National Library
of Canada

Acquisitions and
Bibliographic Services Branch

395 Wellington Street
Ottawa, Ontario
K1A 0N4

Bibliothèque nationale
du Canada

Direction des acquisitions et
des services bibliographiques

395, rue Wellington
Ottawa (Ontario)
K1A 0N4

Your file Votre référence

Our file Notre référence

NOTICE

The quality of this microform is heavily dependent upon the quality of the original thesis submitted for microfilming. Every effort has been made to ensure the highest quality of reproduction possible.

If pages are missing, contact the university which granted the degree.

Some pages may have indistinct print especially if the original pages were typed with a poor typewriter ribbon or if the university sent us an inferior photocopy.

Reproduction in full or in part of this microform is governed by the Canadian Copyright Act, R.S.C. 1970, c. C-30, and subsequent amendments.

AVIS

La qualité de cette microforme dépend grandement de la qualité de la thèse soumise au microfilmage. Nous avons tout fait pour assurer une qualité supérieure de reproduction.

S'il manque des pages, veuillez communiquer avec l'université qui a conféré le grade.

La qualité d'impression de certaines pages peut laisser à désirer, surtout si les pages originales ont été dactylographiées à l'aide d'un ruban usé ou si l'université nous a fait parvenir une photocopie de qualité inférieure.

La reproduction, même partielle, de cette microforme est soumise à la Loi canadienne sur le droit d'auteur, SRC 1970, c. C-30, et ses amendements subséquents.

Canada

UNIVERSITY OF ALBERTA

MAGNETOTELLURIC SURVEY IN WEST-CENTRAL ALBERTA

BY

ANAND RAO KALVEY ©

A THESIS SUBMITTED TO THE FACULTY OF GRADUATE STUDIES AND
RESEARCH IN PARTIAL FULFILLMENT OF THE REQUIREMENTS FOR
THE DEGREE OF MASTER OF SCIENCE

IN

GEOPHYSICS

DEPARTMENT OF PHYSICS

EDMONTON, ALBERTA
SPRING, 1994

National Library of Canada
Acquisitions and Bibliographic Services Branch
395 Wellington Street
Ottawa, Ontario
K1A 0N4

Bibliothèque nationale du Canada
Direction des acquisitions et des services bibliographiques
395, rue Wellington
Ottawa (Ontario)
K1A 0N4

Your file Votre référence

Our file Notre référence

The author has granted an irrevocable non-exclusive licence allowing the National Library of Canada to reproduce, loan, distribute or sell copies of his/her thesis by any means and in any form or format, making this thesis available to interested persons.

L'auteur a accordé une licence irrévocable et non exclusive permettant à la Bibliothèque nationale du Canada de reproduire, prêter, distribuer ou vendre des copies de sa thèse de quelque manière et sous quelque forme que ce soit pour mettre des exemplaires de cette thèse à la disposition des personnes intéressées.

The author retains ownership of the copyright in his/her thesis. Neither the thesis nor substantial extracts from it may be printed or otherwise reproduced without his/her permission.

L'auteur conserve la propriété du droit d'auteur qui protège sa thèse. Ni la thèse ni des extraits substantiels de celle-ci ne doivent être imprimés ou autrement reproduits sans son autorisation.

ISBN 0-612-11248-9

Canada

UNIVERSITY OF ALBERTA

RELEASE FORM

NAME OF AUTHOR: ANAND RAO KALVEY

TITLE OF THESIS: MAGNETOTELLURIC SURVEY IN WEST-CENTRAL ALBERTA

DEGREE: MASTER OF SCIENCE

YEAR THIS DEGREE GRANTED: SPRING 1994

Permission is hereby granted to the University of Alberta Library to reproduce single copies of this thesis and to lend or sell such copies for private, scholarly or scientific research purpose only.

The author reserves all other publication and other rights in association with the copyright in the thesis, and except as hereinbefore provided neither the thesis nor any substantial portion thereof may be printed or otherwise reproduced in any material form whatever without the author's prior written permission.

Anand rao Kalvey

Permanent address:
Qr.No. B-170
Indian Institute of Technology
Kharagpur - 721 302
India

Date Dec. 13, 1993

UNIVERSITY OF ALBERTA

FACULTY OF GRADUATE STUDIES AND RESEARCH

The undersigned certify that they have read, and recommended to the Faculty of Graduate Studies and Research for acceptance, a thesis entitled MAGNETOTELLURIC SURVEY IN WEST-CENTRAL ALBERTA submitted by ANAND RAO KALVEY in partial fulfillment of the requirements for the degree of MASTER OF SCIENCE in GEOPHYSICS.

Dr. F W Jones
(Supervisor)

Dr. E R Kanasewich

Dr. D Hube

Dr. J Toth

Date Dec. 13, 1993

ABSTRACT

Magnetotelluric(MT) measurements in the frequency range approximately 0.01-130Hz were made at thirteen sites in west-central Alberta between 53.1°N-53.6°N and 116.6°W-117.8°W in the Hinton-Edson-Robb area. The objective was to investigate the electrical structure of the area, particularly with reference to a geothermal gradient anomaly that occurs there.

MT data collected from the area, in the form of time series, were processed to obtain plots of apparent resistivities and phases against frequency. These processed data have been used to construct pseudosections (contour plots of apparent resistivities and phases against frequency) along five profiles across the area. The processed data, from each site, were inverted using one-dimensional Fischer inversion to obtain the layer parameters (resistivities and depths). The results from the inversions were used to construct depth section plots along the five profiles. Plan view plots were constructed at various depths. Finally, some preliminary two-dimensional modelling was carried out.

The results of the survey show that the region has relatively low resistivities ranging from 8Ωm to 320Ωm. Although these values are generally expected for

sediments, there is indication that the basement resistivities are low compared to other parts of central Alberta. Low resistivities in the sedimentary part of the section may be caused by highly conductive saline fluids. Their presence is consistent with the presence of the geothermal anomaly and the presence of gas pools. It is possible that migration of warm saline fluids upward along faults and fractures from depth in the southwest transports heat to the upper sediments and so produces the thermal anomaly and the high electrical conductivities. The presence of hydrocarbon accumulations (the Lambert and Banshee gas pools) support this suggestion. The low basement resistivities are unaffected, but are consistent with the presence of a magnetovariational anomaly at depth that may be associated with partial melt of tectonic origin.

Attempts were made to compare the MT resistivities with resistivities from petroleum exploration well logs for five sites. The objective was to investigate the correlation between the two resistivities but the available log data were found to be inadequate for the purpose.

ACKNOWLEDGMENT

I am grateful to Dr. F.W. Jones who proposed the problem and gave me the freedom to work. During the entire course of the research, I received his continuous support, financial and otherwise, his supervision, guidance and constructive criticism. Without his support, work of this kind could never be complete.

Thanks are due to Canadian Hunter Exploration and PanCanadian Petroleum Limited for their financial assistance. I also thank Mr. L. Kelsch of PanCanadian Petroleum Limited, for providing the seismic sections, and Mr. A.R. Fink of Gulf Canada Resources Limited for providing the well logs.

I am grateful to my colleagues Mr. Antonio Correia and Mr. Miles Ertman for their suggestions and comments and for some very lively coffee table discussions, academic and otherwise.

I thank Dr. H. Sherif for his help and acknowledge the financial support provided by the department in the form of a teaching assistantship for my entire stay in the university.

My sincere thanks to Mr. Pranob Banerjee for the help extended to me in hard times. I also thank my room mates, present and past, for all their help and support.

Last, but not the least, I am forever indebted to my parents who have always given me so much and asked for so little.

TABLE OF CONTENTS

CHAPTER PAGE

1. INTRODUCTION 1

1.1 Objective and previous work 2

1.2 Electrical properties of rocks 5

1.3 Geology of the area 8

2. THE MAGNETOTELLURIC METHOD 12

2.1 Introduction 13

2.2 The source field 14

2.3 The magnetotelluric theory 17

2.4 Estimation of tensor elements 28

2.5 Preliminary Estimates 30

3. DATA ACQUISITION AND PROCESSING 34

3.1 Sensors 35

3.2 The SPAM system 41

3.3 Details of data acquisition and analysis 46

4. ANALYSIS OF THE RESULTS 63

4.1 Analysis of processed data 64

4.2 Two-dimensional modelling 88

4.3 Discussion and conclusion 108

4.4 Suggestions for further work 131

5. COMPARISON OF WELL LOGS WITH MAGNETOTELLURIC RESISTIVITIES 133

BIBLIOGRAPHY 143

APPENDIX A 157

APPENDIX B 219

List of Tables

Table Page

3.1 Default SPAM system settings 43

List of Figures

Figure Page

1.1 Map of Hinton-Edson-Robb area showing the 13 magnetotelluric sites 3

1.2 Geothermal gradient (in $^{o}C/km$) contour plot in the Hinton-Edson area (after Lam et al, 1982) 4

1.3 Fence diagram of Hinton and adjacent areas (modified after Lam et al, 1985) 9

1.4 Fence diagram of Edson and adjacent areas (modified after Lam et al, 1985) 10

3.1 A three dimensional field layout of detectors 36

3.2 A typical data acquisition system 42

3.3a Upward and downward biased RHOXY and RHOYX .. 51

3.3b Average RHOXY and RHOYX 52

3.3c Upward and downward biased MAJOR, MINOR and INVARIANT 53

3.3d Average MAJOR, MINOR and INVARIANT 54

3.3e Parameters for Parkinson arrows 55

3.4 A typical data processing flow chart 56

4.1 Pseudosections for profile 1. (a) apparent resistivity (contour values in Ω.m on log scale); (b) Phase (contour values in degrees) 65

4.2 Pseudosections for profile 2. (a) apparent resistivity (contour values in Ω.m on log scale); (b) Phase (contour values in degrees) 67

4.3 Pseudosections for profile 3. (a) apparent resistivity (contour values in Ω.m on log scale); (b) Phase (contour values in degrees) 68

4.4 Pseudosections for profile 4. (a) apparent resistivity (contour values in Ω.m on log scale); (b) Phase (contour values in degrees) 69

4.5 Pseudosections for profile 5. (a) apparent resistivity (contour values in Ω.m on log scale); (b) Phase (contour values in degrees) 70

4.6a Output from one dimensional Fischer inversion 72

4.6b Resistivity against depth plot from 1-D Fischer inversion 73

4.7 Depth section for profile 1 (contour values in Ω.m on log scale) 77

4.8 Depth section for profile 2 (contour values in Ω.m on log scale) 78

4.9 Depth section for profile 3 (contour values in Ω.m on log scale) 79

4.10 Depth section for profile 4 (contour values in Ω.m on log scale) 80

4.11 Depth section for profile 5 (contour values in Ω.m on log scale) 81

4.12 Plan view at 1km(contours in Ω.m on log scale) 84

4.13 Plan view at 2km(contours in Ω.m on log scale) 84

4.14 Plan view at 3km(contours in Ω.m on log scale) 85

4.15 Plan view at 4km(contours in Ω.m on log scale) 85

4.16 Plan view at 5km(contours in Ω.m on log scale) 86

4.17 Plan view at 6km(contours in Ω.m on log scale) 86

4.18 Plan view at 9km(contours in Ω.m on log scale) 87

4.19 Plan view at 18km(contours in Ω.m on log scale) 87

4.20a Resistivity configuration for two dimensional model for profile 1 (resistivity values in Ω.m) 91

4.20b Resistivity configuration for two dimensional model for profile 2 (resistivity values in Ω.m) 92

4.20c Resistivity configuration for two dimensional model for profile 3 (resistivity values in Ω.m) 93

4.20d Resistivity configuration for two dimensional model for profile 4 (resistivity values in Ω.m) 94

4.20e Resistivity configuration for two dimensional model for profile 5 (resistivity values in Ω.m) 95

4.21 Model pseudosections for profile 1 for E-polarization. (a) Apparent resistivity (contour values in Ω.m on log scale); (b) Phase (contour values in degrees) 98

4.22 Model pseudosections for profile 1 for H-polarization. (a) Apparent resistivity (contour values in Ω.m on log scale); (b) Phase (contour values in degrees) 99

4.23 Model pseudosections for profile 2 for E-polarization. (a) Apparent resistivity (contour values in Ω.m on log scale); (b) Phase (contour values in degrees) 100

4.24 Model pseudosections for profile 2 for H-polarization. (a) Apparent resistivity (contour values in Ω.m on log scale); (b) Phase (contour values in degrees) 101

4.25 Model pseudosections for profile 3 for E-polarization. (a) Apparent resistivity (contour values in Ω.m on log scale); (b) Phase (contour values in degrees) 102

4.26 Model pseudosections for profile 3 for H-polarization. (a) Apparent resistivity (contour values in Ω.m on log scale); (b) Phase (contour values in degrees) 103

4.27 Model pseudosections for profile 4 for E-polarization. (a) Apparent resistivity (contour values in Ω.m on log scale); (b) Phase (contour values in degrees) 104

4.28 Model pseudosections for profile 4 for H-polarization. (a) Apparent resistivity (contour values in Ω.m on log scale); (b) Phase (contour values in degrees) 105

4.29 Model pseudosections for profile 5 for E-polarization. (a) Apparent resistivity (contour values in Ω.m on log scale); (b) Phase (contour values in degrees) 106

4.30 Model pseudosections for profile 5 for H-polarization. (a) Apparent resistivity (contour values in Ω.m on log scale); (b) Phase (contour values in degrees) 107

4.31 Lambert (L) and Banshee (B) gas pools with 13 sites and 5 profiles 116

4.32 The geological section. The fifth meridian corresponds to longitude 114°W 118

4.33a Fischer inversion composite plot for profile 1. The numbers indicate resistivities in Ω.m 120

4.33b Fischer inversion composite plot for profile 2. The numbers indicate resistivities in Ω.m 121

4.33c Fischer inversion composite plot for profile 3. The numbers indicate resistivities in Ω.m 122

4.33d Fischer inversion composite plot for profile 4. The numbers indicate resistivities in Ω.m 123

4.33e Fischer inversion composite plot for profile 5. The numbers indicate resistivities in Ω.m 124

4.34a Apparent resistivity against frequency plot for 13 sites showing static shift in the data 126

4.34b Phase against frequency plot for 13 sites showing the independence of phase on static shift 127

5.1a Resistivity and model responses for site 152 138

5.1b Phase and model responses for site 152 138

5.2a Resistivity and model responses for site 163 139

5.2b Phase and model responses for site 163 139

5.3a Resistivity and model responses for site 201 140

5.3b Phase and model responses for site 201 140

5.4a Resistivity and model responses for site 204 141

5.4b Phase and model responses for site 204 141

5.5a Resistivity and model responses for site 205 142

5.5b Phase and model responses for site 205 142

CHAPTER 1

INTRODUCTION

1.1 OBJECTIVE AND PREVIOUS WORK

Magnetotelluric measurements in the frequency range of approximately 0.01-130Hz were made at 13 sites in west-central Alberta between 53.1°N-53.6°N and 116.6°W-117.8°W in the Hinton-Edson-Robb area (Fig.1.1). The purpose of the work was to investigate the electrical structure, particularly with reference to a geothermal gradient anomaly that occurs there (Lam et al, 1982), and its relationship to a deep electrical conductivity anomaly previously discovered from geomagnetic depth sounding studies using a magnetometer array (Ingham et al, 1983).

The geothermal gradient anomaly was discovered from analysis of bottom hole temperatures from 3360 petroleum exploration wells in the area 53°-54°N and 116°-118°W (Lam et al, 1982). A contour plot of the average gradients through the sedimentary section is given in Fig.1.2. The average geothermal gradients range from approximately 24°C/km to 36°C/km. The original interpretation of these data was that ground water motion from recharge areas to the south and west transports heat northeastward from depth along faults and fractures to produce the anomaly.

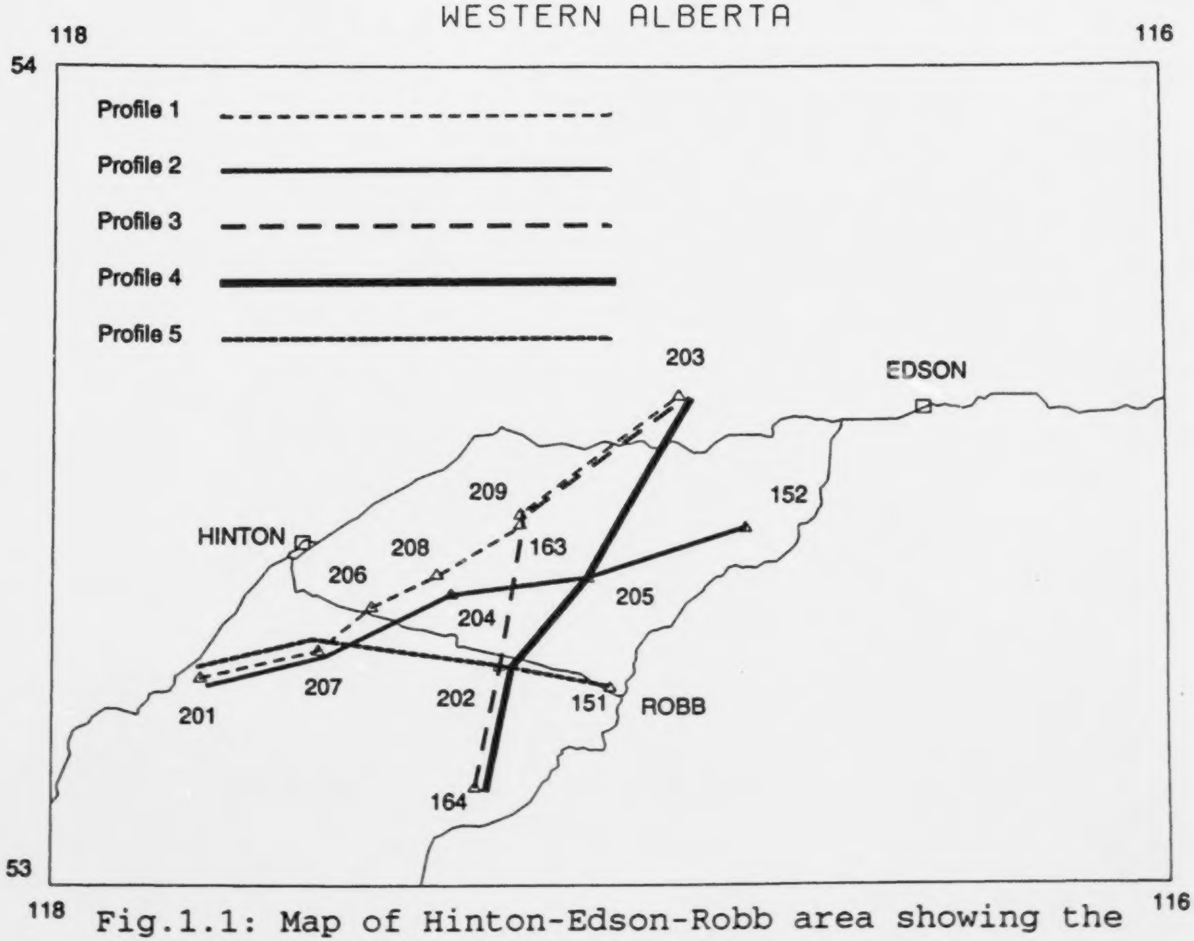

Fig.1.1: Map of Hinton-Edson-Robb area showing the 13 magnetotelluric sites.

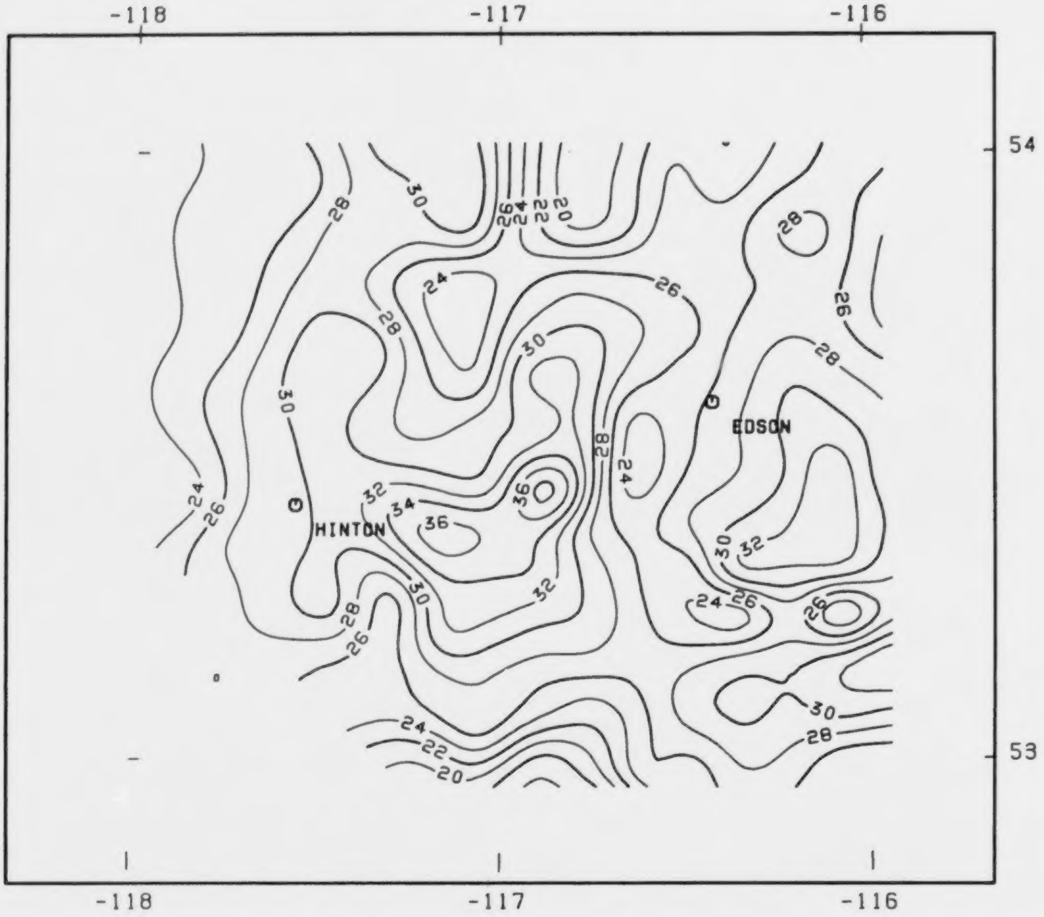

Fig.1.2: Geothermal gradient (in °C/km) contour plot in the Hinton-Edson area (after Lam et al, 1982).

Following the above work, Ingham et al(1983) carried out a magnetometer study of the area with 31 magnetometers. They discovered an electrical conductivity anomaly coincident with the thermal anomaly. They concluded that their results indicated the presence of a highly conducting volume of rock below the geothermal anomaly with its top at greater than 5km depth and which extends to lower crustal depths. They suggested that this may be caused by partial melt of tectonic origin and is the source of both the electrical anomaly and the geothermal anomaly.

Subsequent work by Majorowicz et al (1984) showed that the pattern of heat flow changes with depth, a pattern that is inconsistent with heat from a volume of rock below, or if the heat does come from a volume of rock at depth, the heat flow pattern is disturbed by water motion. It is now acknowledged that both a geothermal gradient anomaly and a magnetovariational anomaly exist in the study area but their causes and interrelationship are still uncertain.

1.2 ELECTRICAL PROPERTIES OF ROCKS

All geophysical methods are unique in the sense that they attempt to measure, directly or indirectly, some physical property or parameter of the earth. In the magnetotelluric method, the measured physical quantity is the electrical resistivity or simply resistivity. It is also possible to determine resistivities in the laboratory from rock samples but this method is not preferred over in situ magnetotelluric measurements primarily because laboratory conditions (such as temperature, porosity, pressure, sample sizes etc.) differ from in situ conditions. It is well known from laboratory measurements that the resistivity (or conductivity which is the reciprocal of resistivity) of a geological formation depends on temperature, porosity, fluid content, chemical composition, phase of the pore fluid, pressure etc. (Keller and Frischknecht, 1966; Shankland and Waff, 1974). Of the several factors, temperature, fluid content, chemical composition and phase play the more important roles in determining conductivities of geological formations.

The dependence of electrical conductivity on temperature(T) is given by the relation (Parkinson, 1983):

$$\sigma = \sigma_e e^{(E_e/kT)} + \sigma_i e^{(E_i/kT)} \qquad (1.1)$$

where σ_e and σ_i are extrinsic and intrinsic conductivities respectively, E_e and E_i are the corresponding activation energies and k is the Boltzmann constant. The first term on the right hand side of equation (1.1), representing extrinsic conductivity, is associated with crystal defects and impurities while the second term, dominant at high temperatures, is associated with thermal motion. In principle it is possible to deduce the temperature distribution in the subsurface from a distribution of conductivity using the above relation.

It is well known that conductivity of a geological formation depends significantly on the water content in that formation. The porosity of a formation depends on the type of rock and the individual formation (e.g. sedimentary rocks are usually more porous than igneous or metamorphic rocks unless the latter are highly fractured). Most of the crustal rocks that are porous are saturated with ground water, which is usually saline (Parkinson, 1983). The conductivity is found to obey Archie's law (Archie, 1942) given by:

$$\sigma = a\sigma_s S^m P^n \tag{1.2}$$

where σ_s is the conductivity of the solution in the pore spaces, S and P are respectively the saturation and porosity and a, m and n are empirical constants. It is evident from the above relation and from experience that conductivity increases with increasing water content.

Electrical conductivities also depend on the chemical compositions of rocks. Rocks with dehydrated minerals will have lower conductivities than those with hydrated minerals such as serpentine, sulfide, magnetite and graphite.

Change of phase is also an important criterion in determination of the conductivity of a geological formation. It has been found that minerals in melt or partial melt phase result in a higher bulk conductivity of a rock than for solid phase. Berdichevsky et al (1972) have interpreted certain observed anomalies in terms of partial melts. Detailed accounts of electrical properties of rocks can be found in Collet and Katsube (1973), Olhoeft (1980), Parkhomenko (1982) and Keller (1987).

1.3 GEOLOGY OF THE AREA

The Edson-Hinton-Robb area is the deepest portion of the western Canadian sedimentary basin that lies between the Canadian shield and the cordilleran foreland thrust belt (Lam and Jones, 1985). The major features and

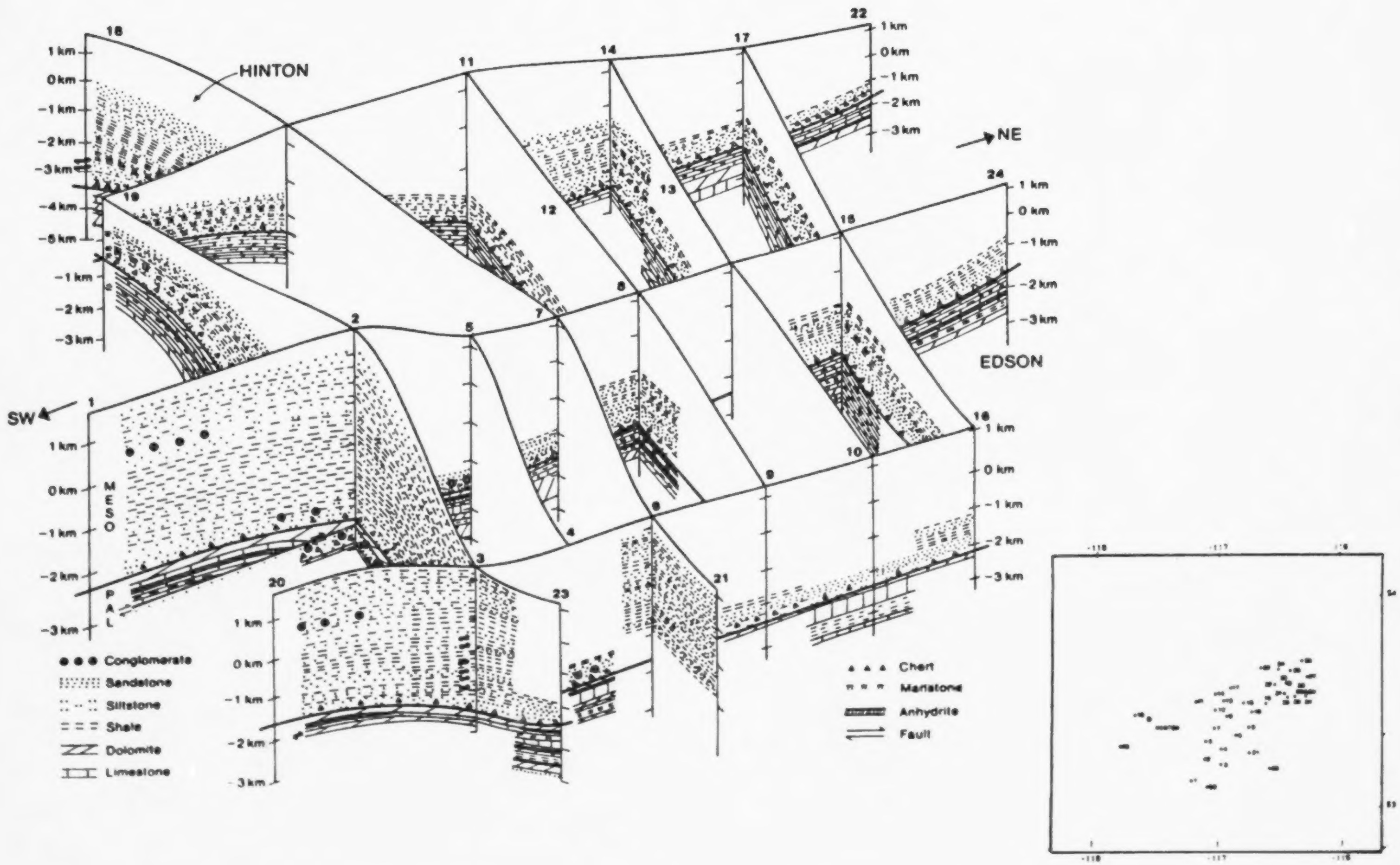

Fig.1.3: Fence diagram of Hinton and adjacent areas (modified after Lam et al, 1985).

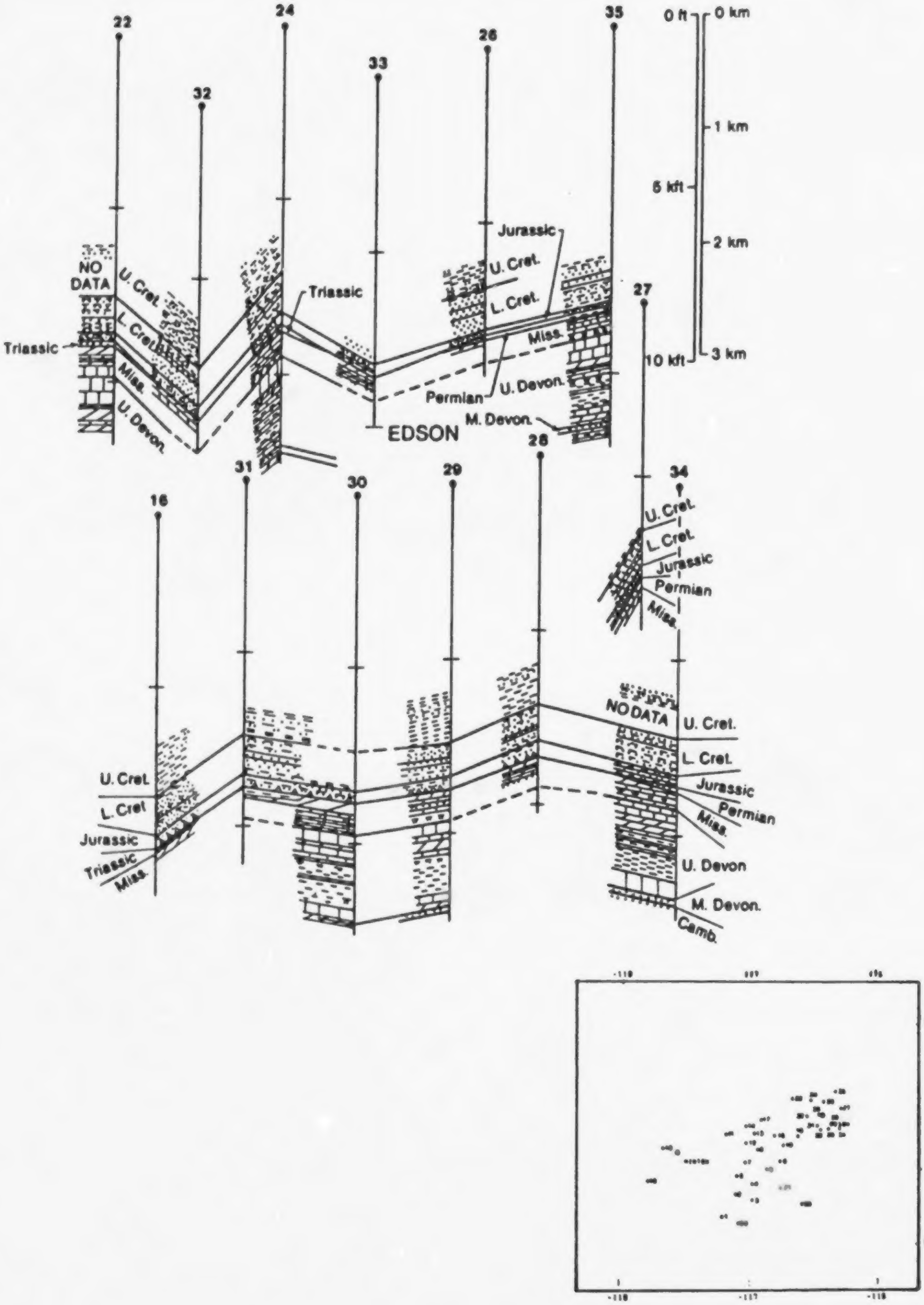

Fig.1.4: Fence diagram of Edson and adjacent areas (modified after Lam et al, 1985).

structures such as rock types, faults etc. are shown in Figs. 1.3 and 1.4. The insets in the two figures show the locations of the wells from which lithological data were used to construct the three dimensional geological fence diagrams.

The major rock types in the region are of Cretaceous, Jurassic, Triassic, Mississippian and Devonian ages. The entire sedimentary sequence consists of two stratigraphic units. These are the upper Mesozoic and lower Paleozoic units respectively. The upper Mesozoic clastic unit consists of Cretaceous sandstone and shale below which lie Jurassic cherts and sandstone. The lower Paleozoic unit is made up mainly of Mississippian and Devonian carbonate sequences. The Mississippian sequence within the lower unit is composed of several layers with the top layer of dolomites followed by limestone, sandstone, siltstones, anhydrites, more limestones and marlstones. The Devonian sequence is mainly comprised of layers of dolomites, limestones, shales and marlstones. The middle Devonian sequence is believed to be silty and sandy. A detailed description of the subsurface geology of the area can be found in Lam and Jones (1985).

CHAPTER 2

THE MAGNETOTELLURIC METHOD

2.1 INTRODUCTION

The magnetotelluric method is one of the most used exploration tools in geophysics that employs the naturally occurring electromagnetic field as the energy source. The theory underlying the method was developed by Tikhonov(1950) in the Soviet Union and Cagniard(1953) in France. The method has been used since the early fifties to investigate the electrical structure of the earth. Tikhonov first recognized the potential of using Earth's natural electromagnetic field in geophysical exploration and Cagniard developed the necessary one dimensional mathematics for obtaining the distribution of conductivity in the subsurface.

The magnetotelluric method is a single site method in which the amplitudes and phases of the mutually perpendicular components of the total (inducing and induced) electromagnetic field at the surface of the earth are measured. It is assumed that the inducing field can be represented by a plane wave and the earth consists of plane horizontal layers. In practice neither of these assumptions is true. Nevertheless, they are approximately satisfied in most situations. Wait(1954) was particularly skeptical about the plane wave assumption. He argued that the finite ionospheric sources do not generate plane waves that are incident at right angles to the surface of the earth. Through extensive computer modeling, however, Madden and Nelson(1964) and Srivastava(1965) proved the validity of the plane wave approximation for periods of up to a thousand seconds.

The mathematics and theory of the MT method were further developed by Neves(1957) and Price(1962) and more recently by Kaufman and Keller(1981), Vozoff(1986), Nabighian(1987) and others.

2.2 THE SOURCE FIELD

The major sources of energy for the magnetotelluric method come from interaction between the charged particles from the solar wind and the Earth's magnetic field and worldwide lightning storm activity. Both these activities cause fluctuations in the natural electromagnetic field near the surface of the earth. These fluctuations occur at all times over the earth (though they may be stronger or weaker at times) and their frequencies include the range most commonly used for exploration purposes, 0.0001-10000 Hz. In the amplitude versus frequency plot of magnetic variations (Patra and Mallick, 1980), a minimum occurs at a frequency of 1Hz and this divides the spectrum into two parts. At frequencies below 1Hz, the interaction of the solar wind with the ionosphere results in micropulsations of the natural electromagnetic field and gives rise to energy that penetrates the earth. The intensity of micropulsations and hence the energy depends mainly on solar activity and is highest during high sunspot activity.

The major source of energy above 1Hz is worldwide thunderstorm activity and lightning associated with it. Lightning stroke signals are called 'sferics'. The three major world thunderstorm centers are located in Brazil, Central Africa and Malaysia. Each of these storm centers has an average of 100 storm days per year (Kaufman and Keller, 1981). The locations of the storm centers are such that at any given time there is a storm at one center or another. Over the entire globe the frequency of lightning flashes is expected to be between 100-1000 flashes per second (Vozoff, 1991). The magnetotelluric(MT) signal depends mainly on the strength and frequency of the lightning flashes and the distance between the point of lightning discharge and the observing location. This implies that MT signals are strongest in tropical regions in summer afternoons.

The sferics travel around the world within the earth-ionosphere cavity which acts as a waveguide. The waveguide dimension changes with time depending on the height of the ionospheric D-layer (height of D-layer being approximately 90km at night and 60km during day time). A range of frequencies is present in the sferics. When the waveguide dimensions change, some frequencies are enhanced while others are suppressed. The enhanced frequencies are the result of resonance effects in the cavity. The resonance peaks occur at 8, 14, 20 and 25Hz and are called Schumann resonance peaks (Schumann, 1957).

The source field may also include unwanted signals due to power line interference or other cultural noise or caused by detector coil movement from ground motion due to wind or other causes. The power line interference can be eliminated by using notch filters. The noise due to coil vibrations can be identified because of lack of correlation between its electric and magnetic field signals and so can be removed from the records.

As mentioned earlier, signals below 1Hz are caused by micropulsations. There are three main types of micropulsations which together result in a wide range of signal amplitudes from a fraction of a nanotesla to a few hundred of nanoteslas. The three types of micropulsations are called P_c(Pulsation continuous), P_i(Pulsation irregular) and P_p(Pulsation pearls). A more detailed account of these can be found in Patra and Mallick(1980), Jacobs (1964), Keller and Frischknecht(1966) and Kaufman and Keller(1981).

2.3 THE MAGNETOTELLURIC THEORY

Micropulsations and thunderstorm activity generate time varying magnetic fields, described by the vector **H**, which in turn generate a plane wave that penetrates into the earth. The plane wave interacts with the subsurface geological structure giving rise to an induced electric field. The interaction can also result in a vertical magnetic field component depending on the dimensionality of the geological structure. Thus on the surface of the earth, three components of magnetic field, H_x, H_y, H_z, and two components of electric field, E_x and E_y, can be measured.

The fundamental equations governing the propagation of electromagnetic waves in a medium are called Maxwell's equations. They are:

$$\nabla . \mathbf{B} = 0 \tag{2.1}$$

$$\nabla x \mathbf{E} = -\frac{\partial \mathbf{B}}{\partial t} \qquad \text{(Faraday's law)} \tag{2.2}$$

$$\nabla x\mathbf{H} = \mathbf{J} + \frac{\partial \mathbf{D}}{\partial t} \qquad \text{(Ampere's law)} \qquad (2.3)$$

$$\nabla . \mathbf{D} = \rho' \qquad \text{(Coulomb's law)} \qquad (2.4)$$

where **B** (=μ**H**) is the magnetic induction (Tesla), **E** is electric field (V/m), **H** is magnetic field intensity (A/m), **J** (=σ**E**) is current density (A/m^2), **D** (=ε**E**) is surface charge density (C/m^2) and ρ' is volume charge density (C/m^3). The quantities μ, σ and ε are respectively magnetic permeability (henry/meter), electrical conductivity (mho/m) and electrical permittivity (farad/meter). Taking curl of (2.2) and manipulating, we get,

$$\nabla x(\nabla x\mathbf{E}) = \nabla x(-\frac{\partial \mathbf{B}}{\partial t}) = -\mu \nabla x \frac{\partial \mathbf{H}}{\partial t} \qquad (2.5)$$

Differentiating (2.3) with respect to t and simplifying, we have,

$$\nabla x \frac{\partial \mathbf{H}}{\partial t} = \frac{\partial \mathbf{J}}{\partial t} + \epsilon \frac{\partial^2 \mathbf{E}}{\partial t^2} \qquad (2.6)$$

Combining (2.5) and (2.6) and remembering the constitutive relation **J**=σ**E**, we get,

$$\nabla x(\nabla x \mathbf{E}) = -\mu\sigma \frac{\partial \mathbf{E}}{\partial t} - \mu \in \frac{\partial^2 \mathbf{E}}{\partial t^2} \qquad (2.7)$$

However,

$$\nabla x(\nabla x \mathbf{E}) = \nabla(\nabla.\mathbf{E}) - \nabla^2 \mathbf{E} \qquad (2.8)$$

$$\therefore \nabla^2 \mathbf{E} = \mu\sigma \frac{\partial \mathbf{E}}{\partial t} + \mu \in \frac{\partial^2 \mathbf{E}}{\partial t^2} \qquad (2.9)^{*}$$

Similarly, it can be shown that

$$\nabla^2 \mathbf{H} = \mu\sigma \frac{\partial \mathbf{H}}{\partial t} + \mu \in \frac{\partial^2 \mathbf{H}}{\partial t^2} \qquad (2.10)$$

Equations (2.9) and (2.10) are called the wave equations.

Applying the Laplacian operator on the rectangular components of **E**, we get

$$\begin{aligned}
\frac{\partial^2 E_x}{\partial x^2} + \frac{\partial^2 E_x}{\partial y^2} + \frac{\partial^2 E_x}{\partial z^2} &= \mu\sigma \frac{\partial E_x}{\partial t} + \mu \in \frac{\partial^2 E_x}{\partial t^2} \\
\frac{\partial^2 E_y}{\partial x^2} + \frac{\partial^2 E_y}{\partial y^2} + \frac{\partial^2 E_y}{\partial z^2} &= \mu\sigma \frac{\partial E_y}{\partial t} + \mu \in \frac{\partial^2 E_y}{\partial t^2} \qquad (2.11) \\
\frac{\partial^2 E_z}{\partial x^2} + \frac{\partial^2 E_z}{\partial y^2} + \frac{\partial^2 E_z}{\partial z^2} &= \mu\sigma \frac{\partial E_z}{\partial t} + \mu \in \frac{\partial^2 E_z}{\partial t^2}
\end{aligned}$$

---

[*] It can be shown that in a region with non vanishing conductivity (Grant and West, 1965), charge density will reach steady state value in a short time implying that charge does not accumulate appreciably during the flow of current. Therefore $\nabla.J = 0$. Hence $\nabla.E = 0$.

For a one dimensional problem, in the z-x plane, $E_y=0=E_z$ and $\partial/\partial x = 0 = \partial/\partial y$. Thus we are left with only

$$\frac{\partial^2 E_x}{\partial z^2} = \mu\sigma\frac{\partial E_x}{\partial t} + \mu \in \frac{\partial^2 E_x}{\partial t^2} \tag{2.12}$$

Let E_x be of the form $E_x = E_o e^{i\omega t}$ (harmonic). Substituting this in equation (2.12) and manipulating, we get,

$$\frac{\partial^2 E_x}{\partial z^2} = i\omega\mu(\sigma + i\omega \in)E_x = k^2 E_x \tag{2.13}$$

where $k^2 = i\omega\mu(\sigma + i\omega \in)$. The solution of equation (2.13) is of the form

$$E_x = (Ae^{kz} + Be^{-kz}) \tag{2.14}$$

For a homogeneous earth E_x becomes negligibly small at great depths (i.e. as $z \to \infty$). Therefore, A in the first term of (2.14) must be zero. Hence,

$$E_x = Be^{-kz} \tag{2.15}$$

Similarly, assuming harmonic nature for $H(=H_0 e^{i\omega t})$, it can be shown that,

$$\nabla x \mathbf{E} = -i\omega\mu\mathbf{H} \tag{2.16}$$

For the one dimensional case under consideration,

$$\frac{\partial E_x}{\partial z} = -i\omega\mu H_y \qquad (2.17)$$

Differentiating (2.15) with respect to z and equating with (2.17) and rearranging, we get,

$$H_y = \frac{k}{i\omega\mu} Be^{-kz} \qquad (2.18)$$

Dividing (2.15) by (2.18), we get an expression for impedance called the Cagniard impedance. The expression is:

$$Z = \frac{E_x}{H_y} = \frac{i\omega\mu}{k} \qquad (2.19)$$

At low frequencies, less than 1000Hz(Keller and Frischknecht; 1966), the displacement current contribution is negligible. Hence,

$$k^2 = i\omega\mu\sigma \qquad (2.20)$$

Therefore,

$$Z = \frac{i\omega\mu}{\sqrt{i\omega\mu\sigma}} = \sqrt{i\omega\mu\rho} \quad . \qquad (2.21)$$

The resistivity is defined as

$$\rho_{xy} = \frac{1}{\omega\mu}\left|\frac{E_x}{H_y}\right|^2 \quad . \qquad (2.22)$$

It can similarly be shown that

$$\rho_{yx} = \frac{1}{\omega\mu}\left|\frac{E_y}{H_x}\right|^2 \quad . \qquad (2.23)$$

Equations (2.22) and (2.23) are the expressions for the apparent resistivities in terms of frequency and mutually perpendicular components of the electromagnetic field[*]. As we shall see later, the expressions are of great significance in data processing.

Another look at equation (2.20) reveals that k($=\sqrt{i\omega\mu\sigma}$) is complex. Thus k can be rewritten as $k=\alpha+i\beta$, where $\alpha=\beta=\sqrt{\omega\mu\sigma/2}$. Substituting this in (2.15), the expression for E_x, we get,

$$E_x = Be^{-\alpha z}e^{-i\beta z} \qquad (2.24)$$

---

[*] These expressions (2.22 and 2.23) can be written as $\rho_{xy} = 0.2T\left|\frac{E_x}{B_y}\right|^2$ and $\rho_{yx} = 0.2T\left|\frac{E_y}{B_x}\right|^2$, where E_x and E_y are in V/km, B_y and B_x are in nano teslas (nT) and T is the period (sec) of the oscillation.

where the presence of $e^{-\alpha z}$ indicates the attenuation of E_x with depth and $e^{-i\beta z}$ indicates a sinusoidal variation with depth. The quantity $e^{-\alpha z}$ in (2.24) can be used to define a quantity called the skin depth- the depth at which the value of E_x reduces to (1/e) times its value at the surface. It can be shown that the skin depth, δ, is given by:

$$\delta = \sqrt{\frac{2}{\omega\mu\sigma}} \tag{2.25}$$

In most cases skin depth is regarded as the depth of penetration. It is obvious from (2.25) that the depth of penetration depends on the frequency of the source signal and the resistivity of the medium. Thus for a higher resistivity and/or a lower frequency, the depth of penetration is greater.

The formulation developed so far is applicable to one dimensional situations. Expressions (2.22) and (2.23) give the resistivities of a homogeneous, isotropic medium. In the case of an n-layered earth, assuming one dimensional variation of resistivity, the expressions (2.22) and (2.23) can be written together as:

$$\rho_a = \frac{1}{\omega\mu}\left|\frac{E_x}{H_y}\right|^2 = \frac{1}{\omega\mu}\left|\frac{E_y}{H_x}\right|^2 \tag{2.26}$$

where apparent resistivity, ρ_a, is an equivalent resistivity. It is as if the entire n layered earth has been replaced by an equivalent homogeneous and isotropic half space of resistivity ρ_a. As we shall see later, ρ_a is of great significance in MT data processing and is normally the first quantity to be obtained from the raw field data.

In the early days of magnetotellurics, it was quite common to use one dimensional analyses. However, over the years, geophysicists realized the inadequacy of 1-D analyses and started developing the theory appropriate for two dimensional analyses. In a two dimensional earth, the variation of resistivity is considered along the vertical direction as well as along one of the horizontal directions(normally perpendicular to the strike). The expressions describing the relationship between the induced and inducing fields, in this case, may be written as:

$$\mathbf{E}=\mathbf{Z}\mathbf{H} \qquad (2.27)$$

which when expanded becomes,

$$\begin{aligned} E_x&=Z_{xx}H_x+Z_{xy}H_y \\ E_y&=Z_{yx}H_x+Z_{yy}H_y \end{aligned} \qquad (2.28)$$

Expression (2.28) can also be written in matrix form as:

$$\begin{bmatrix} E_x \\ E_y \end{bmatrix} = \begin{bmatrix} Z_{xx} & Z_{xy} \\ Z_{yx} & Z_{yy} \end{bmatrix} \begin{bmatrix} H_x \\ H_y \end{bmatrix} \quad (2.29)$$

The quantity **Z** in (2.27) is a tensor and is known as the impedance tensor. Z_{xx}, Z_{xy}, Z_{yx}, Z_{yy} are the impedance tensor elements. For a two dimensional case, $Z_{xx}=-Z_{yy}\neq 0$ and $Z_{xy}\neq Z_{yx}\neq 0$.

Using the impedance tensor elements, it is possible to define three invariant quantities (Rokityanski, 1982). They are:

$$I_1=Z_{xx}Z_{yy}-Z_{xy}Z_{yx} \quad (2.30a)$$

$$I_2=Z_{xx}+Z_{yy} \quad (2.30b)$$

$$I_3=Z_{xy}-Z_{yx} \quad (2.30c)$$

Thus, if I_2 is zero at a site, it can be concluded that the subsurface has a two dimensional geoelectrical nature.

A two dimensional problem can be simplified by breaking it into two separate modes - the TE mode and the TM mode. In TE mode, also called E-parallel($E_{\|}$), the electric field component is parallel to the strike and the magnetic field component is perpendicular to it. In the TM mode, also called E-perpendicular(E⊥), the electric field is perpendicular to strike while the magnetic field is parallel to it[*]. Rewriting equations (2.2) and (2.3) and neglecting displacement currents, we get,

$$\nabla x\mathbf{E} = -i\omega\mu\mathbf{H} \tag{2.31}$$

$$\nabla x\mathbf{H} = \sigma\mathbf{E} \tag{2.32}$$

For a two dimensional problem, the equations (2.31) and (2.32) reduce to (Jones and Price, 1970),

$$\frac{\partial H_z}{\partial y} - \frac{\partial H_y}{\partial z} = \sigma E_x \tag{2.33}$$

$$\frac{\partial H_x}{\partial z} = \sigma E_y \tag{2.34}$$

$$\frac{\partial H_x}{\partial y} = -\sigma E_z \tag{2.35}$$

$$\frac{\partial E_z}{\partial y} - \frac{\partial E_y}{\partial z} = -i\omega\mu H_x \tag{2.36}$$

---

[*] These modes are sometimes called E-polarization (TE mode) and H (or B)-polarization (TM mode).

$$\frac{\partial E_x}{\partial z} = -i\omega\mu H_y \tag{2.37}$$

$$\frac{\partial E_x}{\partial y} = i\omega\mu H_z \tag{2.38}$$

Equations (2.33), (2.37) and (2.38) correspond to E-polarization(TE mode) while (2.34), (2.35) and (2.36) correspond to H-polarization(TM mode). Eliminating H_y and H_z from (2.33), (2.37) and (2.38) and E_y and E_z from (2.34), (2.35) and (2.36), we get,

$$\frac{\partial^2 E_x}{\partial y^2} + \frac{\partial^2 E_x}{\partial z^2} = i\omega\mu\sigma E_x \tag{2.39}$$

$$\frac{\partial^2 H_x}{\partial y^2} + \frac{\partial^2 H_x}{\partial z^2} = i\omega\mu\sigma H_x \tag{2.40}$$

It is possible to solve the two equations above analytically for some special cases. However, numerical techniques are generally used. There are a number of numerical techniques in use. Four of these are: (i) the finite difference method(Jones and Price, 1970), (ii) the finite element method(Coggon, 1971; Reddy and Rankin, 1973), (iii) the transmission line analogy(Madden and Thompson, 1965; Swift, 1967,1971) and (iv) the integral equation method(Hohmann, 1971; Patra and Mallick, 1980). These techniques, however, will not be discussed here.

2.4 ESTIMATION OF TENSOR ELEMENTS

In order to solve the magnetotelluric problem or estimate the apparent resistivities, it is necessary to obtain an estimate of the tensor elements. This can be done using the expressions (2.28). Note that each of the equations in (2.28) contains two unknowns. Therefore, we must have at least two independent measurements of each of the components of electromagnetic field in order to obtain a unique solution for the impedance tensors. In practice, however, a large number of independent measurements are made and the following system of equations is set up (Vozoff, 1986, 1991):

$$\begin{gathered} E_x^1 = Z_{xx} H_x^1 + Z_{xy} H_y^1 \\ E_x^2 = Z_{xx} H_x^2 + Z_{xy} H_y^2 \\ \dots\dots\dots\dots\dots\dots \\ \dots\dots\dots\dots\dots\dots \\ E_x^n = Z_{xx} H_x^n + Z_{xy} H_y^n \end{gathered} \tag{2.41}$$

and

$$\begin{aligned} E_y^1 &= Z_{yx}H_x^1 + Z_{yy}H_y^1 \\ E_y^2 &= Z_{yx}H_x^2 + Z_{yy}H_y^2 \\ &\cdots\cdots\cdots\cdots\cdots \\ &\cdots\cdots\cdots\cdots\cdots \\ E_y^n &= Z_{yx}H_x^n + Z_{yy}H_y^n \end{aligned} \tag{2.42}$$

The system of equations above can be solved by the least squares technique to obtain a solution for the unknowns Z_{xx}, Z_{xy}, Z_{yx} and Z_{yy}. The least squares solution can be obtained by minimizing the quantity Ψ, given by,

$$\Psi = \sum_{i=1}^{n}(E_{xi} - Z_{xx}H_{xi} - Z_{xy}H_{yi})(E_{xi}^{*} - Z_{xx}^{*}H_{xi}^{*} - Z_{xy}^{*}H_{yi}^{*}) \tag{2.43}$$

where * represents the complex conjugate. Differentiating Ψ with respect to the real and imaginary parts of Z_{xx}, Z_{xy} and equating the differentials to zero, we get,

$$\begin{aligned} \sum_{i=1}^{n} E_{xi}H_{xi}^{*} &= Z_{xx}\sum_{i=1}^{n} H_{xi}H_{xi}^{*} + Z_{xy}\sum_{i=1}^{n} H_{yi}H_{xi}^{*} \\ \sum_{i=1}^{n} E_{xi}H_{yi}^{*} &= Z_{xx}\sum_{i=1}^{n} H_{xi}H_{yi}^{*} + Z_{xy}\sum_{i=1}^{n} H_{yi}H_{yi}^{*} \end{aligned} \tag{2.44}$$

Similarly,

$$\sum_{i=1}^{n} E_{yi}H_{xi}^{*} = Z_{yx}\sum_{i=1}^{n} H_{xi}H_{xi}^{*} + Z_{yy}\sum_{i=1}^{n} H_{yi}H_{xi}^{*}$$

$$\sum_{i=1}^{n} E_{yi}H_{yi}^{*} = Z_{yx}\sum_{i=1}^{n} H_{xi}H_{yi}^{*} + Z_{yy}\sum_{i=1}^{n} H_{yi}H_{yi}^{*} \qquad (2.45)$$

The above set of equations can be solved for the unknowns Z_{xx}, Z_{xy}, Z_{yx} and Z_{yy}. Operations under the summations represent auto and cross power spectra. In principle, it is possible to set up a number of equations similar to (2.44) and (2.45) using different combinations of E_x, E_y, H_x and H_y for auto and cross spectra in terms of the tensor elements. It has, however, been found that the above set of equations gives the best results. An excellent discussion on reasons for using (2.44) and (2.45) and neglecting any other combination is given in Sims et al (1971). This is discussed further in section 3.3.

2.5 PRELIMINARY ESTIMATES

It is customary in geophysics to make preliminary estimates of certain parameters that help in narrowing down a problem under investigation. With the tensor elements known, it is now possible to make semi-quantitative predictions about an MT site. The known values of the tensor elements may be substituted in equation (2.28) to obtain the so called predicted values of the electric field components. These predicted values are designated by E_{xp} and E_{yp}. A comparison between the predicted and observed components is a measure of the goodness of the impedance tensor elements. The quantity that measures the goodness is called the coherency and is mathematically given by(Swift,1967):

$$\mathrm{coh} = \frac{E_x E_{xp}^*}{\sqrt{(E_x E_x^*)(E_{xp} E_{xp}^*)}} \qquad (2.46)$$

The value of coherency varies between 0 and 1. A value of 0 represents totally uncorrelated data while a value of 1 is an indicator that the estimated tensor elements are perfect.

There are a number of other parameters such as the skew, the ellipticity and the tipper that aid in geological interpretation of magnetotelluric data. The quantity skew is the ratio of the absolute values of the invariants I_2 and I_3 given by:

$$S = \frac{|Z_{xx} + Z_{yy}|}{|Z_{xy} - Z_{yx}|} \quad . \qquad (2.47)$$

Ideally in one and two dimensional cases, skew should be zero. But in most practical cases S is never zero because there is always some noise present in the data. For a three dimensional case skew is very high but there is no single value of skew that differentiates a 2-D structure from a 3-D one. However, Reddy et al (1977), suggested a value of 0.4 while Ting and Hohmann(1981) and Park et al.(1983) suggested the values 0.12 and 0.5 respectively.

Ellipticity is yet another parameter that may be used to predict the dimensionality of a geoelectrical structure. Mathematically, it is given by:

$$\beta(\theta) = \frac{\left|Z_{xx}(\theta) - Z_{yy}(\theta)\right|}{\left|Z_{xy}(\theta) + Z_{yx}(\theta)\right|} \tag{2.48}$$

where $Z(\theta)$ is the impedance tensor element when rotated through an angle θ. For noise free data $\beta(\theta)$ is zero for one and two dimensional cases.

As mentioned earlier the vertical component, H_Z, of the magnetic field is induced depending upon the dimensionality of the geoelectrical structure. The vertical component is induced when the subsurface has 3-D geoelectrical structure. As in section 2.3, for electric fields, we can write a mathematical equation describing the interaction between H_x, H_y and H_z. The relation is:

$$H_z=T_xH_x+T_yH_y \qquad (2.49)$$

where T_x and T_y are complex and are functions of frequency. Once again we can set up a number of equations, from n independent measurements of the components, in two unknowns. The resulting equations can be solved using the least squares technique. Using the known values of T_x and T_y, it is possible to calculate a quantity called tipper, given by the expression:

$$T=\sqrt{T_x^2+T_y^2} \qquad (2.50)$$

For a one dimensional case, the tipper is always zero. For a two dimensional case, T_x is zero for the TM mode. Thus in a 2-D situation, T_x is zero along the strike direction. Tipper can also be used for detection of the high conductivity side of a contact(Vozoff, 1991; Orange, 1989). A more detailed discussion on the dimensionality parameters can be found in Beamish(1986).

CHAPTER 3

DATA ACQUISITION AND PROCESSING

3.1 SENSORS

The instrumental set up for MT data acquisition can be divided into two parts - the sensing system and the recording system. The sensing system is comprised of a number of sensors which detect the time varying electric and magnetic fields. The recording unit is responsible for recording and storing the data. The recording unit may include computer capability for initial in-field analysis and evaluation of the data.

A typical sensing system consists of three magnetic field sensors and two pairs of electric field sensors. A three dimensional field arrangement of sensors is shown in Fig.3.1. The two pairs of electrodes, AB and CD, are used for recording the potential differences between the two pairs of points. When divided by the distances between the electrodes these potential differences yield the electric field components. It is assumed that the electric fields are constant across the intervals between the electrodes so the results give the average values at the point of reference (normally the center of the spread). The horizontal x component, E_x, of the electric field is obtained along the line joining the electrodes in the x direction. Similarly, E_y is obtained along the line joining the electrodes in the y direction. The choice of electrode spacing is important. If the spacing

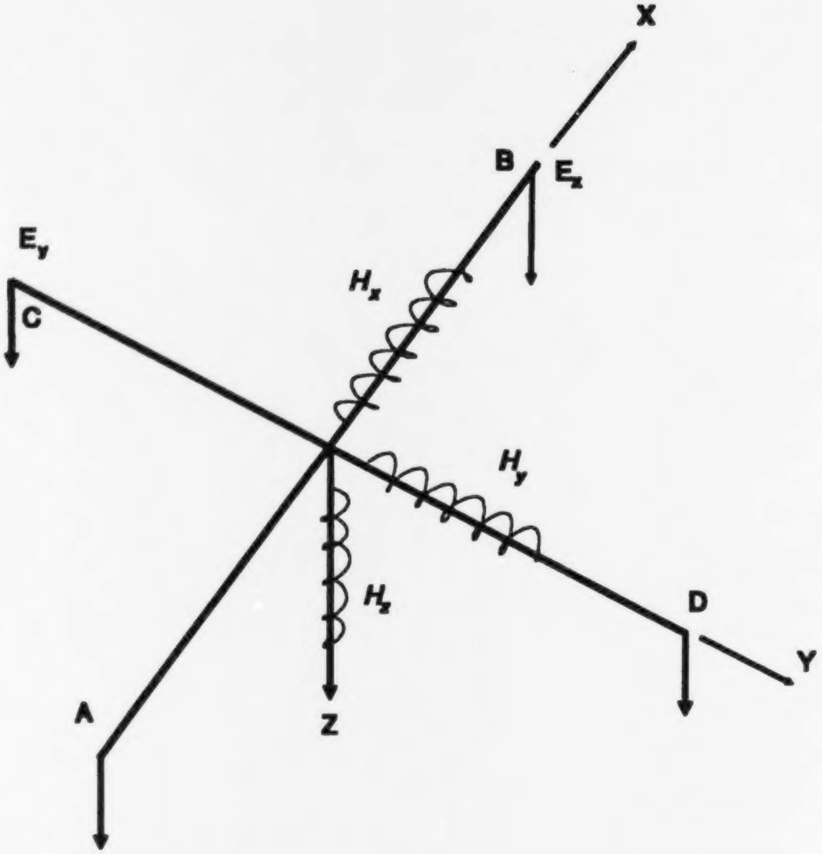

Fig.3.1: A three dimensional field layout of detectors.

is too large, the magnetotelluric signal between the electrodes may be overshadowed by noise. On the other hand, if the spacing is too small, noise generated by the electrodes may overpower the signals. Therefore, an optimum spacing must be used so that the noise effects are minimal. Normally a spacing of 50-300m is considered to be appropriate in most practical situations (Dobrin and Savit, 1988). To minimize motion induced noise, such as that due to sensor and wire movements due to wind and ground vibrations, the wires and electrodes must be firmly fixed on the ground. Also at high frequencies, the wires joining the electrodes must not contain loops or additional voltages will be induced in the wire by time variations in H_z(Swift, 1967).

The electric field measuring electrodes are made from a highly conducting material such as copper, cadmium, silver or lead and make contact with the ground through copper sulfate, cadmium chloride, silver chloride or lead chloride solutions so as to be non-polarizing and low noise. Generally cadmium electrodes are not recommended because of their toxic nature. Petiau and Dupis(1980) describe a $Pb-PbCl_2$ system in Plaster of Paris or clay which is stable if properly made and the electrodes used in this study are of this type. An electrode, when planted in the earth, can be considered as an electrochemical cell that gives rise to a voltage at the interface between the electrode and the earth. This voltage is of no use in magnetotelluric prospecting and is considered as noise. It depends on the chemical interaction between the materials in contact and the ambient temperature. Often it is advisable to install the electrodes a day before the measurements are to be made, to enable the system to attain equilibrium. It is also advisable to select measurement sites that are as far away from power lines as possible since earth currents caused by these can saturate the input amplifiers and so the magnetotelluric signal becomes buried in the power line noise. Nearby lightning also affects the magnetotelluric signal and can appear as spurious peaks unless the preamplifiers have high common mode noise rejection and rapid response(Vozoff, 1991).

The magnetic field is measured using magnetic sensors along three mutually perpendicular directions. Sensors buried just below the surface of the earth (to prevent disturbance by wind) in the x-y plane measure H_x and H_y components. The vertical component, H_z, is measured by a third sensor which is buried vertically. The magnetic sensors and electrodes are connected to a preamplifier and the signals are then sent to the recording unit through a co-axial cable.

The three components of the magnetic field are measured using either a SQUID(Super Conducting Quantum Interference Device) or a set of induction coils. The induction coil system consists of three coils, one for recording each of the three, H_x, H_y and H_z, components of the magnetic field. Each induction coil has thousands of turns of copper wire wound around a metallic core. Each coil produces a voltage that is proportional to the product of its cross sectional area and the time derivative of magnetic induction, B, through its area. For a sinusoidal variation in magnetic induction, the output voltage increases with increasing frequency. In most practical situations, the magnitudes of the fields to be measured are small. Therefore, it is advisable to attempt to increase the voltages before the signals are fed into the preamplifiers. The area of the coil can be increased substantially if it is to be laid out flat on the surface to sense the vertical component(Vozoff, 1991). It is also known that the output is proportional to the number of turns in the coil. Therefore, the greater the number of turns, the higher the output. This, however, should be within practical limits. For sensing the horizontal components of the magnetic field, wire is wound (fewer turns as compared to that for the vertical component sensor) around a core of high magnetic permeability material such as mumetal, molly-permalloy or alloys of molybdenum and nickel in steel. Non-conductive ceramics such as MN-60 (Ceramics Magnetics Inc.; Vozoff, 1991) are used for higher frequency signals.

The high performance induction coils also have many built in circuits including distributed resistance, inductance and capacitance as well as core losses. The voltage output from the circuit decreases with increasing frequency above the resonant frequency of the circuit. Also when designing a coil it is important to have proper impedance matching between the coils and the amplifiers. Detailed accounts of coil design can be found in Clerc(1971), Karmann(1975, 1977) and Stanley and Tinkler(1982).

The second type of magnetometer, called SQUID, also known as a cryogenic magnetometer, is a sensitive device capable of detecting even the slightest variation (of the order of 10^{-5} γ) of the magnetic field. It is based on the principle of the Josephson junction effect in superconductors. A SQUID has a high dynamic range and low inherent noise. The system is compact and lightweight and all the components are packed in a single unit. The instrument requires, for its operation, a continuous supply of liquid helium to keep the system superconducting. A detailed discussion on SQUIDS, in geophysics, is available in Weinstock and Overton(1981).

In the field, all the coils and electrodes are connected to preamplifiers where the signals are given an initial stage of amplification. The preamplifiers are in turn connected to a recording unit (normally in a recording truck) via a coaxial cable. Various stages in a typical data acquisition system are shown in Fig.3.2. The preamplifier outputs are fed into input amplifiers where the signals are further amplified before removing the 60Hz transmission line signal and its harmonics by means of notch filters. The signals are next passed through various gain controls and finally fed into an analog to digital converter (A/D). The digitized signals are then fed into an onboard computer for preliminary analysis and quality checks on data before finally storing the data on a magnetic medium. There may be a number of peripheral devices connected to the computer such as a printer and a monitor. These peripheral devices are used for monitoring and controlling the entire recording system.

3.2 THE SPAM SYSTEM

The SPAM (**S**hort **P**eriod **A**utomatic **M**agnetotelluric) data acquisition system at the University of Alberta has a frequency range of 0.01-128Hz. The entire frequency range of SPAM is divided into four bands with different sampling intervals and within which different numbers of

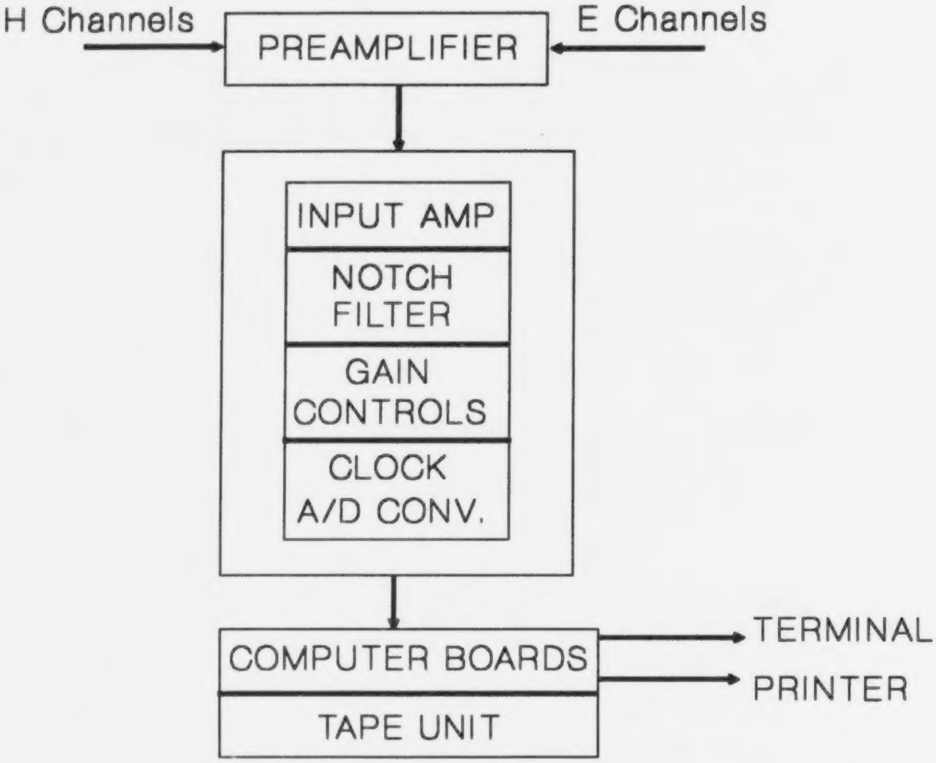

Fig.3.2 : A typical data acquisition system.

frequencies are chosen for analysis. The four frequency bands are numbered 0 through 3 with nominal frequency ranges and sampling intervals as shown in Table 3.1. Data are recorded in each band for a number of time periods called windows. A typical number of windows recorded in each band is 48. In each window, the system records 256 samples of each of the five components of the electromagnetic field as indicated in Table 3.1. Typical data from a site require 512 kilobytes of disk space when stored in uncompressed binary format.

Band No.	**0**	**1**	**2**	**3**
Frequency range(Hz)	16-128	2-16	.25-2	.0125-.25
Sampling frequency(Hz)	512	64	8	1
No. of windows	48	48	48	48
No. of components	5	5	5	5
Samples/component	256	256	256	256

Table 3.1: Default SPAM system settings.

When at a site, the SPAM data are recorded on magnetic cartridges. Normally, two cartridges are required per site, with each cartridge containing two bands of data. The data recording format is as follows (SPAM reference manual):

Cartridge structure

* 512 blocks(numbered 0-511) of 512 bytes each

* logically 4 tracks (2 physically) of 128 blocks each

* each SPAM band occupies one or more consecutive logical tracks

* each track consists of a header(2 blocks), time series data(up to 120 blocks) and results of preliminary analysis(6 blocks) in order.

Header structure

* a header block is written to the first block of each track which is repeated for safety on the second block

* all the information is in 2 byte integer or character

* assume first 128 bytes of block read into an array INTEGER*2 HEAD(64)

* (1) : A2 '**' for valid header block

* (2) : site number (1-999) as entered

* (3) : band number (0-3) as entered

* (4) : logical track number (1-4)

* (5) : cartridge mode (1-3; 3=time series stored)

* (6) : number of samples (128/256); normally 256

* (7) : maximum number of tracks allowed(1-4)

```
*    ( 8)      : digitizing rate in
                 Hz(16384,8192,...,4,2,1)
*    ( 9)      : gain shift normalization number
*    (10)      : wait before digitize cycle
*    (11)      : number of channels used(3-7)
*    (12-20)   : 9I2 physical channel numbers in use for
                 each logical channel name
*    (21-38)   : 9A4 logical channel name sequence
*    (39-45)   : 7I2 where logical channel is telluric,
                 the  telluric line lengths in cm
*    (46)      : spare
*    (47)      : number of coil set in use (1-2)
*    (48)      : SPAM analysis program version number
*    (49)      : spare
*    (50-55)   : 6A2 SPAM identification name
*    (56-64)   : spare
```

The above structure is repeated for all subsequent logical tracks on a cartridge.

The SPAM system also writes the results of some preliminary analysis at the end of each track. The SPAM computer is capable of doing preliminary processing and inversion of data at the end of a site. It takes approximately 12 hours to complete a site on a day when the signal is good. The recorded data, in the form of time series, is brought to The University for detailed processing and interpretation.

3.3 DETAILS OF DATA ACQUISITION AND ANALYSIS

In west central Alberta, the area under investigation, magnetotelluric data were acquired using the sensor layout shown in Fig. 3.1. On the plane of the earth the center of the layout was taken as the origin, the north being the positive x-axis and the east being the positive y-axis. Before starting the SPAM system, it is customary to measure the resistances and self potentials across the two pairs of electrodes. It is also necessary to measure the spacing between the electrodes. The electrode spacing for all the sites in west central Alberta was about 50-100m.

The process of data acquisition and recording is initiated by activating a program called SPAM that prepares the system for receiving and recording the data. Input to the program is the site number, the recording mode of the cartridge, the recording format, some hardware information, electrode spacings in kilometers and the acceptance criteria. The electrode spacings are required to calculate the electric fields from the measured potential differences across the electrodes.

They are recorded in the units of milli-volts/km. Data are accepted for recording only if required standards, as defined by certain acceptance criteria, are met. In most cases the acceptance criteria of 8 frequencies, 0.1 power and 0.8 coherency were used.

The coherency criterion is the minimum coherency for a frequency to be accepted. A low coherency (e.g. 0.7) will accept data of poor quality while a high coherency(e.g. 0.9) will accept only good quality data. It may not always be possible to obtain highly coherent data.

The power criterion is the minimum power, in milli-gammas, of both H_x and H_y for the frequency to be accepted. The minimum power setting depends on the magnetic sensor noise, defining an acceptable signal to noise ratio. The value used will vary from band to band due to the natural power versus frequency distribution. A high setting will only accept frequencies which have high power. A suitable value can be found after a few trials.

The frequency criterion is the least number of frequencies to be accepted, satisfying both the coherency and power criteria in a window. All the analysis sets in use must satisfy their own minimum frequency criteria. All accepted windows are written to the cartridge and the accepted frequencies are stacked. A high value (e.g. 9 frequencies) will accept wide band data whereas a low value(e.g. 4 frequencies) will accept a few good frequencies. If the value is set to zero then the signal quality for that analysis set does not affect the acceptance of other sets.

The data from the field, acquired using the SPAM system, are then brought to The University for processing on the University of Alberta mainframe computer system called the Michigan Terminal System (MTS). The data are first transferred to IBM formatted diskettes from the SPAM cartridges and then transferred to MTS using a file transfer program.

The magnetotelluric data processing package on MTS consists of a number of modules, each module doing a specific job. The first module, which consists of a number of sub modules, reads the data and converts them to appropriate format after performing some preliminary checks on the data. The formatted data are stored in four files, each file corresponding to a band. Data from these four files are then fed into the second module where they are processed to create the spectra files. Once again, there are four spectra files each one corresponding to a band. In the third module, data are processed further to yield the tensor elements for all the frequencies. The fourth and last module is responsible for calculation of apparent resistivities and phases along with other quantities (to be explained later). The fourth module also creates a plot file that is compatible with the plotting library on MTS called plotlib. The processed results are finally stored in files beginning with names AMAVTLS followed by a site number. Finally the results from the AMAVTLS files are plotted graphically on a Calcomp colour plotter. For several practical reasons, however, all the plots in this compilation are shown in black and white. One such plot is shown on the next five pages for site 163. A typical data processing flow chart is shown in Fig.3.4. Plots for all the other sites are appended to the thesis in Appendix A. All the basic processing is performed using the equations developed in Chapter 2.

The first plot of site 163, numbered as Fig.3.3a, is comprised of graphs of apparent resistivities, phases, coherency, skew and number of estimates, all plotted against frequency. There are two apparent resistivity and phase plots. The first two graphs, titled RHOXY, show the apparent resistivity and phase, ρ_{xy} and ϕ_{xy}, along the north-south direction (in the field, x is normally taken as magnetic north and y as magnetic east) with two values at each frequency. One value corresponds to the so called upward biased estimate of the tensor elements while the other corresponds to the downward biased estimate. Similarly the two graphs under the title RHOYX show the apparent resistivity and phase, ρ_{yx} and ϕ_{yx}, along the east-west direction at each frequency, both with upward and downward biased estimates.

It was stated in section 2.4 that many equations could be set up using different combinations of the components of the time varying electromagnetic field for estimation of a particular tensor element. In fact, it is possible to set up six independent equations for estimation of each one of the four tensor elements. The six equations for one such tensor element Z_{xy} (Sims et al., 1971), are as follows:

$$\overline{Z_{xy}} = \frac{\langle H_x E_x^* \rangle \langle E_x E_y^* \rangle - \langle H_x E_y^* \rangle \langle E_x E_x^* \rangle}{\langle H_x E_x^* \rangle \langle H_y E_y^* \rangle - \langle H_x E_y^* \rangle \langle H_y E_x^* \rangle} \tag{3.1}$$

$$\overline{Z_{xy}} = \frac{\langle H_x E_x^* \rangle \langle E_x H_x^* \rangle - \langle H_x H_x^* \rangle \langle E_x E_x^* \rangle}{\langle H_x E_x^* \rangle \langle H_y H_x^* \rangle - \langle H_x H_x^* \rangle \langle H_y E_x^* \rangle} \tag{3.2}$$

$$\overline{Z_{xy}} = \frac{\langle H_x E_x^* \rangle \langle E_x H_y^* \rangle - \langle H_x H_y^* \rangle \langle E_x E_x^* \rangle}{\langle H_x E_x^* \rangle \langle H_y H_y^* \rangle - \langle H_x H_y^* \rangle \langle H_y E_x^* \rangle} \tag{3.3}$$

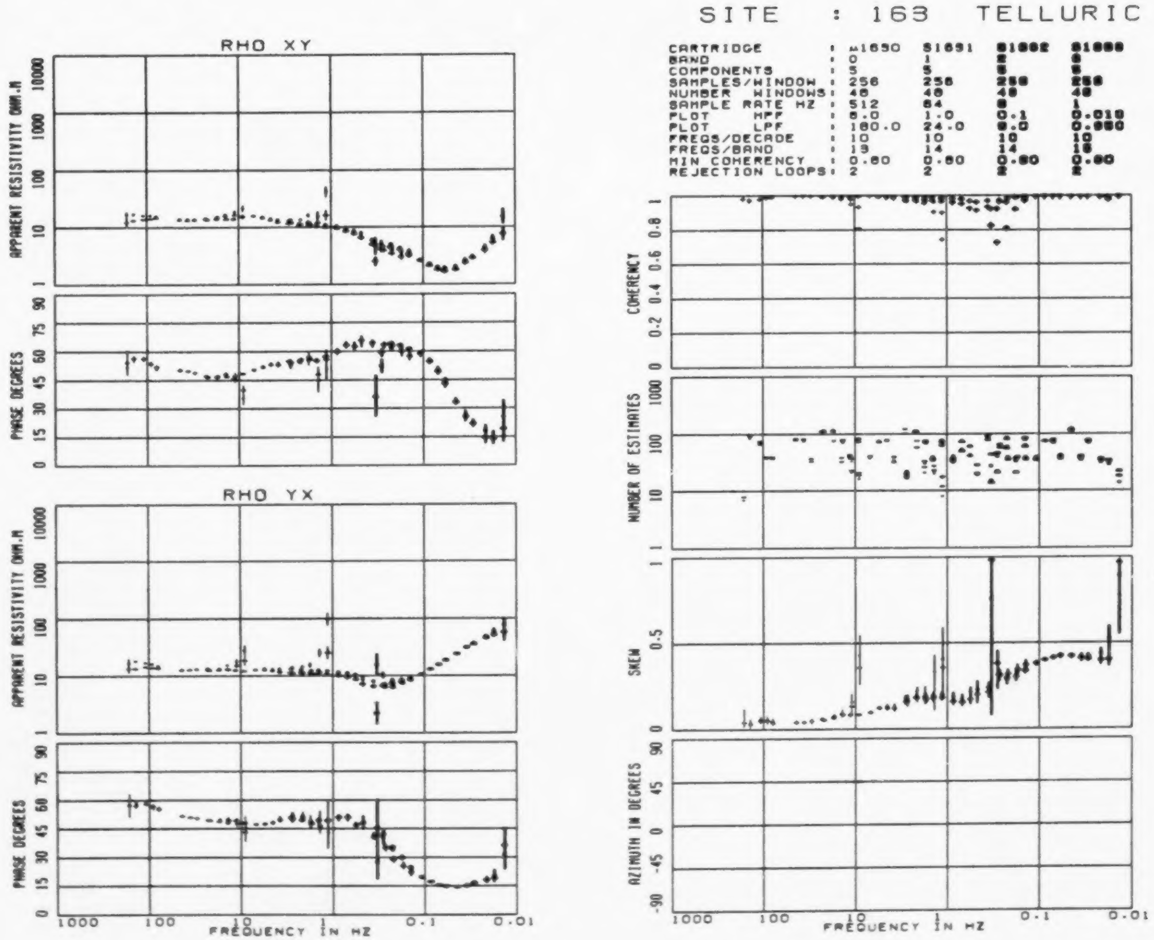

CARTRIDGE	: S1650	S1651	S1002	S1000
BAND	: 0	1	2	3
COMPONENTS	: 5	5	5	5
SAMPLES/WINDOW	: 256	256	256	256
NUMBER WINDOWS	: 48	48	48	48
SAMPLE RATE HZ	: 512	64	8	1
PLOT HPF	: 8.0	1.0	0.1	0.010
PLOT LPF	: 180.0	24.0	[illegible]	[illegible]
FREQS/DECADE	: 10	10	10	10
FREQS/BAND	: 13	14	14	18
MIN COHERENCY	: 0.80	0.80	0.80	0.80
REJECTION LOOPS	: 2	2	2	2

Fig.3.3a: Upward and downward biased RHOXY and RHOYX.

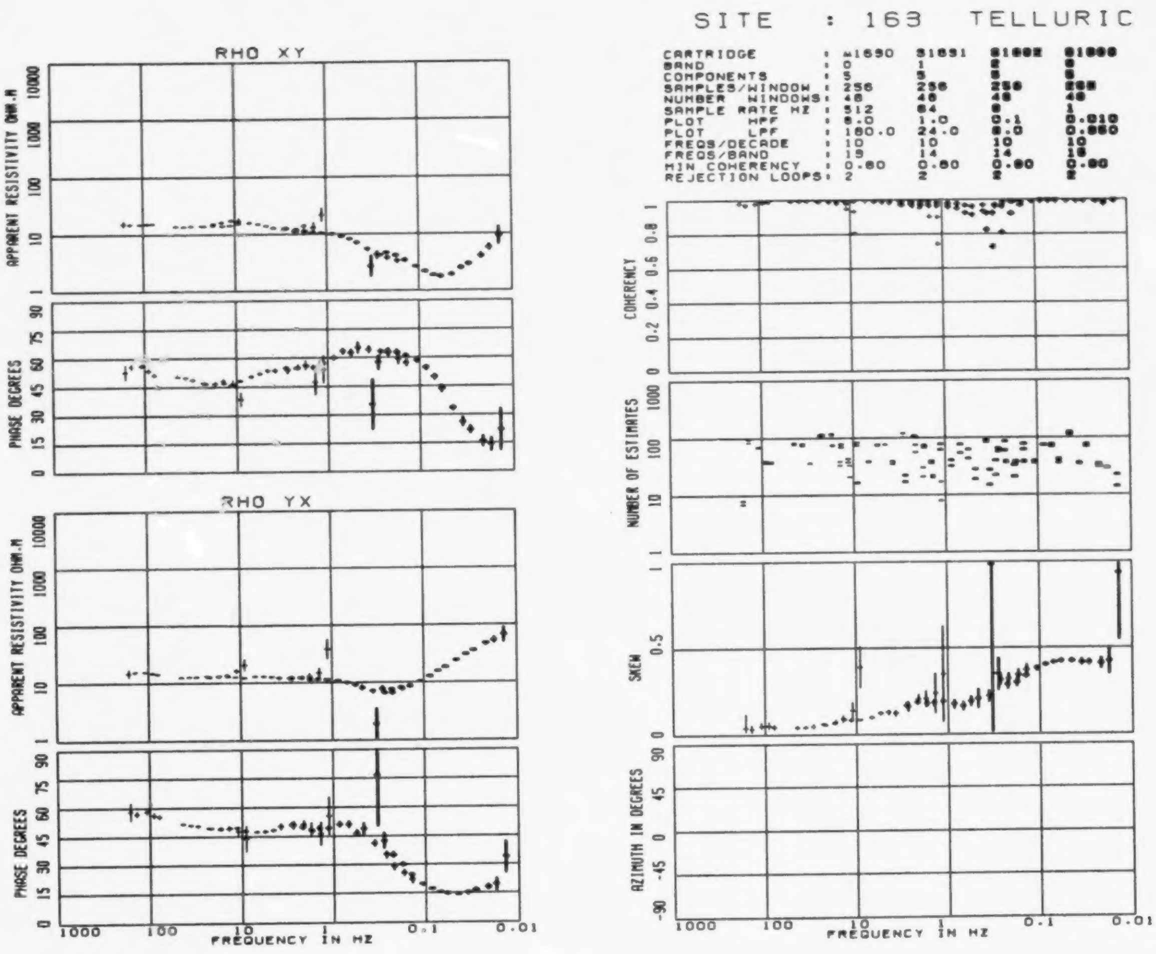

CARTRIDGE	:	M1690	S1691	S1692	S1693
BAND	:	0	1	2	3
COMPONENTS	:	5	5	5	5
SAMPLES/WINDOW	:	256	256	256	256
NUMBER WINDOWS	:	48	48	48	48
SAMPLE RATE HZ	:	512	64	8	1
PLOT HPF	:	8.0	1.0	0.1	0.010
PLOT LPF	:	160.0	24.0	3.0	0.350
FREQS/DECADE	:	10	10	10	10
FREQS/BAND	:	19	14	14	18
MIN COHERENCY	:	0.80	0.80	0.80	0.80
REJECTION LOOPS	:	2	2	2	2

Fig.3.3b: Average RHOXY and RHOYX.

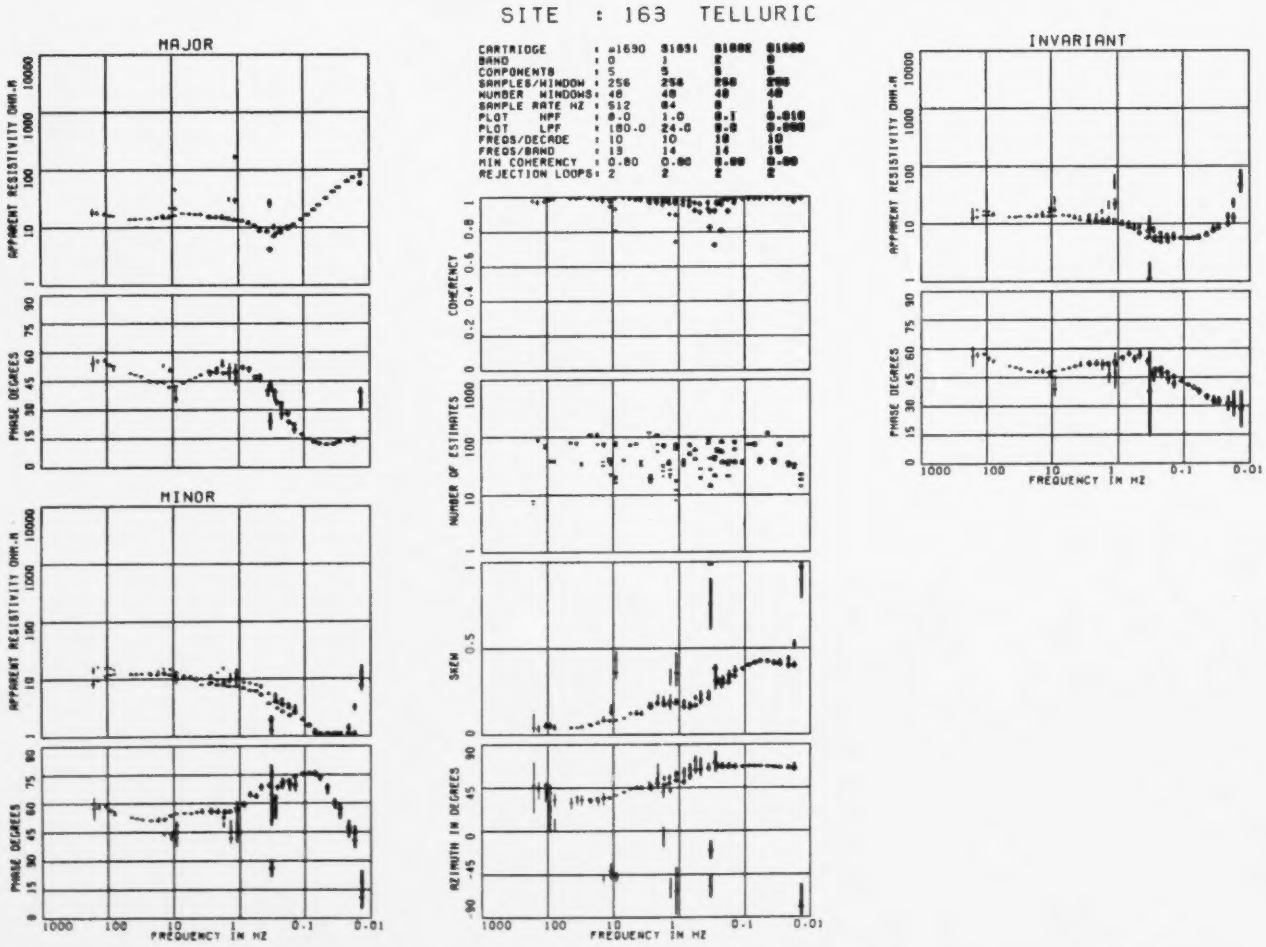

CARTRIDGE	=1630	S1631	[illegible]	[illegible]
BAND	0	1	2	3
COMPONENTS	5	5	5	5
SAMPLES/WINDOW	256	256	[illegible]	[illegible]
NUMBER WINDOWS	48	48	48	48
SAMPLE RATE HZ	512	64	8	1
PLOT HPF	8.0	1.0	0.1	0.010
PLOT LPF	180.0	24.0	[illegible]	[illegible]
FREQS/DECADE	10	10	10	10
FREQS/BAND	13	14	14	15
MIN COHERENCY	0.80	0.80	[illegible]	[illegible]
REJECTION LOOPS	2	2	2	2

Fig.3.3c: Upward and downward biased MAJOR, MINOR and INVARIANT.

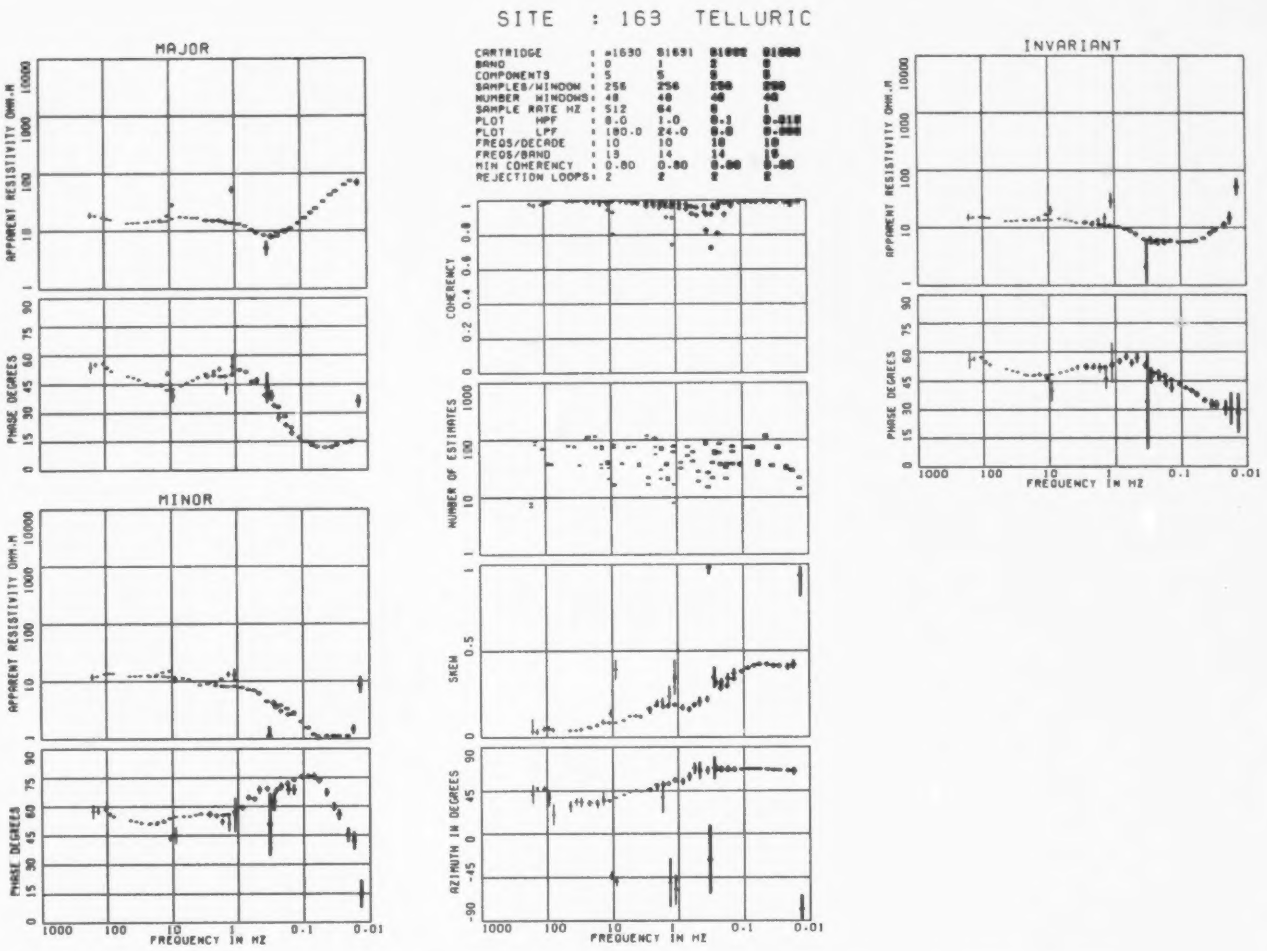

CARTRIDGE	:	81630	81691	[illegible]	[illegible]
BAND	:	0	1	2	3
COMPONENTS	:	5	5	5	5
SAMPLES/WINDOW	:	256	256	256	256
NUMBER WINDOWS	:	48	48	48	48
SAMPLE RATE HZ	:	512	64	8	1
PLOT HPF	:	8.0	1.0	0.1	0.010
PLOT LPF	:	180.0	24.0	8.0	[illegible]
FREQS/DECADE	:	10	10	10	10
FREQS/BAND	:	13	14	14	15
MIN COHERENCY	:	0.80	0.80	0.80	0.80
REJECTION LOOPS	:	2	2	2	2

Fig.3.3d: Average MAJOR, MINOR and INVARIANT.

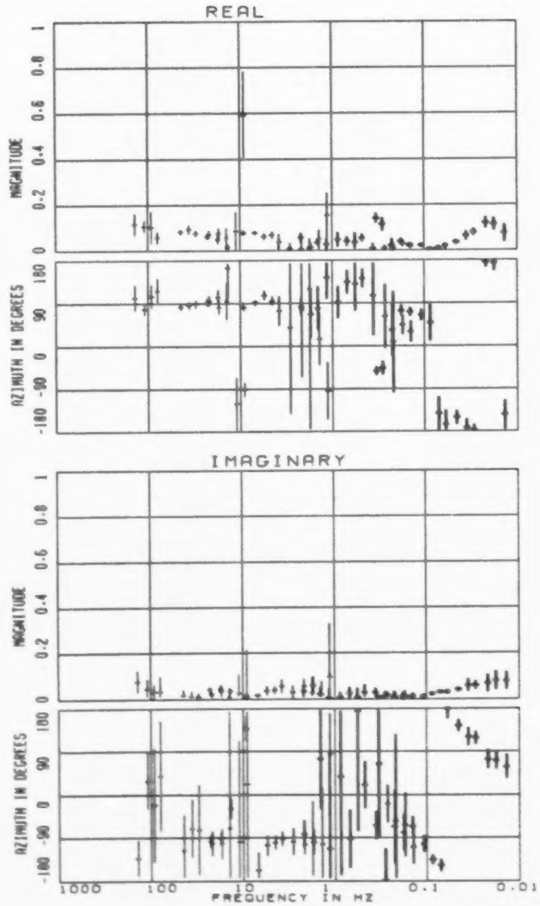

```
SITE   : 163   MAGNETIC

CARTRIDGE       : W1690   S1691   S1692   S1693
BAND            : 0       1       2       3
COMPONENTS      : 5       5       5       5
SAMPLES/WINDOW  : 256     256     256     256
NUMBER  WINDOWS : 48      48      48      48
SAMPLE RATE HZ  : 512     64      8       1
PLOT     HPF    : 8.0     1.0     0.1     0.010
PLOT     LPF    : 180.0   24.0    3.0     0.380
FREQS/DECADE    : 10      10      10      10
FREQS/BAND      : 19      14      14      18
MIN COHERENCY   : 0.70    0.70    0.70    0.70
REJECTION LOOPS : 2       2       2       2
```

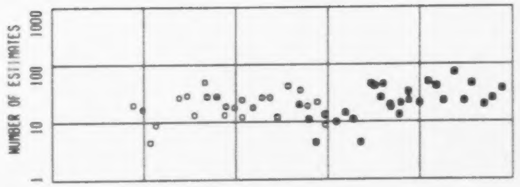

Fig.3.3e: Parameters for Parkinson arrows.

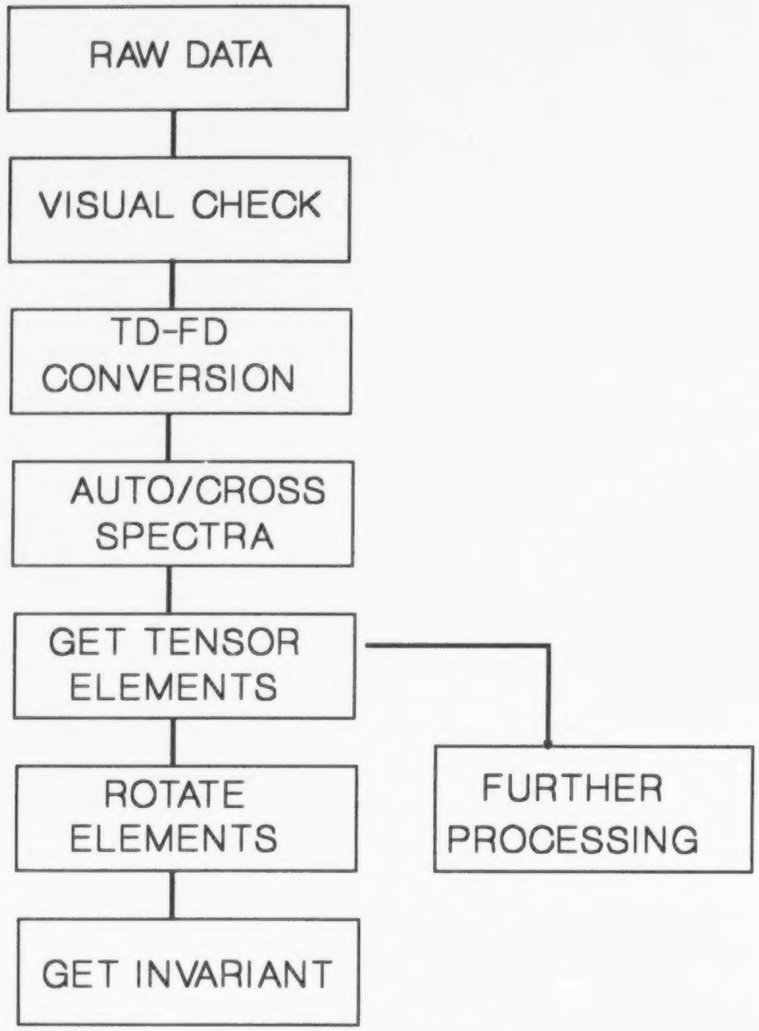

Fig.3.4 : A typical data processing flow chart.

$$\overline{Z_{xy}} = \frac{\langle H_x E_y^* \rangle \langle E_x H_x^* \rangle - \langle H_x H_x^* \rangle \langle E_x E_y^* \rangle}{\langle H_x E_y^* \rangle \langle H_y H_x^* \rangle - \langle H_x H_x^* \rangle \langle H_y E_y^* \rangle} \tag{3.4}$$

$$\overline{Z_{xy}} = \frac{\langle H_x E_y^* \rangle \langle E_x H_y^* \rangle - \langle H_x H_y^* \rangle \langle E_x E_y^* \rangle}{\langle H_x E_y^* \rangle \langle H_y H_y^* \rangle - \langle H_x H_y^* \rangle \langle H_y E_y^* \rangle} \tag{3.5}$$

$$\overline{Z_{xy}} = \frac{\langle H_x H_x^* \rangle \langle E_x H_y^* \rangle - \langle H_x H_y^* \rangle \langle E_x H_x^* \rangle}{\langle H_x H_x^* \rangle \langle H_y H_y^* \rangle - \langle H_x H_y^* \rangle \langle H_y H_x^* \rangle} \tag{3.6}$$

where $\overline{Z_{xy}}$ denotes a measured estimate of Z_{xy} and products of the type $\langle A_i B_j \rangle$ represent auto and cross power spectra. It has been observed that the expressions (3.3) and (3.4) become unstable for one dimensional cases, particularly when the incident fields are unpolarized (Sims et al., 1971). For that case $\langle E_x E_y^* \rangle \langle E_x H_x^* \rangle \langle E_y H_y^* \rangle$ and $\langle H_x H_y^* \rangle$ tend toward zero so that equations (3.3) and (3.4) become indeterminate. The other four equations are stable and correctly predict Z_{xy} provided the incident fields are not highly polarized. The same is true for the other three tensor elements.

Equation (3.6) corresponds to that used for estimation of Z_{xy} by Swift(1967). He showed that the estimates of Z_{ij} were biased down by random noise on the H signal but were not affected by random noise on the E-signal. It was similarly argued that of the other stable estimates, two are biased down by random noise on H and are not biased by random noise on E (e.g. equations (3.5) and (3.6)) while the other two (e.g. (3.1) and (3.2)) are biased up by random noise on E and are not biased by random noise on H. This is what is meant by upward and downward biased estimates.

Coherency in Fig.3.3a is plotted against frequency and, as mentioned earlier, is a measure of the goodness of the estimates. This is plotted for both upward and downward biased estimates. Similarly skew, plotted against frequency, is calculated using the expression (2.47) for upward and downward biased estimates. Skew, as explained in Chapter 2, is a dimensionality parameter.

The number of estimates is the maximum number of windows that were used at a particular frequency for which the power and coherency criteria were satisfied. The greater the number of estimates, the better the results.

The second plot of site 163 is named as Fig.3.3b and is an average of upward and downward estimates of Fig.3.3a. Such average estimates are of immense importance in cases where it is not possible to use each of the individual biased estimates for further analyses and interpretation.

Fig.3.3c shows the third part of the plot for site 163. The figure contains graphs of major and minor apparent resistivities and phases, coherency, number of estimates, skew, azimuth and invariant apparent resistivity and phase, all plotted against frequency for both upward and downward biased estimates. The plots of apparent resistivity and phase against frequency, headlined as MAJOR corresponds to E-polarization while the plot headlined as MINOR corresponds to H-polarization. These plots are obtained after rotation of tensor elements in such a way that the off diagonal elements are minimized. The angle through which the tensor elements are rotated to obtain minimum off diagonal elements is called the azimuth and defines the strike direction at a particular frequency.

Ideally the off diagonal elements should be zero along the strike direction. This, however, is not true in real earth situations because the data are always contaminated with noise. To understand the procedure of rotation, consider the field measurement co-ordinate system defined by the right hand Cartesian co-ordinate system X, Y and Z. Let the geological strike direction be defined by the co-ordinate system X', Y' and Z'. If the angle, θ, between the X direction and strike direction is known then the rotated tensor elements are given by the relation (Swift, 1967):

$$\begin{bmatrix} Z'_{xx} \\ Z'_{xy} \\ Z'_{yx} \\ Z'_{yy} \end{bmatrix} = \begin{bmatrix} C^2 & CS & CS & S^2 \\ -CS & C^2 & -S^2 & CS \\ -CS & -S^2 & C^2 & CS \\ S^2 & -CS & -CS & C^2 \end{bmatrix} \begin{bmatrix} Z_{xx} \\ Z_{xy} \\ Z_{yx} \\ Z_{yy} \end{bmatrix} \tag{3.7}$$

where C=cos θ and S=sin θ.

In almost all practical situations, angle θ is not known at the beginning. Therefore, it is necessary to determine a criterion to rotate the impedance tensor through an angle θ_0 that will make Z'_{xx} and Z'_{yy} minima. This was suggested by Swift(1967) and later described by Vozoff(1972). The aim is to maximize the value of $|Z'_{xy}(\theta)|^2 + |Z'_{yx}(\theta)|^2$ for a particular angle θ_0. This can be achieved by differentiating $Z'_{xy}(\theta)$ and $Z'_{yx}(\theta)$ given by equation (3.7) and finding the value of θ_0, measured in clockwise direction. The angle θ_0 is given by:

$$\theta_0 = \frac{1}{4}\tan^{-1}\frac{(Z_{xx} - Z_{yy})(Z_{xy} + Z_{yx})^* + (Z_{xx} - Z_{yy})^*(Z_{xy} + Z_{yx})}{|Z_{xx} - Z_{yy}|^2 - |Z_{xy} + Z_{yx}|^2} \tag{3.8}$$

where * indicates complex conjugate. Equation (3.8) has four solutions at 90^0 intervals implying two mutually perpendicular strike directions. To choose between them, it is necessary to have some other independent information such as the relationship between the magnitudes of measured vertical and horizontal components of the magnetic field or some kind of geological information.

Fig. 3.3c also shows the plot of azimuth against frequency for upward and downward biased estimates. This plot gives an idea of the strike direction. It is interesting to note the variation of strike with frequency.

The plot of apparent resistivity and phase against frequency, titled INVARIANT, for upward and downward biased estimates is also shown in Fig.3.3c. The determinant invariant resistivity (ρ_{inv}) and phase (ϕ_{inv}) are given by:

$$\rho_{inv} = \frac{1}{\omega\mu}\left|Z_{det}\right|^2 \tag{3.9a}$$

and

$$\phi_{inv} = \tan^{-1}\frac{\mathrm{Im}[Z_{det}]}{\mathrm{Re}[Z_{det}]} \tag{3.9b}$$

where Z_{det} is given by the following (Berdichevsky and Dimitriev, 1976):

$$Z_{det} = \sqrt{(Z_{xx}Z_{yy} - Z_{xy}Z_{yx})} \tag{3.10}$$

The fourth plot of site 163, named Fig.3.3d shows the average of upward and downward biased estimates of all the quantities displayed in Fig.3.3c. The quantities in Fig.3.3d are used for further analyses and interpretation.

The fifth plot of site 163, Fig.3.3e, gives the parameters to plot Parkinson induction arrows(Parkinson, 1962, 1983). The figure shows the magnitudes and azimuths of REAL and IMAGINARY parts of the induction arrows along with the number of estimates.

CHAPTER 4

ANALYSIS OF THE RESULTS

4.1 ANALYSIS OF PROCESSED DATA

The process of interpretation of magnetotelluric data can be divided into two types - semi-quantitative and quantitative. The semi-quantitative interpretation is done using a set of plots called pseudosections while quantitative interpretation is done by inversion of the data and production of depth sections.

It is customary in magnetotellurics to construct pseudosections. These plots give the distributions of apparent resistivities and phases against frequency along a profile. The plotted phase is the difference in phase between the mutually perpendicular electric and magnetic field components. Typical pseudosections are shown in Figs.4.1a and b. These are the apparent resistivity and phase pseudosections for profile number 1 of Fig.1.1. Fig. 4.1a gives the apparent resistivity against frequency, with frequency decreasing downwards (indicating an increase in depth due to the skin depth effect). The site numbers and distances are marked along the horizontal direction. The plotted contours and their values are logarithms to the base 10 of the apparent resistivities. The plot shows a general increase in resistivity with decreasing frequency except beneath sites 208, 163 and 203 where the apparent resistivities

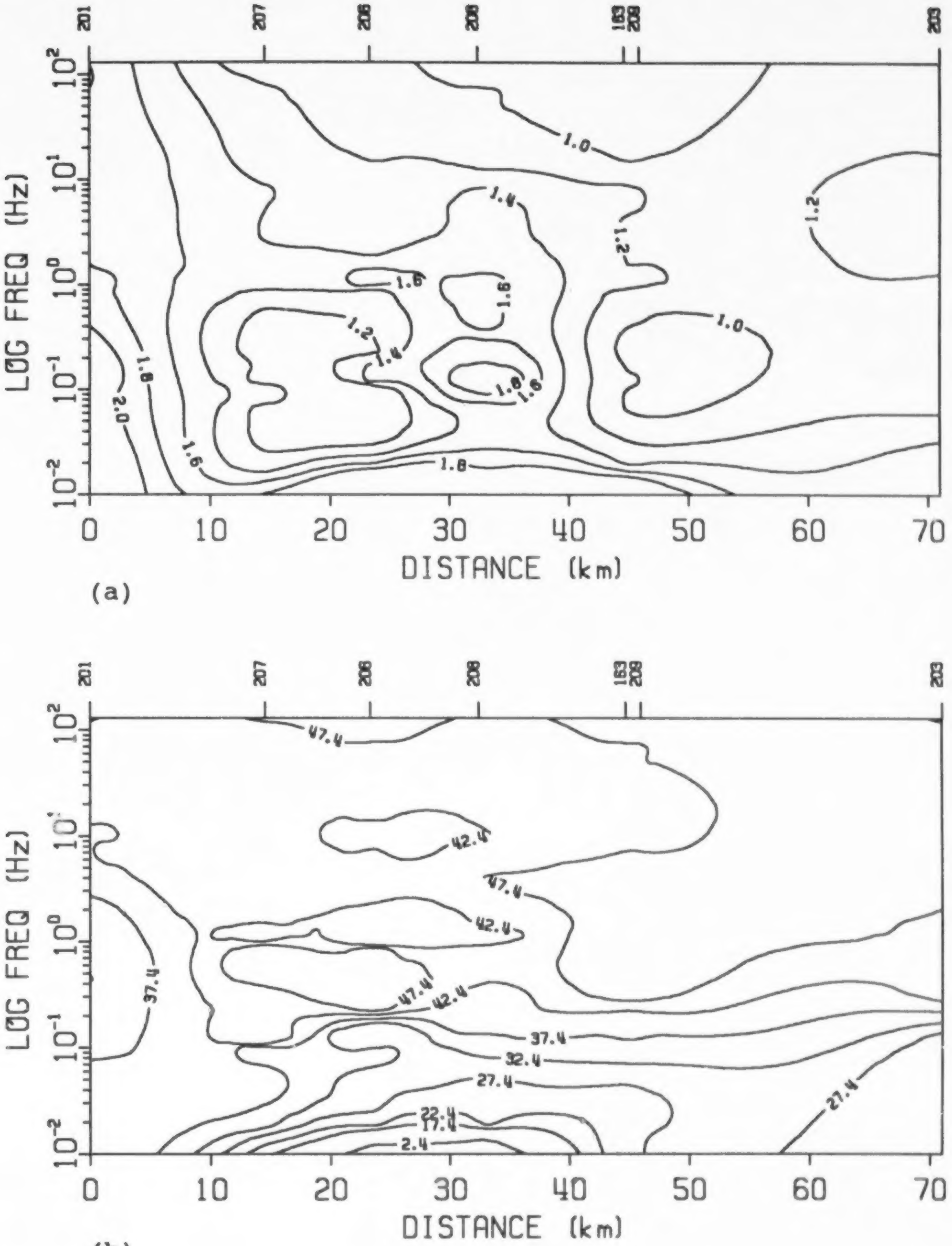

(a)

(b)

Fig.4.1: Pseudosections for profile 1. (a) Apparent resistivity (contour values in Ω.m on log scale); (b) Phase (contour values in degrees).

are lower as compared to the surroundings. Moreover, the nature of the contour lines at low frequencies suggests horizontal layering at depth except toward the left boundary where the contour lines tend toward the vertical.

The pseudosection for phase, shown in Fig.4.1b is similar in nature but different quantitatively. It is evident that the phase decreases with decrease in frequency. The nature of the phase contours at low frequencies again suggests layering, particularly beneath sites 207, 206, 208, 163 and 209. In general, low phase values correspond to high resistivity.

The pseudosections for profile 2 (see Fig.1.1) in Fig.4.2a and b show fairly low apparent resistivity (hence high conductivity) of 6.3 Ωm in the frequency range of 100 to 10Hz. The apparent resistivity increases with decreasing frequency. The nature of the contour lines at low frequencies indicates layering.

Profile 3 is approximately perpendicular to profile 1 (see Fig.1.1). The pseudosections of this profile shown in Figs. 4.3a and b reflect this by the nature of the almost vertical contour lines beneath sites 163 and 209. A region of low resistivity (2.51 Ωm) in the frequency

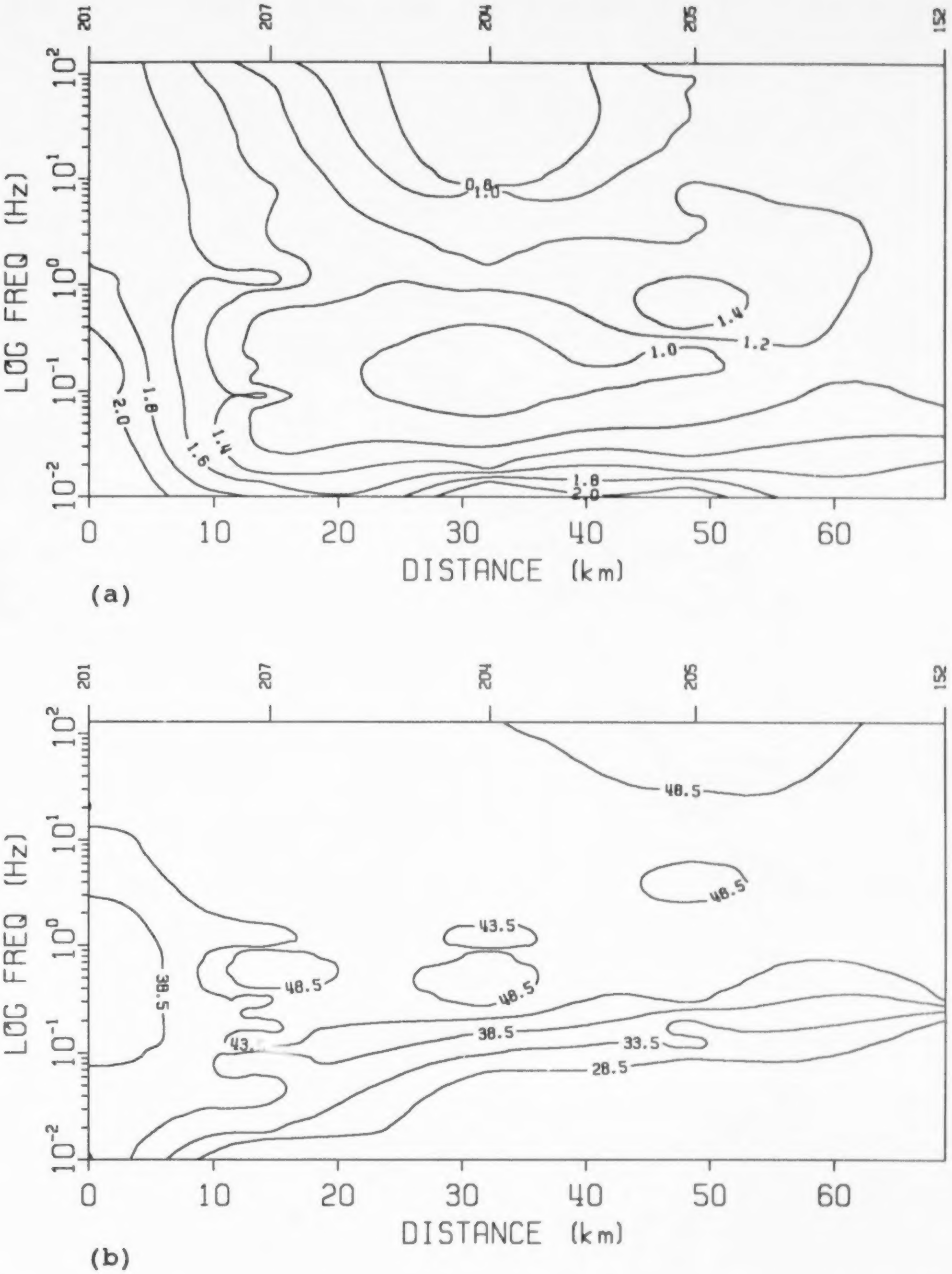

Fig.4.2: Pseudosections for profile 2. (a) Apparent resistivity (contour values in Ω.m on log scale); (b) Phase (contour values in degrees).

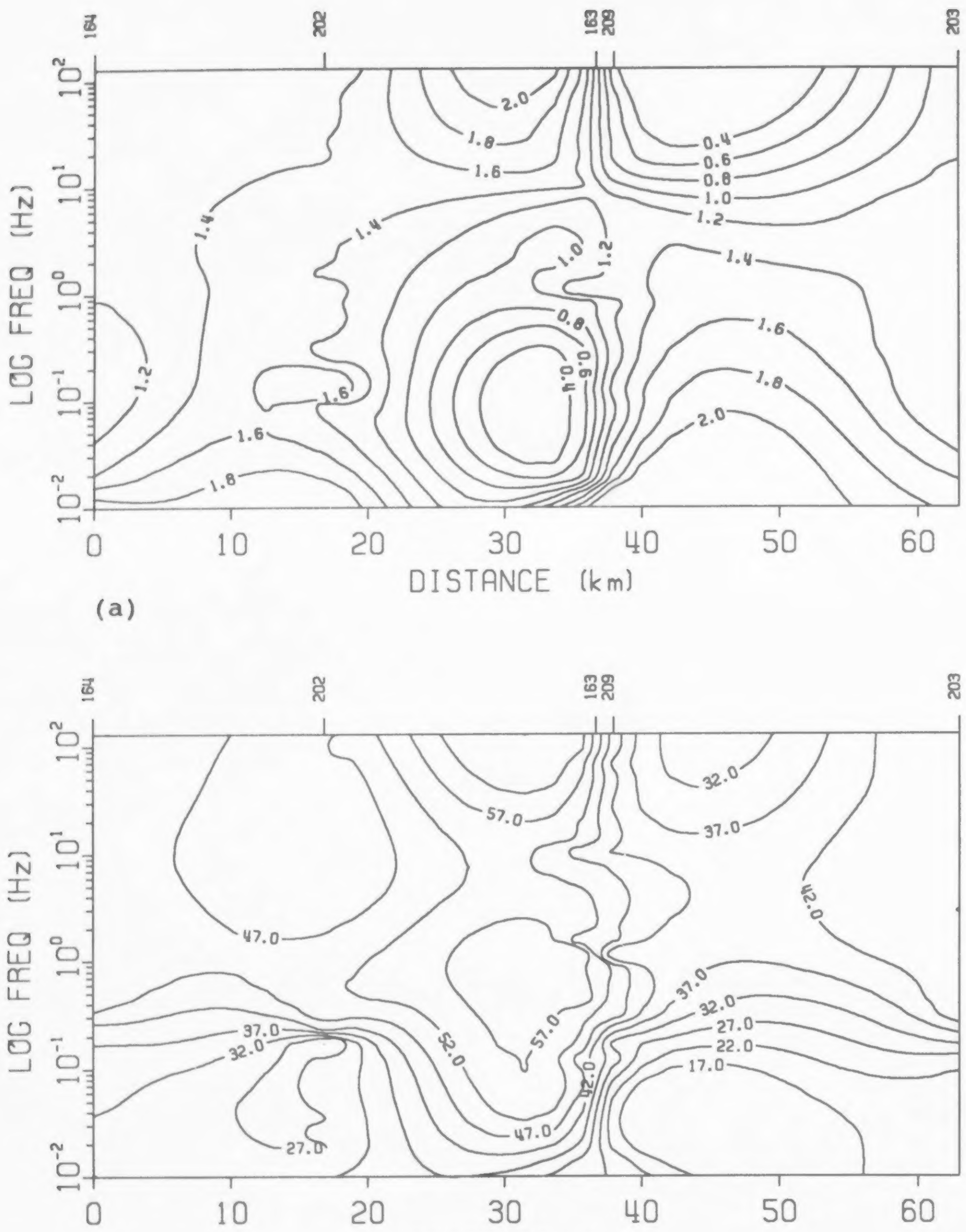

(a)

(b)

Fig.4.3: Pseudosections for profile 3. (a) Apparent resistivity (contour values in Ω.m on log scale); (b) Phase (contour values in degrees).

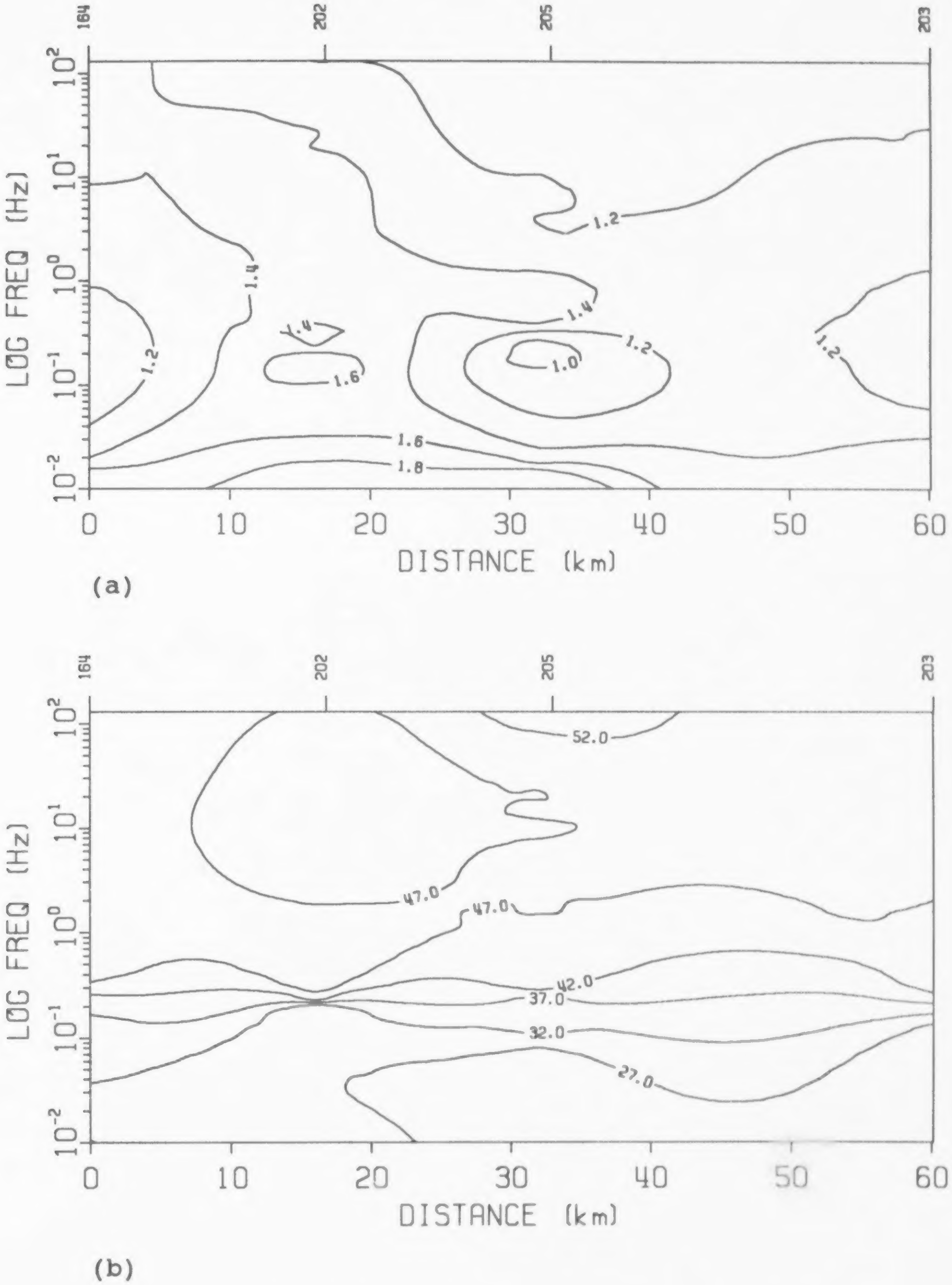

Fig.4.4: Pseudosections for profile 4. (a) Apparent resistivity (contour values in Ω.m on log scale); (b) Phase (contour values in degrees).

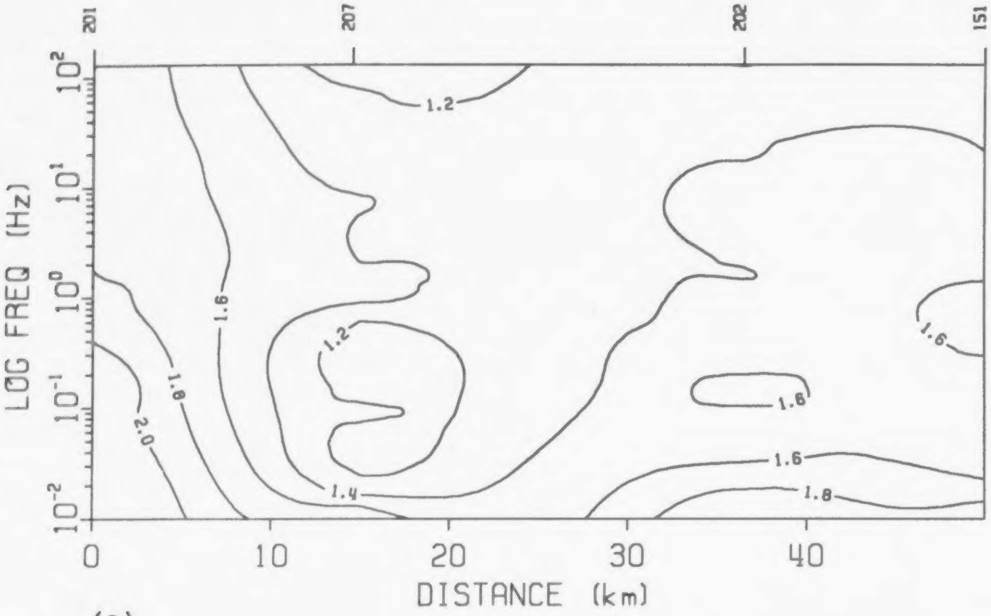

(a)

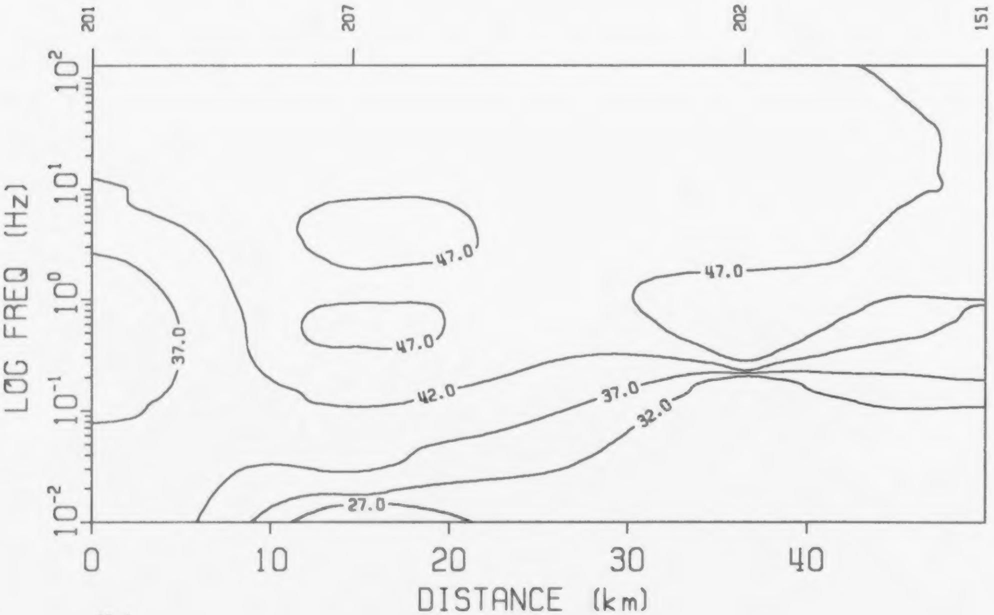

(b)

Fig.4.5: Pseudosections for profile 5. (a) Apparent resistivity (contour values in Ω.m on log scale); (b) Phase (contour values in degrees).

range 0.01-1Hz is indicated between sites 209 and 202 and a further low resistivity zone in the range 10-100Hz between sites 209 and 203.

Profiles 4 and 5 in Figs. 4.4a, b and 4.5a, b again indicate layering at depth with a general increase in apparent resistivity with decreasing frequency, as well as some smaller features.

One of the most important steps in interpretation of magnetotelluric data is to convert the distribution of apparent resistivity against frequency into a distribution of true resistivity against depth. Such a transformation yields the layer parameters (layer resistivities and thicknesses) and can be performed by the process of inversion. In this work, the invariants from the processed data from each of the thirteen sites were inverted using the Fischer (Fischer and Le Quang, 1982; Weaver and Fischer, 1990) inversion technique to obtain the layer parameters.

An output from a one dimensional Fischer inversion, for site 163, is shown in Figs. 4.6a and b. Inputs to the inversion program are the apparent resistivities, phases, frequencies and errors in apparent resistivities and phases at each frequency. Data with large errors were not

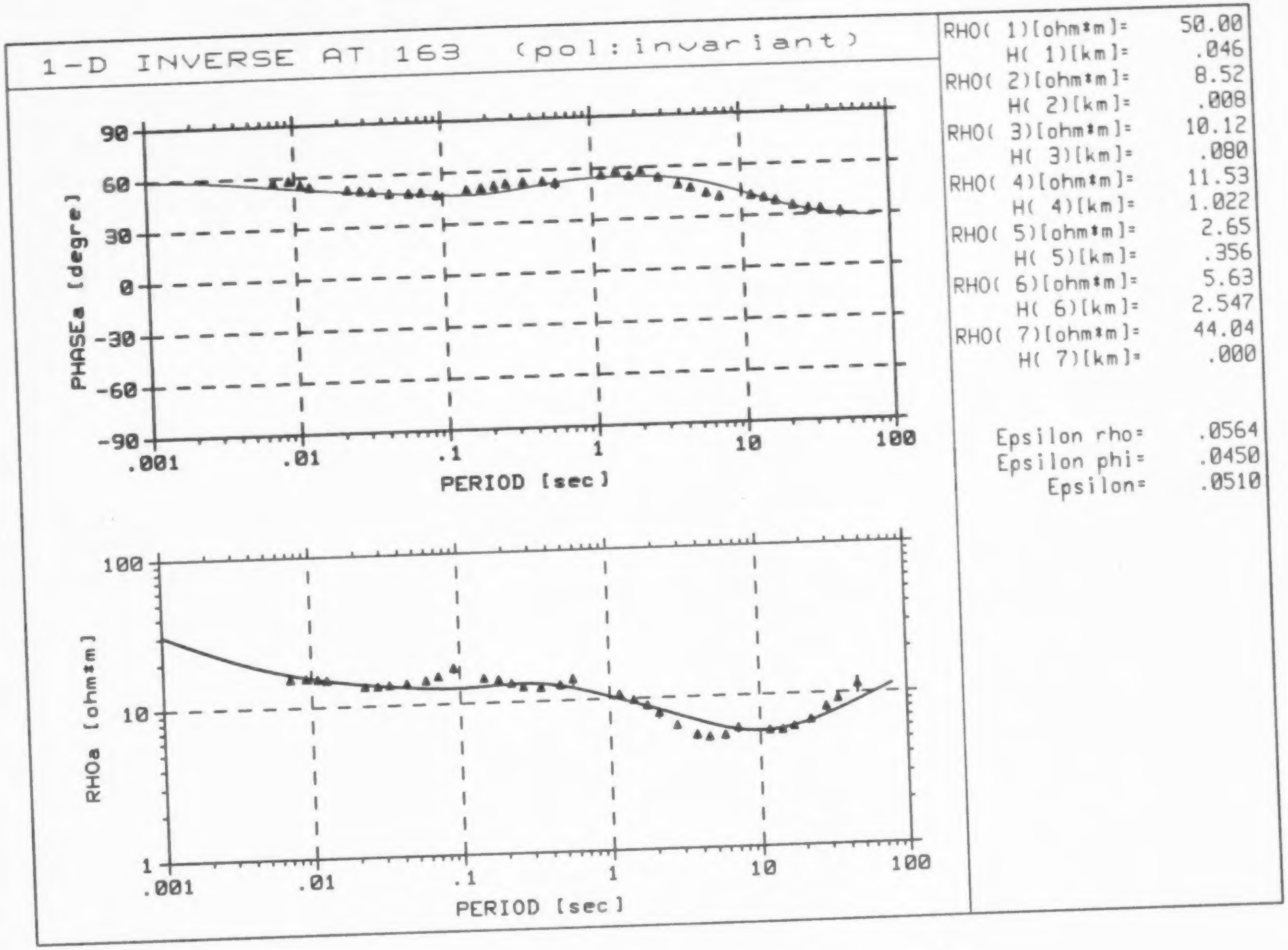

```
RHO( 1)[ohm*m]=     50.00
    H( 1)[km]=       .046
RHO( 2)[ohm*m]=      8.52
    H( 2)[km]=       .008
RHO( 3)[ohm*m]=     10.12
    H( 3)[km]=       .080
RHO( 4)[ohm*m]=     11.53
    H( 4)[km]=      1.022
RHO( 5)[ohm*m]=      2.65
    H( 5)[km]=       .356
RHO( 6)[ohm*m]=      5.63
    H( 6)[km]=      2.547
RHO( 7)[ohm*m]=     44.04
    H( 7)[km]=       .000


  Epsilon rho=      .0564
  Epsilon phi=      .0450
     Epsilon=       .0510
```

Fig.4.6a: Output from one dimensional Fischer inversion.

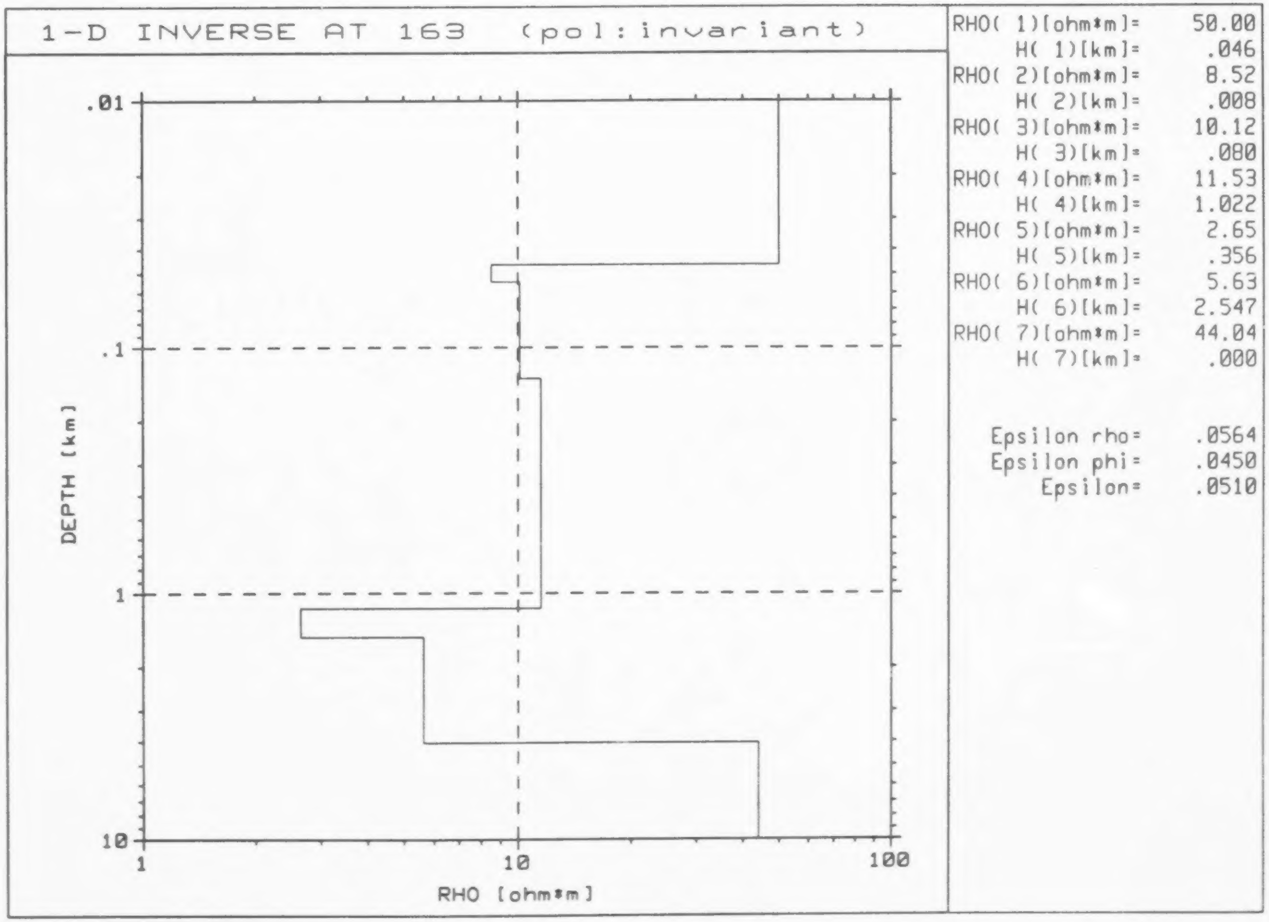

```
RHO( 1)[ohm*m]=    50.00
    H( 1)[km]=      .046
RHO( 2)[ohm*m]=     8.52
    H( 2)[km]=      .008
RHO( 3)[ohm*m]=    10.12
    H( 3)[km]=      .080
RHO( 4)[ohm*m]=    11.53
    H( 4)[km]=     1.022
RHO( 5)[ohm*m]=     2.65
    H( 5)[km]=      .356
RHO( 6)[ohm*m]=     5.63
    H( 6)[km]=     2.547
RHO( 7)[ohm*m]=    44.04
    H( 7)[km]=      .000


  Epsilon rho=     .0564
  Epsilon phi=     .0450
      Epsilon=     .0510
```

Fig.4.6b: Resistivity against depth plot from 1-D Fischer inversion.

included. In Fig.4.6a, the uninverted data are represented by triangles. The solid curves are the responses calculated from the layer parameters obtained through inversion. Fig.4.6b shows the distribution of resistivity with depth. The layer parameters are listed on the right hand sides of the plots. The outputs from Fischer inversions for the 12 other sites are attached in Appendix B. A careful look at all the plots shows a fairly good degree of match between the field curves and the curves obtained through inversion.

The Fischer inversion program used in this work is a combination of techniques developed by Bostick(1977), Fischer and LeQuang(1982) and Weaver and Fischer(1990). The inversion procedure developed by Bostick directly provides the layer parameters (resistivities and depths) from which an appropriate and smooth resistivity curve can be drawn. The Fischer-LeQuang procedure, on the other hand, calculates a best fitting forward model under certain physical constraints. The program used in this work combines the Bostick inversion procedure with the Fischer-LeQuang forward modelling technique, so that a best fitting model with appropriate number of layers is found automatically. The technique, though computationally intensive, yields good results. The detailed algorithm can be found in Weaver and Fischer(1990).

In the processing and interpretation of magnetotelluric data, it is essential to obtain a distribution of layer resistivities with depths along profiles - thus describing the subsurface resistivity distribution in a vertical plane. A plot showing such a distribution is called a depth section. In this work, depth sections were constructed along the five profiles (Fig.1.1). These depth sections are shown in Figs. 4.7 through 4.11. Depth (vertical), increasing downwards, and distance (horizontal), increasing to the right, are shown on a linear scale. The values on the contour lines are logarithms (base 10) of the resistivities.

The depth section for profile 1, Fig.4.7, shows a general increase in resistivity with increasing depth along the entire profile. The layers tend to be relatively horizontal at shallow depths but inclined in deeper regions. The lowest resistivity on the section is between the sites 209 and 203 at a depth of 1km and has a value of 7.9Ωm. There is also a low of 20Ωm under site 206 at a depth of approximately 4km and a relatively high resistivity zone at 8km depth beneath site 208 compared with the rest of the section at that depth.

Sections in Figs.4.8 and 4.9 for profiles 2 and 3 respectively show a general increase in resistivity with increasing depth. There do not appear to be any localized regions of high or low resistivity in these sections. The contour lines in the two figures indicate the presence of layering. Two interesting structures are evident under site 205 (Fig.4.8) corresponding to resistivity contours of 15.8Ωm and 251.2Ωm (contour values 1.2 and 2.4). The first structure is approximately at a depth of 4km while the second is at 7-8km and below. The nature of the two contour lines suggests faulting. The deeper regions of profile 3 (Fig.4.9) show vertical layering with high resistivity in the left half (i.e to the south). The right half (sites 163,209 and 203) appears to be of higher conductivity and may reflect the deep conductive structure found by Ingham et al(1983) which they suggested has its top at approximately 5-10km and extends to great depth.

The depth section for profile 4 (Fig.4.10) is of particular interest. It shows the general trend of increasing resistivity with increasing depth. The variation in slopes of contour lines is gentle at shallow depths. Once again the nature of the contour lines suggests layering. The most interesting feature in this depth section is the presence of a high resistivity

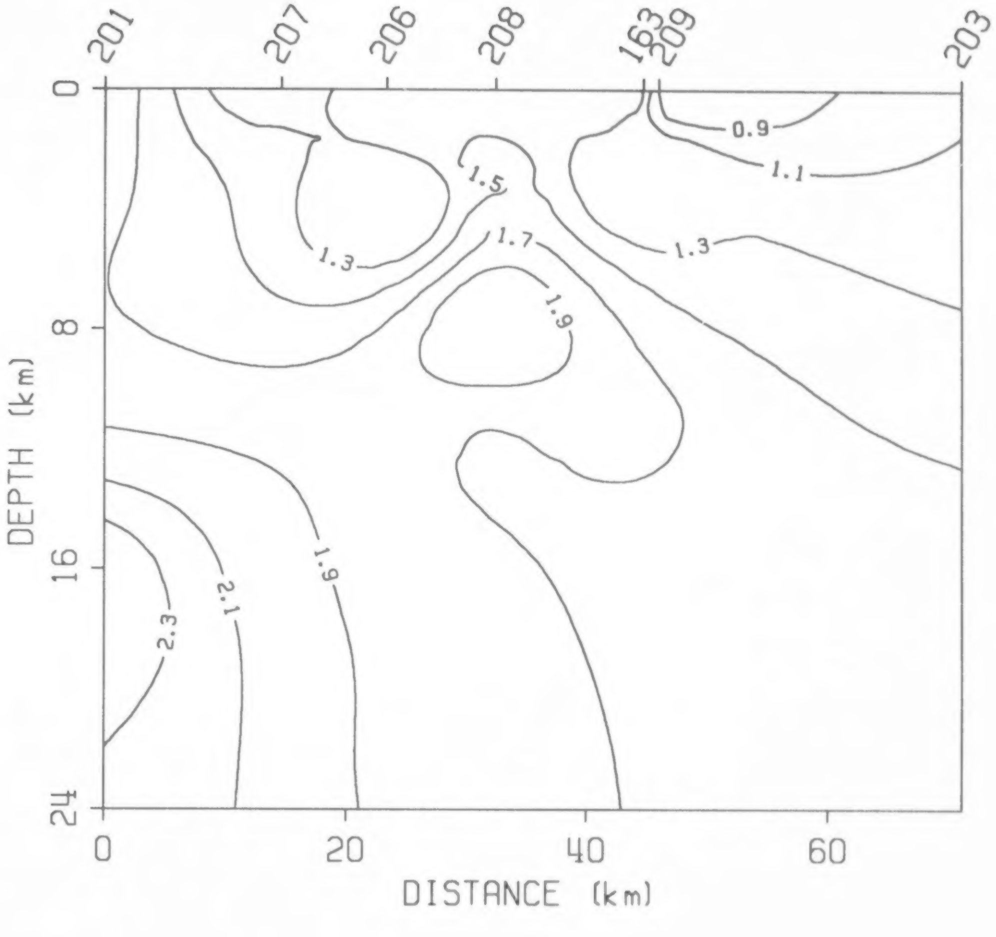

Fig.4.7: Depth section for profile 1 (contour values in Ω.m on log scale).

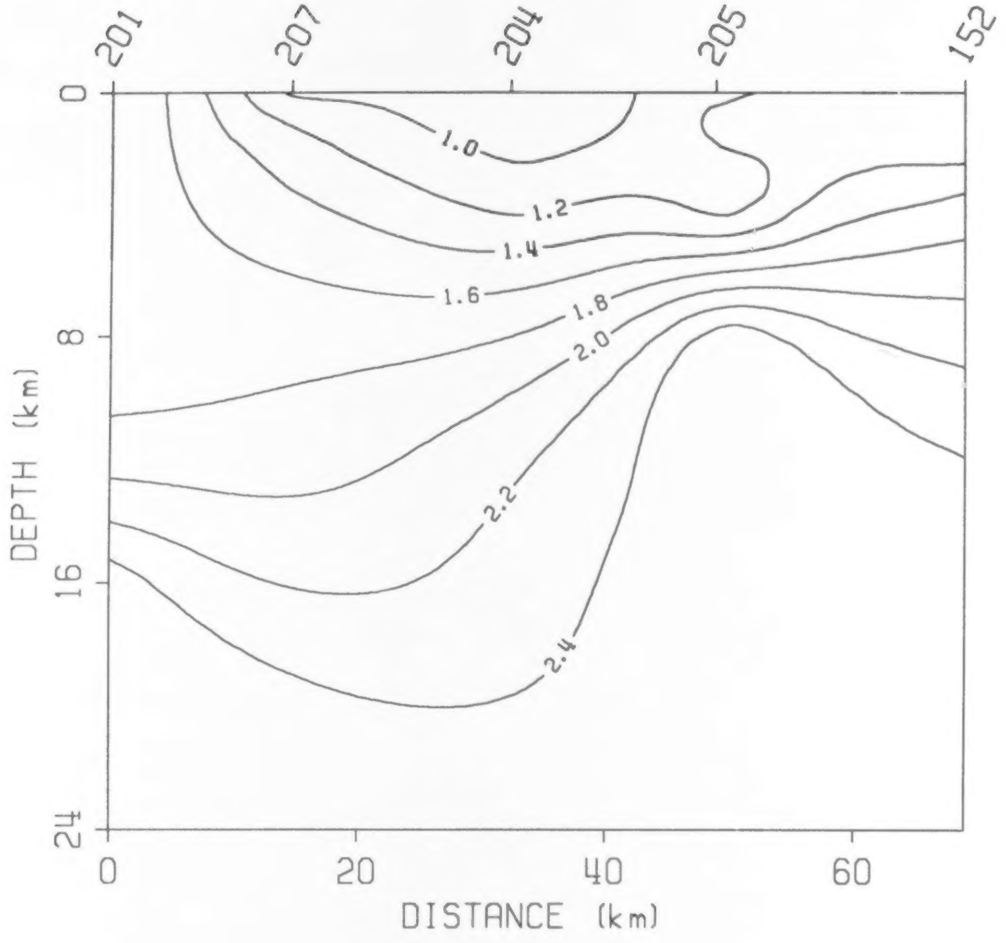

Fig.4.8: Depth section for profile 2 (contour values in Ω.m on log scale).

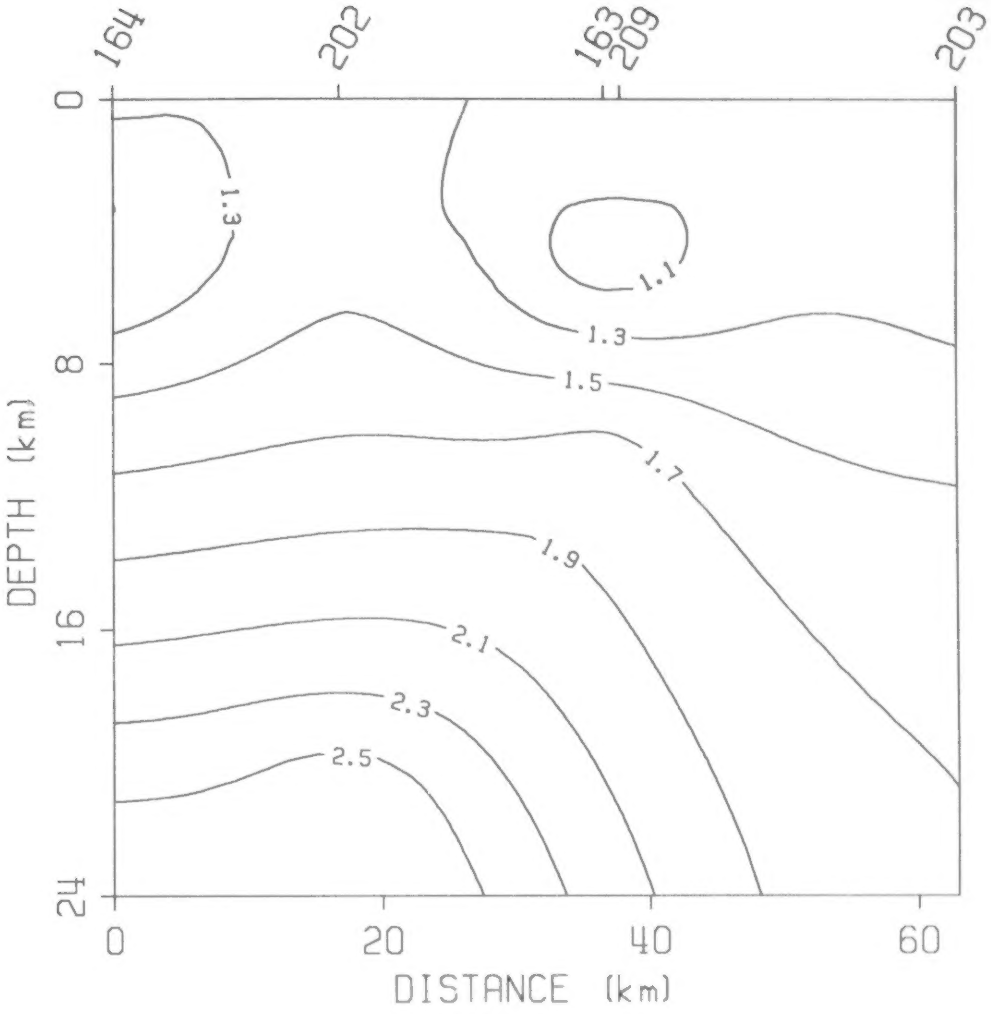

Fig.4.9: Depth section for profile 3 (contour values in Ω.m on log scale).

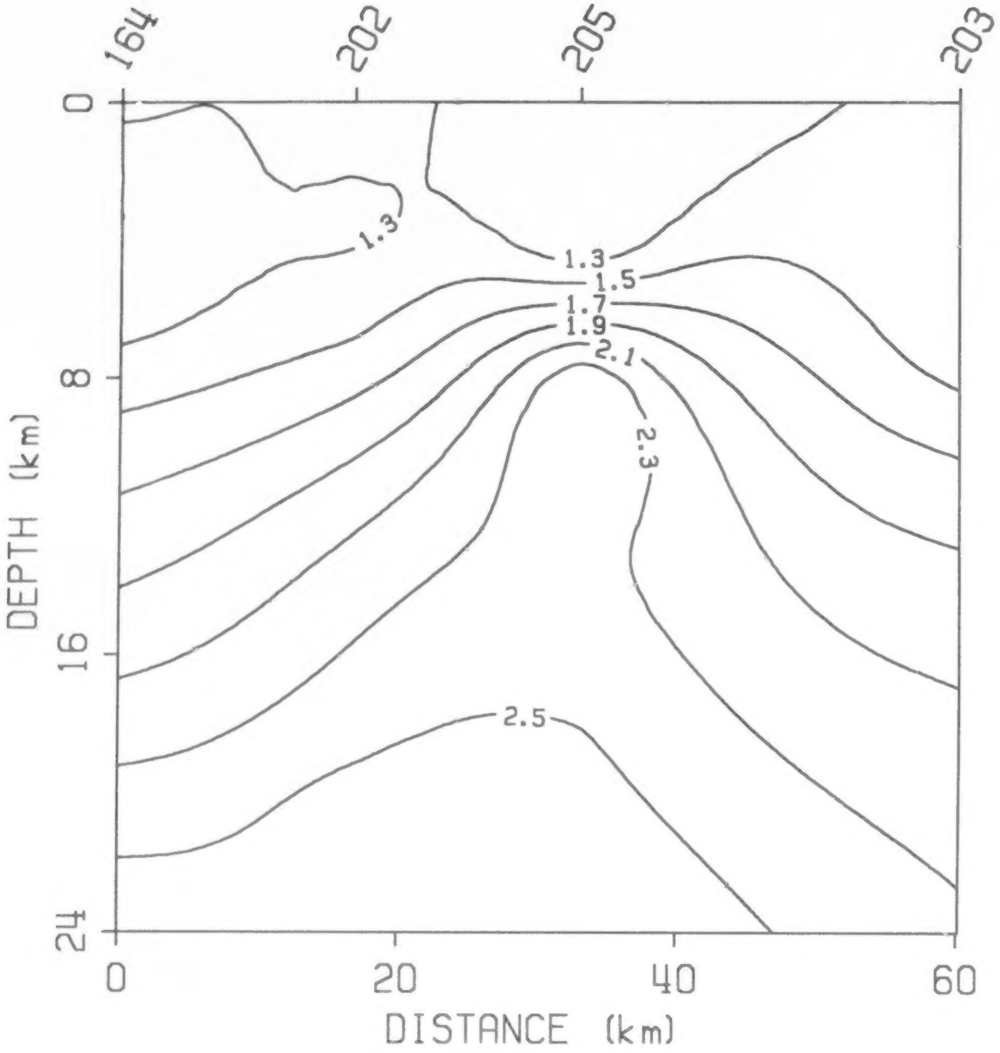

Fig.4.10: Depth section for profile 4 (contour values in Ω.m on log scale).

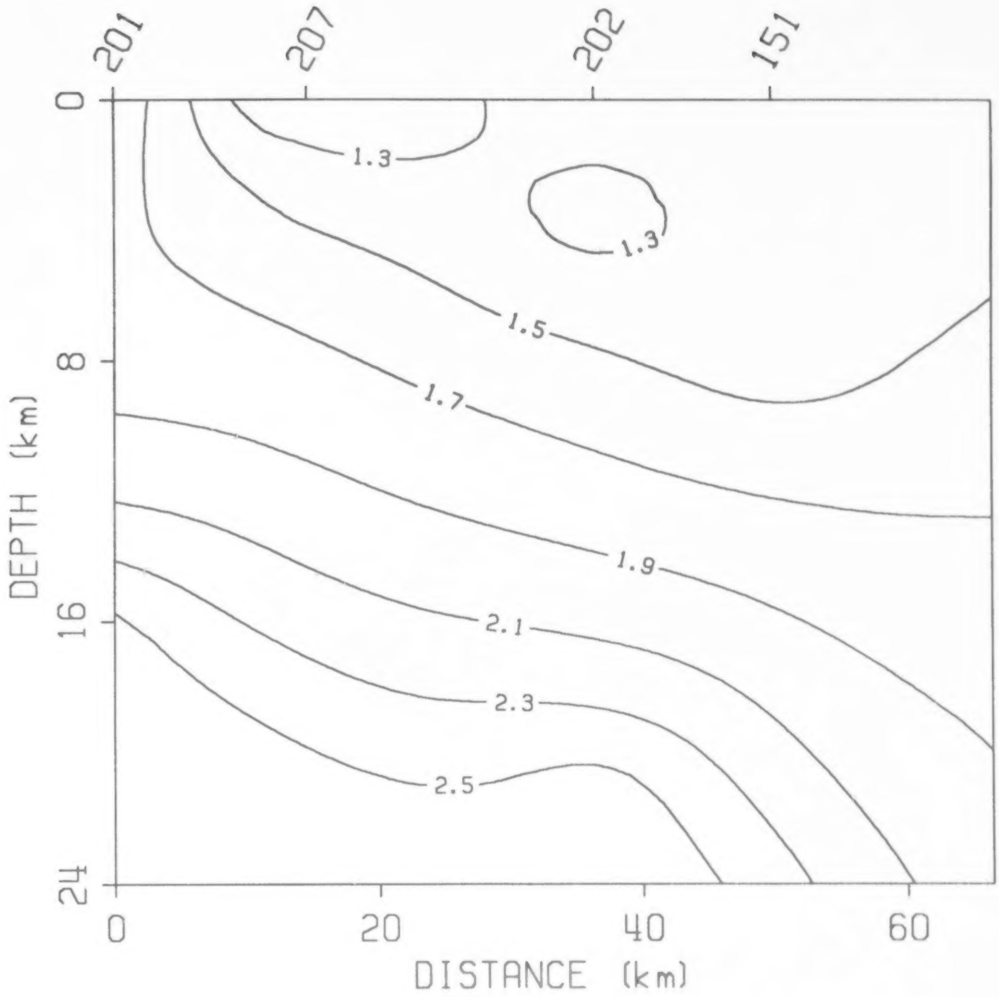

Fig.4.11: Depth section for profile 5 (contour values in Ω.m on log scale).

structure under site 205 - the same one that appears in profile 2 (Fig.4.8).

The fifth depth section, Fig.4.11, is similar to the others in most ways. There is a general increase in resistivity with increasing depth. There are no isolated zones of high or low resistivities. The general trend of contour lines indicates stratification. As in the case of profile 3, the right half (in this case the eastern part) is of higher conductivity than the left (to the west).

Another way to show the resistivity distribution in an area is to construct plan maps of the distributions for different depths. Since the planer coordinates (latitude and longitude) of all the sites are known, contour maps of resistivities at different depths (from the Fischer inversions) can be prepared for the entire area. One such plan view is shown in Fig.4.12 for a depth of 1km. The vertical scale represents the latitude while the horizontal scale represents the longitude. The contour values are the logarithms(base 10) of the true resistivities. Asterisks mark the site locations. Similar maps of the resistivity distributions for 7 additional depths between 2 and 18km are given in Figs. 4.13-4.19.

The plan maps (Figs.4.12 through 4.19) show that there is a general increase in resistivity with depth.

However, zones of lower resistivities occur at all depths. One such interesting zone lies in the region approximately 53.25-53.4°N and 117.4-117.5°W. This zone appears prominently at 2km and is present to a depth of 5km with resistivity values over that depth interval ranging from about 9Ωm to about 25Ωm. Below 5km, the resistivity increases over part of this area (to 250Ωm at 6km), though the low resistivity zone persists to great depths in the southwest of the zone (near 53.27°N and 117.53°W at 9km on Fig.4.18).

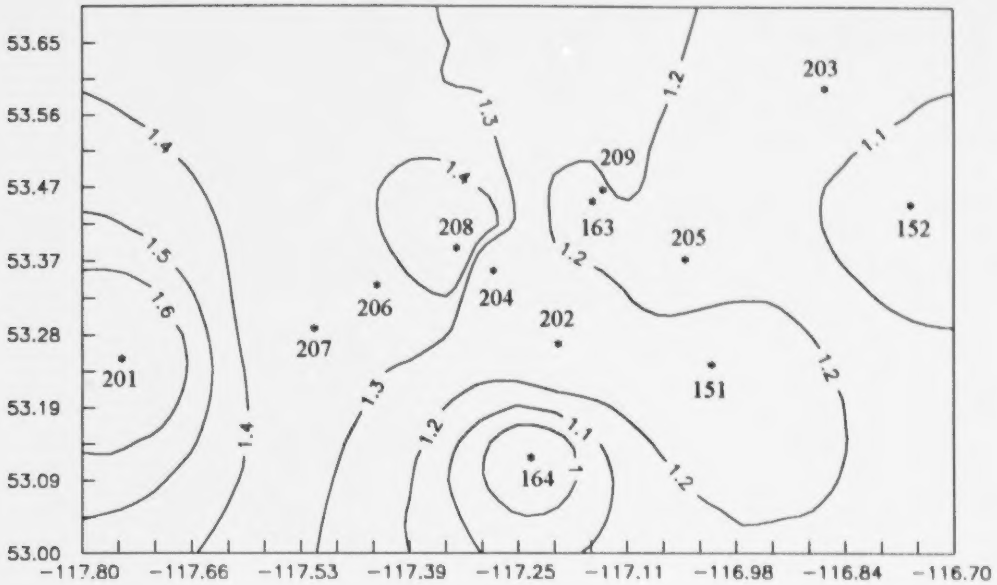

Fig.4.12: Plan view at 1km(contours in Ω.m on log scale).

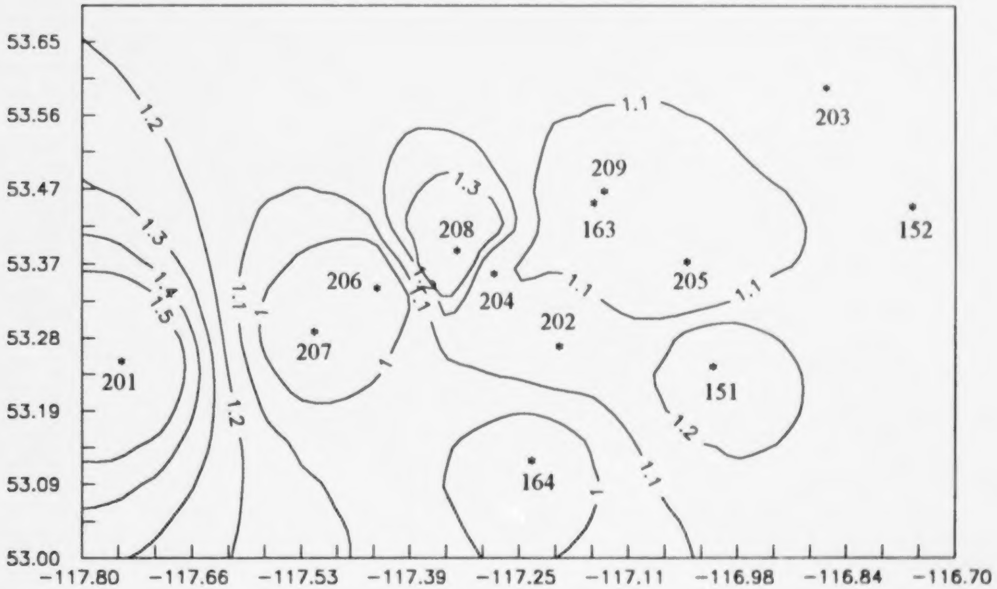

Fig.4.13: Plan view at 2km(contours in Ω.m on log scale).

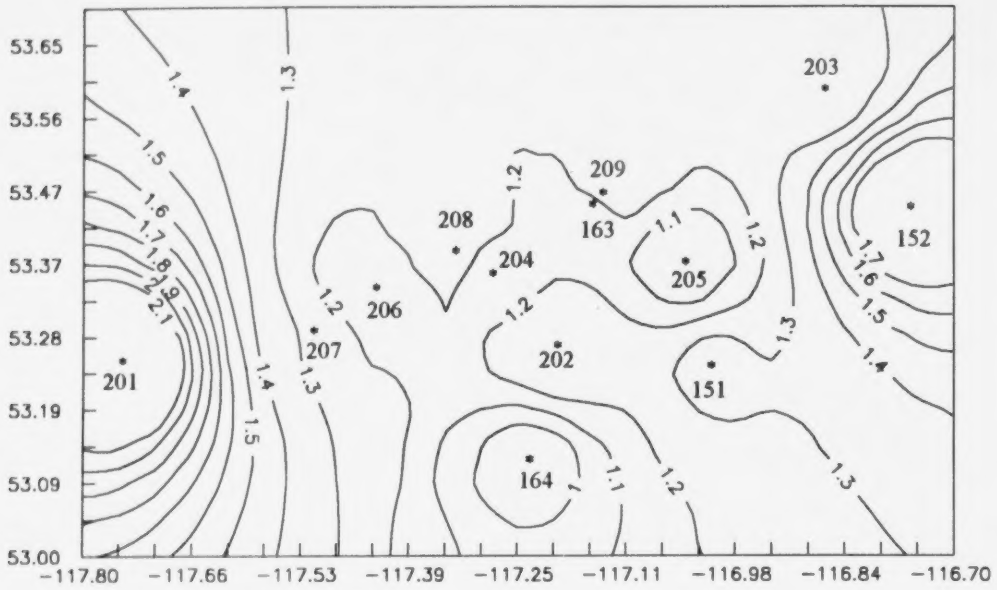

Fig.4.14: Plan view at 3km(contours in Ω.m on log scale).

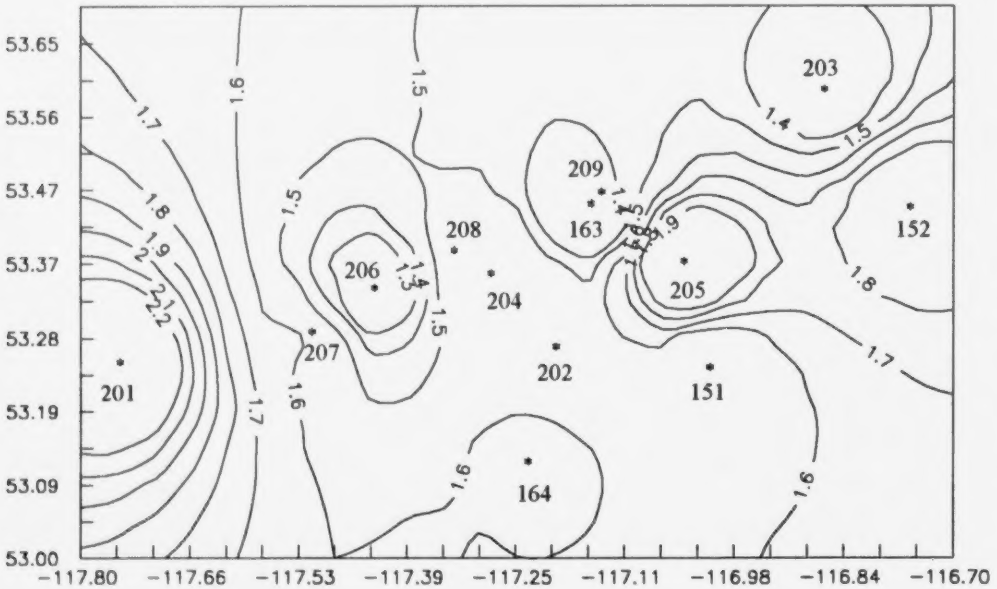

Fig.4.15: Plan view at 4km(contours in Ω.m on log scale).

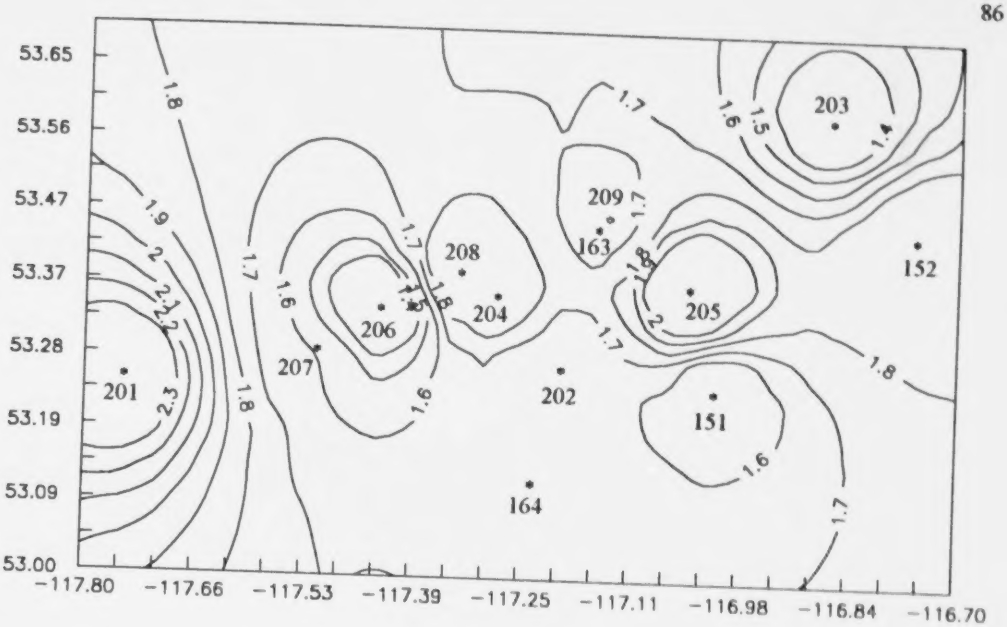

Fig.4.16: Plan view at 5km(contours in Ω.m on log scale).

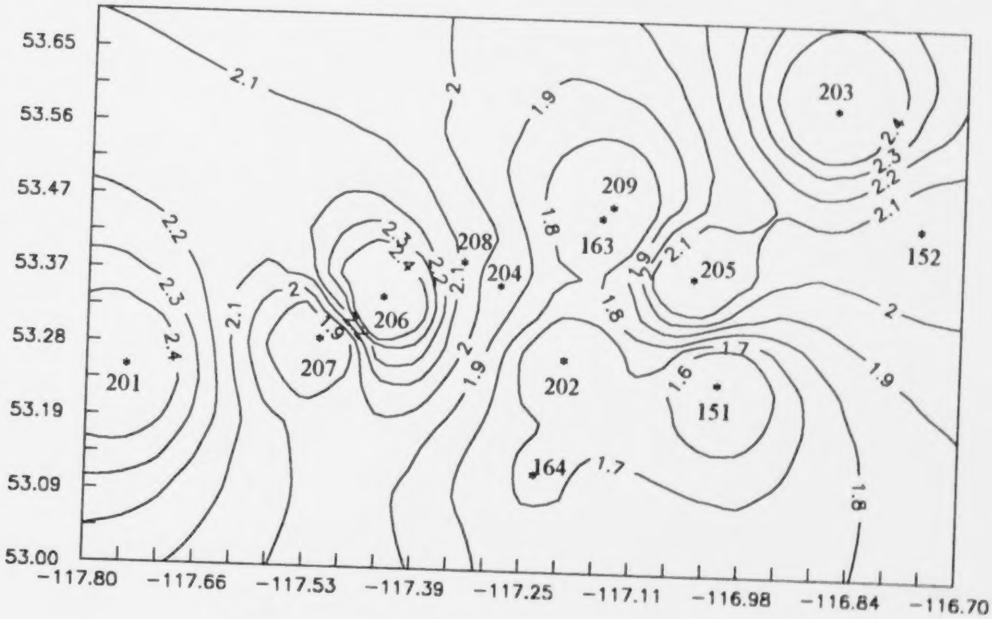

Fig.4.17: Plan view at 6km(contours in Ω.m on log scale).

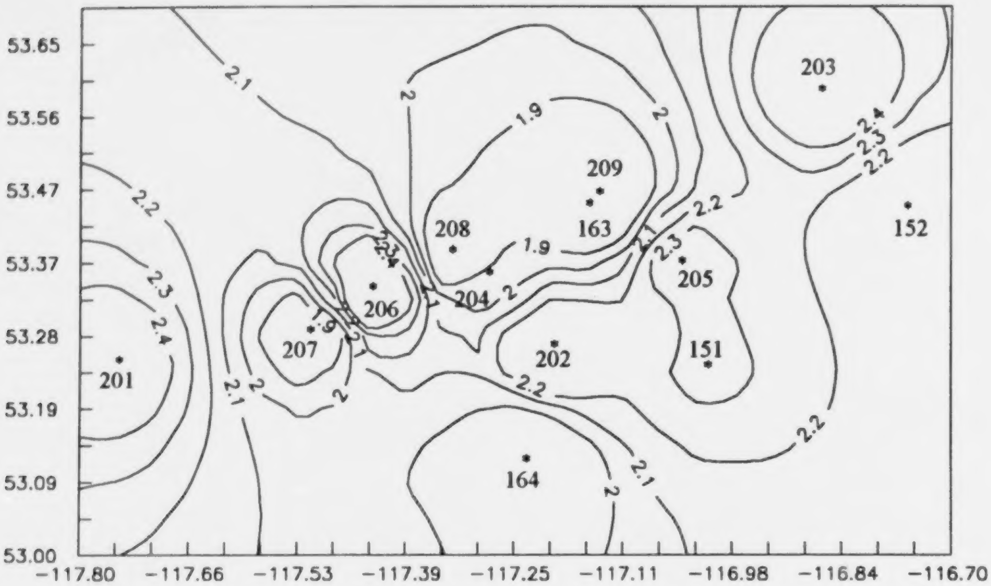

Fig.4.18: Plan view at 9km(contours in Ω.m on log scale).

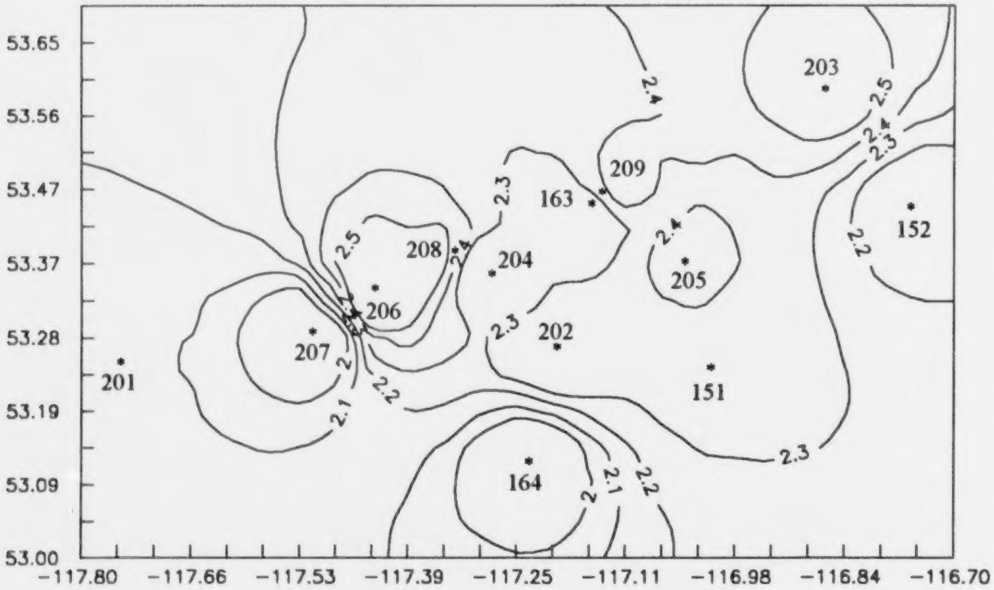

Fig.4.19:Plan view at 18km(contours in Ω.m on log scale).

4.2 TWO-DIMENSIONAL MODELLING

Modelling and inversion are important aspects of geophysical interpretation, and this is particularly true in magnetotellurics. Depending on the type of problem, modelling and inversion may be one dimensional (1D), two dimensional (2D) or three dimensional (3D). One dimensional modelling and inversion have already been discussed. Detailed accounts of 1D-modelling and inversion can be found in Rokitiyanski(1982), Vozoff(1991), Oldenburg(1978) and Wu(1968). There are several well developed schemes for 2D and 3D forward modelling but schemes for 2D and 3D inversions are yet to be perfected. Most of the 2D inversion schemes so far available are essentially forward modelling schemes that use the results of one dimensional inversion. Moreover, true two dimensional inversion procedures are found to work well only on synthetic data. The same is true for three dimensional procedures. Because of the complexity, non-uniqueness and uncertainties of the models and their responses, 2D inversion and 3D modelling and inversion were not applied in this work. Hence, these will not be discussed. A two dimensional forward modelling scheme was, however, applied here. A brief description follows.

Two dimensional forward modelling involves the solution of the set of equations (2.33 through 2.38) developed in Chapter 2. The differential equations governing two dimensional modelling were solved using the finite difference approach developed by Jones and Price(1970), Jones(1971, 1972) and Jones and Pascoe(1971), though some modifications have been made by a number of subsequent users. The most recent versions were modified to run on NEXT workstations and IBM microcomputers. All the programs are in FORTRAN 77.

Construction of any two dimensional model is a difficult task partly because of non-uniqueness and partly because of the inherent uncertainties associated with the field data. A forward model can be expected to give perfect results only when its response is compared to the corresponding synthetic data. Two dimensional models were constructed in this work using the results from the one dimensional Fischer inversions. Along a profile, each station was assigned the layer parameters, in the subsurface, based on the one dimensional results. The boundary between two successive stations was chosen at the mid point between the two stations. At the extremes, the boundaries were set at infinity (at very large distances compared to the station spacings).

The resulting resistivity configurations for the five profiles used for the forward modelling are shown in Figs.4.20a through e. The units of length and resistivity in the figures are in kilometers and ohm-m respectively. Both E-polarization and H-polarization cases were considered in the modelling. The responses of the models for the range of frequencies 0.05-100Hz were calculated and pseudosections constructed. The model responses, as contour plots of resistivities and phases (model pseudosections), for each of the five profiles and for both E and H polarizations are given in Figs.4.21-4.30.

The responses of the two-dimensional models can be compared with the results from the field data. Such comparison provides a measure of the adequacy of constructing the 2D sections from the 1D inversions and as such provide the starting point for more detailed modelling if desired.

A careful inspection of the model pseudosections, constructed from model responses (Figs.4.21 through 4.30), and field pseudosections (Figs.4.1 through 4.5) reveals the degree of similarity between the two. The nature of the contour line labeled 1.2, at the top right corner of the plots, is similar for profile 1 in the model pseudosections and the field pseudosection.

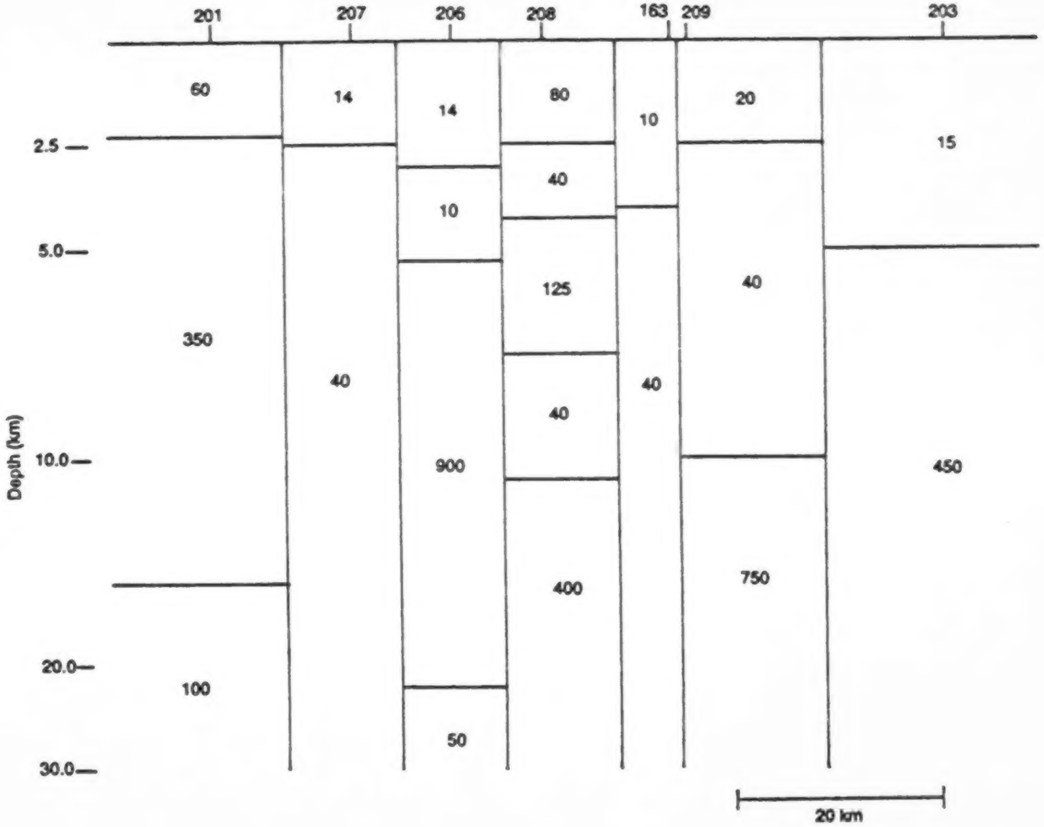

Fig.4.20a: Resistivity configuration for two dimensional model for profile 1 (resistivity values in Ω.m).

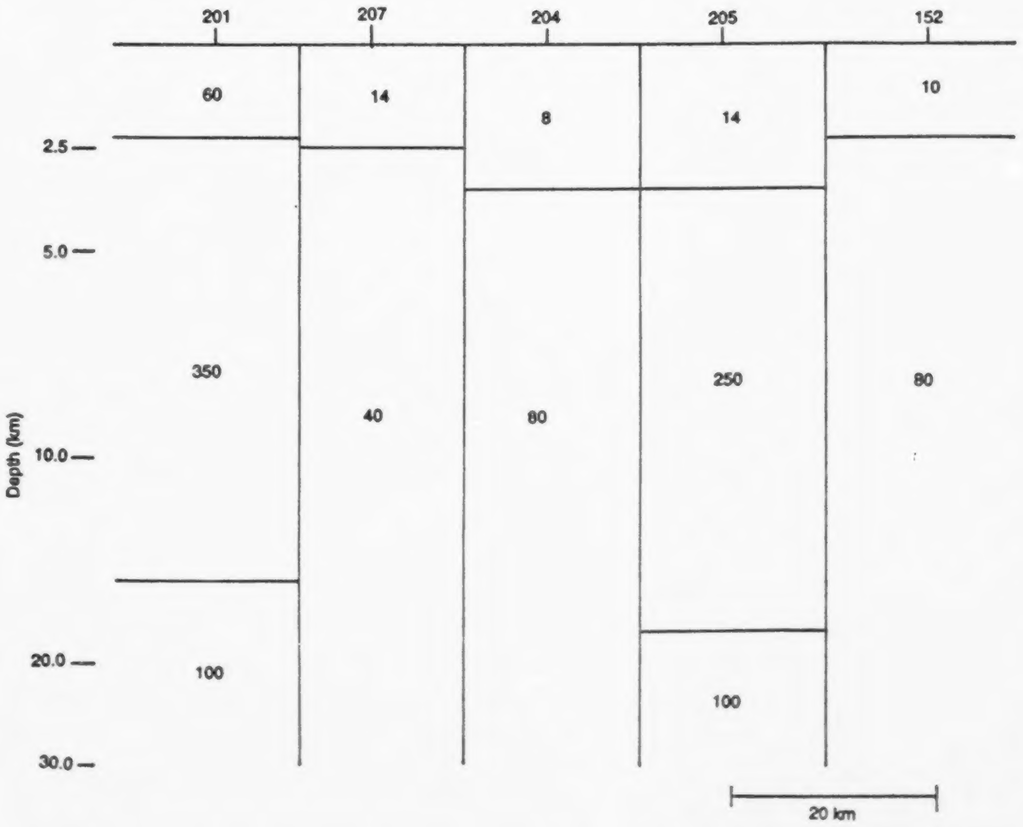

Fig.4.20b: Resistivity configuration for two dimensional model for profile 2 (resistivity values in Ω.m).

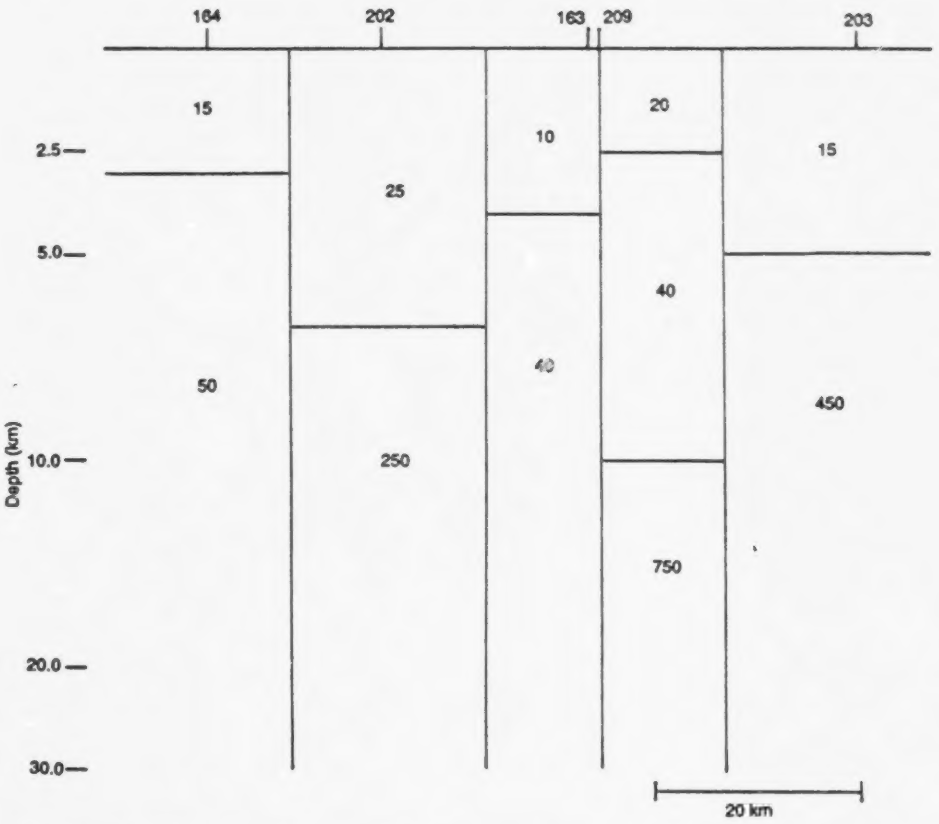

Fig.4.20c: Resistivity configuration for two dimensional model for profile 3 (resistivity values in Ω.m).

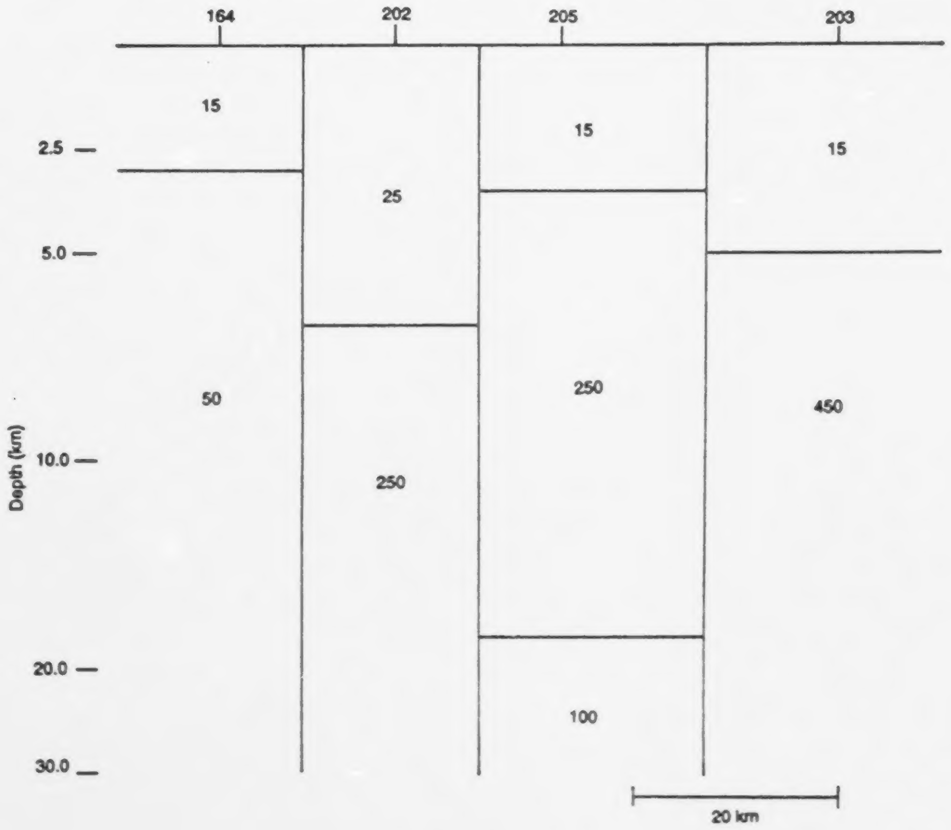

Fig.4.20d: Resistivity configuration for two dimensional model for profile 4 (resistivity values in Ω.m).

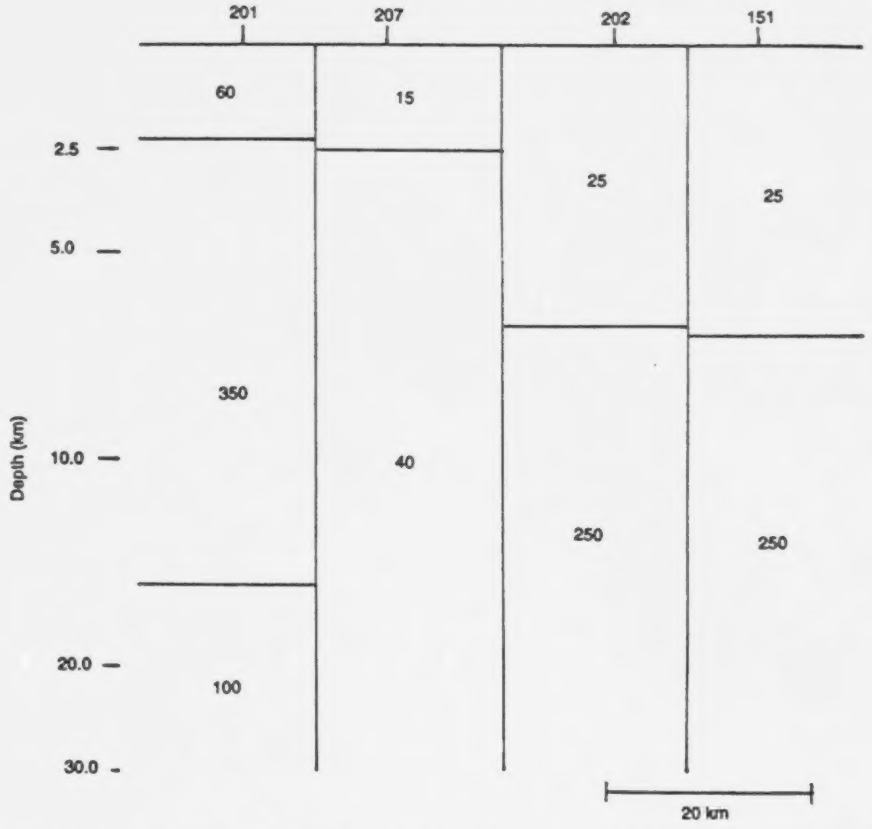

Fig.4.20e: Resistivity configuration for two dimensional model for profile 5 (resistivity values in Ω.m).

Likewise, the appearance of the contours beneath sites 207 and 205 are somewhat similar. There is a distinct similarity in contours, which tend to be horizontal at low frequencies, indicating horizontal stratification in deeper regions.

For profile 2, the contour line labeled 1.0 and originating at the surface is similar in the model pseudosections and the field pseudosection. The line in the model pseudosections, however, appears to penetrate deeper. As in profile 1, horizontal layering is evident at lower frequencies.

The degree of similarity for profile 3 is not as great as those for profiles 1 and 2. However, the natures of the contour lines labeled 1.4 and originating near the surface around sites 163 and 209, are similar in model and field pseudosections. Once again, as in profiles 2 and 3, layers tend to be horizontal at lower frequencies.

The results for profile 4 are disappointing. This may be due to the inadequacy of the model in describing the subsurface and demonstrates the fact that construction of 2D models is uncertain when dealing with an inherently 3D earth. Usually, a number of modifications to the models are required to obtain acceptable solutions through modelling.

The similarity between model and field pseudosections, for profile 5, is better than that for profile 4. The contours in the left portion of the pseudosections indicate that the layers in that region tend to be inclined while the contours in the bottom right corner of the plots suggest horizontal stratification at lower frequencies and in deeper regions.

Overall, the 2D modelling based on results from the 1D Fischer inversions produce pseudosections that are similar to the pseudosections from the field data. This means that to a first approximation, the electrical structure of the region is described by the 2D models.

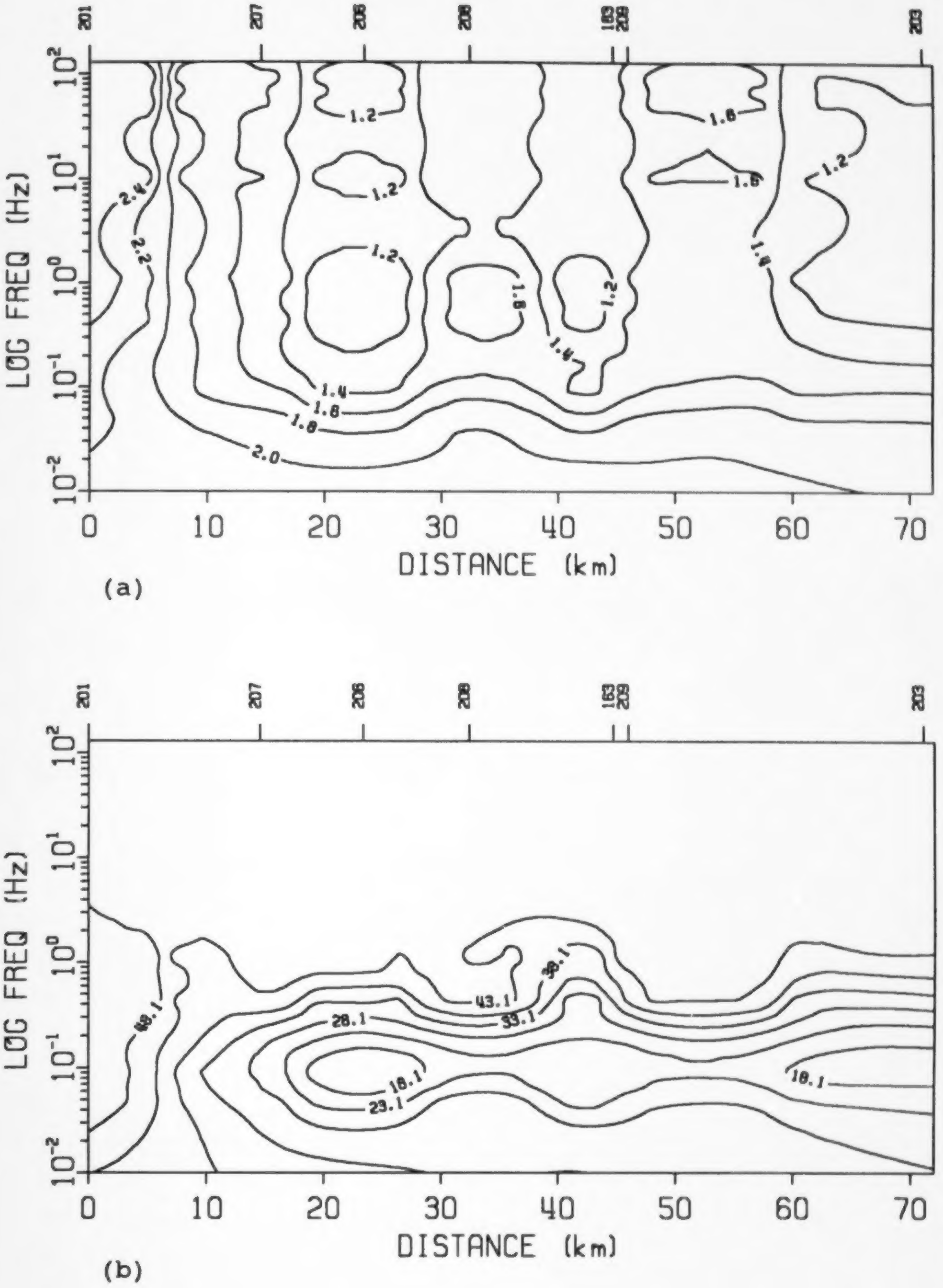

Fig.4.21: Model pseudosections for profile 1 for E-polarization. (a) Apparent resistivity (contour values in Ω.m on log scale); (b) Phase (contour values in degrees).

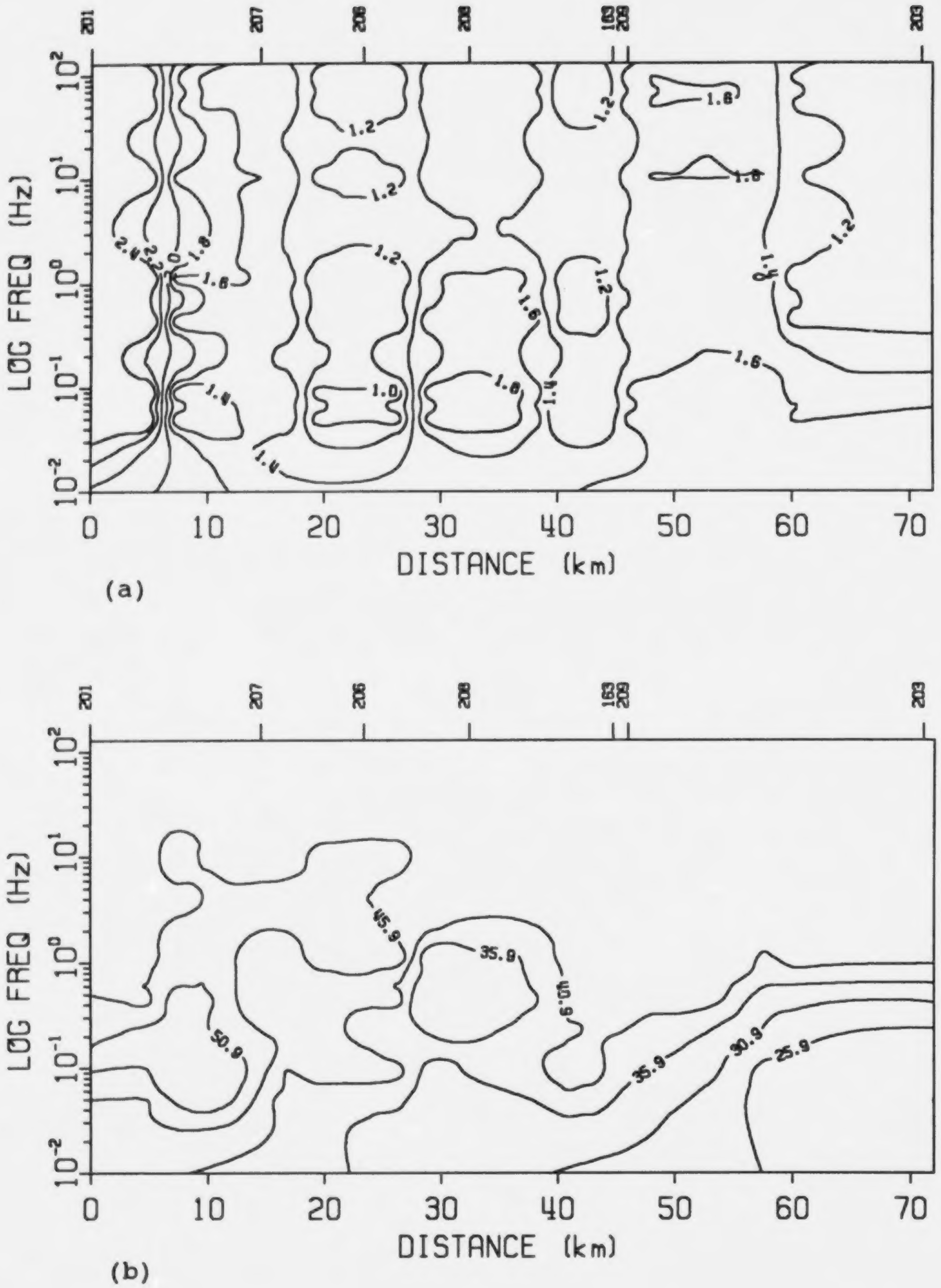

Fig.4.22: Model pseudosections for profile 1 for H-polarization. (a) Apparent resistivity (contour values in Ω.m on log scale); (b) Phase (contour values in degrees).

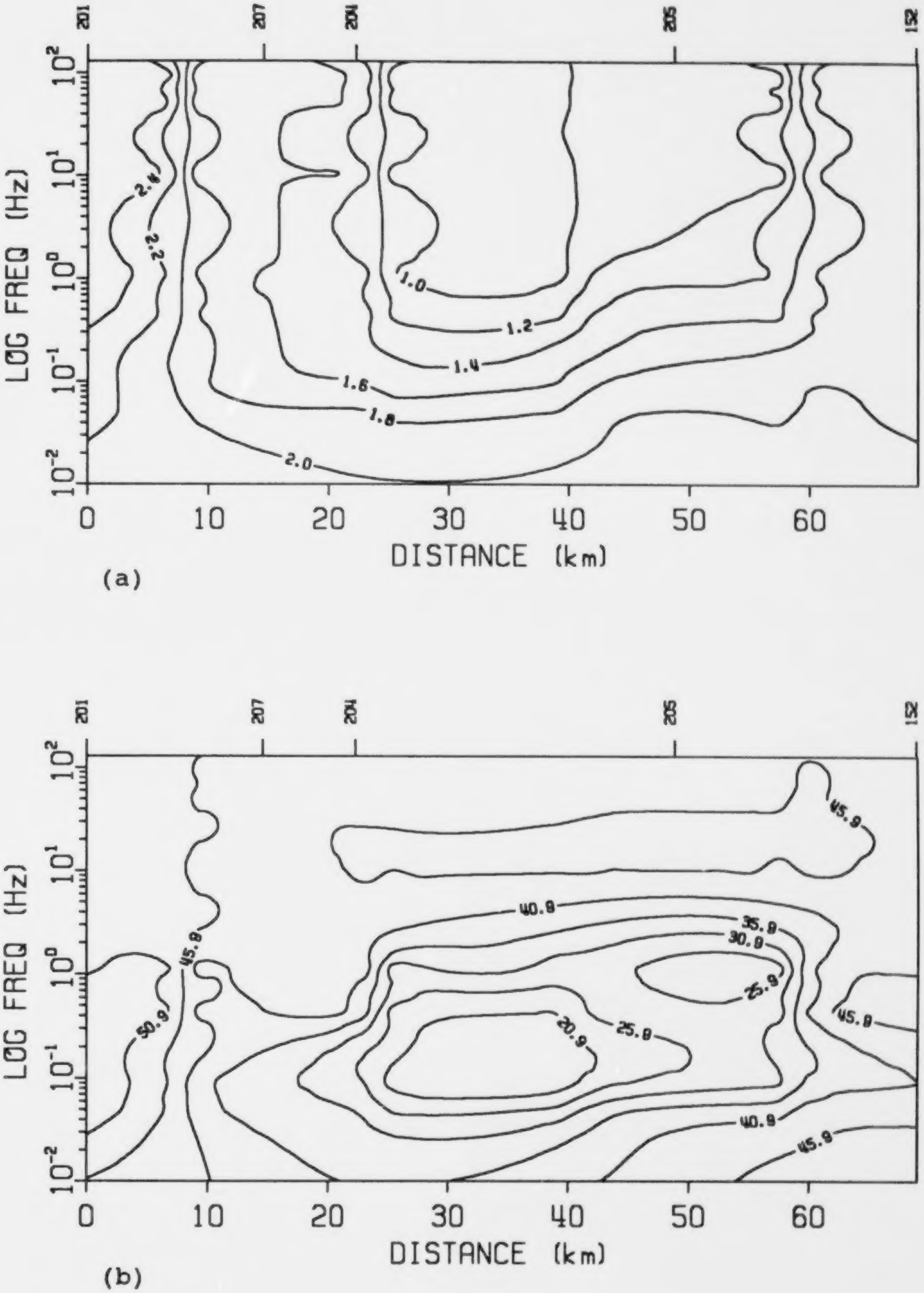

Fig.4.23: Model pseudosections for profile 2 for E-polarization. (a) Apparent resistivity (contour values in Ω.m on log scale); (b) Phase (contour values in degrees).

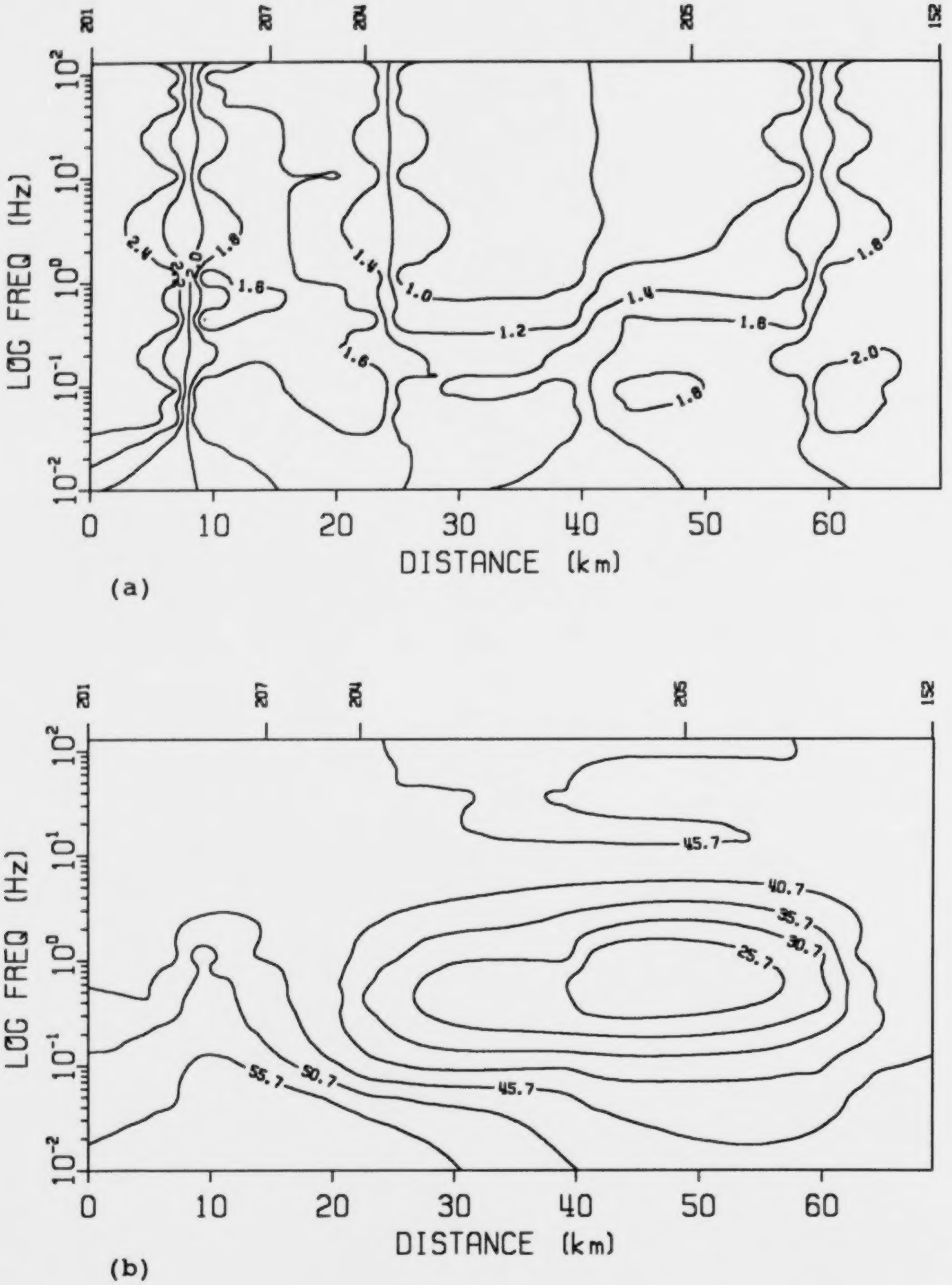

Fig.4.24: Model pseudosections for profile 2 for H-polarization. (a) Apparent resistivity (contour values in Ω.m on log scale); (b) Phase (contour values in degrees).

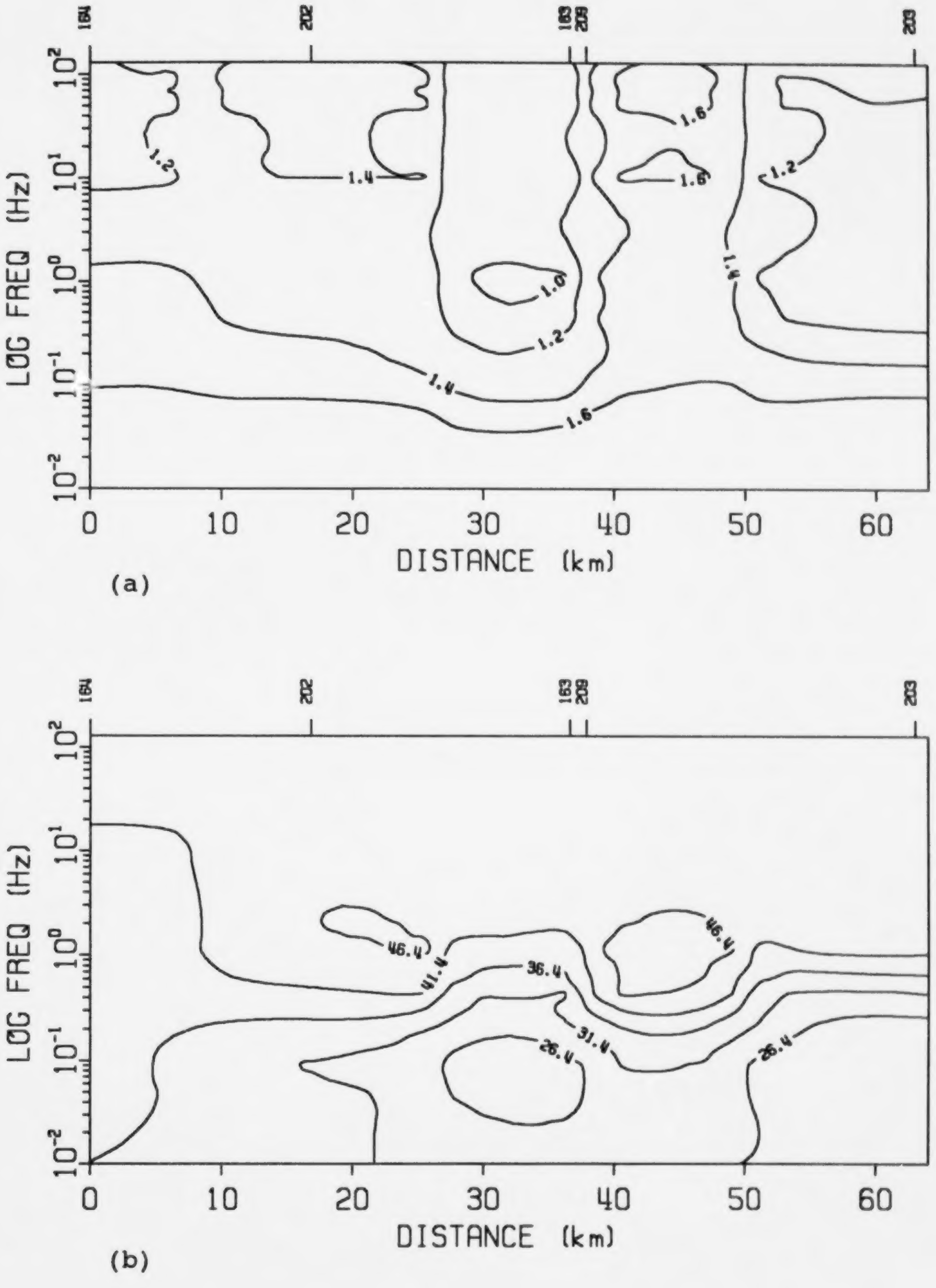

Fig.4.25: Model pseudosections for profile 3 for E-polarization. (a) Apparent resistivity (contour values in Ω.m on log scale); (b) Phase (contour values in degrees).

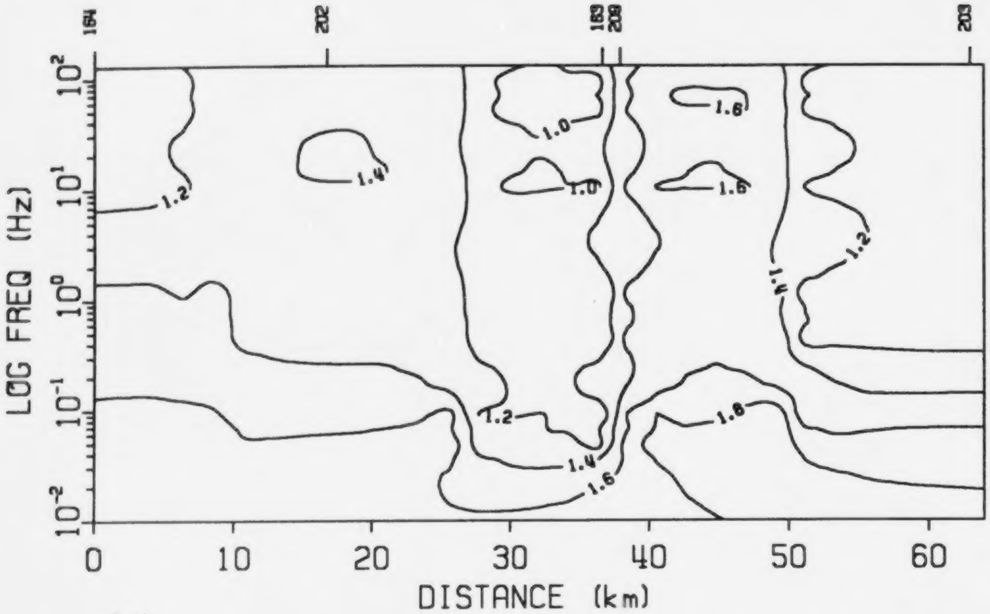

(a)

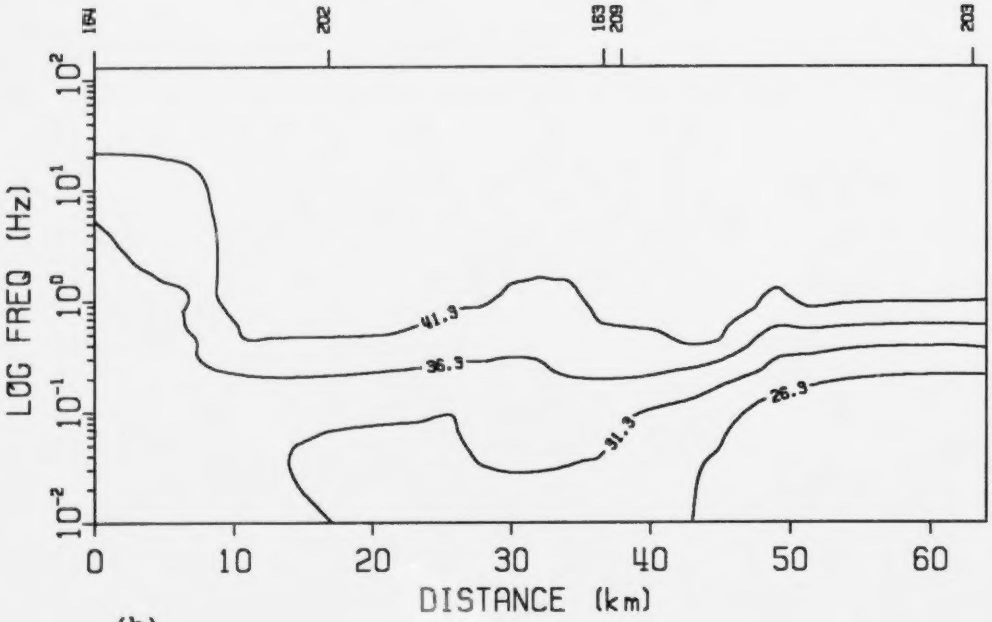

(b)

Fig.4.26: Model pseudosections for profile 3 for H-polarization. (a) Apparent resistivity (contour values in Ω.m on log scale); (b) Phase (contour values in degrees).

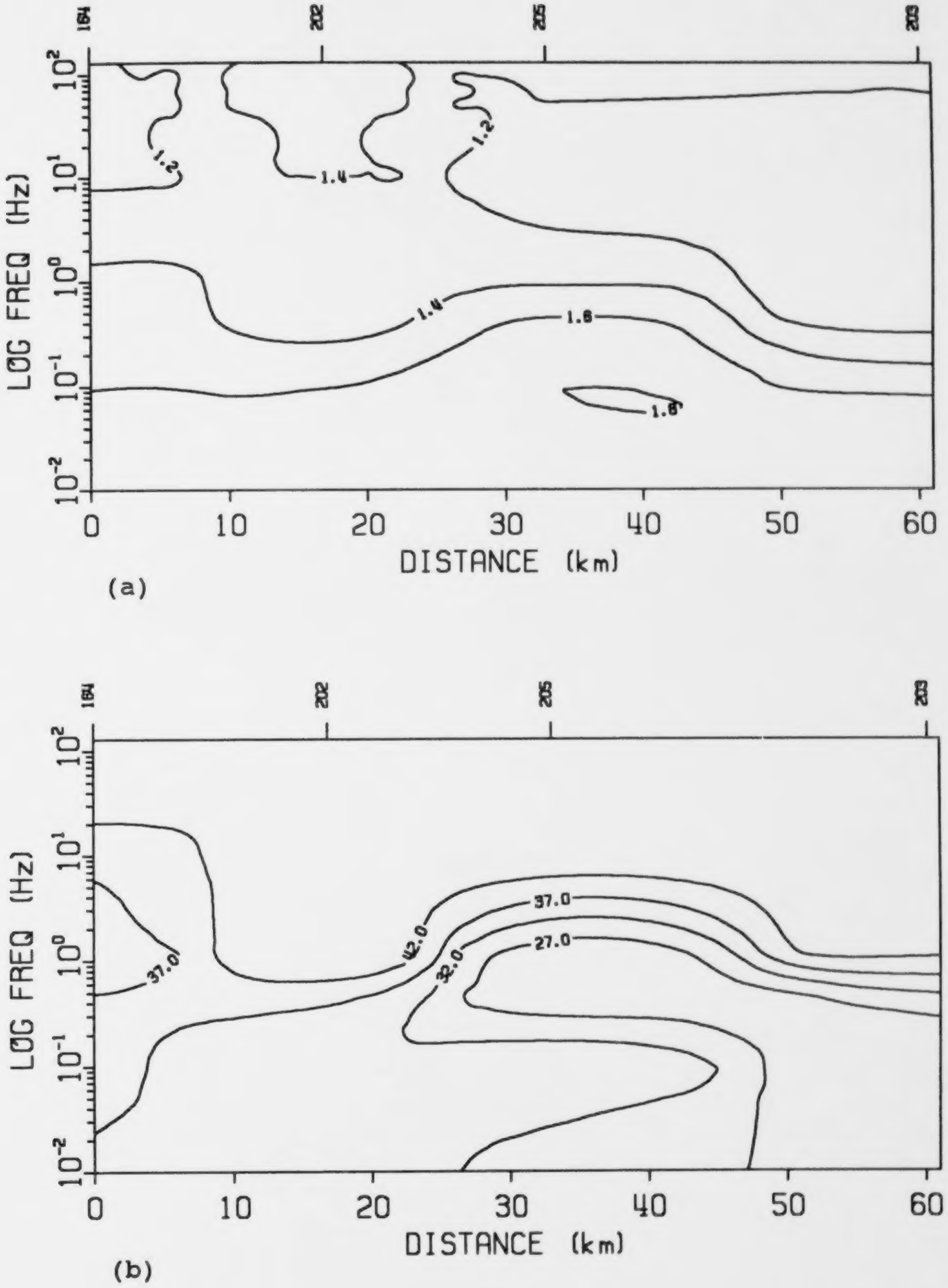

Fig.4.27: Model pseudosections for profile 4 for E-polarization. (a) Apparent resistivity (contour values in Ω.m on log scale); (b) Phase (contour values in degrees).

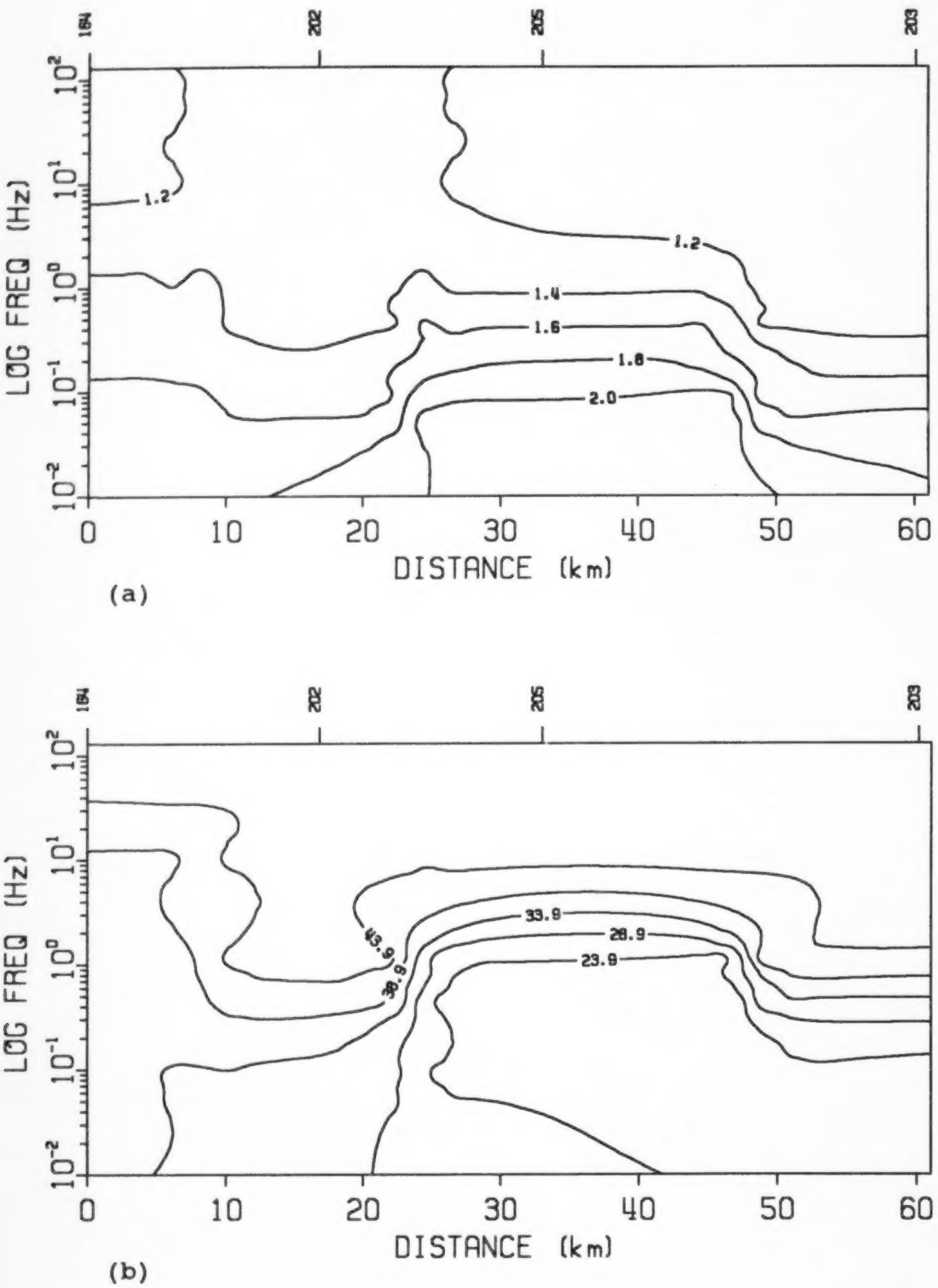

Fig.4.28: Model pseudosections for profile 4 for H-polarization. (a) Apparent resistivity (contour values in Ω.m on log scale); (b) Phase (contour values in degrees).

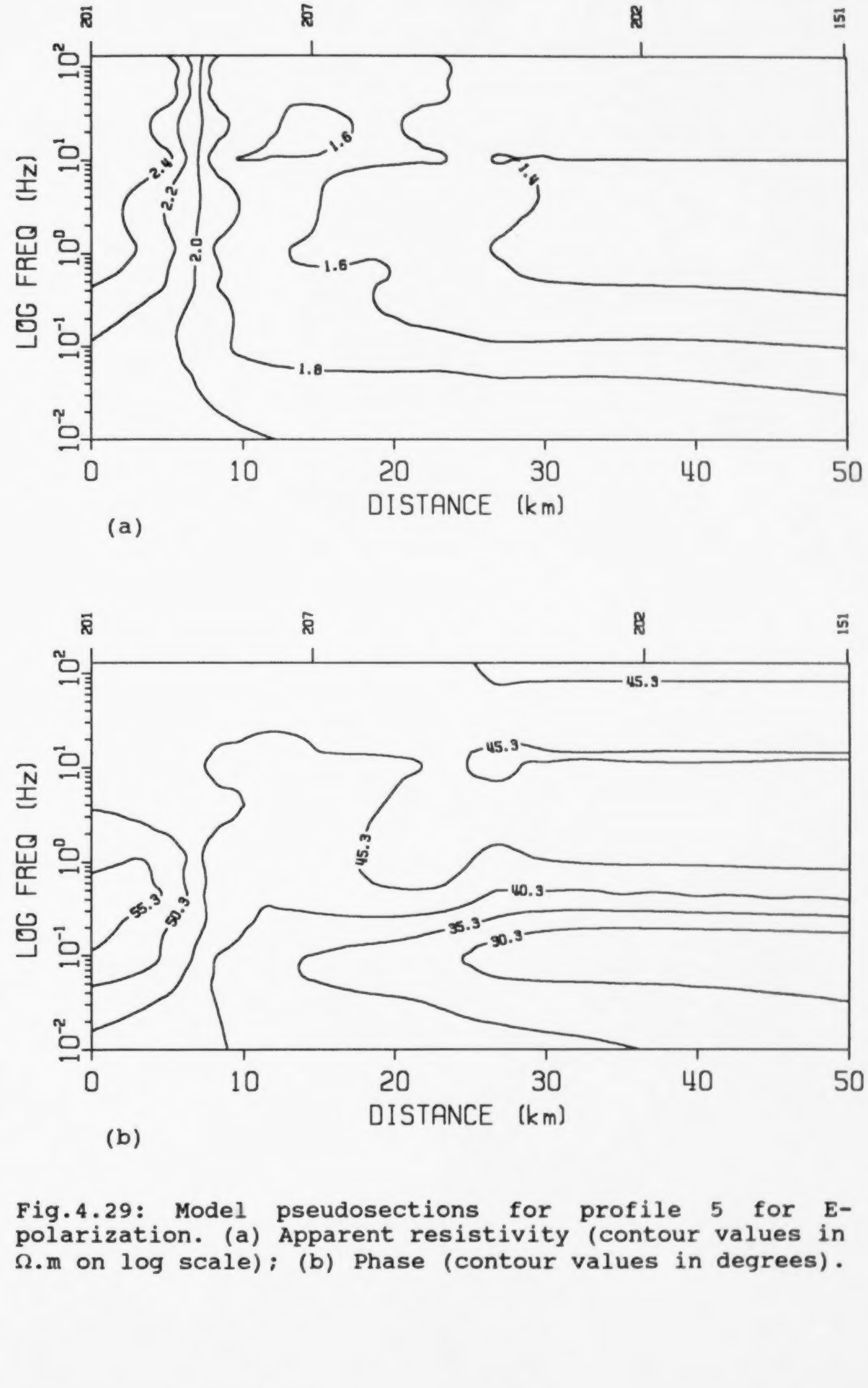

(a)

(b)

Fig.4.29: Model pseudosections for profile 5 for E-polarization. (a) Apparent resistivity (contour values in Ω.m on log scale); (b) Phase (contour values in degrees).

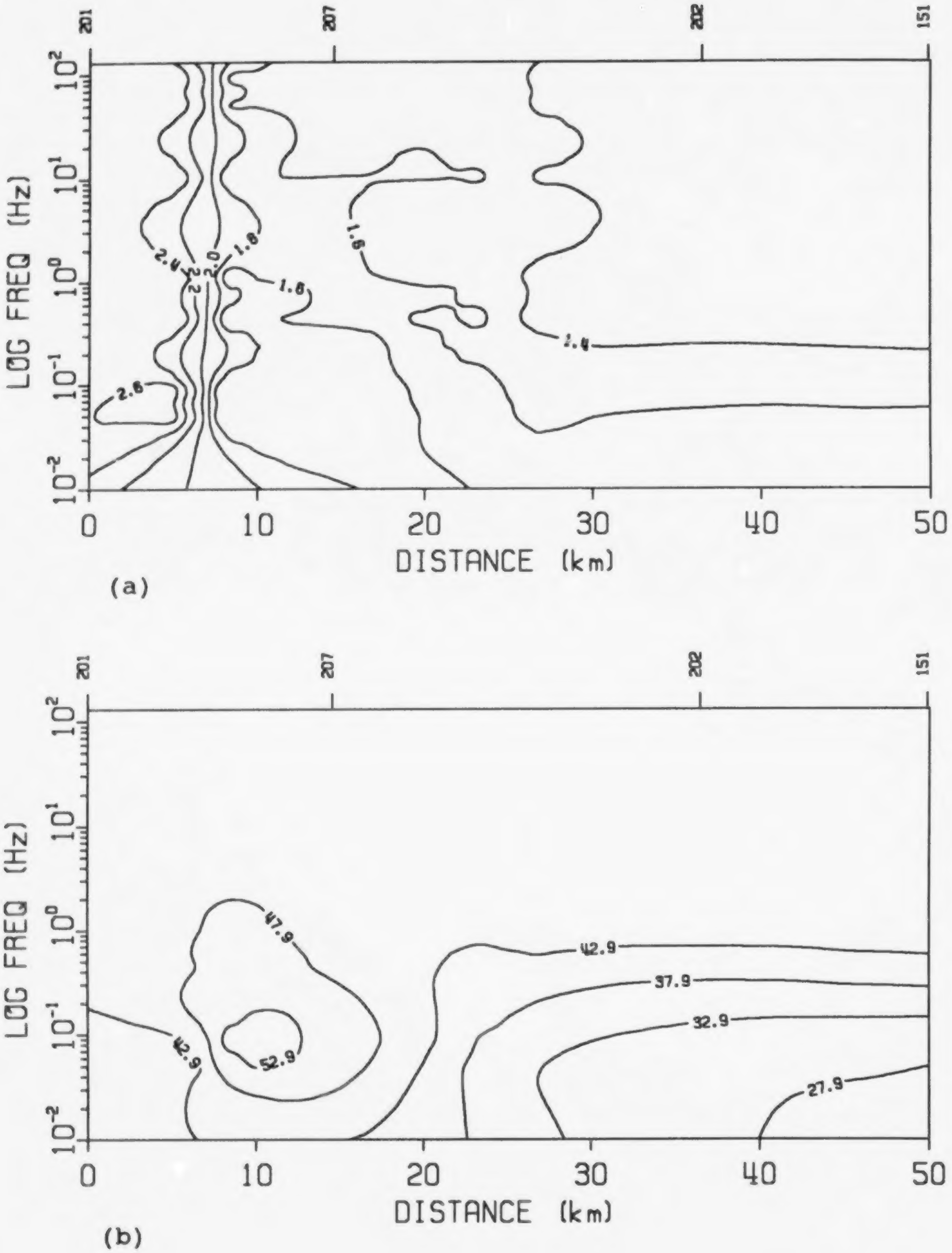

Fig.4.30: Model pseudosections for profile 5 for H-polarization. (a) Apparent resistivity (contour values in Ω.m on log scale); (b) Phase (contour values in degrees).

4.3 DISCUSSION AND CONCLUSION

Several general trends such as layering, resistivity contrasts etc. have been identified so far in earlier sections. In this section , the emphasis will be on pinpointing the various features which are visible from the plots (in particular, from the depth section and plan view plots) and suggesting the possible causes for some of these features.

In the depth section for profile 1, there are at least three noticeable features. These are - (i) the low resistivity contour(1.3) of resistivity 20Ωm (approximately) beneath sites 207 and 206, (ii) the low resistivity contour(0.9) of resistivity 8Ωm at a depth of about 1.5km, originating beneath site 209 and (iii) a relatively higher resistivity pocket, indicated by the contour line labeled as 1.9, of resistivity 80Ωm. A simultaneous inspection of the plan view plots (Figs.4.12 through 4.19) along the line joining sites 201, 207, 206, 208, 163, 209 and 203 reveals that there is a whole range of resistivities present in the region, from the surface all the way down to the depth of 18km. The lowest resistivity of about 10Ωm occurs along profile 1 at a depth of 2km surrounding sites 207 and 206. The highest resistivity of 316Ωm occurs along the profile at a depth of 18km. At all depths, for profile 1, there are no abrupt changes in resistivities. It is interesting to note that most of the sites along profile 1 exhibit a resistivity of about 16Ωm at 3km depth.

As in the case of profile 1, several observations can be made from profile 2. As mentioned earlier, there is a general increase in resistivity with depth. The highest and the lowest resistivities along the profile are 316Ωm and 9Ωm which occur at depths of 18km and 2km respectively. The most interesting feature in the depth section plot for profile 2 (Fig.4.8) is the contour(2.4) of resistivity 251Ωm. The contour line originates at a depth of 15km beneath site 201 and terminates below site 152 at a depth of 12km. The middle portion of this resistivity contour shows a depression beneath site 204 and a hump beneath 205. It is difficult to confirm at this stage what the hump signifies. It, however, appears to be a structural feature, possibly a fault that appears as a rounded hump on the magnetotelluric depth section. A seismic line north of site 205, shot by Pan Canadian, shows a subtle hump on the migrated seismic section. It is, however, difficult to relate the two directly, primarily because the hump on the seismic section occurs at a depth of roughly 3.5km while the top of the rounded hump on the magnetotelluric section is at a depth approximately 8km. Moreover, site 205 is at a distance of approximately 6km from the seismic line. Pan Canadian have interpreted the seismic sections as indicating a triangle zone in which a thrust fault and a conjugate fault form two opposite faces of a triangle. This triangle zone produces the subtle feature on the seismic section at a depth of about 3km. The formation of the triangle zone may have been associated with a deeper structural disturbance the effects of which are reflected in the magnetotelluric data and produce the high resistivity zone at greater depth. Data from closely spaced magnetotelluric sites in that region should help to better define the triangle zone and the deeper structure beneath it.

Profile 3, as in the other depth sections, shows a general increase in resistivity with depth. There are three important features which can be noted from the depth section (Fig.4.9). A region of low resistivity(12.5 Ωm) is present beneath sites 163 and 209. This low resistivity region extends from 3km to a depth of 6km and has a lateral extent of about 10km. This is clearly reflected in the plan view sections, particularly for depths of 1-3km (Figs.4.12 through 4.14). The same is also reflected in the deeper plan view plots at 4km, 5km and 6km (Figs.4.15 and 4.17) with somewhat higher resistivities. The contours(1.3) of resistivity 20Ωm in the upper part of the depth section(Fig.4.9) extend from close to the surface to a depth of about 7km enclosing a fairly large high conductivity region. The third interesting feature is the low resistivity layer (about 32Ωm) at a depth of 10km that roughly separates the high and low resistivity regions. The resistivity contours below this low resistivity layer are inclined.

The low resistivity layer mentioned above also appears on the depth section plot for profile 4 (Fig.4.10). This is because sites 164 and 202 are common to both profiles 3 and 4. The region above this layer has lower resistivities. In the region below the low resistivity layer, there is an increase in resistivity with depth. The same hump as that of profile 2 occurs beneath site 205 with its top at a depth of approximately 8km and displays a resistivity of about 200Ωm. A resistivity of this value is generally considered to be moderate, but with respect to the surroundings here it is relatively high.

The depth section for profile 5 (Fig.4.11) shows two important features. The first is the presence of a low resistivity pocket of resistivity 20Ωm beneath site 202. This low resistivity pocket lies between 2km and 5km depth and has a lateral extent of about 10km. The resistivity in the vicinity of site 202 on the plan view plots (Figs.4.13 through 4.16) varies from about 13Ωm to 63Ωm over 2-5km depth. The second noticeable feature in

Fig.4.11 is the tendency of the layers to be inclined in deeper regions.

There are several possible causes of high conductivities in the earth's crust. High conductivity taken alone in the earth's crust may be associated with anelastic deformation processes in the lower crust or tectonic processes involving the whole crust which may form interconnected accumulations of carbon or minerals such as magnetite (Stesky and Brace, 1973; de Beer, van Zyl and Gough, 1982; Shankland and Waff, 1977). High conductivity may also be associated with mineralization containing metallic sulfides or graphite (Camfield et al, 1971; Camfield and Gough, 1977), or it may be associated with hydrated rocks (Hyndman and Hyndman, 1968; Cochrane and Hyndman, 1974), serpentinized rocks in buried oceanic crust (de Beer et al., 1982), or fracture zones containing interconnected saline water or with partial melting.

Hyndman and Hyndman(1968) suggested that rocks saturated with water in the lower crust may account for high conductivity at shallower depths. Greenhouse and Bailey(1981) suggested that it may be due to electrolytic conduction through pores and fractures, formation of hydrous compounds with silicates and lowering of melting points of crystalline rocks resulting in partial melting.

Dvorak (1975) on the other hand has shown that free water in interconnected pores is unlikely to provide high conductivity at depths greater than 10km, where pressure reduces the porosity of crustal rocks. This reasoning seems to hold good in the area under investigation because of the general trend of increasing resistivity with depth. It may still be noted, however, that the numerically high resistivities on the depth section plots are considered to be moderate and higher only in relative terms.

Stesky and Brace(1973) showed through experiments on serpentinized rocks from the Indian ocean that these were 3-4 orders of magnitude more conductive than unserpentinized oceanic rocks of similar compositions. The process of formation and the conductive mechanisms of serpentinized marine rocks were discussed by de Beer et al(1982). They showed that such rocks in the lower crust could account for high conductivity.

In the present work, several high conductivity zones have been observed in the area under investigation. There are several low resistivity (high conductivity) layers, visible on the depth sections, with resistivities ranging from about 32Ωm to about 63Ωm and with depth extent being 8-12 km. The high conductivity region characterized by several layers may correspond to the conductive anomaly discovered by Ingham et al (1983) who placed the depth to the top of the anomaly at about 10km but could not ascribe a resistivity value to the anomaly. The geothermal anomaly found by Lam et al (1982) was interpreted by them to be the result of migration of heated water from the Miette region along ascending fault planes in the lower Devonian and Cambrian sediments which underlie the area at a depth of 3-4km. This effect may explain the presence of the two isolated pockets with high electrical conductivities which are visible on the depth section plots of profiles 3 and 5 and so may be associated with saline water. Another possible explanation, suggested by Ingham et al(1983) is that the source of the geothermal and magnetovariational anomalies is a body of partially molten rock at a much greater depth in the earth. Such a possibility is indicated from the magnetotelluric results in Fig.4.9, but more data are needed to the north and west of the area to explain this further.

It is difficult at this stage to ascertain the cause of the hump (discussed earlier) that appears beneath site 205. This hump can be seen on the depth section plots of profiles 2 and 4. It is not a mathematical manifestation or the influence of the surrounding resistivity contours because the isoline labeled 1.5 appears at approximately the same depths in Figs. 4.9 and

4.10. It appears that this hump is associated with the triangle zone as discovered in the seismic data with faults that act as a physical medium for upward migration of saline water (and hence also heat transport) which results in a low electrical resistivity zone as portrayed by the presence of isolines just above the hump and the conductivity anomaly as described by Ingham et al(1983).

It is well known that west-central Alberta is rich in hydrocarbons. Figure 4.31 shows the locations of two gas pools, Lambert and Banshee, which are in the vicinity of sites 163, 209, 202 and 205. The two gas pools are labeled as L and B in the figure. Information about the two gas pools was obtained from the Geological Survey of Canada (map 1558A, Gas Pools of Western Canada, June 30, 1981) and the ERCB (Alberta's Reserves of Crude Oil, Gas, Natural Gas Liquids and Sulphur; at December 31, 1982). The mean depths to the formations of Lambert and Banshee pools are 4430.8m and 4580.6m respectively. Both pools produce saline water with the gas. This is consistent with the results from the Fischer inversions for sites 163 and 209 which display low resistivities of about 45Ωm at depths of approximately 4.5km. Interestingly, the mean depth below the surface of the Upper Devonian Formation to the west of the fifth meridian is approximately 4km as can be seen from the geological section in Fig.4.32. This figure also shows

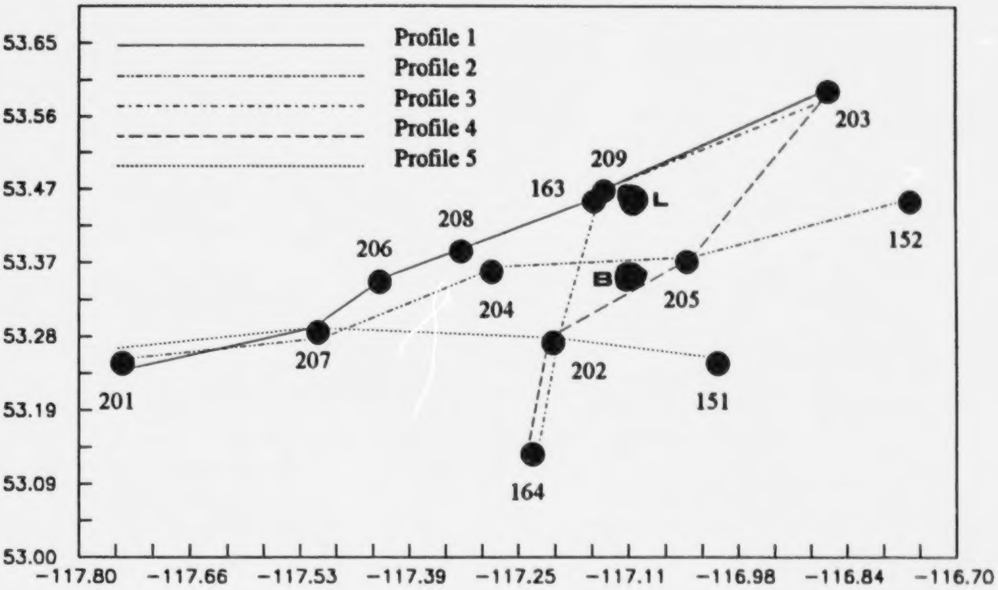

Fig.4.31: Lambert (L) and Banshee (B) gas pools along with 13 sites and 5 profiles.

several reefs with hydrocarbons to the east of the fifth meridian. Since the area under study is known to have concentrations of hydrocarbons, it is possible that the low resistivities in the region are associated with hydrocarbon traps in the Upper Devonian. The lithological logs near sites 163 and 203 also show the Upper Devonian at a mean depth of approximately 4km. These concordant facts clearly suggest that the area under investigation is indeed highly conducting and the high conductivity may be associated with hydrocarbons as well as the presence and movement of saline water (Lam et al, 1982). The work of Lam et al (1985) shows that the highest geothermal gradient of 36^0C/km (Fig. 1.2) is in the vicinity of sites 163 and 209. They also show that a high value, 158400 mg/L, of total dissolved solids (TDS) occurs in the Upper Devonian. These data were acquired from a well located near sites 163 and 209. These results suggest that the MT method may be capable of detecting high conductivity zones associated with high salinity fluids and possibly hydrocarbons. However, to better pinpoint hydrocarbon traps, a spatially high resolution MT survey would be needed.

The resistivity values obtained for site 202, through Fischer inversion, indicate a resistivity at 4.5km is 28Ωm which is considered to be low. This depth corresponds to the mean depth of the Banshee gas pool

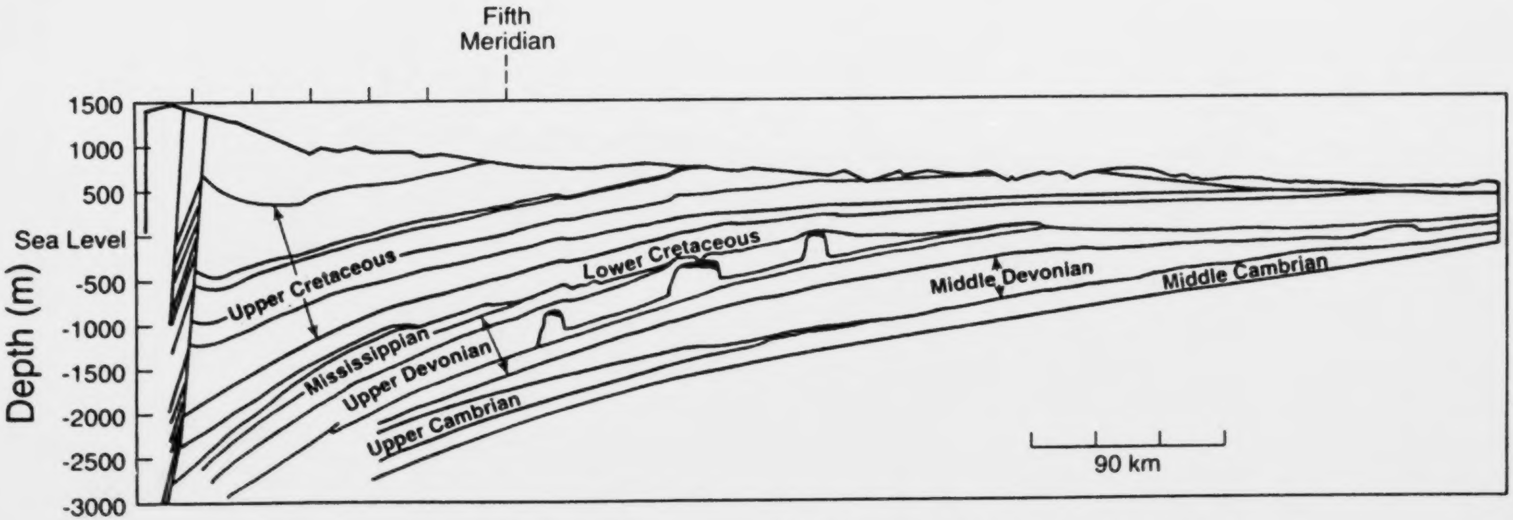

Fig.4.32: The geological section. The fifth meridian corresponds to longitude 114°W.

which is 4580.6m. The Fischer inversion for site 205, which is also near Banshee, shows a somewhat higher resistivity of more than 100Ωm at 4.5km. It is below this site that the high resistivity hump occurs on the depth section plots. It is possible that the hump represents a dome shaped dolomitic limestone trap that lacks hydrocarbons but seems to deflect saline water and gas upward to form the Banshee pool. The hump is seen in magnetotelluric data from only one site (205) and so it is important that more data be obtained in that area to confirm its existence and to better delineate its nature.

The presence of low resistivity zones is also reflected in the Fischer inversion composite plots along the five profiles as shown in Figs.4.33a through e. The solid lines joining the sites on the five profiles indicate what is believed to be the electrical basement with depth varying between about 3km to almost 10km. The electrical basement depth may differ from that of the geological basement. The depth of the geological basement in this area is greater than 5km as can be seen from the geological section of Fig.4.32 with apparent difference between its depth and the electrical basement. Lithological logs from wells near sites 163 and 209 indicate that the top of the Precambrian lies at about 5km while the MT data indicate a greater depth. It is possible that the several thin low resistivity zones in

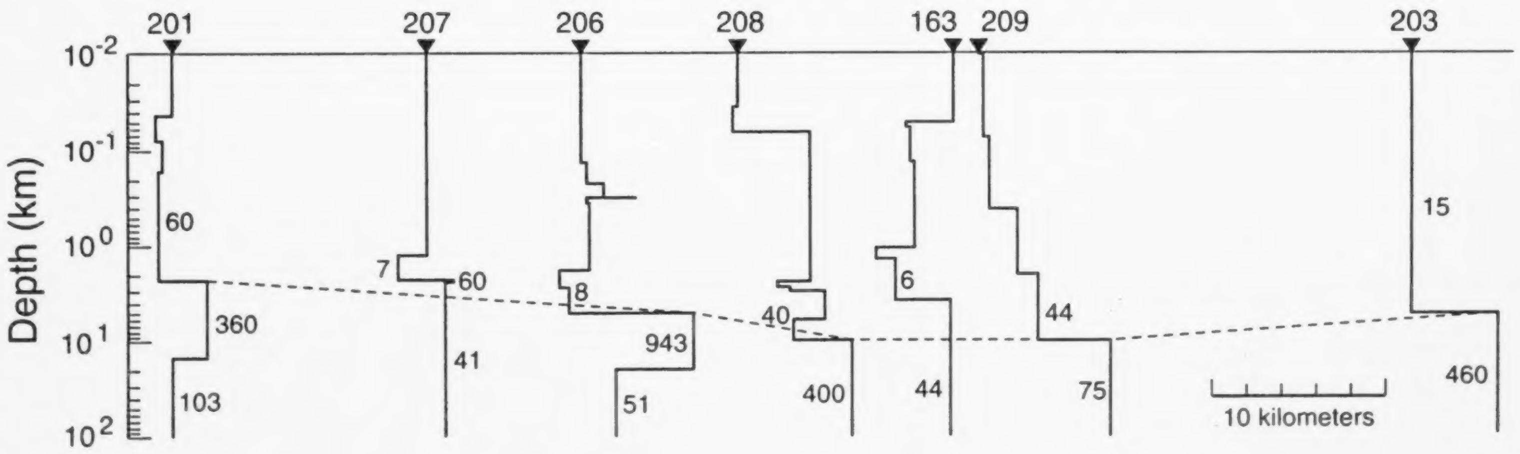

Fig.4.33a: Fischer inversion composite plot for profile 1. The numbers indicate resistivities in Ω.m.

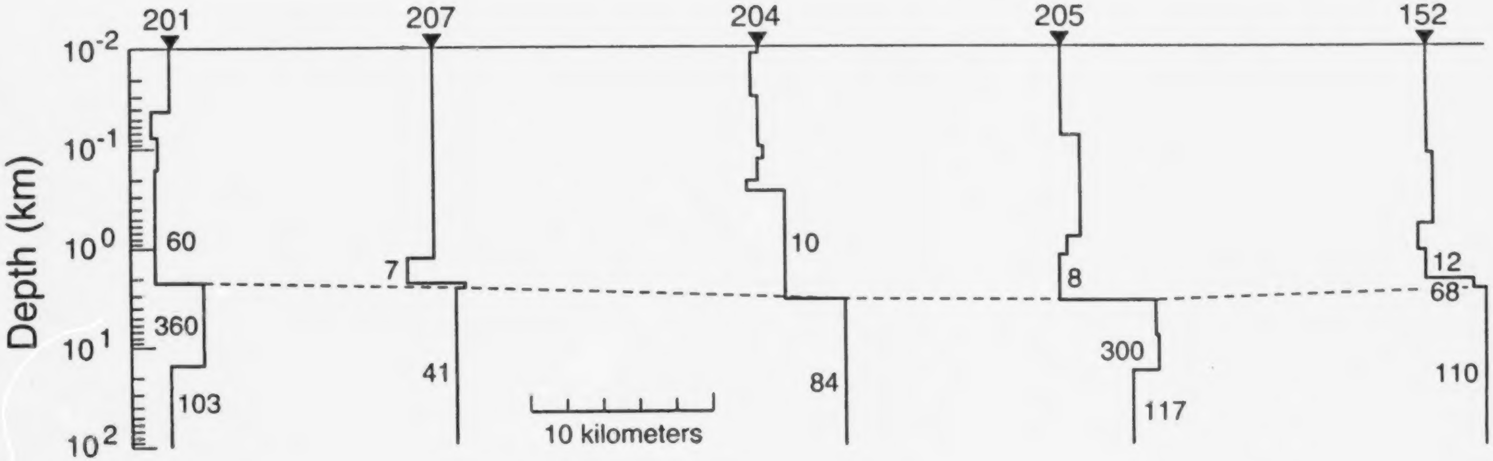

Fig.4.33b: Fischer inversion composite plot for profile 2. The numbers indicate resistivities in Ω.m.

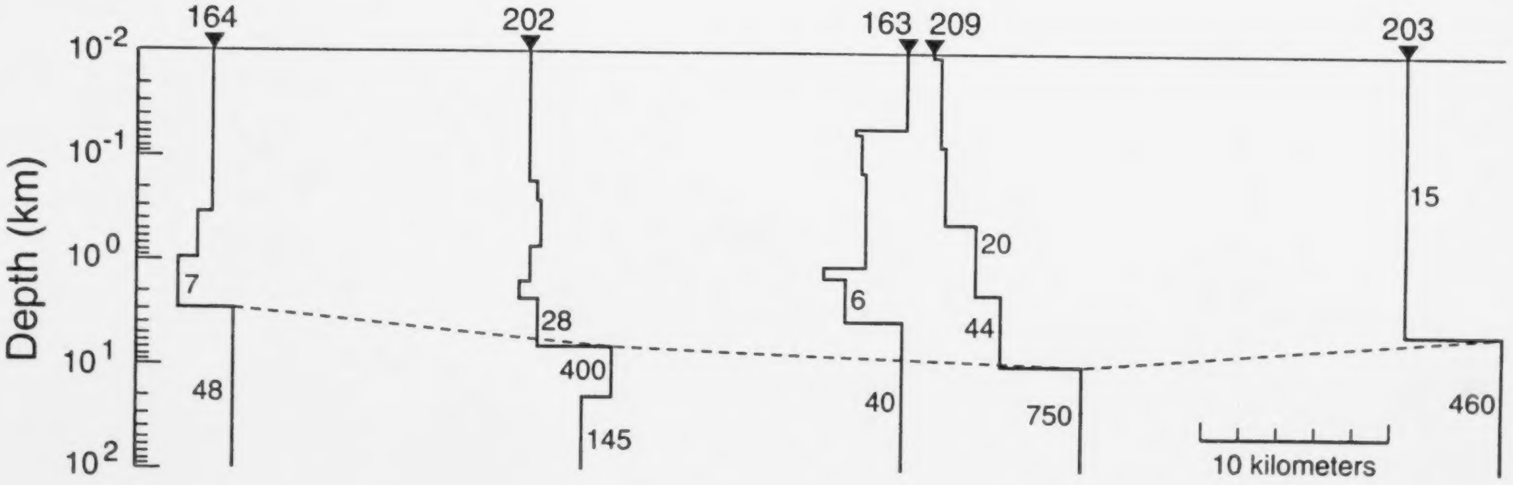

Fig.4.33c: Fischer inversion composite plot for profile 3. The numbers indicate resistivities in Ω.m.

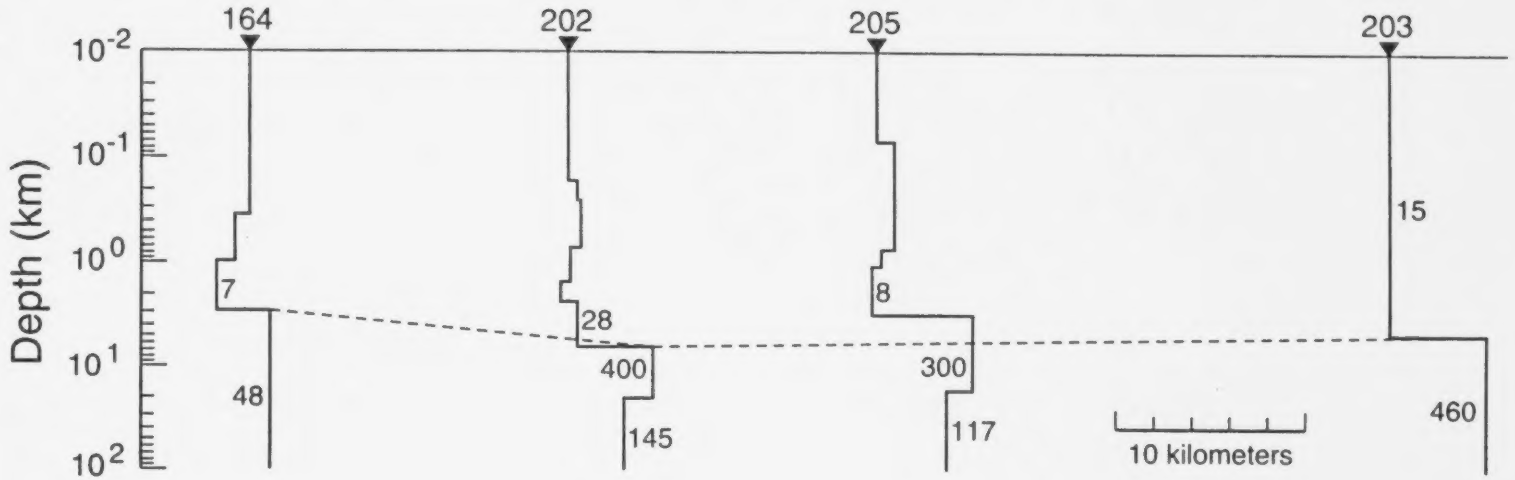

Fig.4.33d: Fischer inversion composite plot for profile 4. The numbers indicate resistivities in Ω.m.

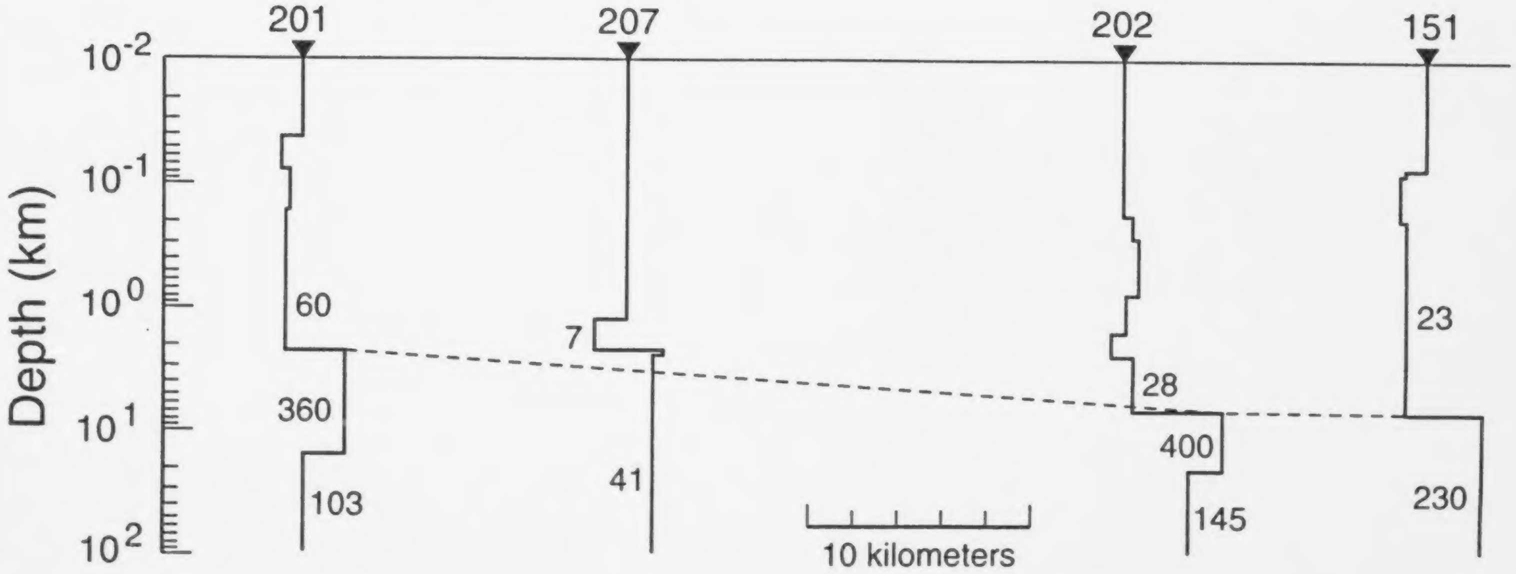

Fig.4.33e: Fischer inversion composite plot for profile 5. The numbers indicate resistivities in Ω.m.

the Fischer inversion composites, above the basement, correspond to hydrocarbon traps, in particular for site 163. It is difficult, at this stage, to ascertain the cause of the discrepancy in depth between the electrical and geological basement but a possible cause could be the presence of static shift in the data.

Static shift in a set of apparent resistivity curves appears as a displacement of one or a number of curves with respect to the others in the set, and is caused by the presence of charges on near surface lateral inhomogeneities (Jones, 1988). This results in erroneous measurement of the horizontal component of the electric field which in turn results in the displacement of the apparent resistivity curves. The static shift effect is essentially a near surface effect but in the measurement of apparent resistivities, the whole apparent resistivity curve is displaced.

It has been shown (Jones, 1988), through model studies, that static shift does not affect the phases of the MT impedance tensor. This independence of phases is due to the finite electrode dipole separation. Figs.4.34a and b show the apparent resistivity and phase plots for all 13 sites. It is seen that the apparent resistivity curves exhibit some displacement relative to one another while the phase curves lie close together. In particular,

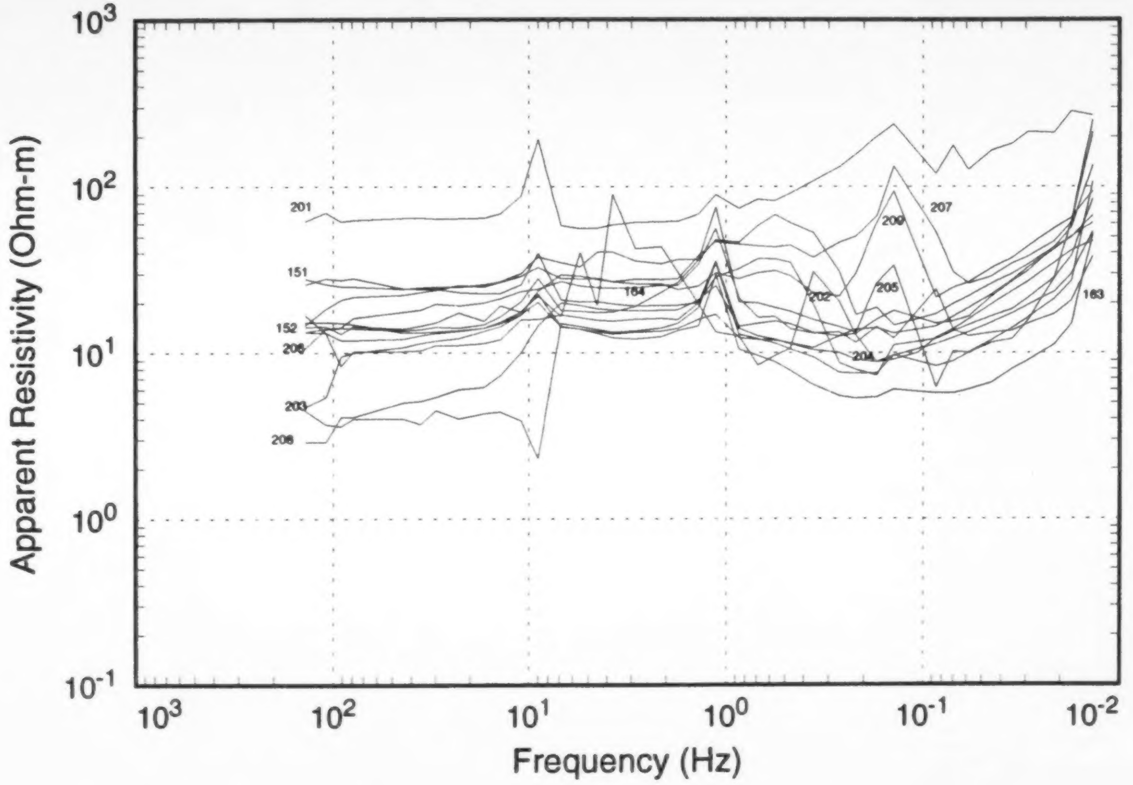

Fig.4.34a: Apparent resistivity against frequency plot for 13 sites showing static shift in the data.

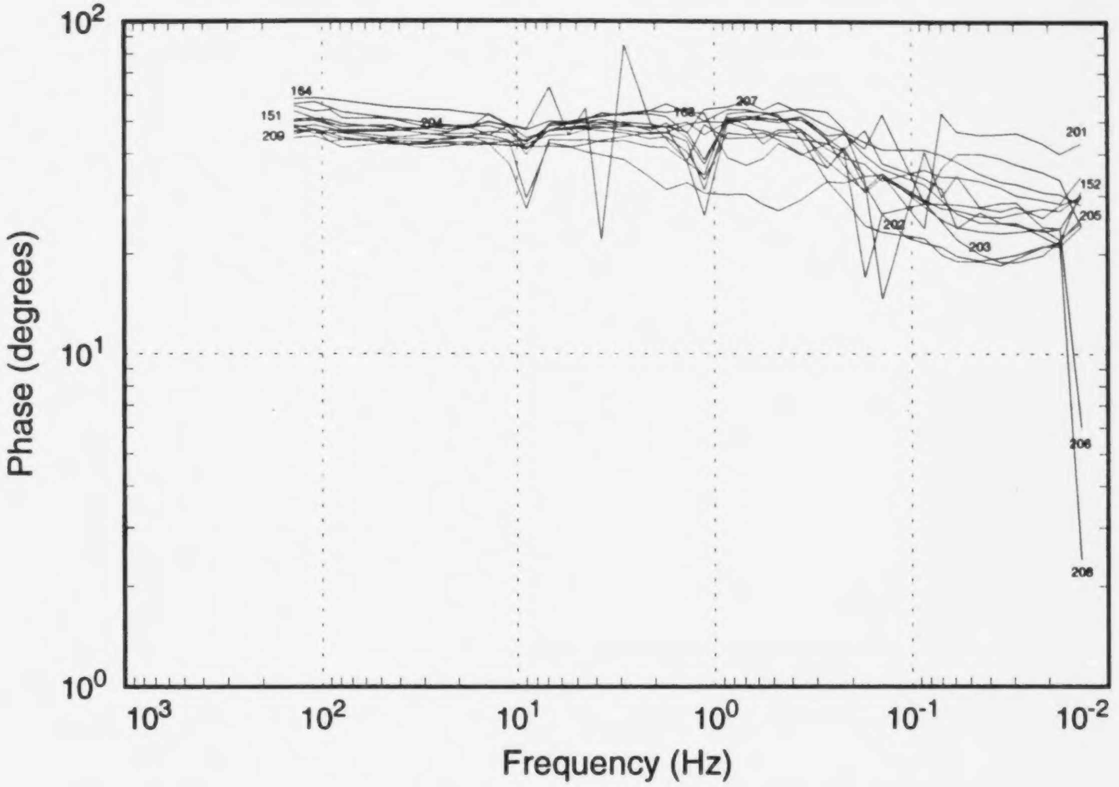

Fig.4.34b: Phase against frequency plot for 13 sites showing the independence of phase on static shift.

the apparent resistivity curve for site 201 is shifted relative to the other sites, the apparent resistivities of which generally lie close together (within one decade) at high frequencies. Site 201 is to the west of Hinton where the geology is structurally complex. The displacement of the apparent resistivity curve may, therefore, reflect geology rather than a static shift effect. For this reason, and since little shift is apparent amongst the other sites, no static shift correction was considered. Whaler and Zengeni (1993) note that static shifts are more common in areas where the surface is highly resistive which is not the situation encountered in west-central Alberta.

Reddy and Rankin(1971) made magnetotelluric measurements in the period range 1-1000 seconds at sixteen sites across central Alberta. They presented detailed results for thirteen of these sites. No detailed results were presented by them from the two sites (Gregg Lake and Foothills) that lie close to our survey area, though they do state that the anomalous results obtained in the rocky mountains (and foothills) probably stem from the complexity of the geology. This is reflected in anomalously large skew values at intermediate periods shown for two of our sites (206 and 207) that are to the west (toward the mountains) in our survey area. Analysis of the data in terms of three dimensional structures must be conducted in future.

Reddy and Rankin(1971) found the resistivities of the sedimentary column to be of the order of a few ohm meters, and this is consistent with what we have found. Basement resistivities were found by them to range from a few hundred to several thousand ohm meters. Their evidence from southeast of our study area (their site Alder Flats) suggests a Precambrian basement resistivity of 7000Ωm at 4.5km. None of our data suggest a resistivity this high. All the resistivities from our data lie below 1000Ωm in our study area even at depths greater than 10km. This suggests that our area is anomalous at depth with relatively low resistivities throughout. It is possible that the deep conductivity anomaly observed by Ingham et al(1983) is a local enhancement of a more widespread low resistivity zone in the upper crust.

It is evident that two effects occur in our study area. Relatively shallower low resistivity zones exist and are probably associated with saline fluids. These fluids have probably migrated upward along faults and fractures from the southwest and have transported heat to produce the thermal anomaly in the upper part of the section as described by Lam et al(1982). These uprising fluids have probably also carried the hydrocarbons from source to the south and west to produce the gas pools that occur in the area. The work of Lam and Jones(1985) has shown fluid salinities as high as 180,000 mg/L TDS in some formations (Mississippian and Upper Devonian). Secondly, it is evident that a relatively low resistivity zone (compared with the rest of central Alberta) occurs and appears to extend to some depth. This may be related to the Ingham et al (1983) magnetovariational anomaly and so supports their evidence of a highly conductive volume of rock that extends through much of the crust and may contain partial melt of tectonic origin. It is unlikely, though, that this relatively widespread conductive zone contributes substantially to the local geothermal anomaly in the upper sediments, though it may contribute to the slightly higher than normal heat flow in the area as a whole.

Attempts were made to compare the magnetotelluric results with seismic sections and available resistivity logs. The comparison with seismic sections was restricted to shallow depths because the seismic sections (proprietary information) supplied by Pan Canadian extended to only about 4-5km depth. The seismic sections revealed the presence of a triangle zone, which is a structural feature and may be related to the magnetotelluric results. The results of comparisons between magnetotelluric data and resistivity logs are presented in Chapter 5.

4.4 SUGGESTIONS FOR FURTHER WORK

There is always a need for additional data, and in particular, it will be beneficial to extend the measurements northward and westward to further explore the low resistivity zone detected there and which may be associated with the Ingham et al(1983) anomaly. In addition, more data from the present area, with more closely spaced stations and at longer period are needed in order to better understand the lateral extent of the observed features and to explore the resistivity structure at greater depth. Although there is no consensus yet on the optimum spacing between the MT stations, Jodicke et al.(1983) and Sule and Hutton(1986) suggested a spacing of the order of a few kilometers or less.

The magnetotelluric measurements provide much data. The present work has been concentrated on analysis and interpretation from the invariant data, but all the processed output such as upward and downward biased RHOXY, RHOYX, MAJOR, MINOR and INVARIANT, average RHOXY, RHOYX, MAJOR, MINOR and INVARIANT and the magnetic component may also be used for further analysis through inversion and modelling. Keeping in view the fact that most subsurface electrical structures are three dimensional, detailed two dimensional modelling and inversion and three dimensional modelling can be carried out. Construction of profiles, at all the sites, from model responses and their comparisons with field profiles may throw additional light on the question of adequacy of two dimensional models. It will be interesting to compare the results in this thesis with the ones obtained using the new package called GEOTOOLS which is an interactive magnetotelluric data processing system. It has been difficult in this work to relate the geophysical results with geology because of the unavailability of adequate published geological information. Extraction of additional geological information from well logs as well as further seismic data will provide a better understanding of the geophysical nature of the area.

There were several computational constraints involved during the course of this work because the programs and packages used were spread across several different computers and platforms. With the acquisition of a number of new computers and GEOTOOLS we hope to have all the programs running on a single operating platform in future.

CHAPTER 5

COMPARISON OF WELL LOGS WITH MAGNETOTELLURIC RESISTIVITIES

It is common practice, in geophysics, to compare the data obtained using different geophysical methods. This type of comparison often gives a better insight into the results primarily because of the inherent uncertainties involved in geophysical processing and interpretation. One of the secondary aims of this work was to compare the results from magnetotelluric data with the available well logs. Of the thirteen magnetotelluric sites in west-central Alberta five were situated at well sites. They are listed below with site numbers and the corresponding well identifiers.

Site Number	**Well Identifier**
152	08-32-51-19-W5 (Nova et al Fickle)
163	10-34-51-22-W5 (Gulf et al Medlod)
201	06-28-49-26-W5 (Shell-Home Brule)
204	11-34-50-23-W5 (Esso Banshee)
205	10-04-51-21-W5 (Citadel et al Lambert)

Several comparisons between the results from the magnetotelluric measurements and the well log data can be made. These are Bostick-log, Fischer-log, MT-log models and statistical correlation. In the Bostick-log and Fischer-log methods, the magnetotelluric data must first be inverted using Bostick or Fischer inversions to obtain the layer parameters and these are then compared with the distributions of resistivities with depth from well logs.

These two methods were not used here primarily because of the inherent non-uniqueness of the inversion schemes. The statistical correlation method was not used for similar reasons.

The MT-log models method used in this work is believed to be the least ambiguous. The procedure involves construction of several one dimensional models from well logs and calculating their forward model responses and then comparing those with the magnetotelluric data. In the present work for the five sites, 1 to 5 models were constructed and their forward responses calculated, the output being apparent resistivities and phases for the given set of frequencies. To construct the models, average resistivities for different depth intervals were determined from well logs. The interval lengths were 50m, 100m, 200m, 400m and 800m respectively for models 1 to 5. The model responses along with the magnetotelluric apparent resistivities and phases are shown in Figs. 5.1 through 5.5. The horizontal axes show the frequencies, in hertz, while the vertical axes show apparent resistivities and phases in Ohm-m and degrees respectively.

A careful look at Figs.5.1 a and b reveals that the general natures of the model responses and the magnetotelluric apparent resistivity curves are similar. The measured curve is displaced from the model curves at higher frequencies. This may be a result of a "static shift" effect in the magnetotelluric results (Jones, 1988; Jiracek, 1990). At lower frequencies, the measured values lie closer to the model 1 results than to the other model results. This may reflect the fact that the model resistivity values at depth are assumed values based on the deepest known log values and may not well represent the true resistivities. The comparison of the phase responses for this well and the models in Fig.5.1b shows that the phase is better represented by models 2 and 3 particularly at lower frequencies. This implies that the values chosen for the models for below the log depths are more appropriate than for the other models.

The results for site 163 (Fig.5.2) are disappointing. The magnetotelluric data from this site are very good and it is not known why the comparison in this figure is so poor.

In Figs.5.3a and b, the natures of the curves are similar with the difference that in Fig5.3a, the resistivity model response curves are shifted downwards. This shift may be related to a static shift in the magnetotelluric data. There is a fairly good degree of match in Figs.5.4a and b between the magnetotelluric data and model response curves at low as well as high frequencies. The match is not good in the medium frequency range. In Fig.5.5a, as in Fig.5.3a, there is a shift in the apparent resistivity model response curve. The phase response shows some degree of match at higher frequencies as seen in Fig.5.5b. The cause of the shift is not known.

It has not been possible to quantify the degree of match or mismatch between the model responses and the field data primarily because of a number of severe limitations. As mentioned, the well data extended over only part of the section and, therefore, the deep resistivities could not be determined and were taken constant and equal to the value of the resistivity in the deepest interval of the well. Similarly, some of the near surface resistivities were not known for the well data. Another limitation was the format of the well data. The data were available only in analog form on charts and not as digitized data. This imposed severe restrictions on data manipulation. Moreover, the well logs were available only for the five sites considered above. To be able to quantify this type of comparison, it necessary to have digitized deep well logs for a large number of sites.

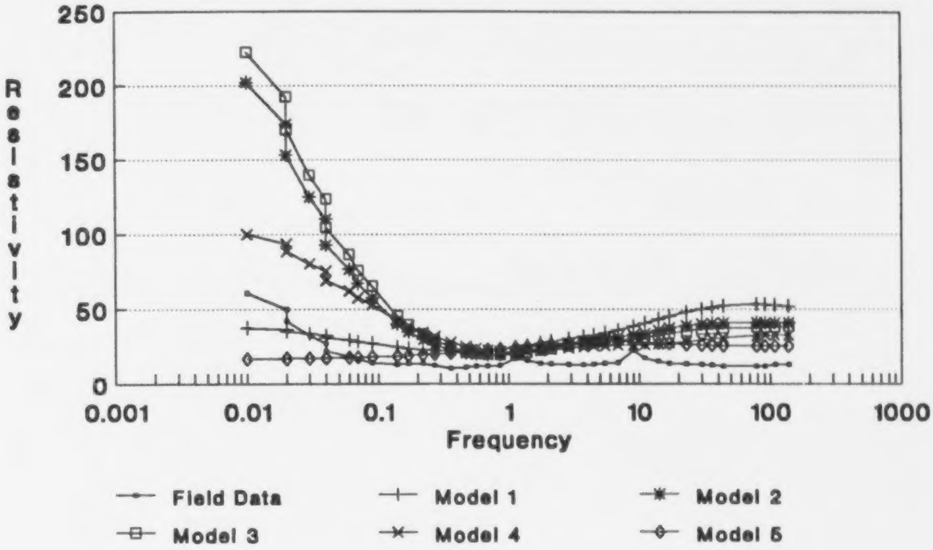

Fig.5.1a: Resistivity and model responses for site 152.

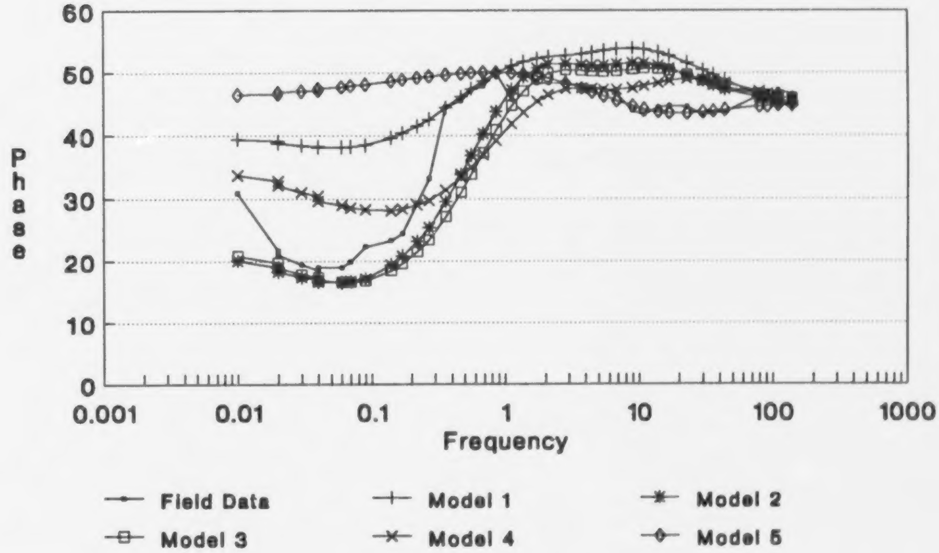

Fig.5.1b: Phase and model responses for site 152.

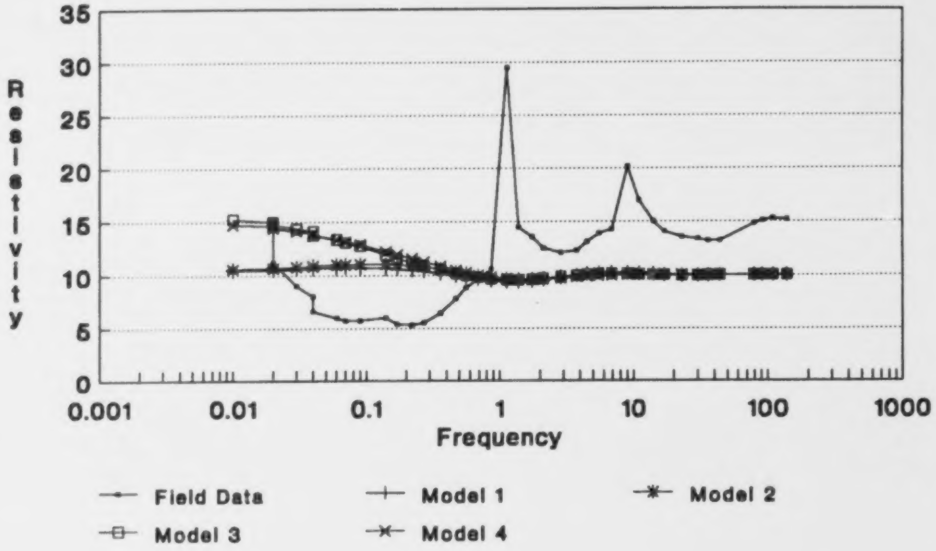

Fig.5.2a: Resistivity and model responses for site 163.

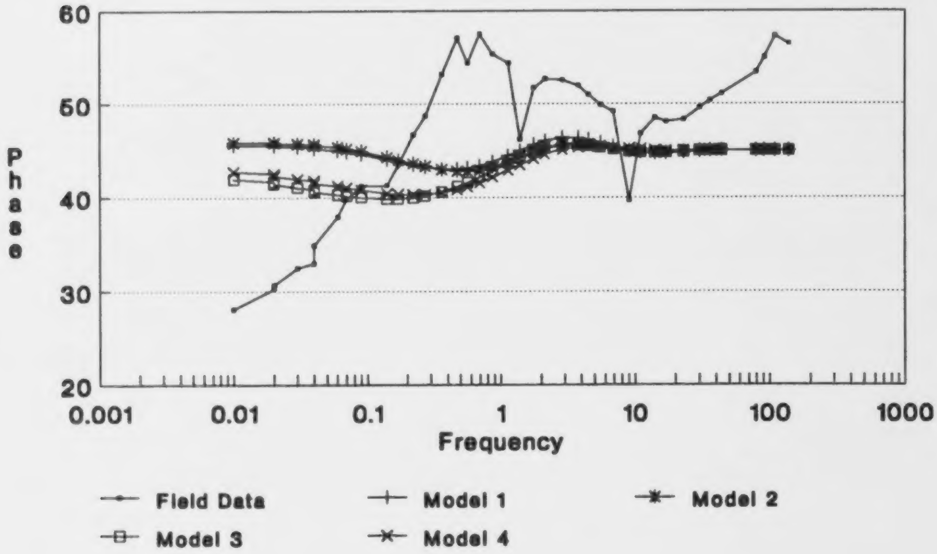

Fig.5.2b: Phase and model responses for site 163.

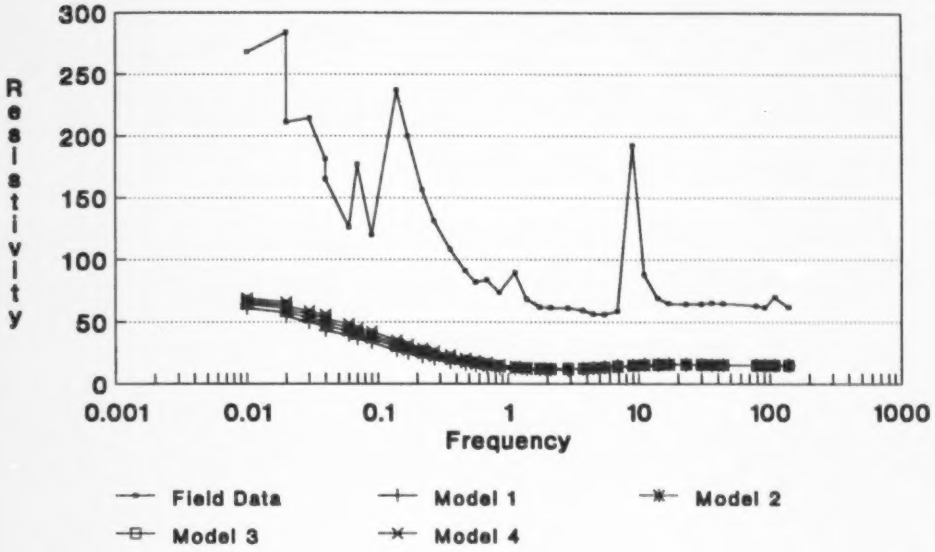

Fig.5.3a: Resistivity and model responses for site 201.

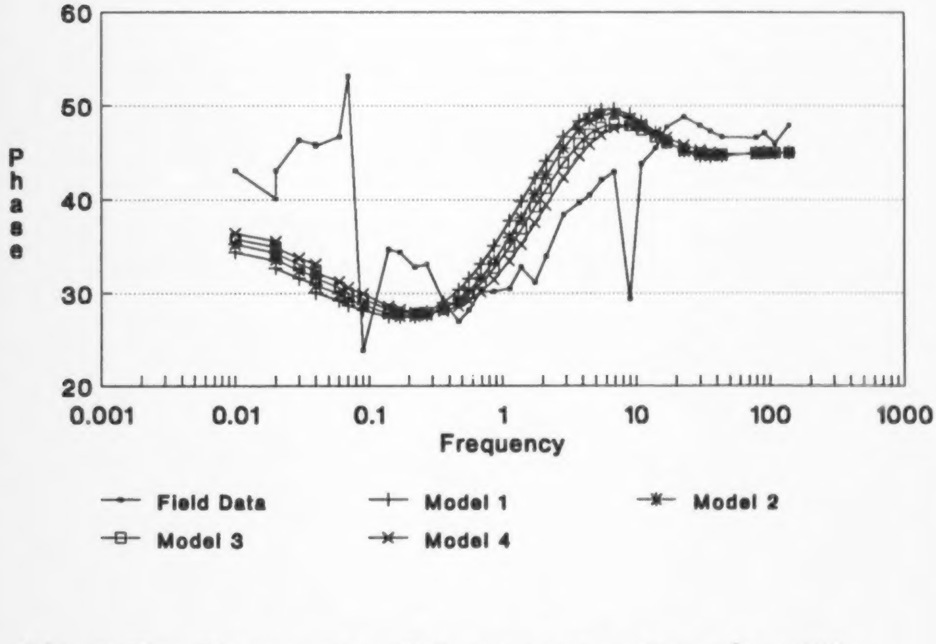

Fig.5.3b: Phase and model responses for site 201.

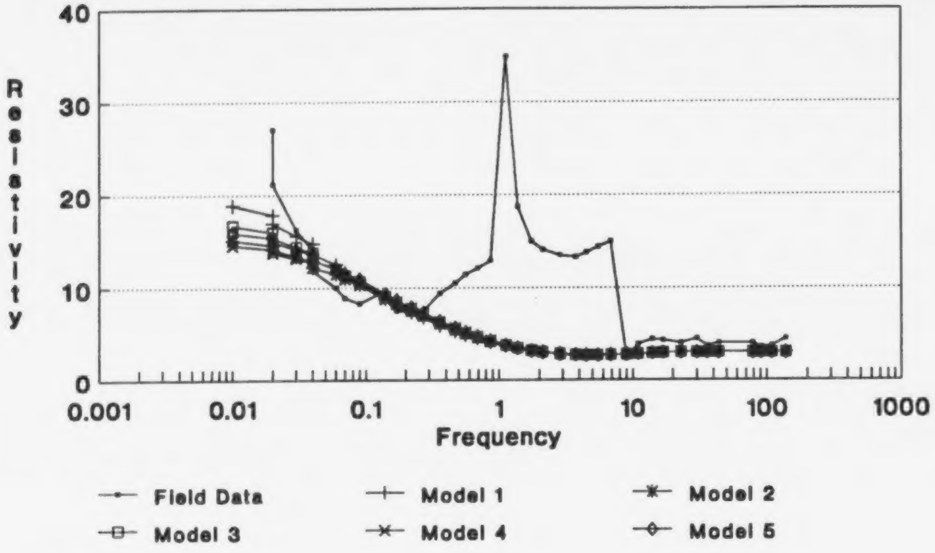

Fig.5.4a: Resistivity and model responses for site 204.

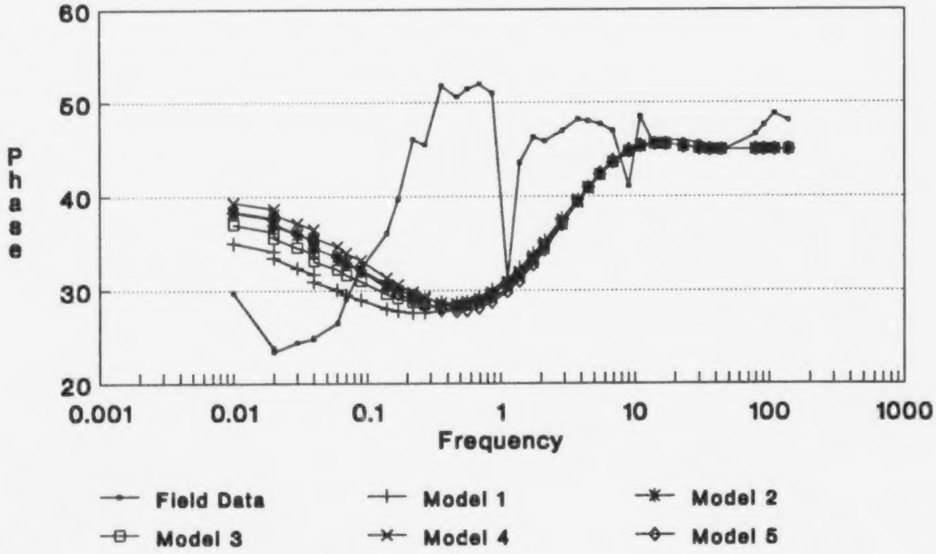

Fig.5.4b: Phase and model responses for site 204.

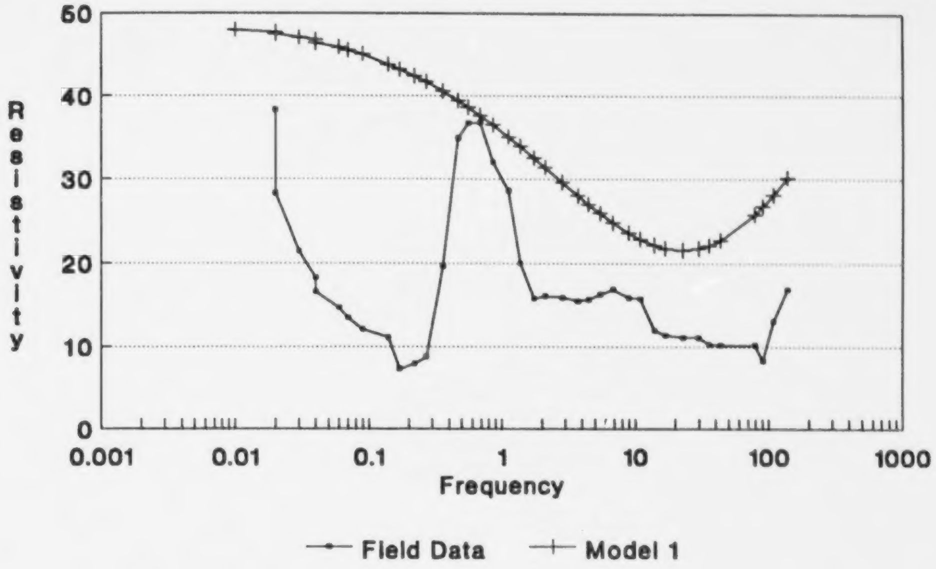

Fig.5.5a: Resistivity and model responses for site 205.

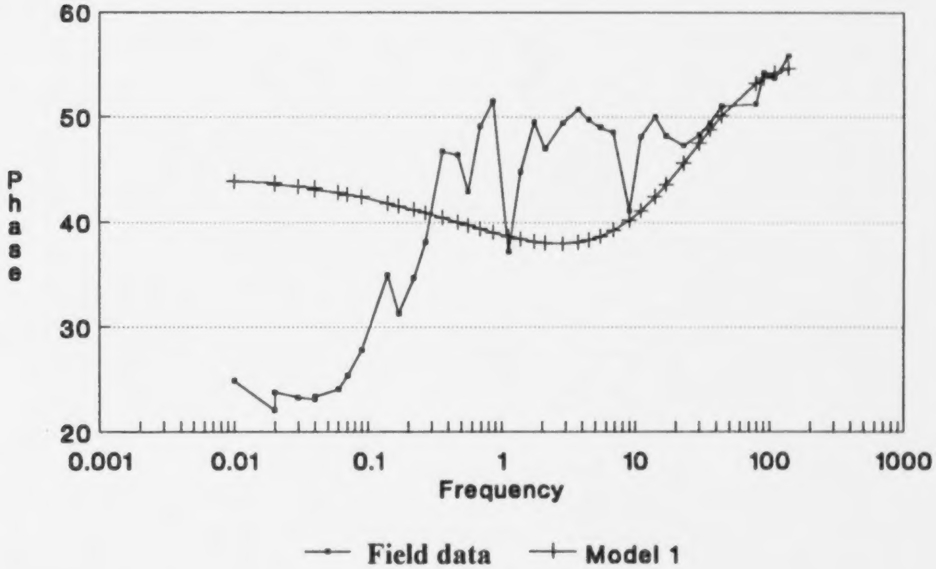

Fig.5.5b: Phase and model responses for site 205.

BIBLIOGRAPHY

Archie, G., 1942, The resistivity log as an aid in determining some reservoir characteristics; Trans. Am. Inst. Min. Metall. Engrs., vol.146, p.54-61.

Beamish, D., 1986, Geoelectric structural dimensions from magnetotelluric data: methods of estimation, old and new; Geophysics, vol.51, 1298-1309.

Berdichevsky, M.N., Vanyan, L.L., Feldman, I.S. and Porstendorfer G., 1972, Conducting layers in the earth's crust and upper mantle; Beitr. Geophys., vol.81, p.187-196.

Berdichevsky, M.N. and Dmitriev, V.I., 1976, Basic principles of interpretation of magnetotelluric curves in geoelectric and geothermal studies; Adam, A., Ed., Akademini Kiado, 165-221.

Bostick, F.X,Jr., 1977, A simple almost exact method of MT analysis; Abstract in Workshop on Electrical Methods in Geothermal Exploration, Snowbird, Utah.

Cagniard, L., 1953, Basic theory of magneto-telluric method of geophysical prospecting; Geophysics, vol.18, p.605-635.

Camfield, P.A., Gough, D.I. and Porath, H., 1971, Magnetometer array studies in north-western United States and south-western Canada; Geophys. J. R. astr. Soc., vol.22, p.202-221.

Camfield, P.A. and Gough, D.I., 1977, A possible Proterozoic plate boundary in North America; Canadian Jour. Earth Sciences, vol.14, p.1229-1238.

Clerc, G., 1971, Contribution of the optimization of sensors designed to measure terrestrial magnetic field variations from (10^{-3} to 10^4 Hz); Thesis, Doctor of Engineering (Physics), University of Paris (in French).

Cochrane, N.A. and Hyndman, 1974, Magneto-telluric and magneto-variational studies in Atlantic Canada; Geophys. J. R. astr. Soc., vol.20, p.385-406.

Coggon, J.H., 1971, Electromagnetic and electrical modelling by the finite element method; Geophysics, vol.36, p.132-155.

Collet, L.S. and Katsube, T.J., 1973, Electrical parameters of rocks in developing geophysical techniques; Geophysics, vol.38, p.76-91.

de Beer, J.H., van Zyl, J.S.V. and Gough, D.I., 1982, The Southern Cape conductive belt (South Africa): its composition, origin and tectonic significance; Tectonophys., vol.83, p.205-225.

Dobrin, M.B. and Savit, C.H., 1988, Introduction to geophysical prospecting; McGraw-Hill Book Company.

Dvorak, Z., 1975, Electrical conductivity models of the crust; Canadian Jour. Earth Sciences, vol.12, p.962-970.

ERCB, 1982, Alberta Reserves of oil, gas, natural gas liquids and sulphur.

Fischer, G. and Le Quang, B.V., 1982, Parameter trade-off in one-dimensional magnetotelluric modelling; J. Geophysics, vol.51, p.206-215.

Geological Survey of Canada, 1981, Gas pools of western Canada; map 1558A.

Grant, F.S and West, G.F., 1965, Interpretation theory in applied geophysics; McGraw-Hill Book Company

Greenhouse, J.P. and Bailey, R.C, 1981, A review of geomagnetic variation measurements in the eastern United

States: implications for continental tectonics; Canadian Jour. Earth Sciences, vol.18, p.1268-1289.

Hohmann, G.W., 1971, Electromagnetic scattering by conductors in the earth near a line source current; Geophysics, vol.36, p.101-131.

Hutton, V.R.S., Gough, D.I., Dawes, G.J.K. and Travassos J., 1987, Magnetotelluric soundings in the Canadian Rocky mountains; Geophys. J. R. astr. Soc., vol.90, p.245-263.

Hyndman, R.D. and Hyndman, D.W., 1968, Water saturation and high electrical conductivity in the lower continental crust; Earth and Planet. Sci. Letters, vol.4, p.427-432.

Ingham, M.R., Bingham, D.K. and Gough, D.I., 1983, A magnetovariational study of a geothermal anomaly; Geophys. J. R. astr. Soc., vol.72, p.597-618.

Jacobs, J.A., 1964, Micropulsations of the earth's electromagnetic field in the frequency range of 0.1 to 10 CPS; in Natural Electromagnetic Phenomena Below 300kc/s, Plenum Press, N.Y.

Jiracek, G.R., 1990, Near surface topographic distortions in electromagnetic induction; Surveys in Geophysics, vol.11, p.163-203.

Jodicke, H., Untiedt, J., Olgemann, W., Schulte L. and Wagenitz, V., 1983, Electrical conductivity structure of the crust and upper mantle beneath the Rhenish Massif, in Plateau Uplift, p.288-362, ed. Fuchs, K. et al, Springer-Verlag, Berlin.

Jones, A.G., 1988, Static shift of magnetotelluric data and its removal in a sedimentary basin environment; Geophysics, vol.53, p.967-978.

Jones, F.W. and Price, A.T., 1970, The perturbations of alternating geomagnetic fields by conductivity anomalies; Geophys. J. R. astr. Soc., vol.20, p.317-334.

Jones, F.W., 1971, Electromagnetic induction in a non-horizontally stratified two-layered conductor; Geophys. J. R. astr. Soc., vol.22, p.17-28.

Jones, F.W. and Pascoe, L.J., 1971, A general computer program to determine the perturbation of alternating electric currents in a two-dimensional model of a region of uniform conductivity with an embedded inhomogeneity; Geophys. J. R. astr. Soc., vol.24, p.3-30.

Jones, F.W., 1972, The electromagnetic perturbation fields of conductivity anomalies within the earth; Geophys. J. R. astr. Soc., vol.30, p.211-228.

Jones, F.W., Kushigbor, C., Lam, H.L., Majorowicz, J.A. and Rahman, M., 1984, Estimates of terrestrial thermal gradients and heat flow variations with depth in the Hinton-Edson area of the Alberta basin derived from petroleum bottom-hole temperature data; Geophys. Pros., vol.32, p.1111-1130.

Karmann, R., 1975, Optimization of the signal/noise ratio of inductance coil magnetometers for magnetotellurics; Thesis, Doctor of Engineering, Brauschweig Technical University.

Karmann, R., 1977, Search coil magnetometers with optimum signal-to-noise ratio; Acta. Geodaet. Geophys. Mont., vol.12, p.353-357.

Kaufman, A.A. and Keller, G.V., 1981, The magnetotelluric sounding method; Elsevier Science Publishing Co. Inc., Amsterdam.

Keller, G.V. and Frischknecht, F.C., 1966, Electrical methods of geophysical prospecting; Pergamon Press, N.Y.

Keller, G.V., 1987, Rock and mineral properties in: Electromagnetic Methods in Applied Geophysics - Theory, Volume 1, Nabighian, M.N. and Corbett, J.D. (eds), Investigations in Geophysics, Volume 3, SEG, p.13-51.

Lam, H.L., Jones, F.W. and Lambert, C., 1982, Geothermal gradients in the Hinton area of west-central Alberta; Canadian Jour. Earth Sciences, vol.19, p.755-766.

Lam, H.L. and Jones, F.W., 1985, Geothermal energy potential in the Hinton-Edson area of west-central Alberta; Canadian Jour. Earth Sciences, vol.22, p.369-383.

Madden, T.R. and Nelson, P.H., 1964, A defense of Cagniard's magnetotelluric method; ONR report, project NR-371-401, Geophysics Lab., M.I.T.

Madden, T.R. and Thompson, W., 1965, Low frequency electromagnetic oscillations of the earth-ionosphere cavity; Reviews of Geophysics, vol.3, p.211-254.

Majorowicz, J.A., Jones, F.W., and Lam, H.L., 1984, A comment on 'A magnetovariational study of a geothermal anomaly' by M.R. Ingham, D.K. Bingham and D.I. Gough; Geophys. J. R. astr. Soc., vol.76, p.667-672.

Nabighian, M.N., 1987, Electromagnetic Methods in Applied Geophysics, Volume 1, Theory; Investigations in Geophysics no.3, SEG, Tulsa, Oklahoma.

Neves, A., 1957, The generalized magnetotelluric method; Unpublished Ph.D. thesis, M.I.T.

Oldenburg, D.W., 1978, One dimensional inversion of natural source magnetotelluric observations; Geophysics, vol.44, p.1218-1244.

Olhoeft, G.R., 1980, Electrical properties of rocks, in: Physical properties of rocks and minerals, Thoulaikian, Y.S., Judd, W.R. and Roy, R.F. (eds), McGraw Hill Book Co., New York, p.257-330.

Orange, A.S., 1989, Magnetotelluric exploration for hydrocarbons; Inst. Elect. and Electron. Eng. Proc., vol.77, p.287-317.

Park, S.K., Orange, A.S. and Madden, T.R., 1983, Effects of three-dimensional structure on magnetotelluric sounding curves; Geophysics, vol.48, p.1402-1405.

Parkinson, W.D., 1962, Influence of continents and oceans on geomagnetic variations; Geophys. J. R. astr. Soc., vol.6, p.441-449.

Parkinson, W.D., 1983, Introduction to Geomagnetism; Scottish Academic Press, Edinburgh, Scotland.

Parkhomenko, E.I., 1982, Electrical resistivity of minerals and rocks at high temperature and pressure; Rev. Geophys. and Space Phys., vol.29, p.193-218.

Patra, H.P. and Mallick, K., 1980, Geosounding Principles, 2; Elsevier Scientific Publishing Company, Amsterdam.

Petiau, G. and Dupis, A., 1980, Noise, temperature coefficient and long time stability of electrodes for telluric observations; Geophys. Prospecting, vol.28, p.792-804.

Price, A.T., 1962, The theory of magnetotelluric method when the source field is considered; J. Geophys. Res., vol.67, p.1907-1919.

Reddy, I.K. and Rankin, D., 1971, Magnetotelluric measurements in Central Alberta; Geophys., vol.36, p.739-753.

Reddy, I.K. and Rankin, D., 1973, Magnetotelluric response of two-dimensional sloping contact by finite element method; Pure Appl. Geophys., vol.105, p.847-857.

Reddy, I.K., Rankin, D. and Phillips, R.J., 1977, Three dimensional modelling in magnetotelluric and magnetic variation sounding; Geophys. J. R. astr. Soc., vol.51, p.313-325.

Rokityanski, I.I., 1982, Geoelectromagnetic investigation of the earth's crust and mantle; Springer-Verlag, Berlin.

Schumann, W.O., 1957, Electrische Eigens Chwingungen des Holraumes Erde-Luft; Ionospare irregt durch Blitzentlardungen. Z. Agnew. Phys., vol.9, p.373-378.

Shankland, T.J. and Waff, H.S., 1974, Conductivity in fluid bearing rocks; J. Geophys. Res., vol.79, p.4863-4868.

Shankland, T.J. and Waff, H.S., 1977, Partial melting and electrical conductivity anomalies in the upper mantle; J. Geophys. Res., vol.82, p.5409-5417.

Sims, W.E., Bostick, F.X. and Smith, H.W., 1971, The estimation of magnetotelluric impedance tensor elements from measured data; Geophysics, vol.36, p.938-942.

SPAM Reference Manual, 1981, University of Edinburgh, UK.

Srivastava, S.P., 1965, Method of interpretation of magnetotelluric data when the source field is considered; J. Geophys. Res., vol.70, p945-954.

Stanley, W.D. and Tinkler, R.D., 1982, A practical low noise coil system for magnetotellurics; Open file report, U.S. Geological Survey.

Stesky, R.M. and Brace, W.F., 1973, Electrical conductivity of serpentinized rocks to kilobars; J. Geophys. Res., vol.78, p.7614-7621.

Sule, P.O. and Hutton, V.R.S., 1986, A broadband magnetotelluric study in SE Scotland - data acquisition analysis and one dimensional modelling, Ann.Geophys., vol.4, p.145-156.

Swift, C.M.,Jr., 1967, A magnetotelluric investigation of an electrical conductivity anomaly in the southwestern United States; Ph.D. thesis, M.I.T.

Swift, C.M.,Jr., 1971, Theoretical magnetotelluric and Turam response from two-dimensional inhomogeneities; Geophysics, vol.36, p.38-52.

Tikhonov, A.N., 1950, On determining electrical characteristics of deep layers of the earth's crust; Dokl. Akad. Nauk., S.S.S.R., vol.73, p295-297.

Ting, S.C. and Hohmann, G.W., 1981, Integral equation modelling of three dimensional magnetotelluric response; Geophysics, vol.46, 182-197.

Vozoff, K., 1972, The magnetotelluric method in exploration of sedimentary basins; Geophysics, vol.37, p.98-141.

Vozoff, K., 1986, Magnetotelluric methods; Geophysics reprint series no.5, SEG, Tulsa, Oklahoma.

Vozoff, K., 1991, The magnetotelluric method; in Electromagnetic Methods in Applied Geophysics, vol.2, part B, Chapter 8, p.641-711, Edited by Misac N. Nabighian, SEG, Tulsa, Oklahoma.

Wait, J.R., 1954, On the relation between telluric currents and the earth's magnetic field; Geophysics, vol.19, p.281-289.

Weaver, J.T. and Fischer, G., 1990, Finding a one dimensional layered model: A combination of the Niblett-Bostick and Fischer-LeQuang Schemes; 10th workshop on EM induction in the earth, Ensenada, Mexico.

Weinstock, H. and Overton, W.C., Jr., 1981, SQUID applications to geophysics; SEG, Tulsa, Oklahoma.

Whaler, K.A. and Zengeni, T.G., 1993, An audiofrequency magnetotelluric traverse across the Mana Pools Basin, northern Zimbabwe; Geophys.J.Int., v.114, p.673-686.

Wu, F.T., 1968, The inverse problem of magnetotelluric sounding; Geophysics, vol.33, p.972-979.

APPENDIX A

All the figures in Appendix A appear in the same order as Figs.3.3a through 3.3e with each figure showing the site number at the top.

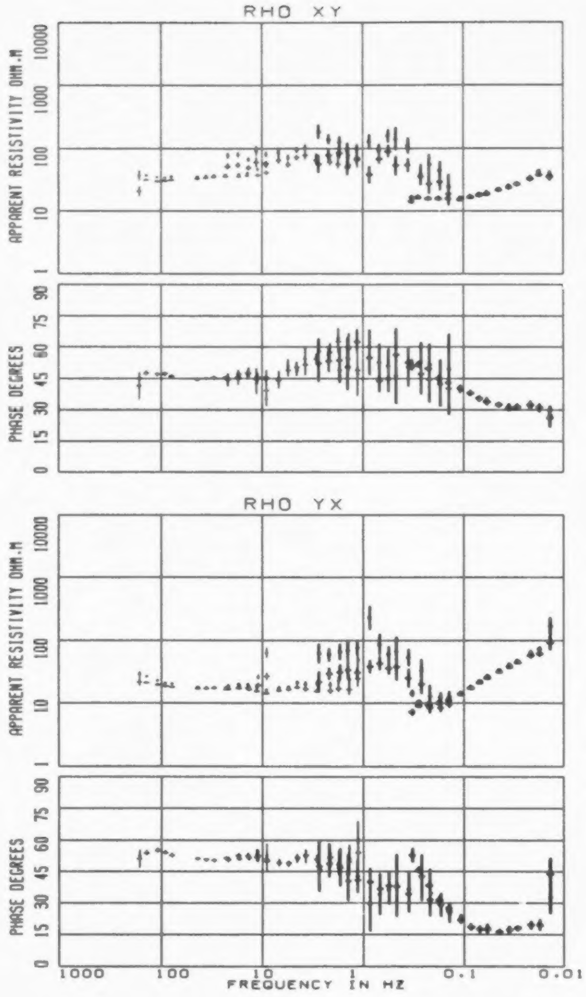

SITE : 151 TELLURIC

CARTRIDGE	:	S1510	S1511	S1512	S1513
BAND	:	0	1	2	3
COMPONENTS	:	5	5	5	5
SAMPLES/WINDOW	:	256	256	256	256
NUMBER WINDOWS	:	96	48	48	48
SAMPLE RATE HZ	:	512	64	8	1
PLOT HPF	:	8.0	1.0	0.1	0.010
PLOT LPF	:	180.0	24.0	3.0	0.350
FREQS/DECADE	:	10	10	10	10
FREQS/BAND	:	13	14	14	15
MIN COHERENCY	:	0.80	0.80	0.80	0.80
REJECTION LOOPS	:	2	2	2	2

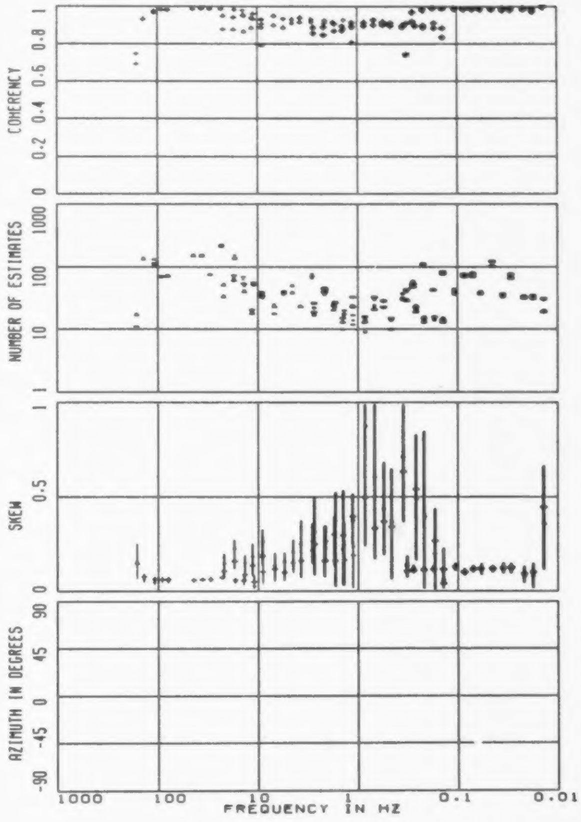

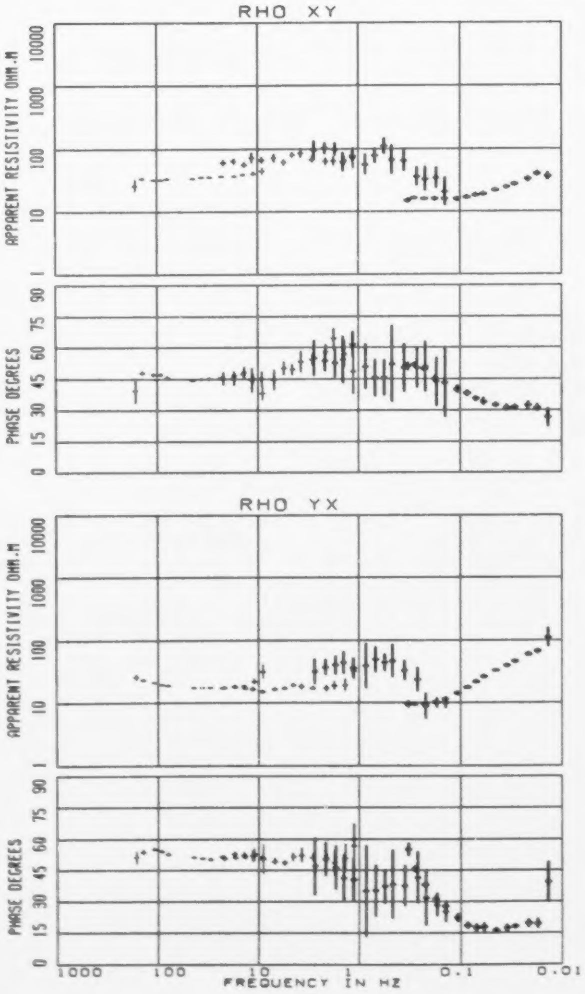

SITE : 151 TELLURIC

CARTRIDGE	:	S1510	S1511	S1512	S1513
BAND	:	0	1	2	3
COMPONENTS	:	5	5	5	5
SAMPLES/WINDOW	:	256	256	256	256
NUMBER WINDOWS	:	96	48	48	48
SAMPLE RATE HZ	:	512	64	8	1
PLOT HPF	:	8.0	1.0	0.1	0.010
PLOT LPF	:	180.0	24.0	3.0	0.350
FREQS/DECADE	:	10	10	10	10
FREQS/BAND	:	19	14	14	15
MIN COHERENCY	:	0.80	0.80	0.80	0.80
REJECTION LOOPS	:	2	2	2	2

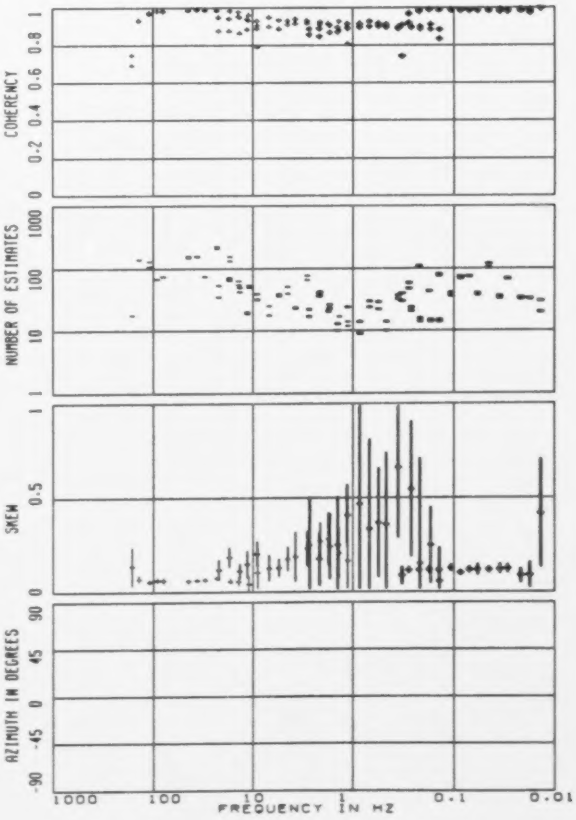

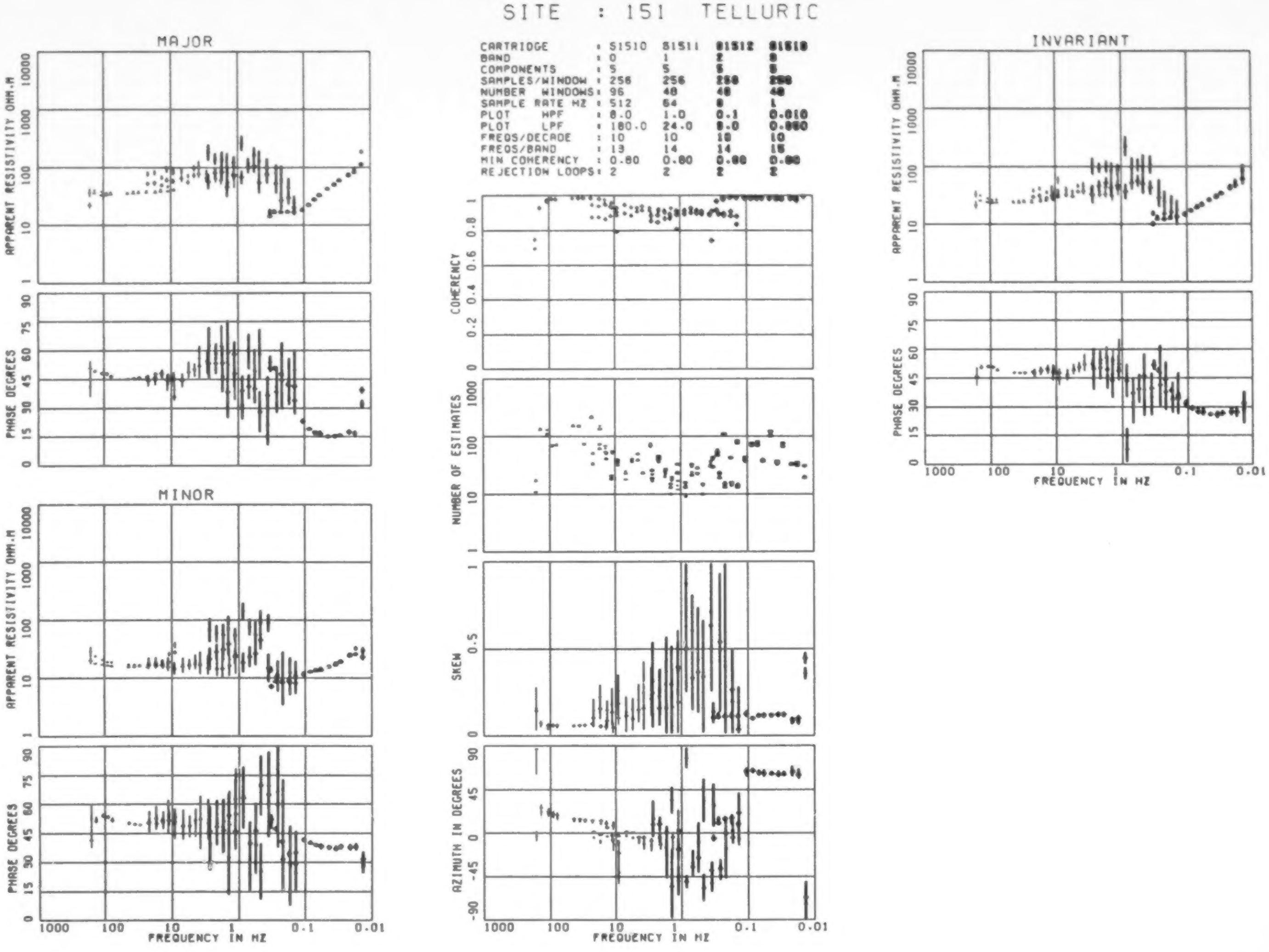

SITE : 151 TELLURIC

CARTRIDGE	S1510	S1511	S1512	S1513
BAND	0	1	2	3
COMPONENTS	5	5	5	5
SAMPLES/WINDOW	256	256	256	256
NUMBER WINDOWS	96	48	48	48
SAMPLE RATE HZ	512	64	8	1
PLOT HPF	8.0	1.0	0.1	0.010
PLOT LPF	180.0	24.0	[illegible]	[illegible]
FREQS/DECADE	10	10	10	10
FREQS/BAND	13	14	14	15
MIN COHERENCY	0.80	0.80	0.80	0.80
REJECTION LOOPS	2	2	2	2

SITE : 151 TELLURIC

CARTRIDGE	: S1510	S1511	S1512	S1513
BAND	: 0	1	2	3
COMPONENTS	: 5	5	5	5
SAMPLES/WINDOW	: 256	256	256	256
NUMBER WINDOWS	: 96	48	48	48
SAMPLE RATE HZ	: 512	64	8	1
PLOT HPF	: 8.0	1.0	0.1	0.010
PLOT LPF	: 180.0	24.0	3.0	0.360
FREQS/DECADE	: 10	10	10	10
FREQS/BAND	: 13	14	14	15
MIN COHERENCY	: 0.80	0.80	0.80	0.80
REJECTION LOOPS	: 2	2	2	2

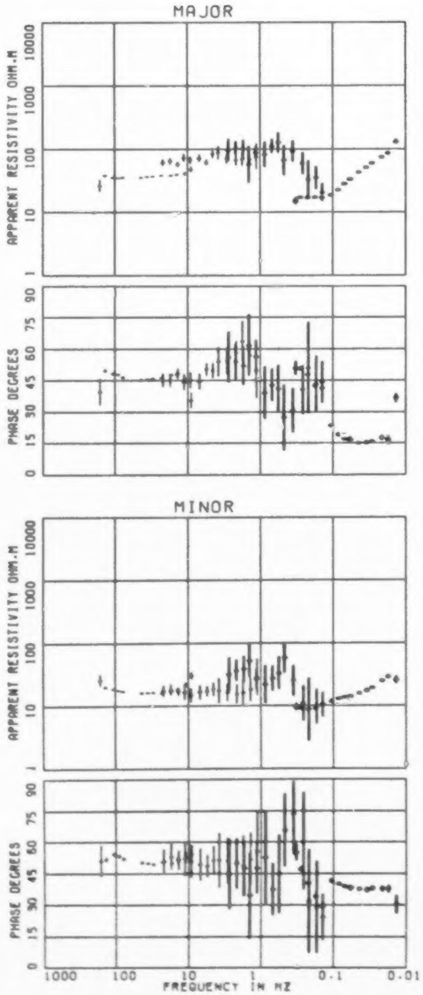

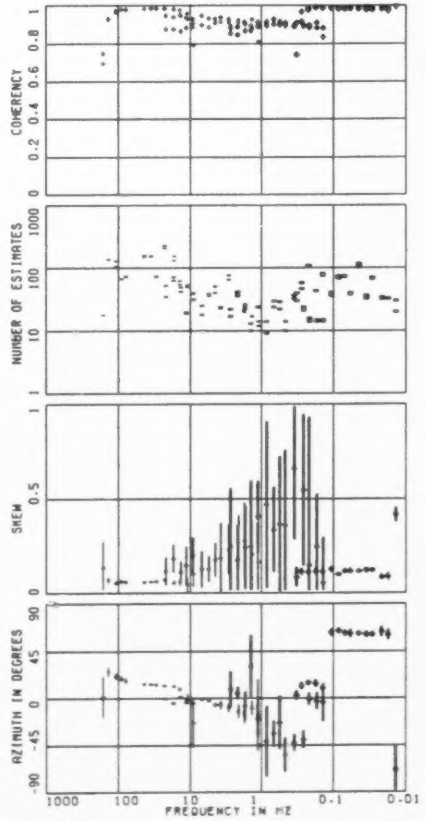

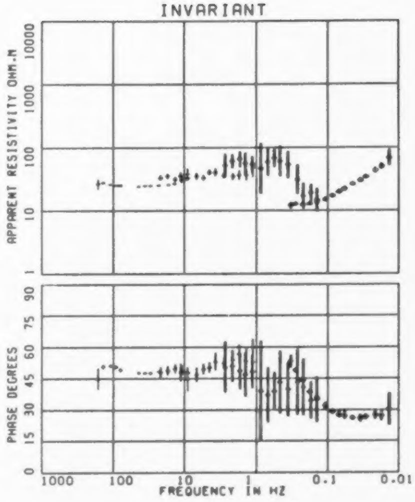

SITE : 151 MAGNETIC

CARTRIDGE :	S1510	S1511	S1512	S1513
BAND :	0	1	2	3
COMPONENTS :	5	5	5	5
SAMPLES/WINDOW :	256	256	256	256
NUMBER WINDOWS :	96	48	48	48
SAMPLE RATE HZ :	512	64	8	1
PLOT HPF :	8.0	1.0	0.1	0.010
PLOT LPF :	180.0	24.0	3.0	0.350
FREQS/DECADE :	10	10	10	10
FREQS/BAND :	13	14	14	13
MIN COHERENCY :	0.70	0.70	0.70	0.70
REJECTION LOOPS :	2	2	2	2

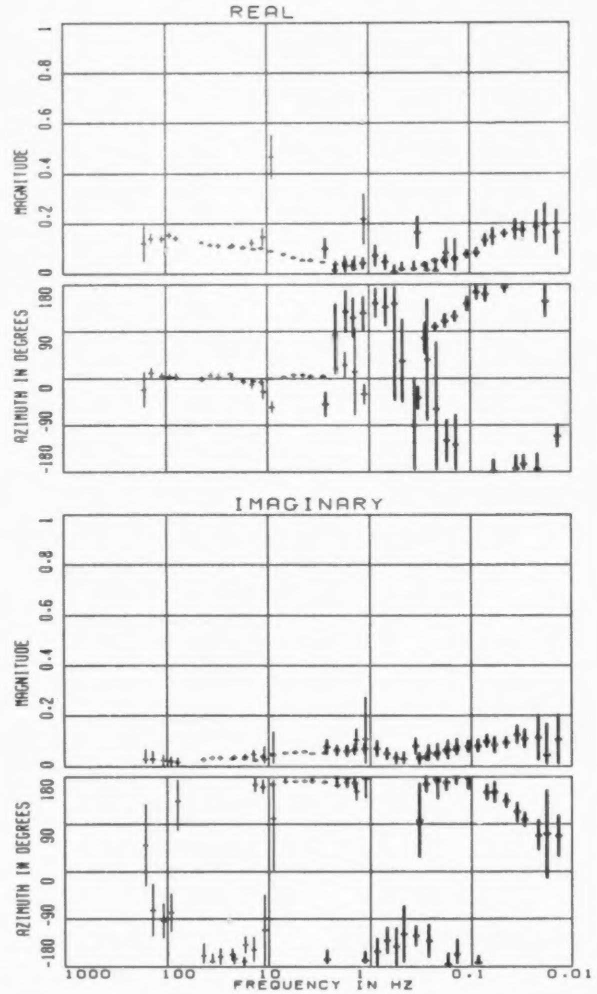

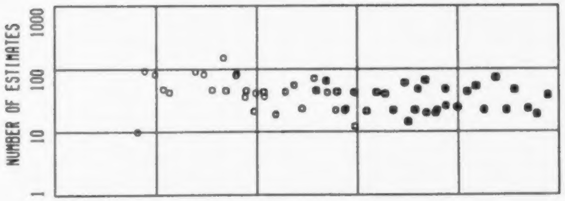

SITE : 152 TELLURIC

CARTRIDGE	:	µ1520	µ1521	µ1522	µ1523
BAND	:	0	1	2	3
COMPONENTS	:	5	5	5	5
SAMPLES/WINDOW	:	256	256	256	256
NUMBER WINDOWS	:	48	48	48	48
SAMPLE RATE HZ	:	512	64	8	1
PLOT HPF	:	8.0	1.0	0.1	0.010
PLOT LPF	:	180.0	24.0	3.0	0.350
FREQS/DECADE	:	10	10	10	10
FREQS/BAND	:	13	14	14	15
MIN COHERENCY	:	0.80	0.80	0.80	0.80
REJECTION LOOPS	:	2	2	2	2

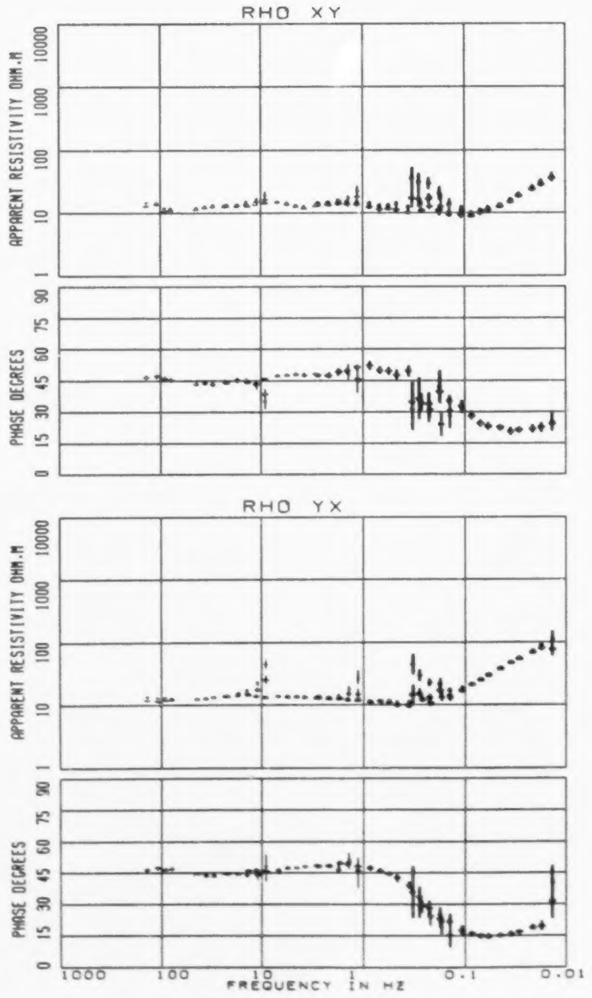

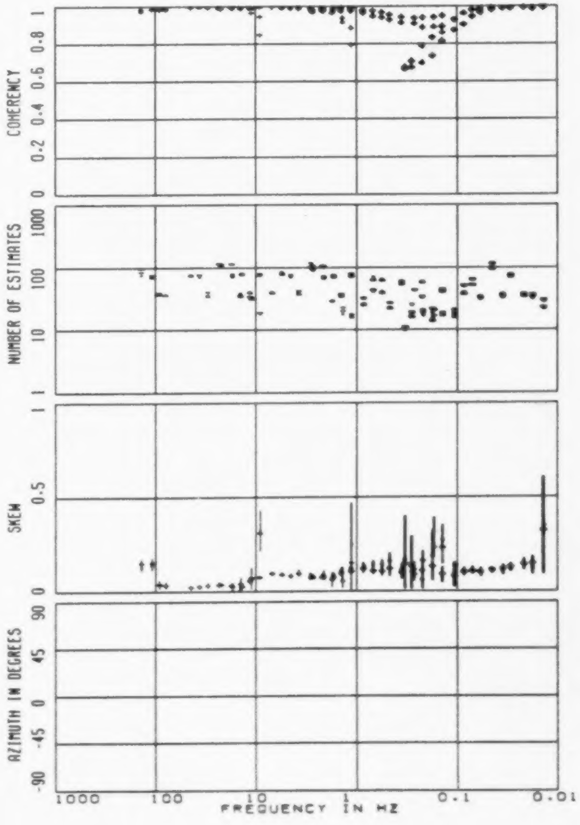

RHO XY

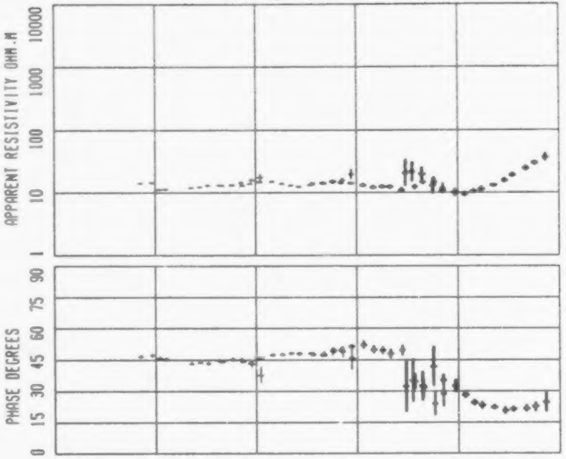

RHO YX

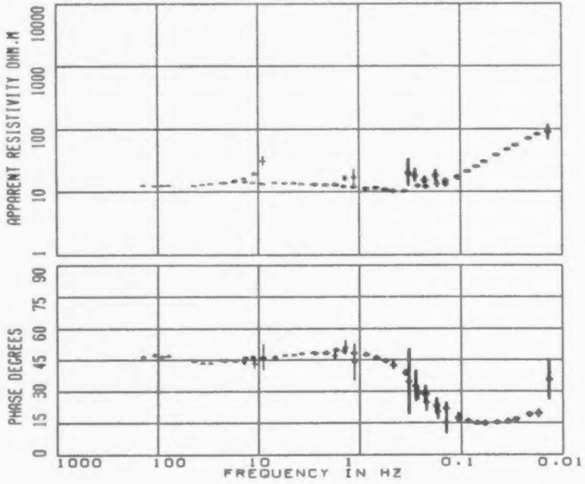

SITE : 152 TELLURIC

CARTRIDGE	:	W1520	W1521	W1522	W1523
BAND	:	0	1	2	3
COMPONENTS	:	5	5	5	5
SAMPLES/WINDOW	:	256	256	256	256
NUMBER WINDOWS	:	48	48	48	48
SAMPLE RATE HZ	:	512	64	8	1
PLOT HPF	:	8.0	1.0	0.1	0.010
PLOT LPF	:	180.0	24.0	3.0	0.350
FREQS/DECADE	:	10	10	10	10
FREQS/BAND	:	13	14	14	15
MIN COHERENCY	:	0.80	0.80	0.80	0.80
REJECTION LOOPS	:	2	2	2	2

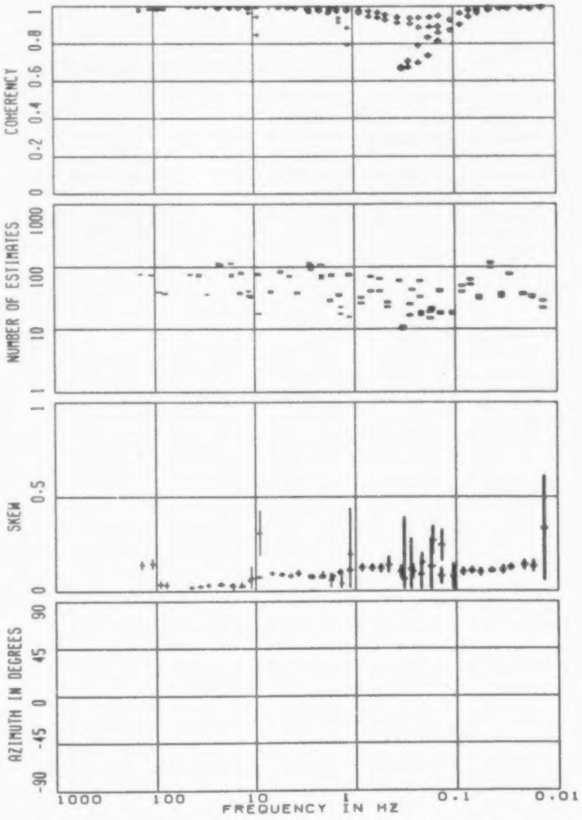

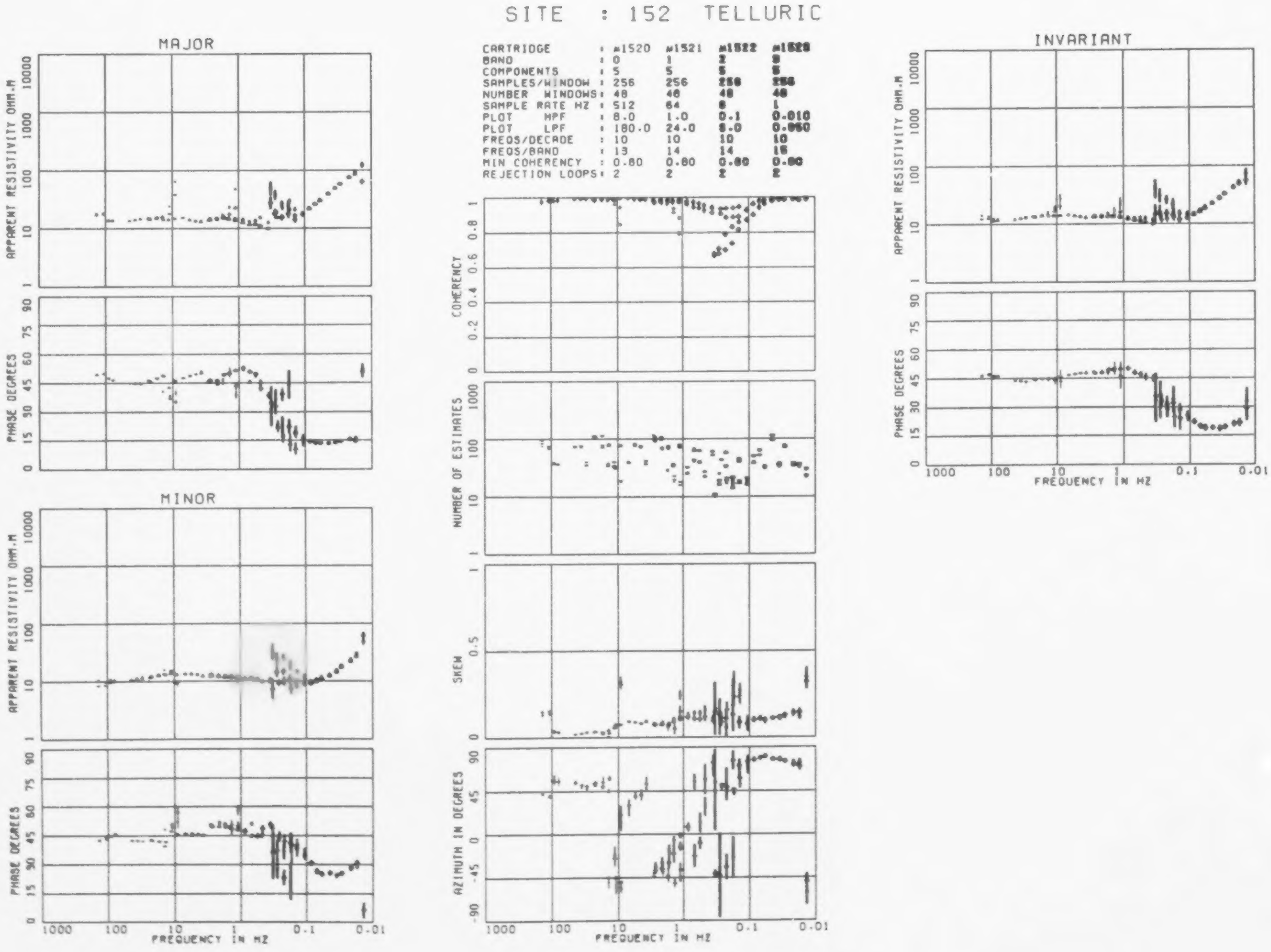

SITE : 152 TELLURIC

CARTRIDGE	#1520	#1521	#1522	#1523
BAND	0	1	2	3
COMPONENTS	5	5	5	5
SAMPLES/WINDOW	256	256	256	256
NUMBER WINDOWS	48	48	48	48
SAMPLE RATE HZ	512	64	8	1
PLOT HPF	8.0	1.0	0.1	0.010
PLOT LPF	180.0	24.0	8.0	0.060
FREQS/DECADE	10	10	10	10
FREQS/BAND	13	14	14	15
MIN COHERENCY	0.80	0.80	0.80	0.80
REJECTION LOOPS	2	2	2	2

SITE : 152 TELLURIC

```
CARTRIDGE         : #1520   #1521   #1522   #1523
BAND              : 0       1       2       3
COMPONENTS        : 5       5       5       5
SAMPLES/WINDOW    : 256     256     256     256
NUMBER  WINDOWS   : 48      48      48      48
SAMPLE RATE HZ    : 512     64      8       1
PLOT    HPF       : 8.0     1.0     0.1     0.010
PLOT    LPF       : 180.0   24.0    8.0     0.080
FREQS/DECADE      : 10      10      10      10
FREQS/BAND        : 13      14      14      15
MIN COHERENCY     : 0.80    0.80    0.80    0.80
REJECTION LOOPS   : 2       2       2       2
```

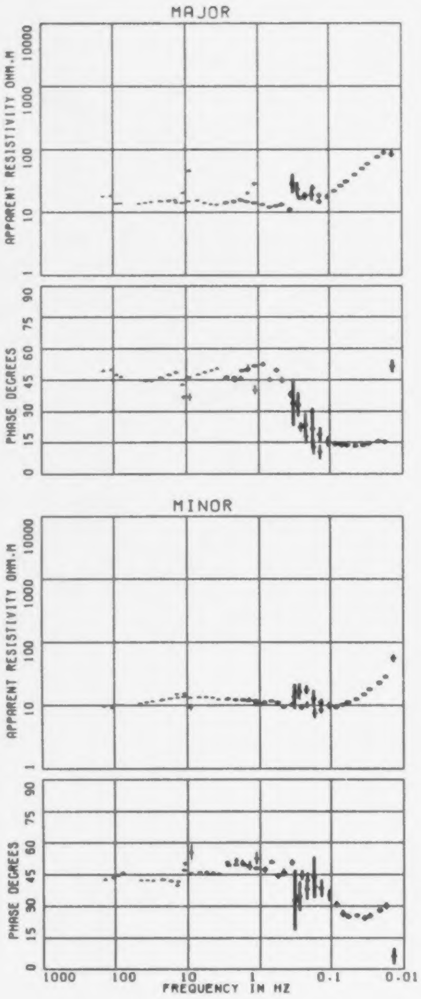

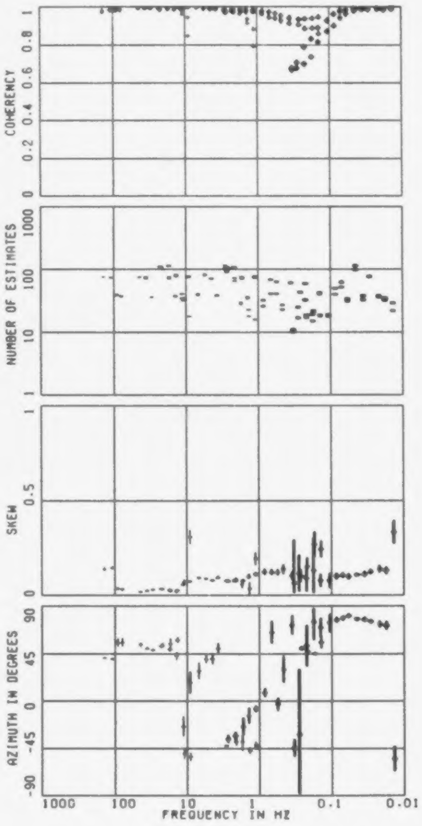

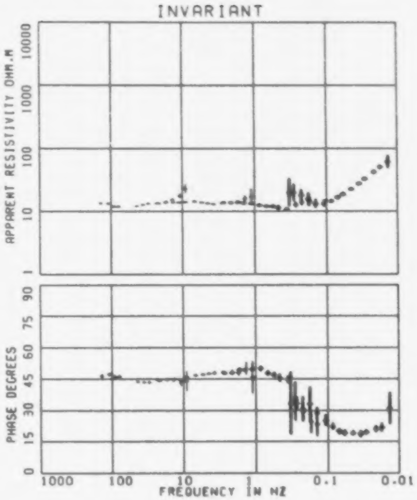

SITE : 152 MAGNETIC

CARTRIDGE	: M1520	M1521	M1522	M1523
BAND	: 0	1	2	3
COMPONENTS	: 5	5	5	5
SAMPLES/WINDOW	: 256	256	256	256
NUMBER WINDOWS	: 48	48	48	48
SAMPLE RATE HZ	: 512	64	8	1
PLOT HPF	: 8.0	1.0	0.1	0.010
PLOT LPF	: 180.0	24.0	3.0	0.350
FREQS/DECADE	: 10	10	10	10
FREQS/BAND	: 13	14	14	15
MIN COHERENCY	: 0.70	0.70	0.70	0.70
REJECTION LOOPS	: 2	2	2	2

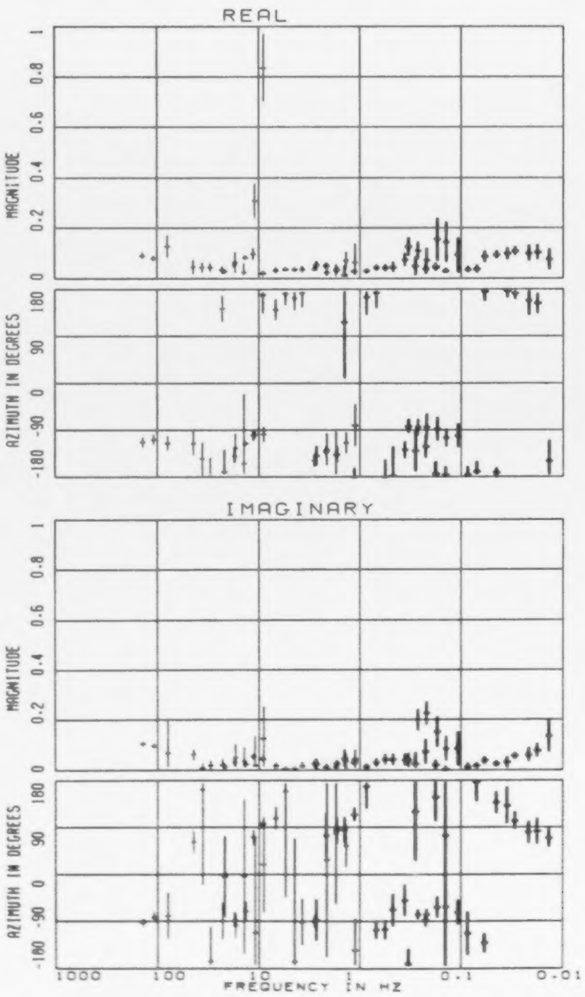

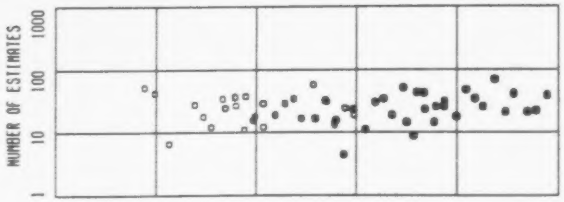

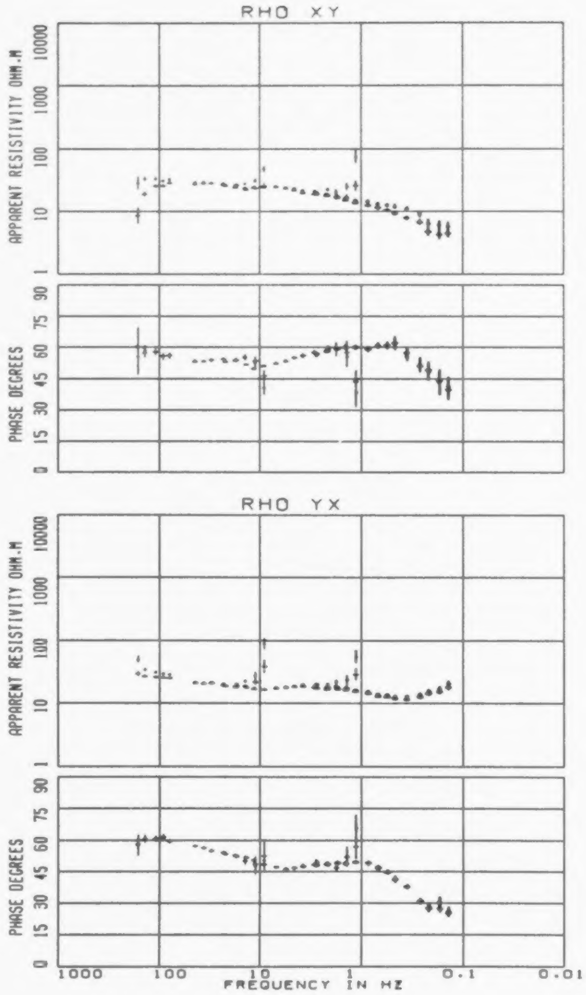

SITE : 164 TELLURIC

CARTRIDGE	: M1640	M1641	M1642
BAND	: 0	1	2
COMPONENTS	: 5	5	5
SAMPLES/WINDOW	: 256	256	256
NUMBER WINDOWS	: 48	48	48
SAMPLE RATE HZ	: 512	64	8
PLOT HPF	: 8.0	1.0	0.1
PLOT LPF	: 180.0	24.0	3.0
FREQS/DECADE	: 10	10	10
FREQS/BAND	: 13	14	14
MIN COHERENCY	: 0.80	0.80	0.80
REJECTION LOOPS	: 2	2	2

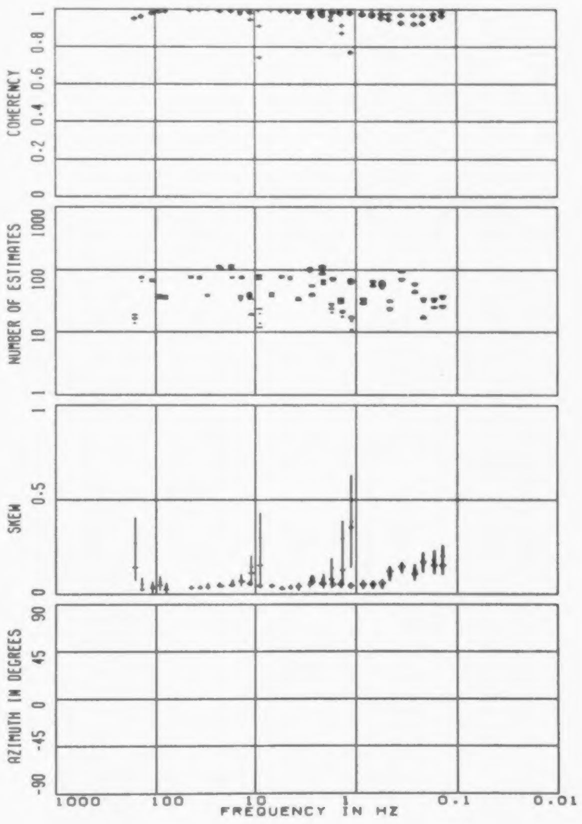

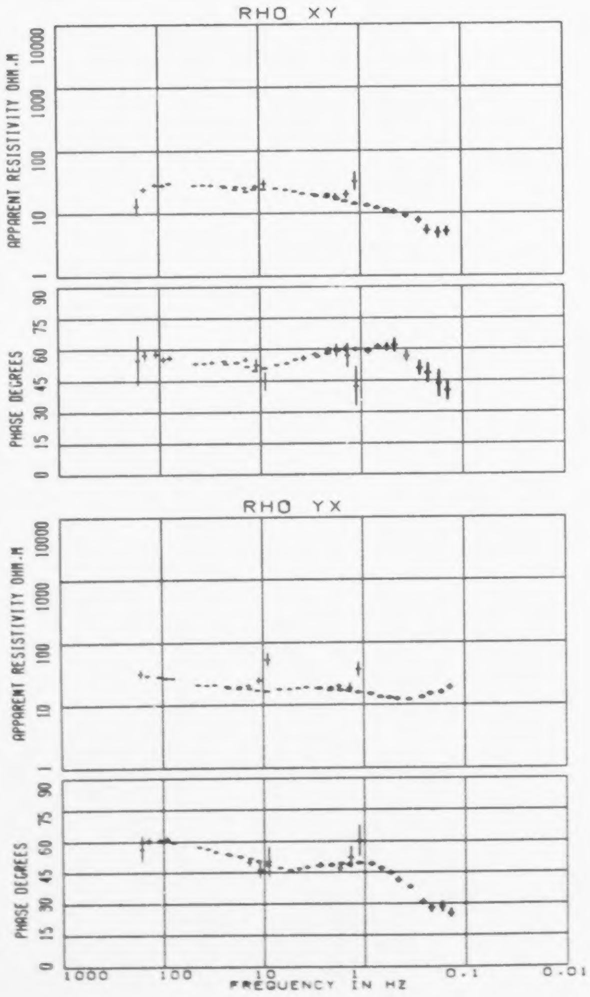

SITE : 164 TELLURIC

CARTRIDGE	: µ1640	µ1641	µ1642
BAND	: 0	1	2
COMPONENTS	: 5	5	5
SAMPLES/WINDOW	: 256	256	256
NUMBER WINDOWS	: 48	48	48
SAMPLE RATE HZ	: 512	64	8
PLOT HPF	: 8.0	1.0	0.1
PLOT LPF	: 180.0	24.0	3.0
FREQS/DECADE	: 10	10	10
FREQS/BAND	: 13	14	14
MIN COHERENCY	: 0.80	0.80	0.80
REJECTION LOOPS	: 2	2	2

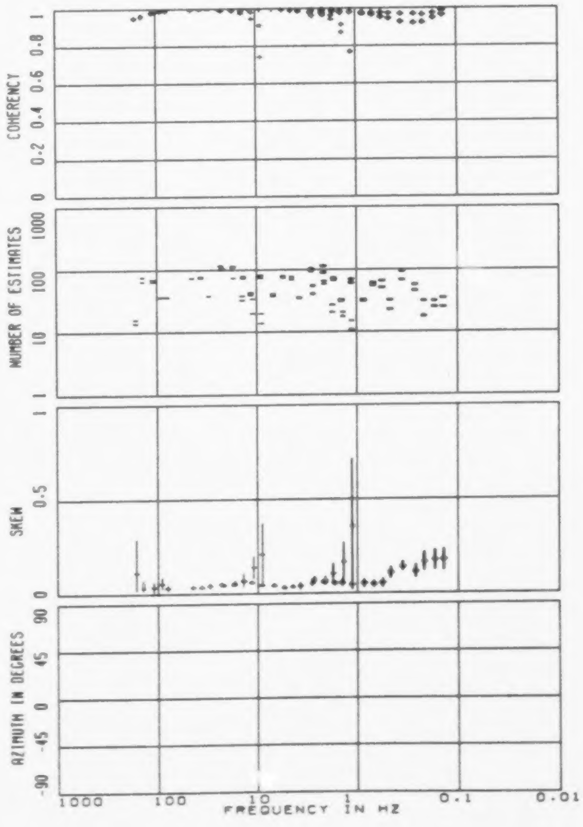

SITE : 164 TELLURIC

CARTRIDGE	: =1640	=1641	=1642
BAND	: 0	1	2
COMPONENTS	: 5	5	5
SAMPLES/WINDOW	: 256	256	256
NUMBER WINDOWS	: 48	48	48
SAMPLE RATE HZ	: 512	64	8
PLOT HPF	: 8.0	1.0	0.1
PLOT LPF	: 180.0	24.0	3.0
FREQS/DECADE	: 10	10	10
FREQS/BAND	: 13	14	14
MIN COHERENCY	: 0.80	0.80	0.80
REJECTION LOOPS	: 2	2	2

MAJOR

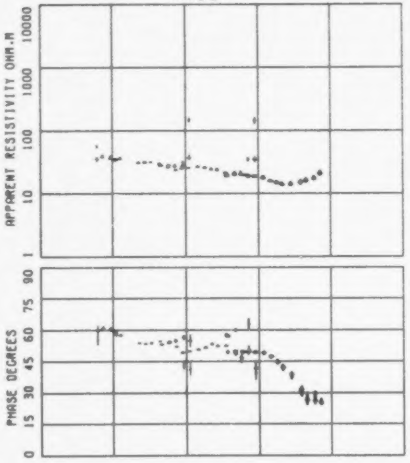

MINOR

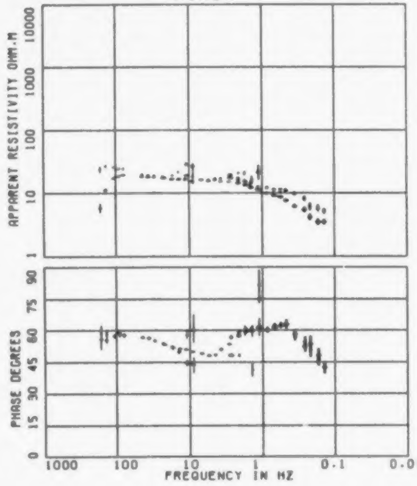

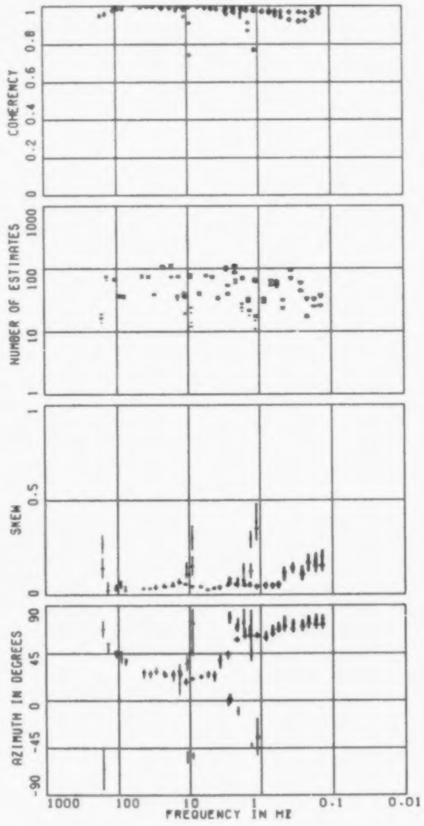

INVARIANT

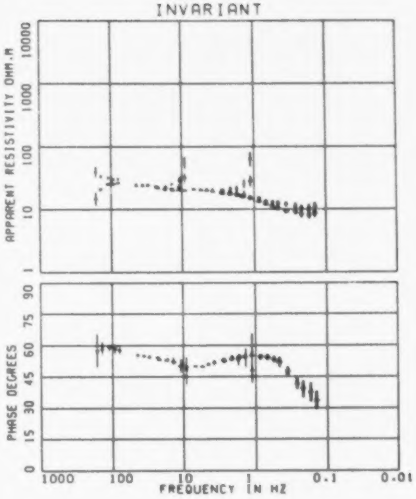

SITE : 164 TELLURIC

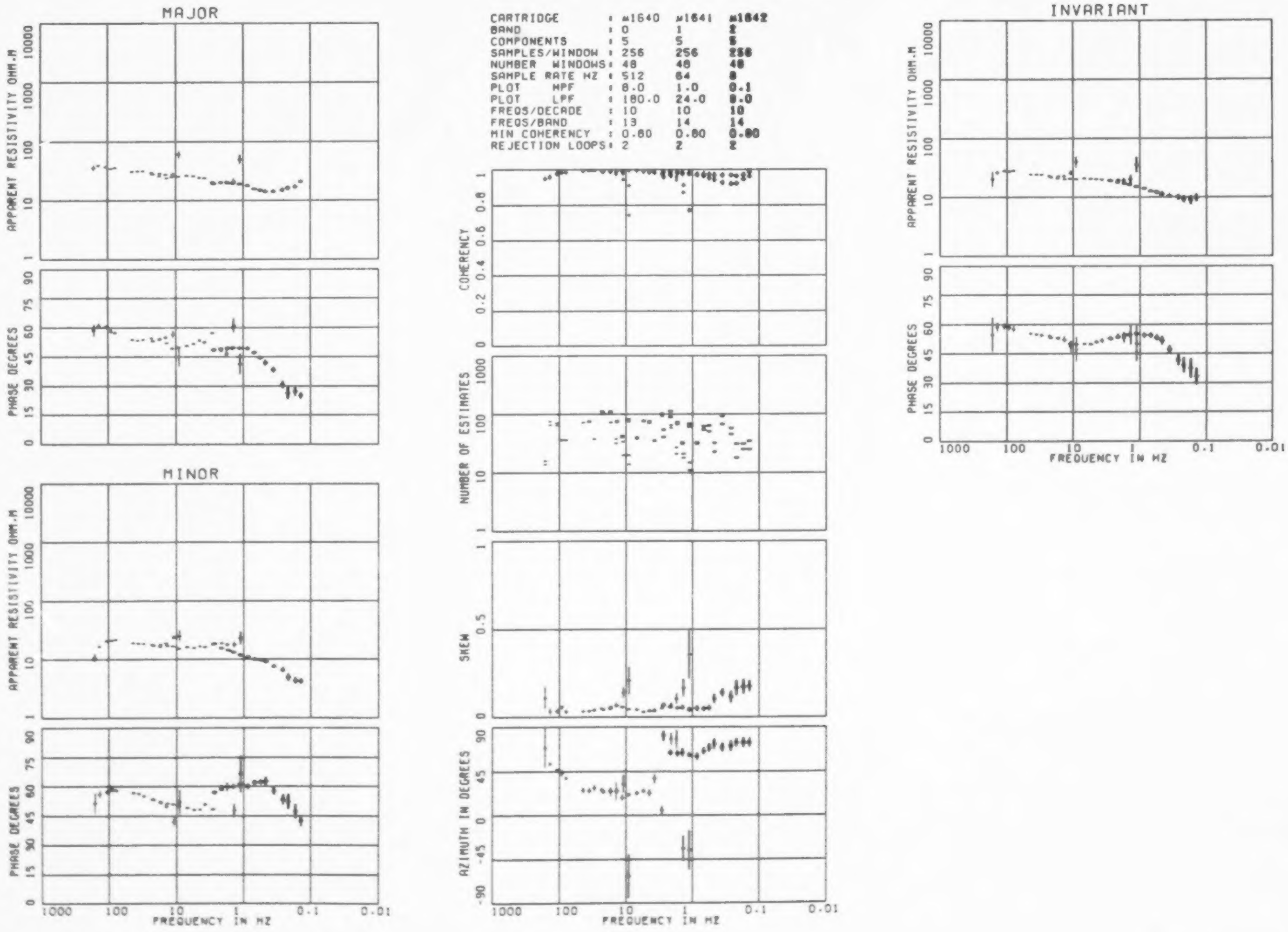

```
CARTRIDGE       : #1640   #1641   #1642
BAND            : 0       1       2
COMPONENTS      : 5       5       5
SAMPLES/WINDOW  : 256     256     256
NUMBER  WINDOWS : 48      48      48
SAMPLE RATE HZ  : 512     64      8
PLOT     HPF    : 8.0     1.0     0.1
PLOT     LPF    : 180.0   24.0    8.0
FREQS/DECADE    : 10      10      10
FREQS/BAND      : 13      14      14
MIN COHERENCY   : 0.80    0.80    0.80
REJECTION LOOPS : 2       2       2
```

SITE : 164 MAGNETIC

CARTRIDGE	: w1640	w1641	w1642
BAND	: 0	1	2
COMPONENTS	: 5	5	5
SAMPLES/WINDOW	: 256	256	256
NUMBER WINDOWS	: 48	48	48
SAMPLE RATE HZ	: 512	64	8
PLOT HPF	: 8.0	1.0	0.1
PLOT LPF	: 180.0	24.0	8.0
FREQS/DECADE	: 10	10	10
FREQS/BAND	: 13	14	14
MIN COHERENCY	: 0.70	0.70	0.70
REJECTION LOOPS	: 2	2	2

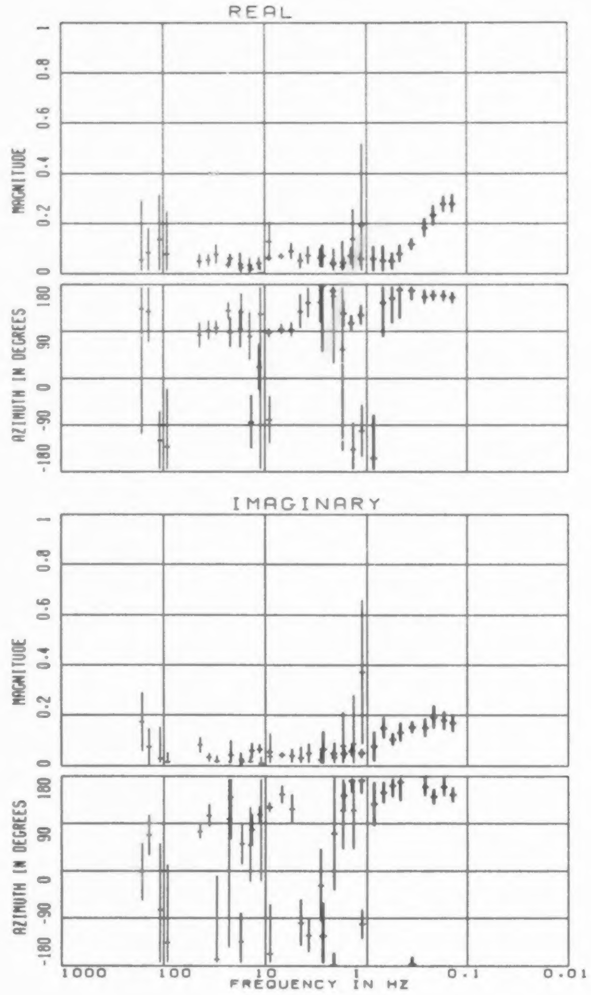

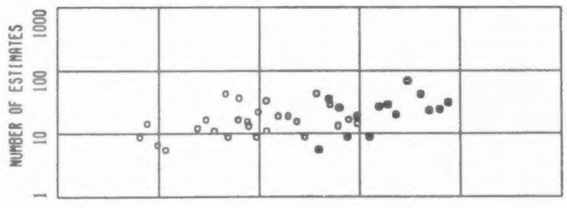

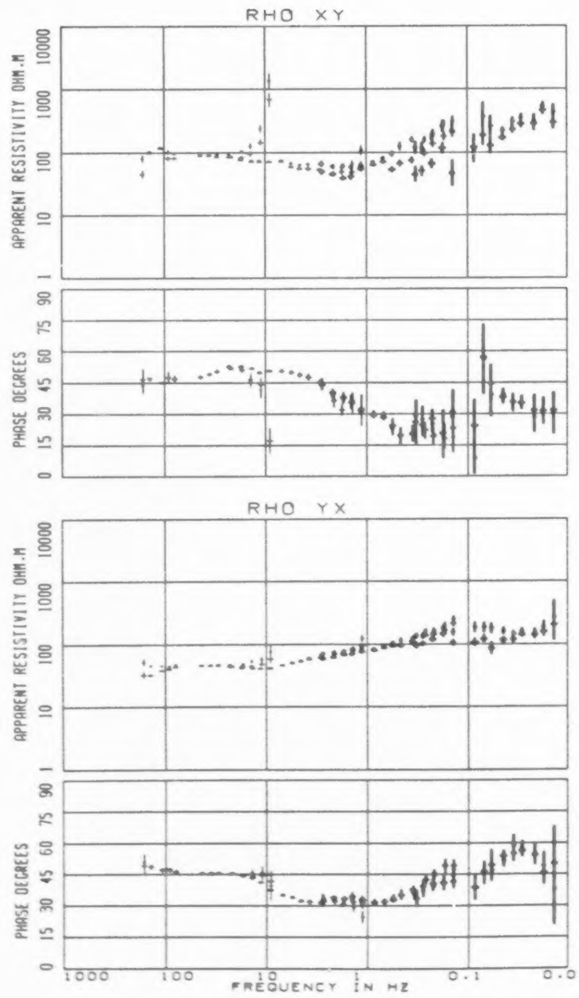

SITE : 201 TELLURIC

CARTRIDGE	: 52010	82011	82012	82013
BAND	: 0	1	2	3
COMPONENTS	: 5	5	5	5
SAMPLES/WINDOW	: 256	256	256	256
NUMBER WINDOWS	: 48	48	48	25
SAMPLE RATE HZ	: 512	64	8	1
PLOT HPF	: 8.0	1.0	0.1	0.010
PLOT LPF	: 180.0	24.0	3.0	0.350
FREQS/DECADE	: 10	10	10	10
FREQS/BAND	: 13	14	14	15
MIN COHERENCY	: 0.80	0.80	0.80	0.80
REJECTION LOOPS	: 2	2	2	2

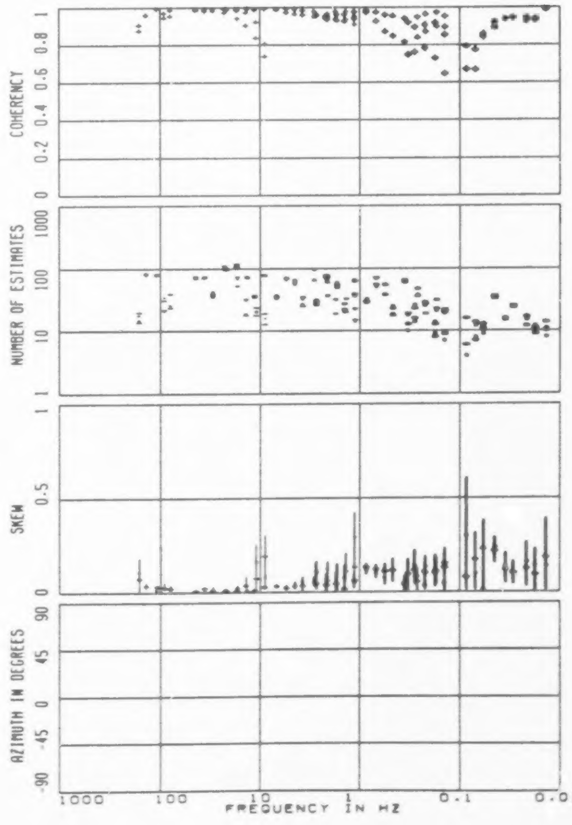

SITE : 201 TELLURIC

CARTRIDGE	:	S2010	S2011	S2012	S2013
BAND	:	0	1	2	3
COMPONENTS	:	5	5	5	5
SAMPLES/WINDOW	:	256	256	256	256
NUMBER WINDOWS	:	48	48	48	28
SAMPLE RATE HZ	:	512	64	8	1
PLOT HPF	:	8.0	1.0	0.1	0.010
PLOT LPF	:	180.0	24.0	3.0	0.350
FREQS/DECADE	:	10	10	10	10
FREQS/BAND	:	13	14	14	15
MIN COHERENCY	:	0.80	0.80	0.80	0.80
REJECTION LOOPS	:	2	2	2	2

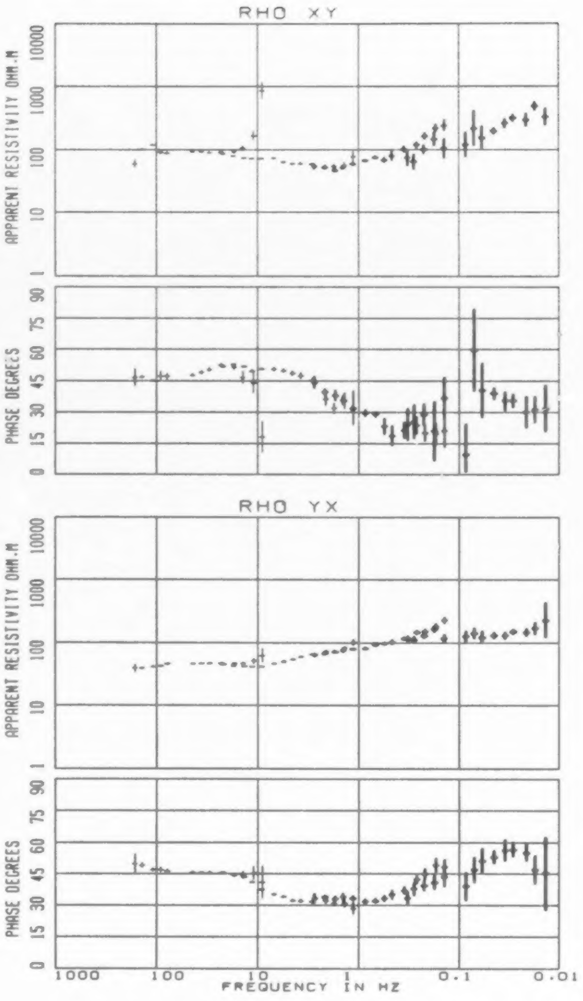

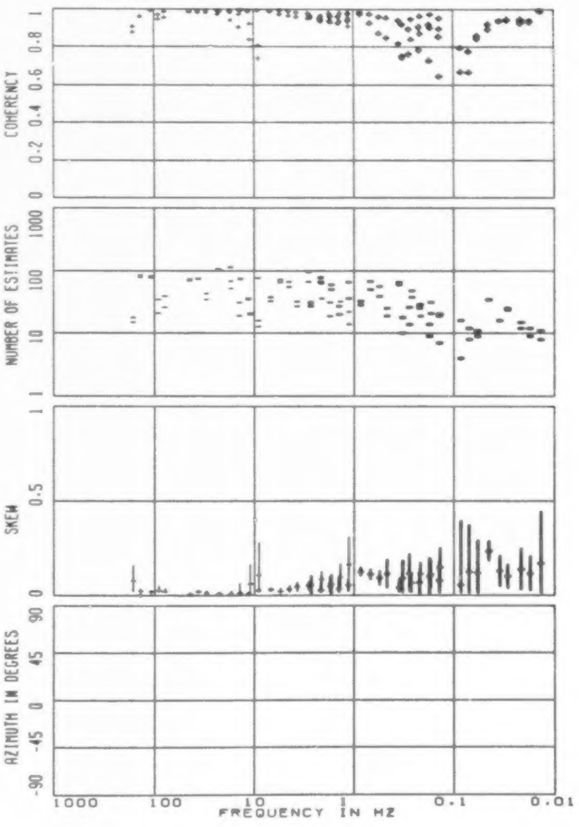

SITE : 201 TELLURIC

CARTRIDGE	S2010	S2011	S2012	S201[illegible]
BAND	0	1	2	[illegible]
COMPONENTS	5	5	5	5
SAMPLES/WINDOW	256	256	256	256
NUMBER WINDOWS	48	48	48	25
SAMPLE RATE HZ	512	64	8	1
PLOT HPF	8.0	1.0	0.1	0.010
PLOT LPF	180.0	24.0	[illegible].0	0.[illegible]50
FREQS/DECADE	10	10	10	10
FREQS/BAND	13	14	14	15
MIN COHERENCY	0.80	0.80	0.80	0.80
REJECTION LOOPS	2	2	2	2

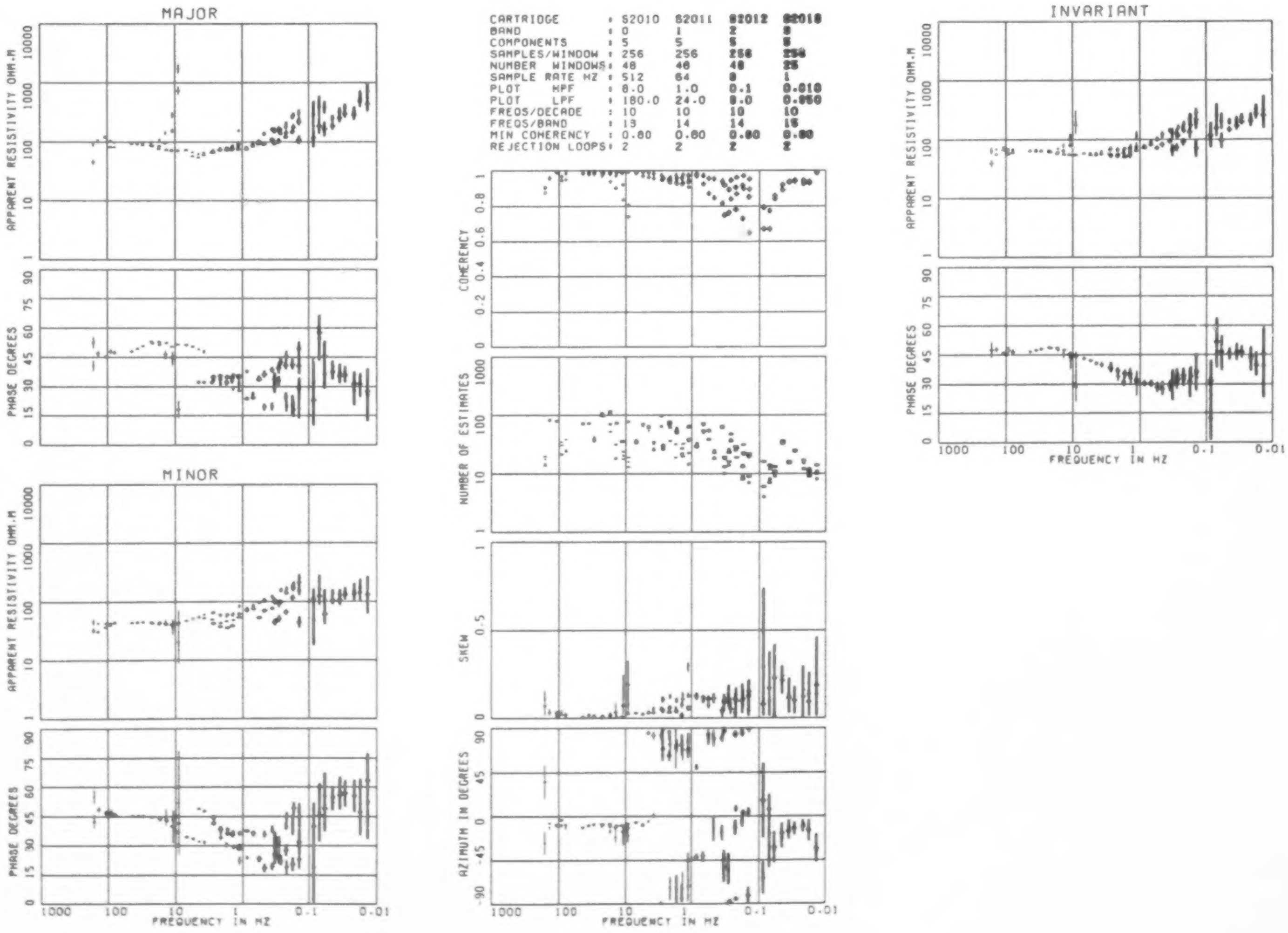

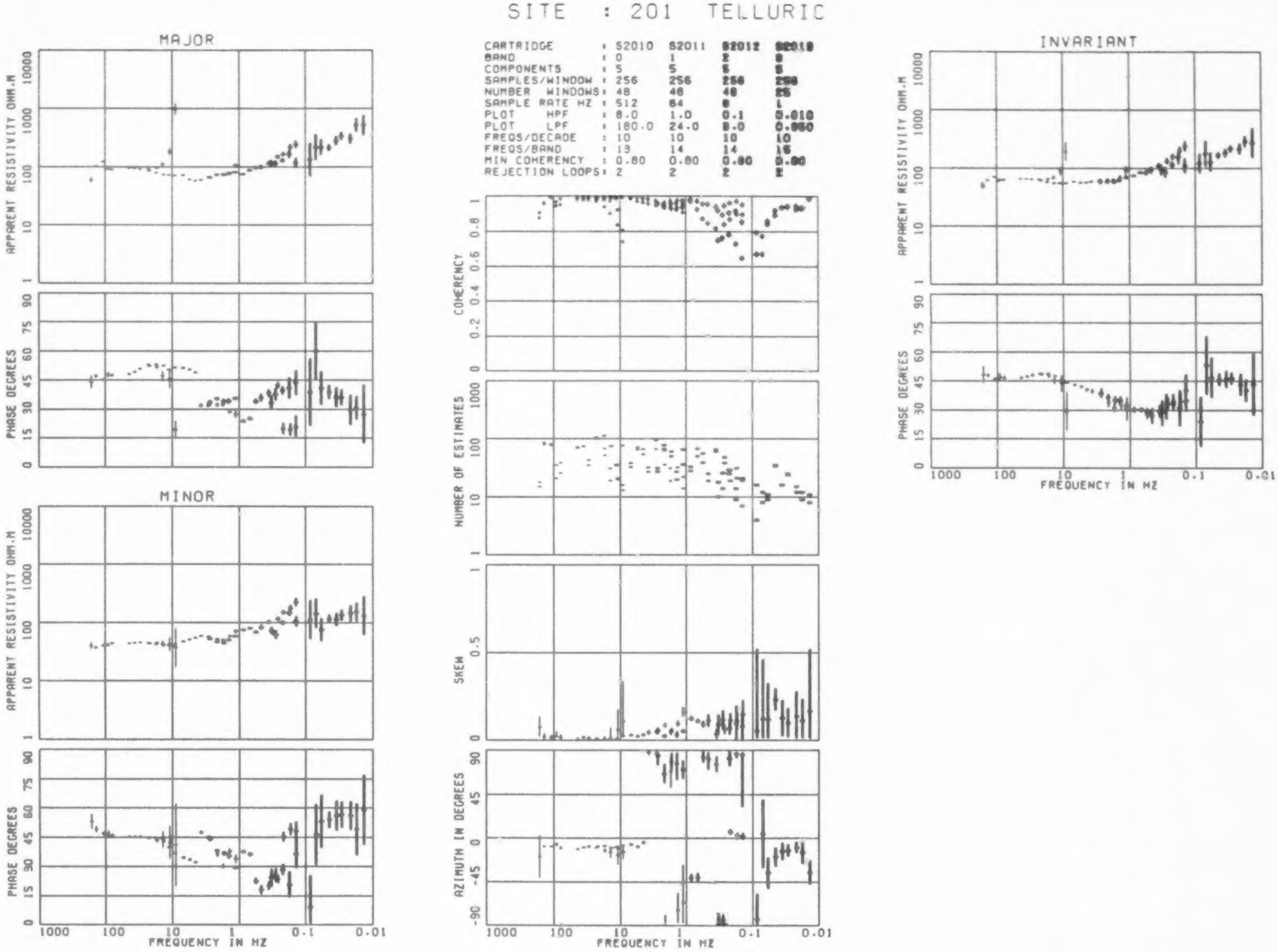
SITE : 201 TELLURIC
CARTRIDGE : S2010 S2011 S2012 S2013
BAND : 0 1 2 3
COMPONENTS : 5 5 5 5
SAMPLES/WINDOW : 256 256 256 256
NUMBER WINDOWS : 48 48 48 25
SAMPLE RATE HZ : 512 64 8 1
PLOT HPF : 8.0 1.0 0.1 0.010
PLOT LPF : 180.0 24.0 8.0 0.060
FREQS/DECADE : 10 10 10 10
FREQS/BAND : 13 14 14 15
MIN COHERENCY : 0.80 0.80 0.80 0.80
REJECTION LOOPS : 2 2 2 2
MAJOR
MINOR
INVARIANT
APPARENT RESISTIVITY OHM.M
1
10
100
1000
10000
PHASE DEGREES
0
15
30
45
60
75
90
COHERENCY
0
0.2
0.4
0.6
0.8
1
NUMBER OF ESTIMATES
1
10
100
1000
SKEW
0
0.5
1
AZIMUTH IN DEGREES
-90
-45
0
45
90
1000
100
10
1
0.1
0.01
FREQUENCY IN HZ

SITE : 201 MAGNETIC

```
CARTRIDGE        : S2010   S2011   S2012   S2013
BAND             : 0       1       2       3
COMPONENTS       : 5       5       5       5
SAMPLES/WINDOW   : 256     256     256     256
NUMBER  WINDOWS  : 48      48      48      25
SAMPLE RATE HZ   : 512     64      8       1
PLOT      HPF    : 8.0     1.0     0.1     0.010
PLOT      LPF    : 180.0   24.0    3.0     0.350
FREQS/DECADE     : 10      10      10      10
FREQS/BAND       : 13      14      14      15
MIN COHERENCY    : 0.70    0.70    0.70    0.70
REJECTION LOOPS  : 2       2       2       2
```

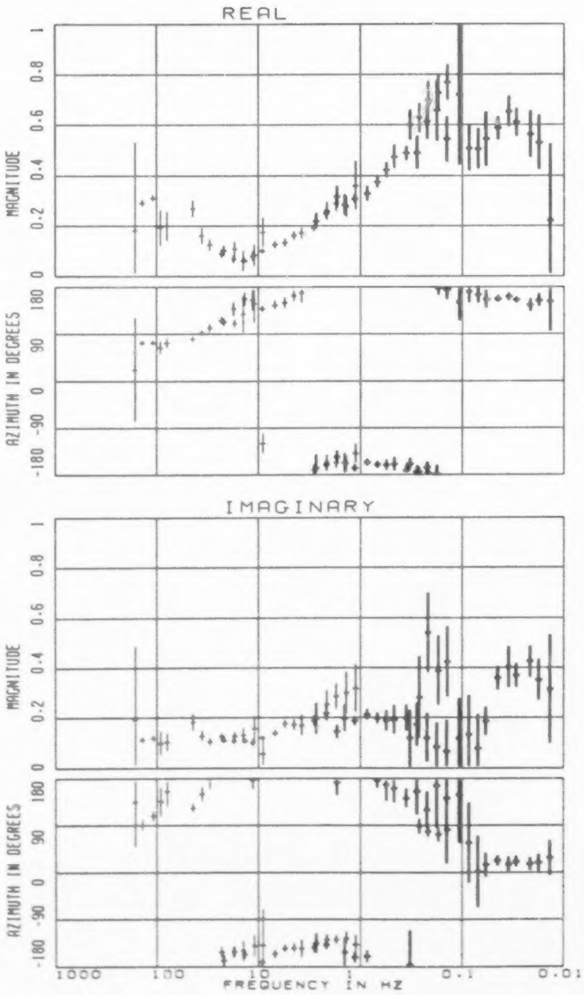

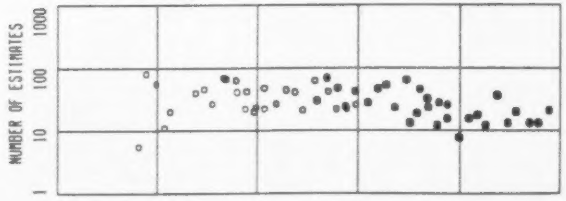

SITE : 202 TELLURIC

```
CARTRIDGE         : M2020   M2021   M2022   M2023
BAND              : 0       1       2       3
COMPONENTS        : 5       5       5       5
SAMPLES/WINDOW    : 256     256     256     256
NUMBER  WINDOWS   : 48      48      48      48
SAMPLE RATE HZ    : 512     64      8       1
PLOT      HPF     : 8.0     1.0     0.1     0.010
PLOT      LPF     : 160.0   24.0    3.0     0.350
FREQS/DECADE      : 10      10      10      10
FREQS/BAND        : 19      14      14      15
MIN COHERENCY     : 0.80    0.80    0.80    0.80
REJECTION LOOPS   : 2       2       2       2
```

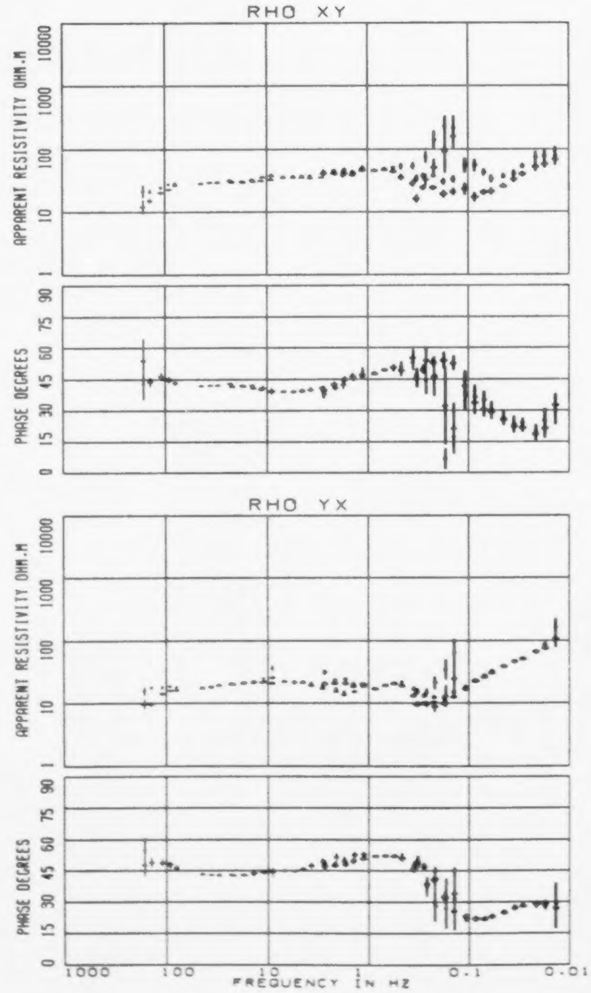

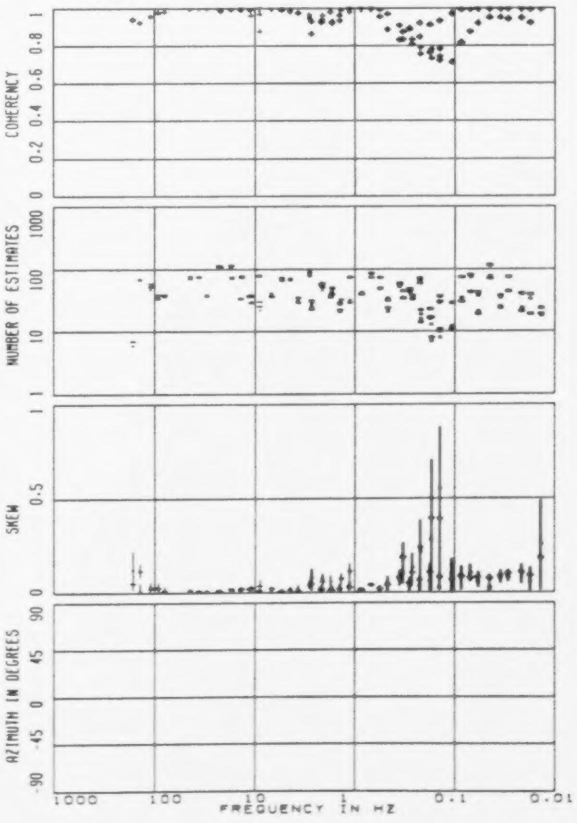

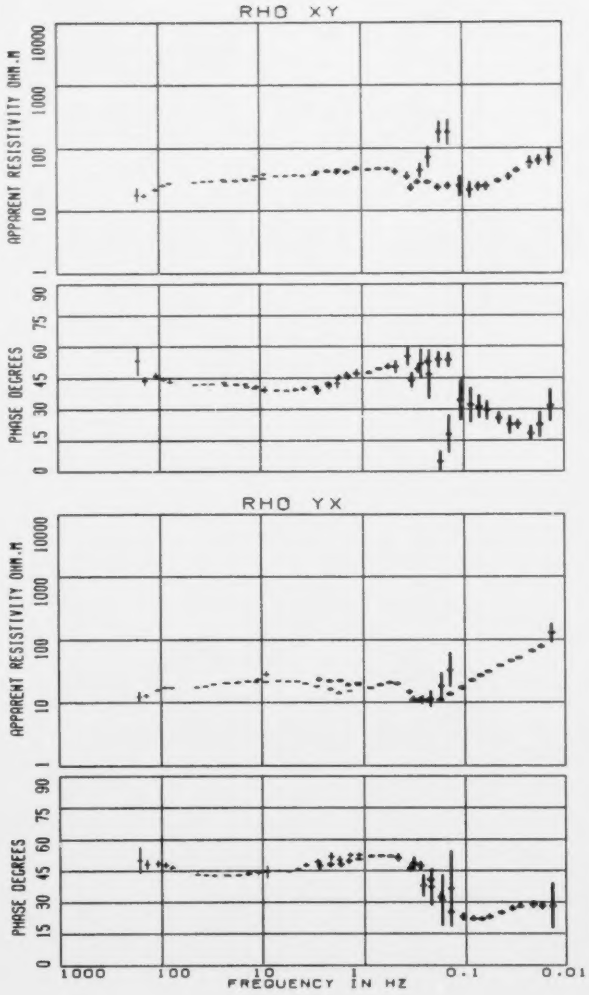

SITE : 202 TELLURIC

CARTRIDGE	: M2020	M2021	M2022	M2023
BAND	: 0	1	2	3
COMPONENTS	: 5	5	5	5
SAMPLES/WINDOW	: 256	256	256	256
NUMBER WINDOWS	: 48	48	48	48
SAMPLE RATE HZ	: 512	64	8	1
PLOT HPF	: 8.0	1.0	0.1	0.010
PLOT LPF	: 180.0	24.0	3.0	0.350
FREQS/DECADE	: 10	10	10	10
FREQS/BAND	: 13	14	14	15
MIN COHERENCY	: 0.80	0.80	0.80	0.80
REJECTION LOOPS	: 2	2	2	2

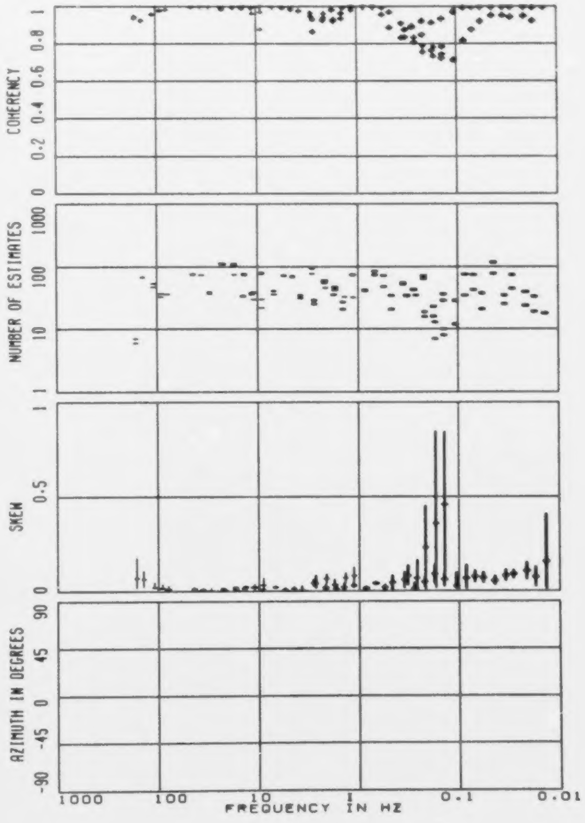

SITE : 202 TELLURIC

CARTRIDGE	:	#2020	#2021	#2022	#2023
BAND	:	0	1	2	3
COMPONENTS	:	5	5	5	5
SAMPLES/WINDOW	:	256	256	256	256
NUMBER WINDOWS	:	48	48	48	48
SAMPLE RATE HZ	:	512	64	8	1
PLOT HPF	:	8.0	1.0	0.1	0.010
PLOT LPF	:	180.0	24.0	8.0	0.050
FREQS/DECADE	:	10	10	10	10
FREQS/BAND	:	13	14	14	15
MIN COHERENCY	:	0.80	0.80	0.80	0.80
REJECTION LOOPS	:	2	2	2	2

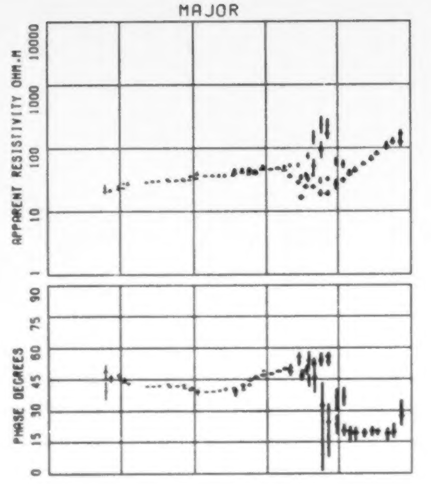

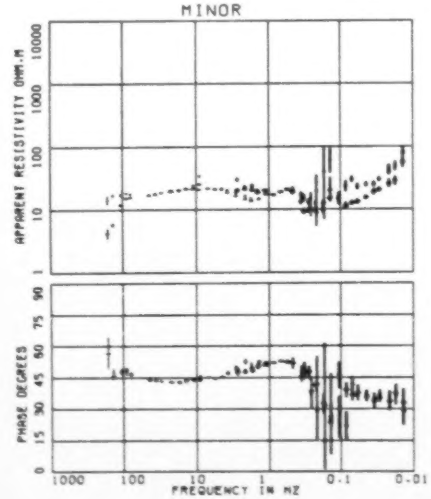

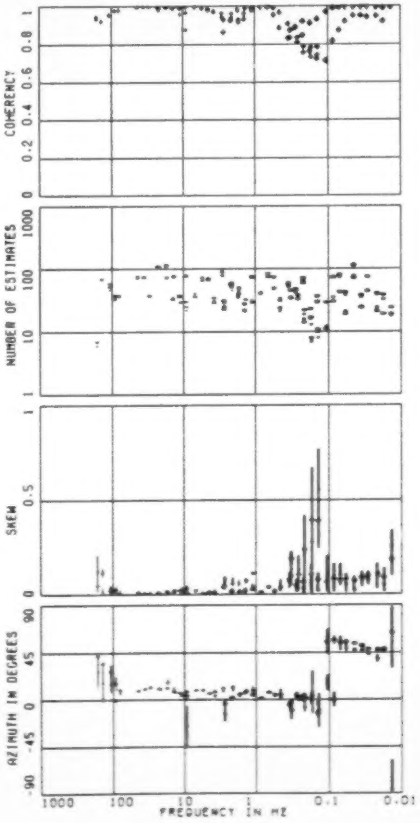

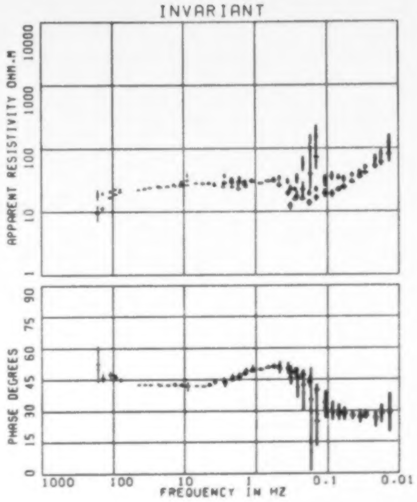

SITE : 202 TELLURIC

CARTRIDGE	:	#2020	#2021	#2022	#2023
BAND	:	0	1	2	3
COMPONENTS	:	5	5	5	5
SAMPLES/WINDOW	:	256	256	256	256
NUMBER WINDOWS	:	48	48	48	48
SAMPLE RATE HZ	:	512	64	8	1
PLOT HPF	:	8.0	1.0	0.1	0.010
PLOT LPF	:	180.0	24.0	3.0	[illegible]
FREQS/DECADE	:	10	10	10	10
FREQS/BAND	:	13	14	14	15
MIN COHERENCY	:	0.80	0.80	0.80	0.80
REJECTION LOOPS	:	2	2	2	2

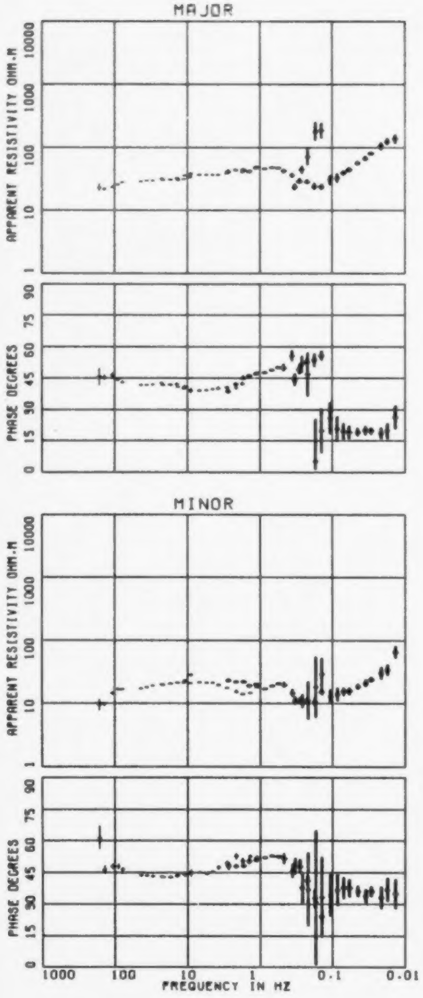

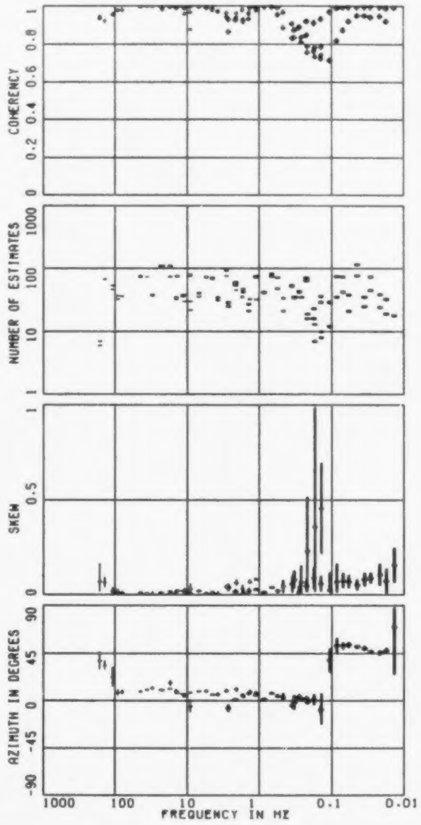

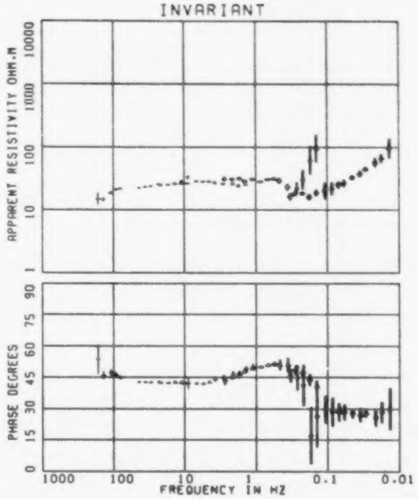

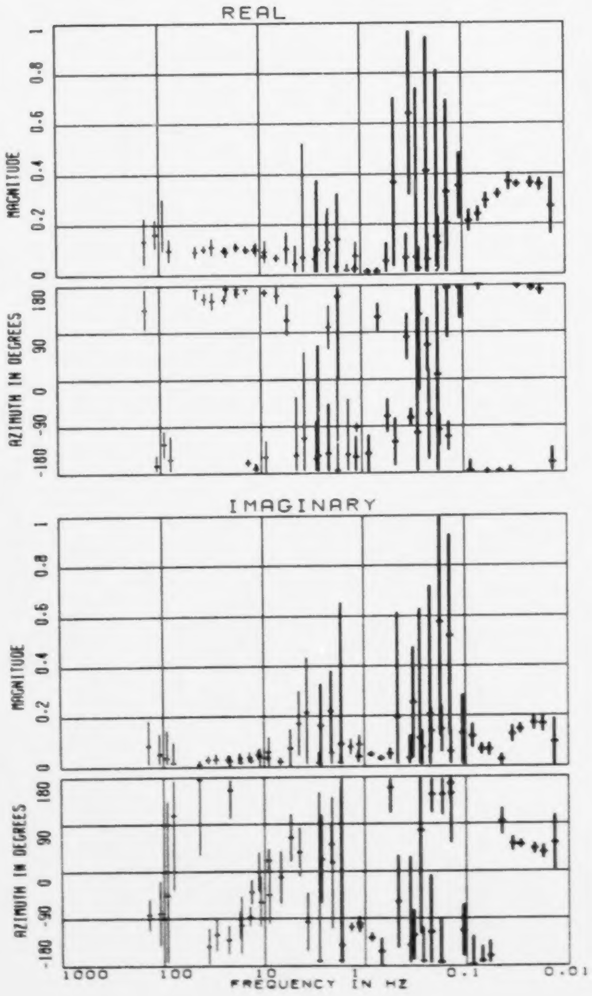

SITE : 202 MAGNETIC

CARTRIDGE	:	μ2020	μ2021	μ2022	μ2023
BAND	:	0	1	2	3
COMPONENTS	:	5	5	5	5
SAMPLES/WINDOW	:	256	256	256	256
NUMBER WINDOWS	:	48	48	48	48
SAMPLE RATE HZ	:	512	64	8	1
PLOT HPF	:	8.0	1.0	0.1	0.010
PLOT LPF	:	180.0	24.0	3.0	0.350
FREQS/DECADE	:	10	10	10	10
FREQS/BAND	:	13	14	14	15
MIN COHERENCY	:	0.70	0.70	0.70	0.70
REJECTION LOOPS	:	2	2	2	2

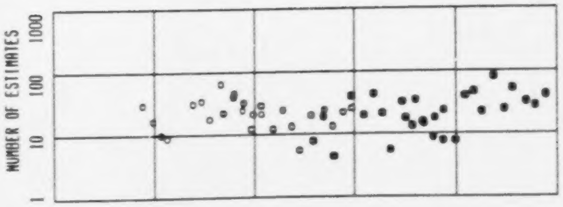

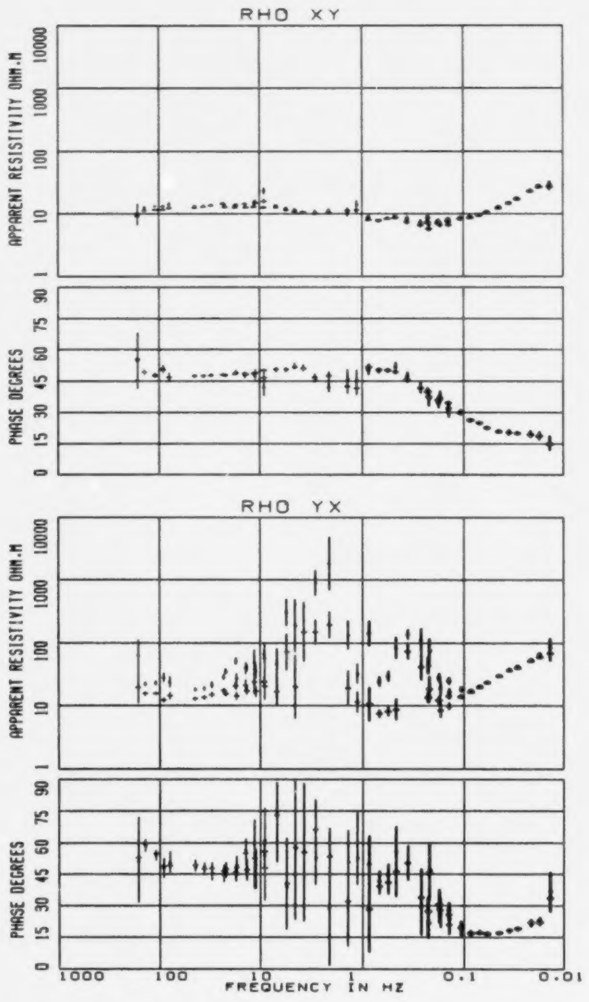

SITE : 203 TELLURIC

CARTRIDGE	: S2090	S2091	S2092	S2093
BAND	: 0	1	2	3
COMPONENTS	: 5	5	5	5
SAMPLES/WINDOW	: 256	256	256	256
NUMBER WINDOWS	: 48	48	48	48
SAMPLE RATE HZ	: 512	64	8	1
PLOT HPF	: 8.0	1.0	0.1	0.010
PLOT LPF	: 180.0	24.0	3.0	0.350
FREQS/DECADE	: 10	10	10	10
FREQS/BAND	: 19	14	14	15
MIN COHERENCY	: 0.80	0.80	0.80	0.80
REJECTION LOOPS	: 2	2	2	2

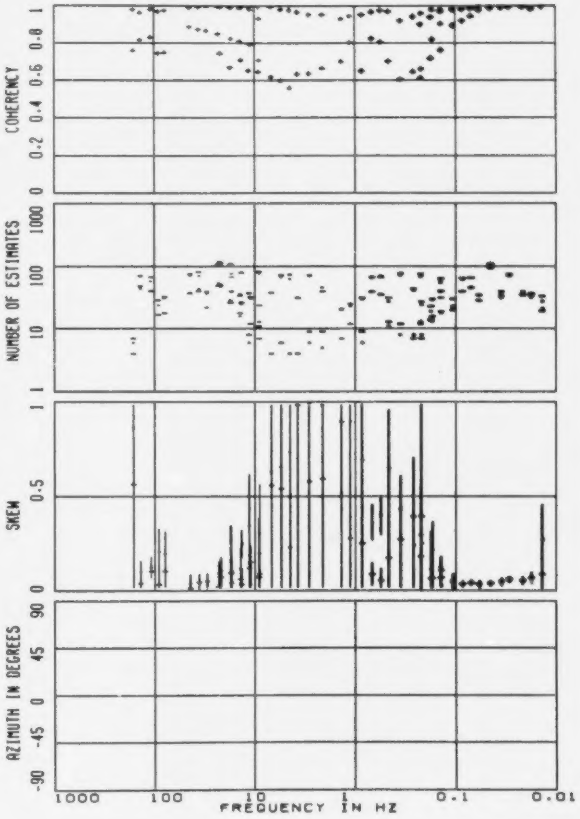

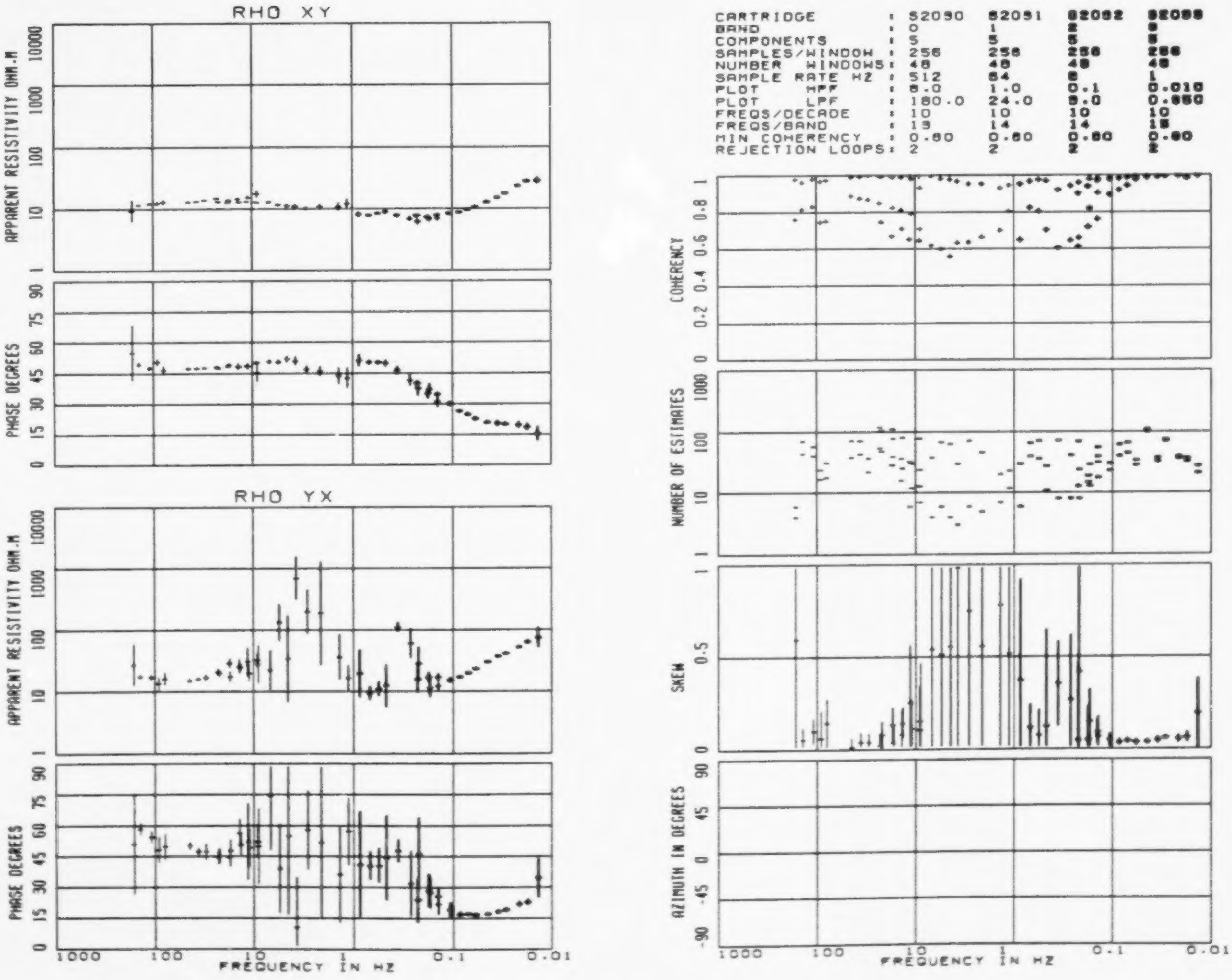

SITE : 203 TELLURIC

```
CARTRIDGE         : 52090   52091   52092   52093
BAND              : 0       1       2       3
COMPONENTS        : 5       5       5       5
SAMPLES/WINDOW    : 256     256     256     256
NUMBER  WINDOWS   : 48      48      48      48
SAMPLE RATE HZ    : 512     64      8       1
PLOT      HPF     : 8.0     1.0     0.1     0.010
PLOT      LPF     : 180.0   24.0    3.0     0.350
FREQS/DECADE      : 10      10      10      10
FREQS/BAND        : 13      14      14      15
MIN COHERENCY     : 0.80    0.80    0.80    0.80
REJECTION LOOPS   : 2       2       2       2
```

SITE : 203 TELLURIC

CARTRIDGE	: S2030	S2031	S2032	S2033
BAND	: 0	1	2	3
COMPONENTS	: 5	5	5	5
SAMPLES/WINDOW	: 256	256	256	256
NUMBER WINDOWS	: 48	48	48	48
SAMPLE RATE HZ	: 512	64	8	1
PLOT HPF	: 8.0	1.0	0.1	0.010
PLOT LPF	: 180.0	24.0	3.0	0.050
FREQS/DECADE	: 10	10	10	10
FREQS/BAND	: 13	14	14	15
MIN COHERENCY	: 0.80	0.80	0.80	0.80
REJECTION LOOPS	: 2	2	2	2

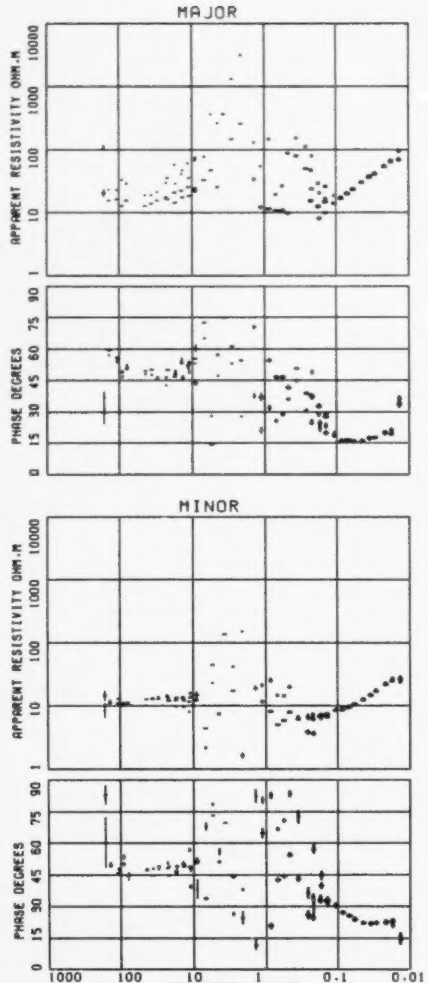

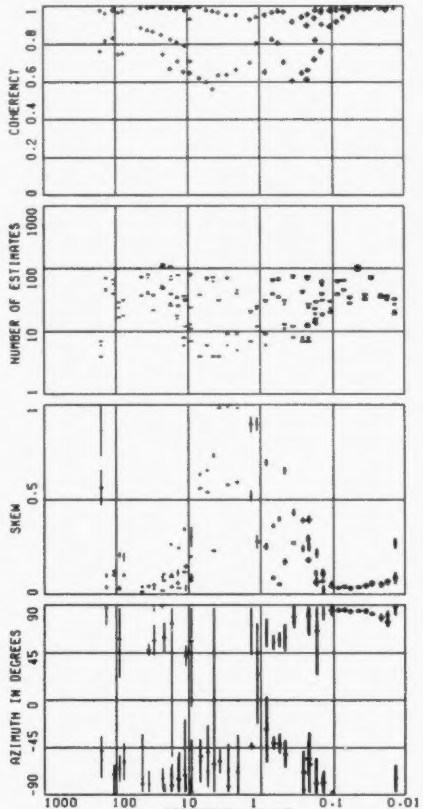

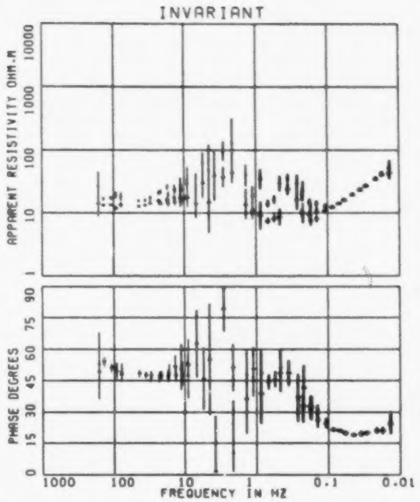

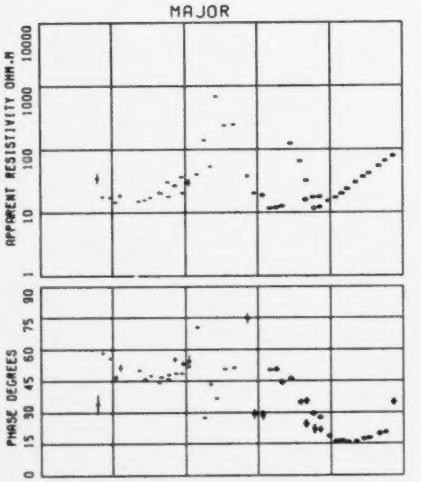

SITE : 203 TELLURIC

CARTRIDGE	: S2030	S2031	S2032	[illegible]
BAND	: 0	1	2	3
COMPONENTS	: 5	5	5	5
SAMPLES/WINDOW	: 256	256	256	256
NUMBER WINDOWS	: 48	48	48	48
SAMPLE RATE HZ	: 512	64	8	1
PLOT HPF	: 8.0	1.0	0.1	0.010
PLOT LPF	: 180.0	24.0	3.0	0.350
FREQS/DECADE	: 10	10	10	10
FREQS/BAND	: 13	14	14	15
MIN COHERENCY	: 0.80	0.80	0.80	0.80
REJECTION LOOPS	: 2	2	2	2

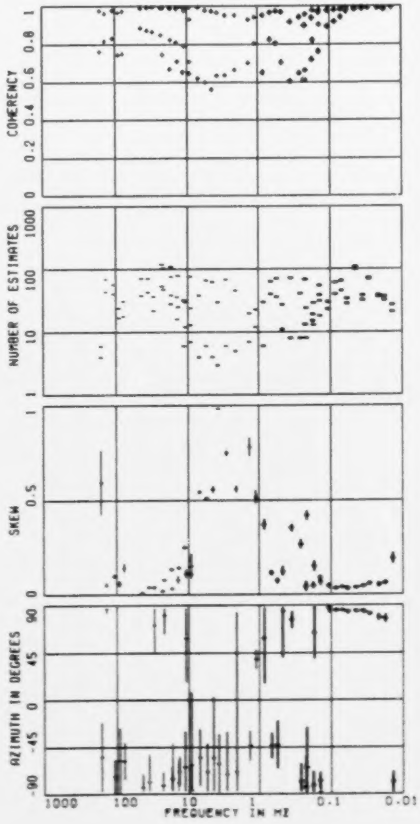

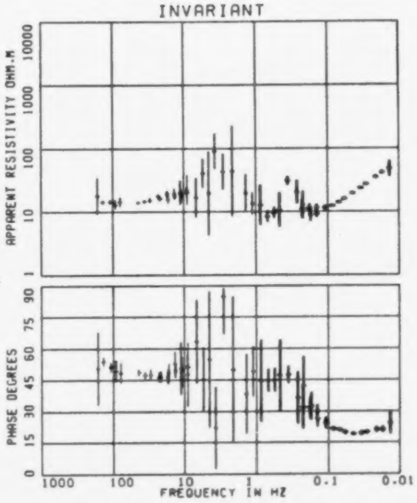

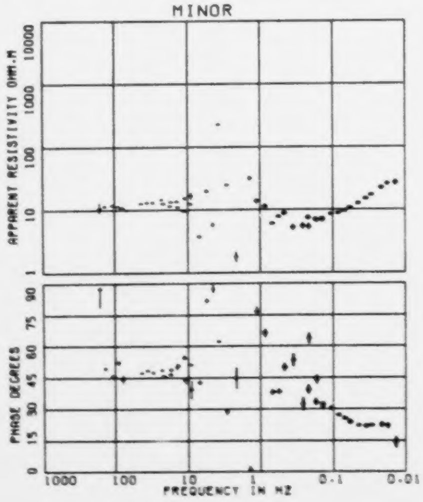

SITE : 203 MAGNETIC

```
CARTRIDGE         : S2090   S2091   S2092   S2093
BAND              : 0       1       2       3
COMPONENTS        : 5       5       5       5
SAMPLES/WINDOW    : 256     256     256     256
NUMBER  WINDOWS   : 48      48      48      48
SAMPLE RATE HZ    : 512     64      8       1
PLOT      HPF     : 8.0     1.0     0.1     0.010
PLOT      LPF     : 180.0   24.0    9.0     0.850
FREQS/DECADE      : 10      10      10      10
FREQS/BAND        : 13      14      14      15
MIN COHERENCY     : 0.70    0.70    0.70    0.70
REJECTION LOOPS   : 2       2       2       2
```

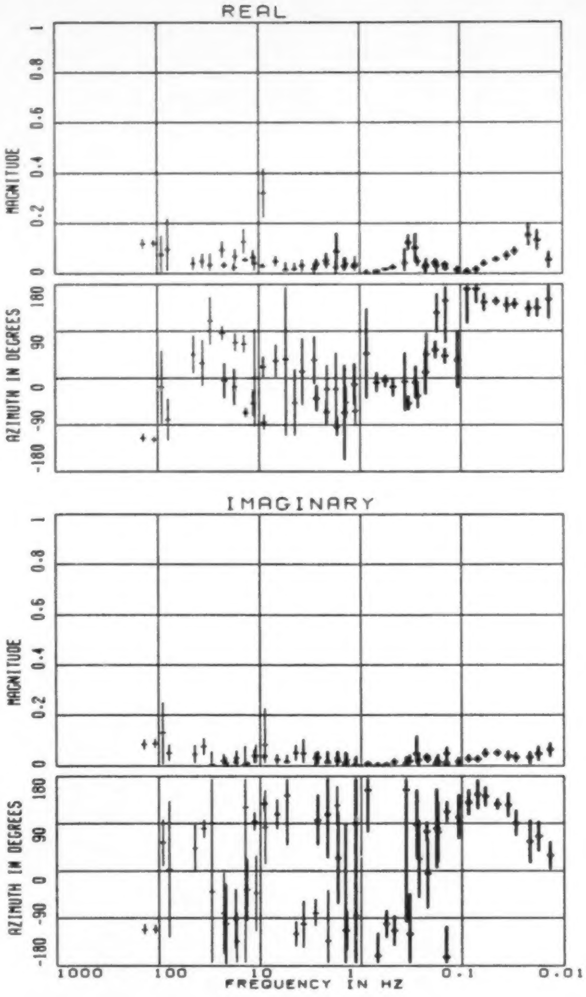

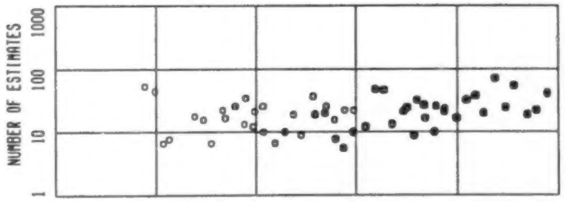

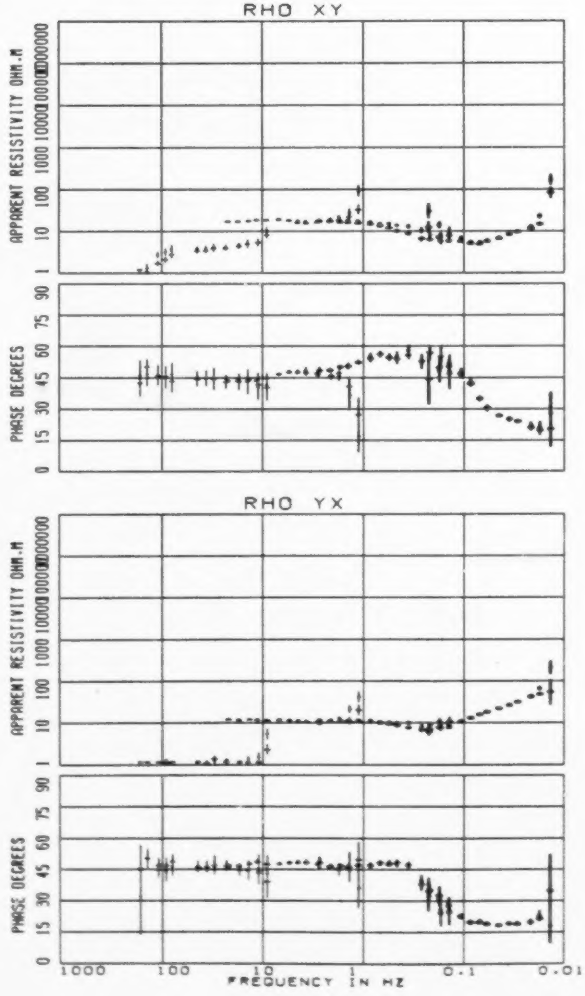

SITE : 204 TELLURIC

```
CARTRIDGE       : 52040   52041   52042   52043
BAND            : 0       1       2       3
COMPONENTS      : 5       5       5       5
SAMPLES/WINDOW  : 256     256     256     256
NUMBER  WINDOWS : 48      48      48      48
SAMPLE RATE HZ  : 512     64      8       1
PLOT     HPF    : 8.0     1.0     0.1     0.010
PLOT     LPF    : 180.0   24.0    3.0     0.380
FREQS/DECADE    : 10      10      10      10
FREQS/BAND      : 19      14      14      15
MIN COHERENCY   : 0.80    0.80    0.80    0.80
REJECTION LOOPS : 2       2       2       2
```

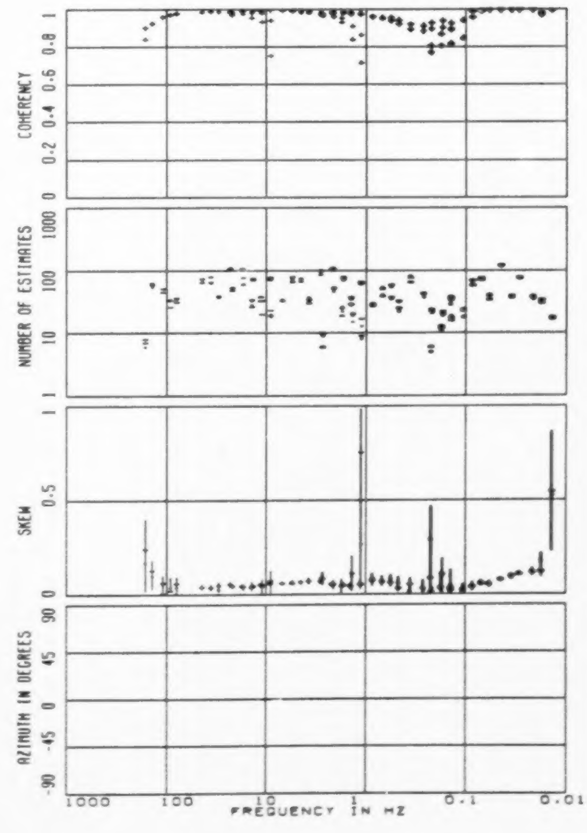

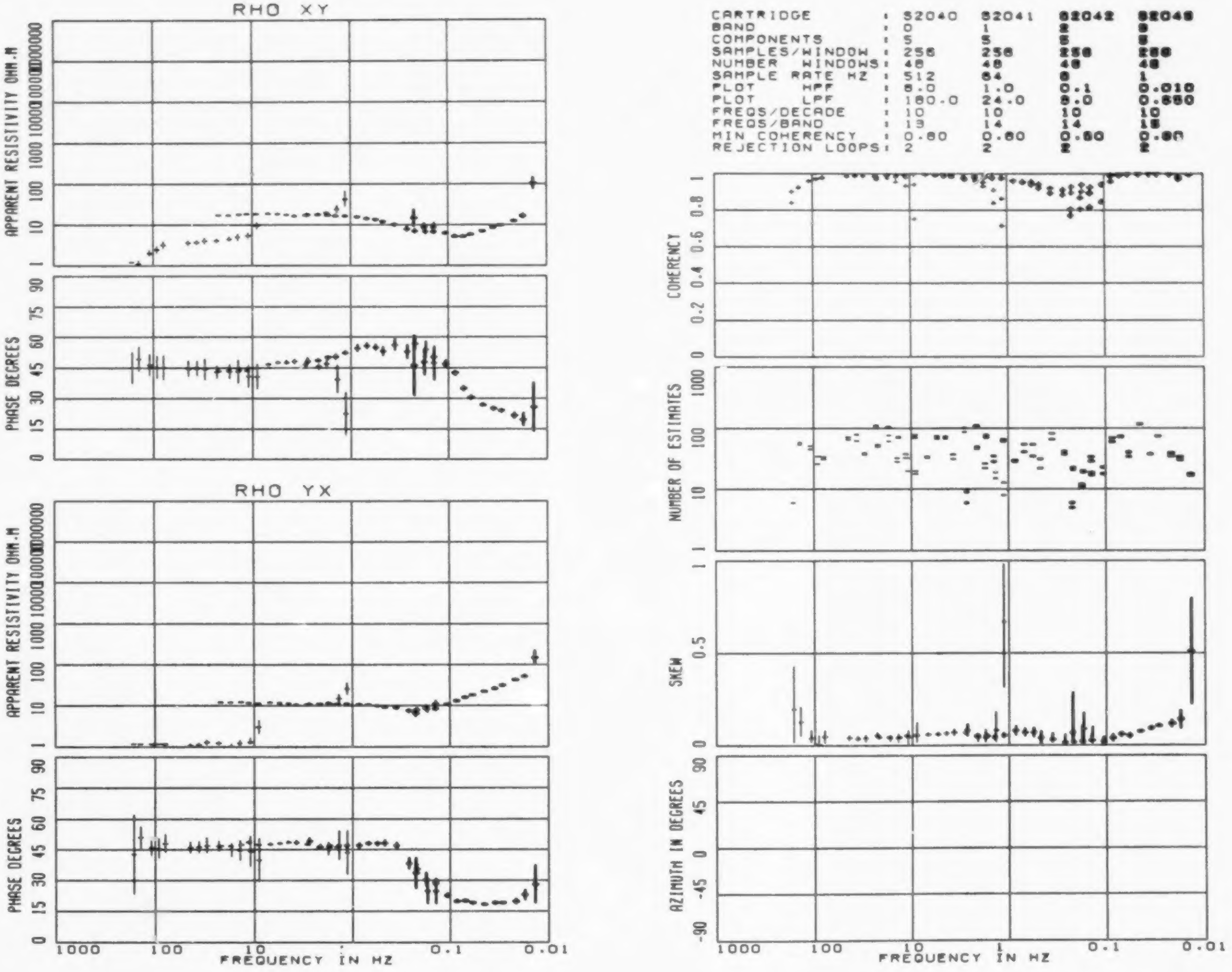

```
SITE   : 204   TELLURIC

CARTRIDGE         : S2040   S2041   S2042   S2043
BAND              : 0       1       2       3
COMPONENTS        : 5       5       5       5
SAMPLES/WINDOW    : 256     256     256     256
NUMBER  WINDOWS   : 48      48      48      48
SAMPLE RATE HZ    : 512     64      8       1
PLOT     HPF      : 8.0     1.0     0.1     0.010
PLOT     LPF      : 180.0   24.0    8.0     0.850
FREQS/DECADE      : 10      10      10      10
FREQS/BAND        : 13      14      14      15
MIN COHERENCY     : 0.80    0.80    0.80    0.80
REJECTION LOOPS   : 2       2       2       2
```

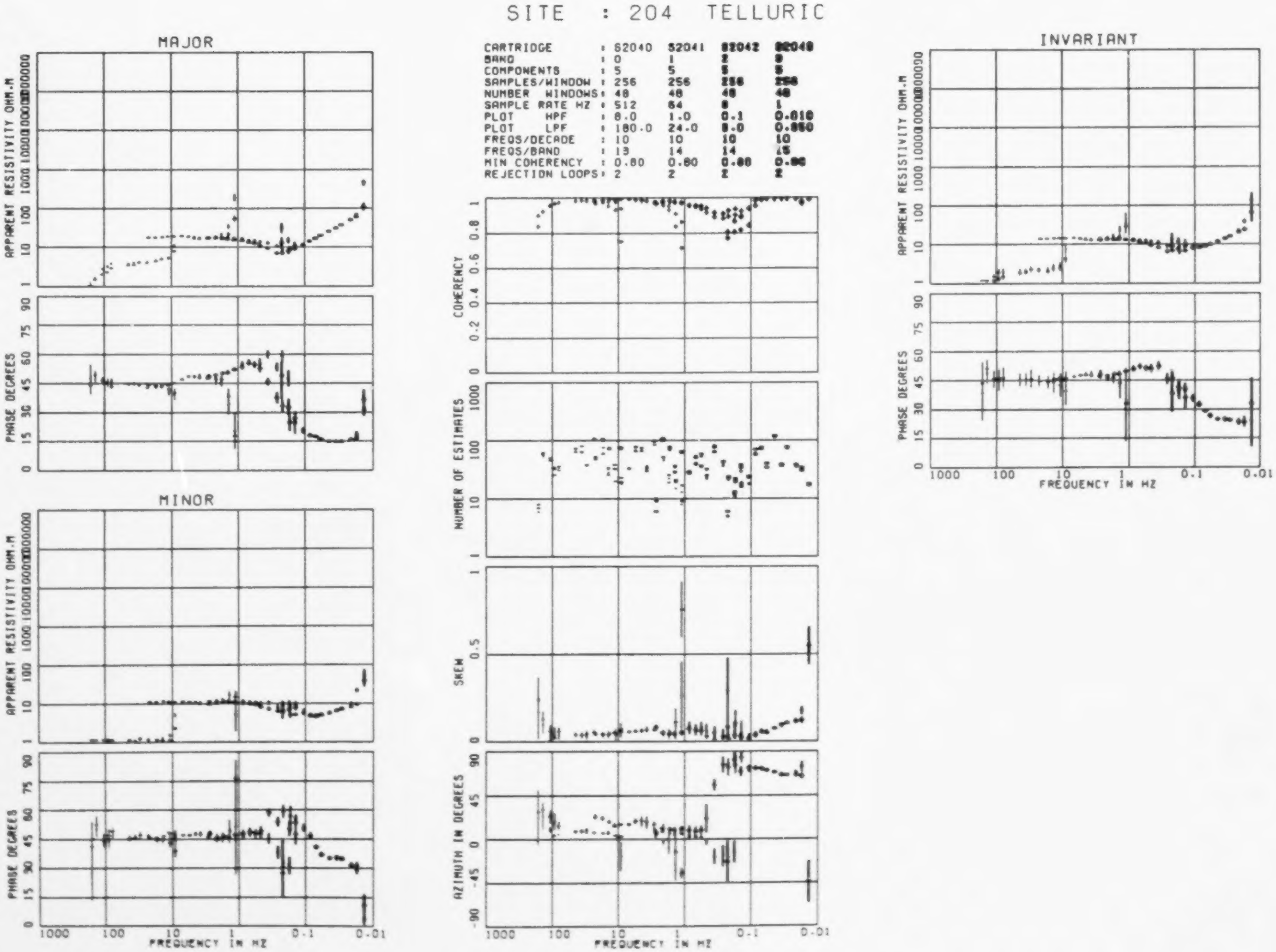

SITE : 204 TELLURIC

CARTRIDGE	: S2040	S2041	S2042	S2043
BAND	: 0	1	2	3
COMPONENTS	: 5	5	5	5
SAMPLES/WINDOW	: 256	256	256	256
NUMBER WINDOWS	: 48	48	48	48
SAMPLE RATE HZ	: 512	64	8	1
PLOT HPF	: 8.0	1.0	0.1	0.010
PLOT LPF	: 180.0	24.0	3.0	0.350
FREQS/DECADE	: 10	10	10	10
FREQS/BAND	: 13	14	14	15
MIN COHERENCY	: 0.80	0.80	0.80	0.80
REJECTION LOOPS	: 2	2	2	2

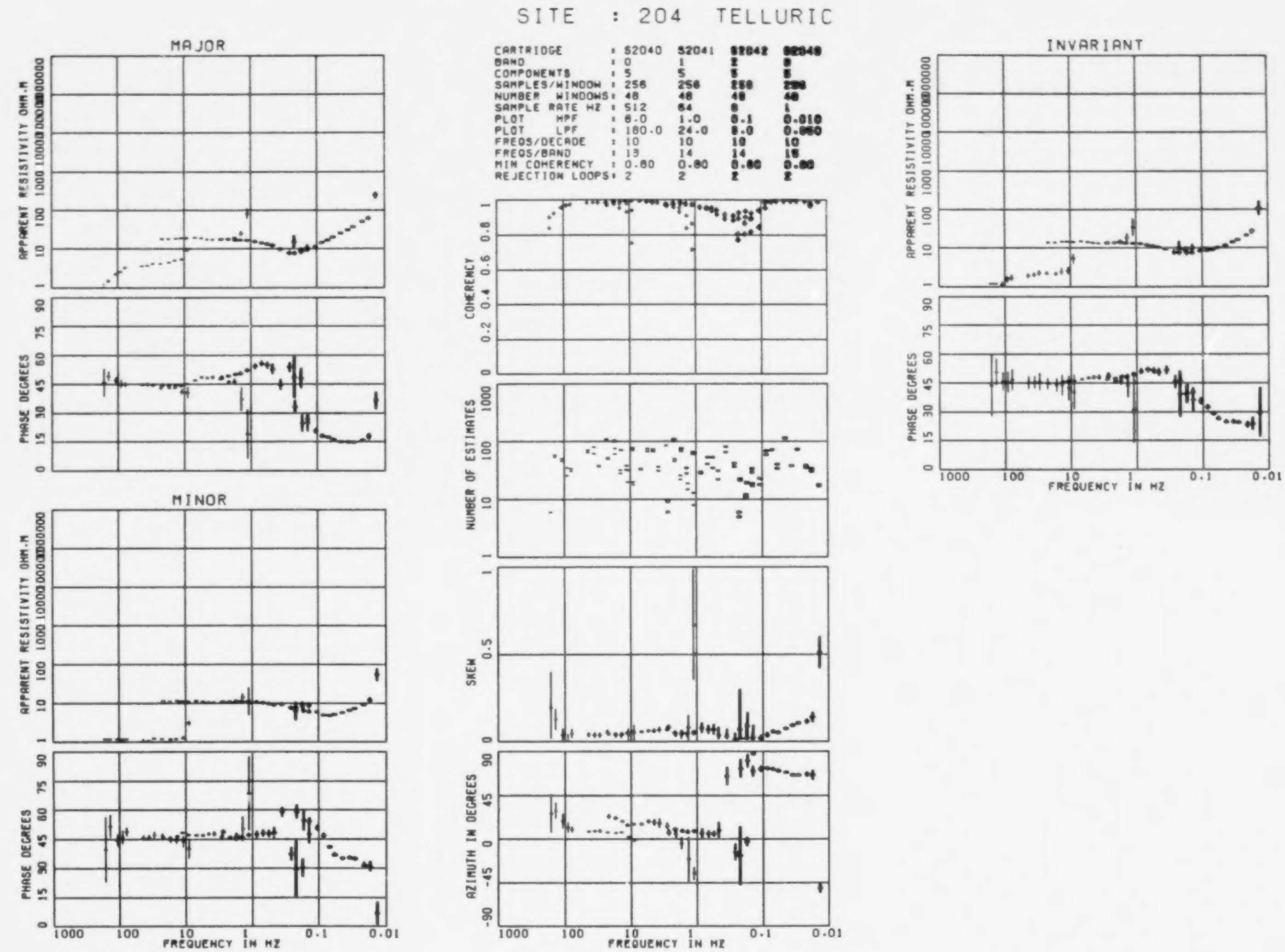

SITE : 204 TELLURIC

```
CARTRIDGE      : S2040   S2041   S2042   S2043
BAND           : 0       1       2       3
COMPONENTS     : 5       5       5       5
SAMPLES/WINDOW : 256     256     256     256
NUMBER  WINDOWS: 48      48      48      48
SAMPLE RATE HZ : 512     64      8       1
PLOT    HPF    : 8.0     1.0     0.1     0.010
PLOT    LPF    : 180.0   24.0    8.0     0.800
FREQS/DECADE   : 10      10      10      10
FREQS/BAND     : 13      14      14      15
MIN COHERENCY  : 0.80    0.80    0.80    0.80
REJECTION LOOPS: 2       2       2       2
```

```
SITE   : 204   MAGNETIC

CARTRIDGE         : 52040  52041  52042  52043
BAND              : 0      1      2      3
COMPONENTS        : 5      5      5      5
SAMPLES/WINDOW    : 256    256    256    256
NUMBER   WINDOWS  : 48     48     48     48
SAMPLE RATE HZ    : 512    64     8      1
PLOT      HPF     : 8.0    1.0    0.1    0.010
PLOT      LPF     : 180.0  24.0   3.0    0.350
FREQS/DECADE      : 10     10     10     10
FREQS/BAND        : 13     14     14     15
MIN COHERENCY     : 0.70   0.70   0.70   0.70
REJECTION LOOPS   : 2      2      2      2
```

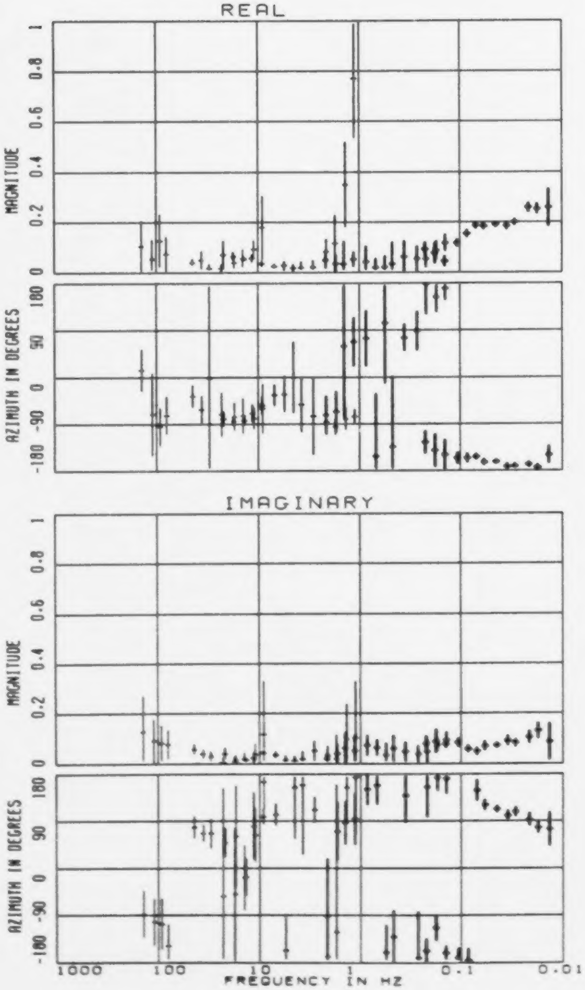

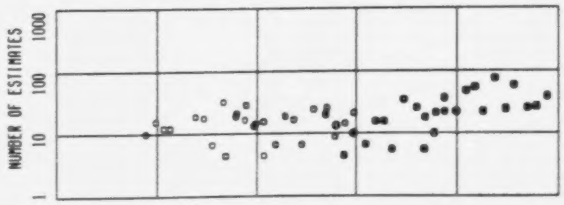

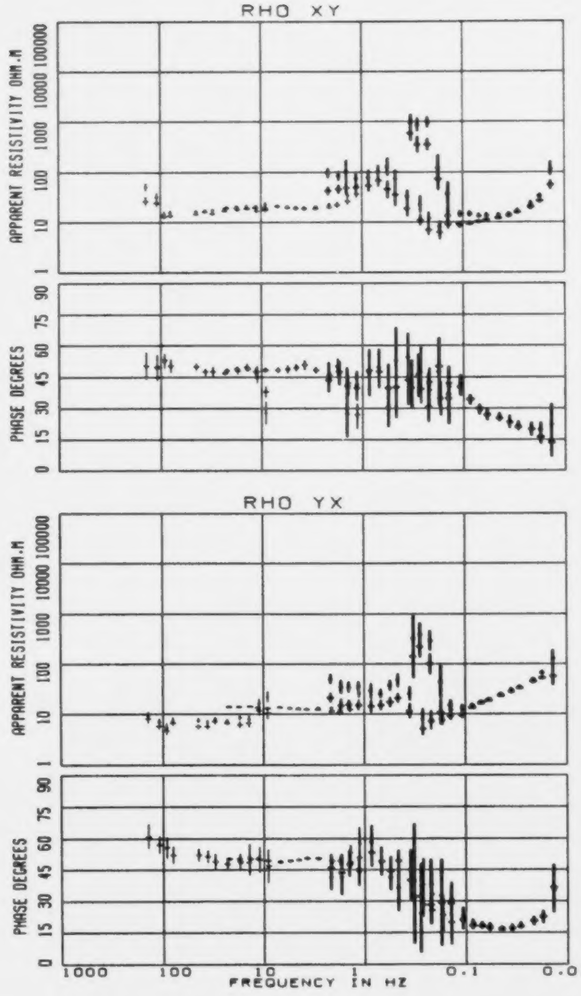

SITE : 205 TELLURIC

CARTRIDGE	: S2050	S2051	S2052	S2053
BAND	: 0	1	2	3
COMPONENTS	: 5	5	5	5
SAMPLES/WINDOW	: 256	256	256	256
NUMBER WINDOWS	: 48	48	24	48
SAMPLE RATE HZ	: 512	64	8	1
PLOT HPF	: 8.0	1.0	0.1	0.010
PLOT LPF	: 180.0	24.0	3.0	0.350
FREQS/DECADE	: 10	10	10	10
FREQS/BAND	: 13	14	14	15
MIN COHERENCY	: 0.80	0.80	0.80	0.80
REJECTION LOOPS	: 2	2	2	2

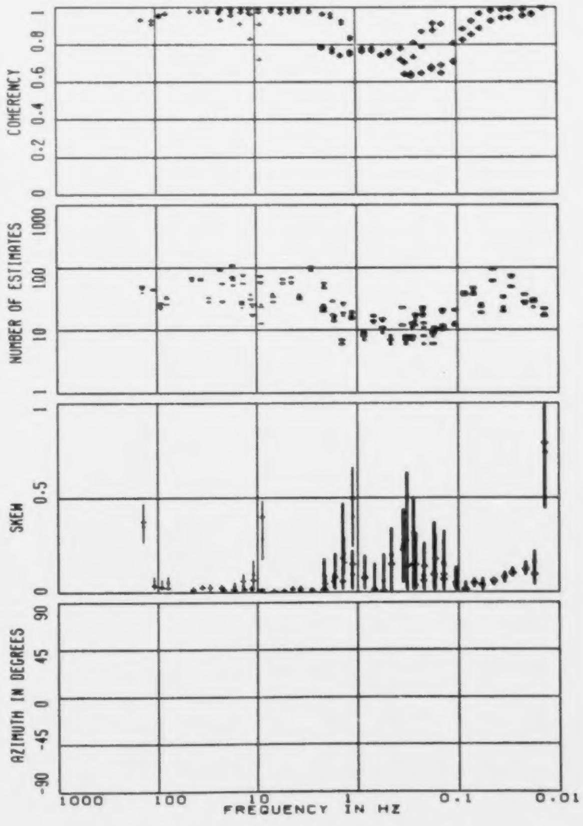

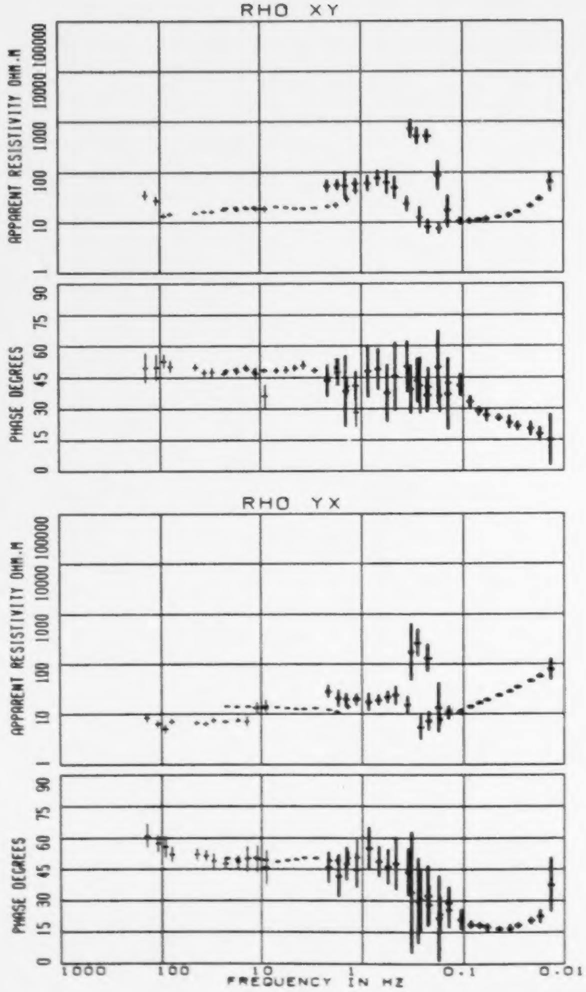

SITE : 205 TELLURIC

```
CARTRIDGE        : S2050  S2051  S2052  S2053
BAND             : 0      1      2      3
COMPONENTS       : 5      5      5      5
SAMPLES/WINDOW   : 256    256    256    256
NUMBER  WINDOWS  : 48     48     24     48
SAMPLE RATE HZ   : 512    64     8      1
PLOT     HPF     : 8.0    1.0    0.1    0.010
PLOT     LPF     : 180.0  24.0   3.0    0.350
FREQS/DECADE     : 10     10     10     10
FREQS/BAND       : 15     14     14     15
MIN COHERENCY    : 0.80   0.80   0.80   0.80
REJECTION LOOPS  : 2      2      2      2
```

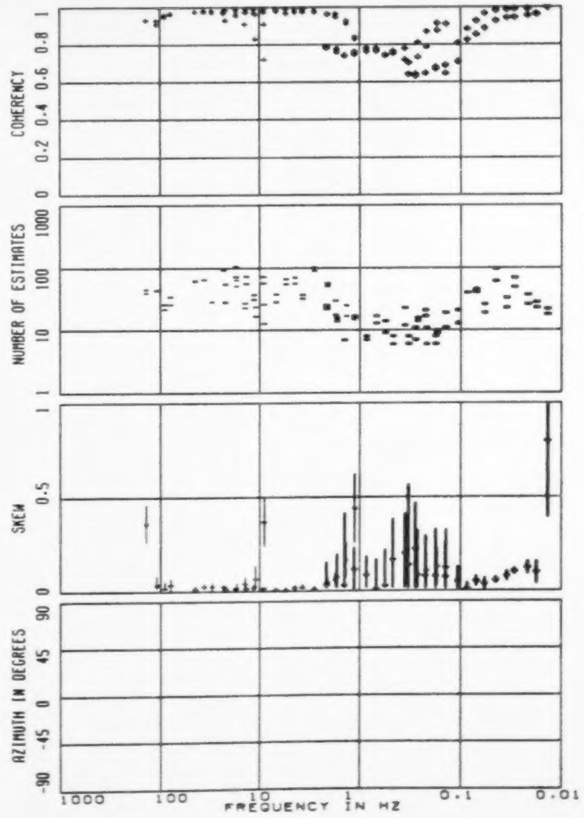

SITE : 205 TELLURIC

CARTRIDGE	: S2050	S2051	S2052	S2053
BAND	: 0	1	2	3
COMPONENTS	: 5	5	5	5
SAMPLES/WINDOW	: 256	256	256	256
NUMBER WINDOWS	: 48	48	24	48
SAMPLE RATE HZ	: 512	64	8	1
PLOT HPF	: 8.0	1.0	0.1	0.010
PLOT LPF	: 180.0	24.0	8.0	0.080
FREQS/DECADE	: 10	10	10	10
FREQS/BAND	: 13	14	14	15
MIN COHERENCY	: 0.80	0.80	0.80	0.80
REJECTION LOOPS	: 2	2	2	2

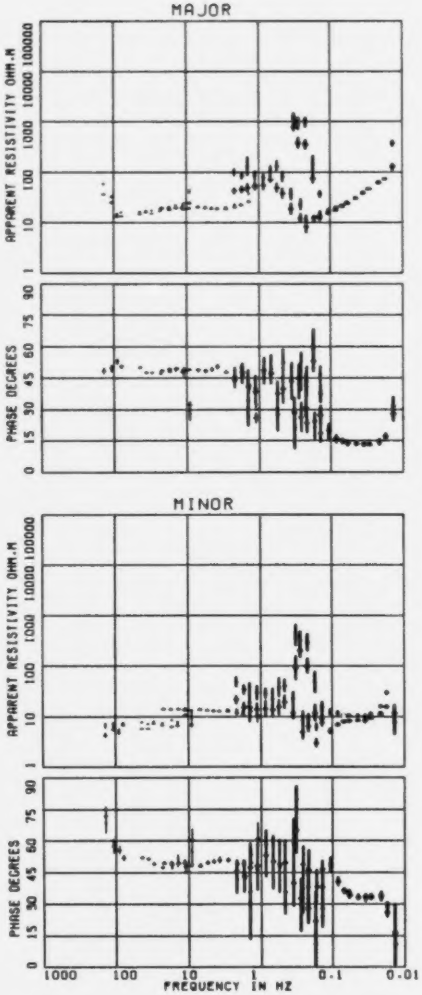

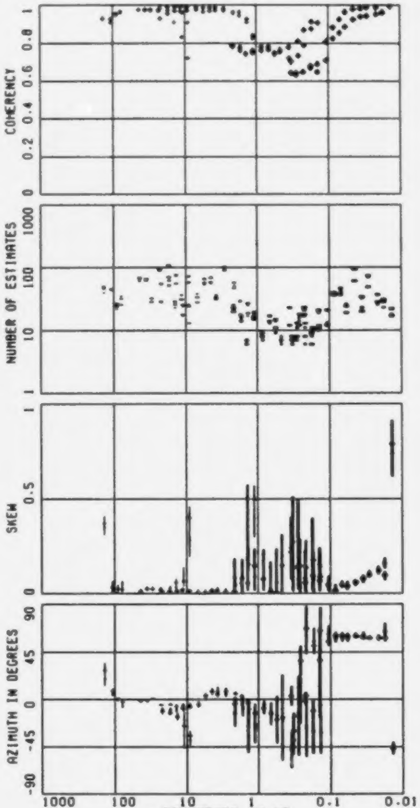

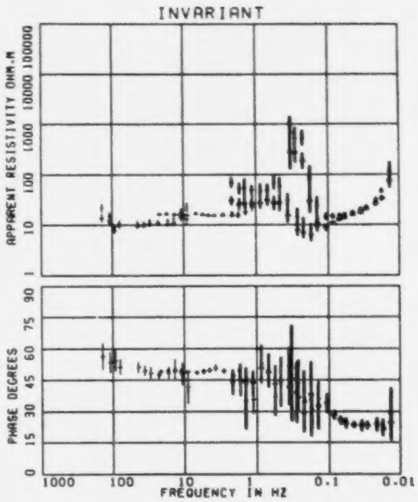

SITE : 205 TELLURIC

CARTRIDGE	: S2050	S2051	S2052	S2053
BAND	: 0	1	2	3
COMPONENTS	: 5	5	5	5
SAMPLES/WINDOW	: 256	256	256	256
NUMBER WINDOWS	: 48	48	24	48
SAMPLE RATE HZ	: 512	64	8	1
PLOT HPF	: 8.0	1.0	0.1	0.010
PLOT LPF	: 180.0	24.0	8.0	0.080
FREQS/DECADE	: 10	10	10	10
FREQS/BAND	: 13	14	14	15
MIN COHERENCY	: 0.80	0.80	0.80	0.80
REJECTION LOOPS	: 2	2	2	2

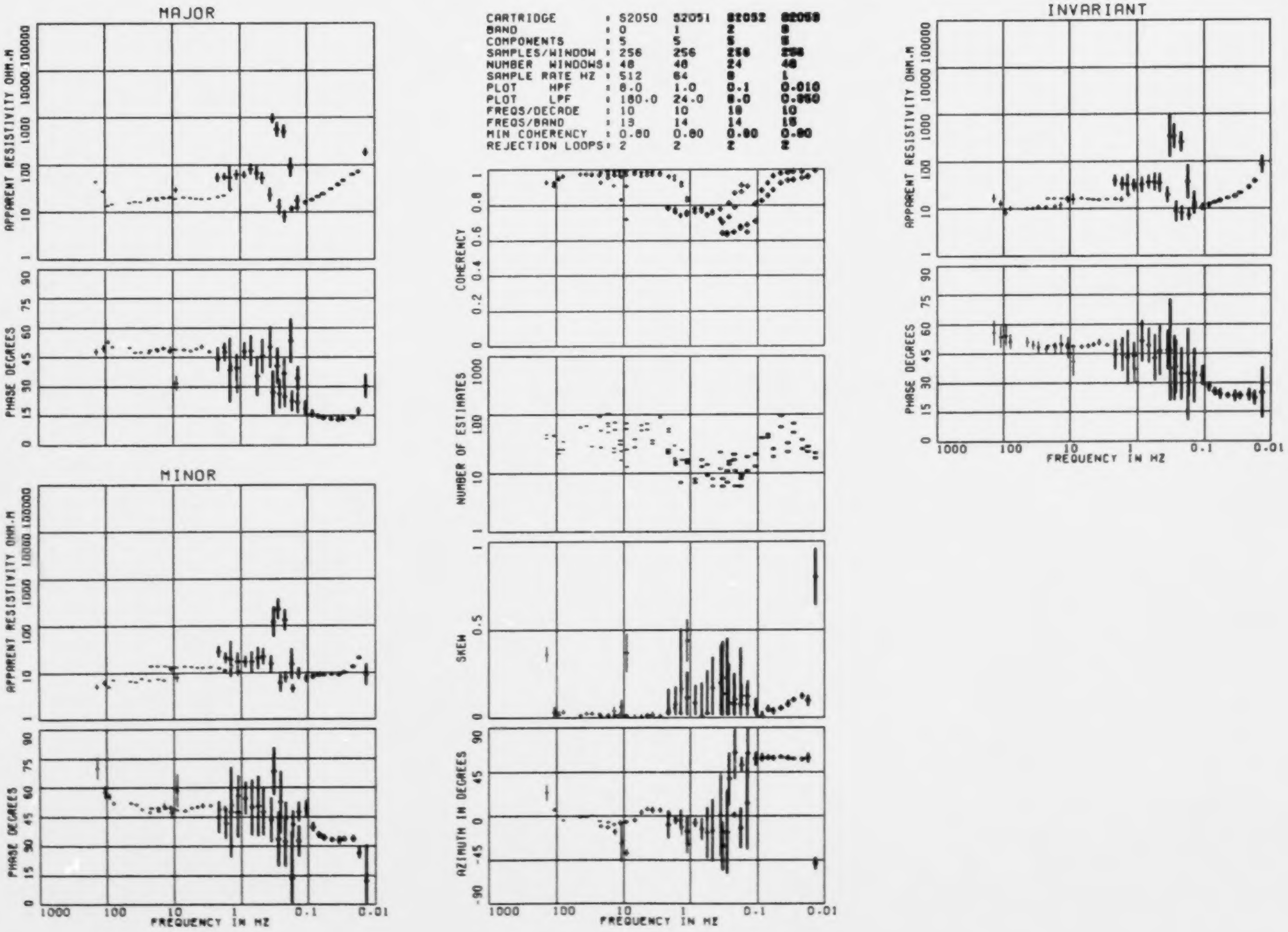

SITE : 205 MAGNETIC

CARTRIDGE	: 52050	52051	52052	52053
BAND	: 0	1	2	3
COMPONENTS	: 5	5	5	5
SAMPLES/WINDOW	: 256	256	256	256
NUMBER WINDOWS	: 48	48	24	48
SAMPLE RATE HZ	: 512	64	8	1
PLOT HPF	: 8.0	1.0	0.1	0.010
PLOT LPF	: 180.0	24.0	3.0	0.850
FREQS/DECADE	: 10	10	10	10
FREQS/BAND	: 19	14	14	15
MIN COHERENCY	: 0.70	0.70	0.70	0.70
REJECTION LOOPS	: 2	2	2	2

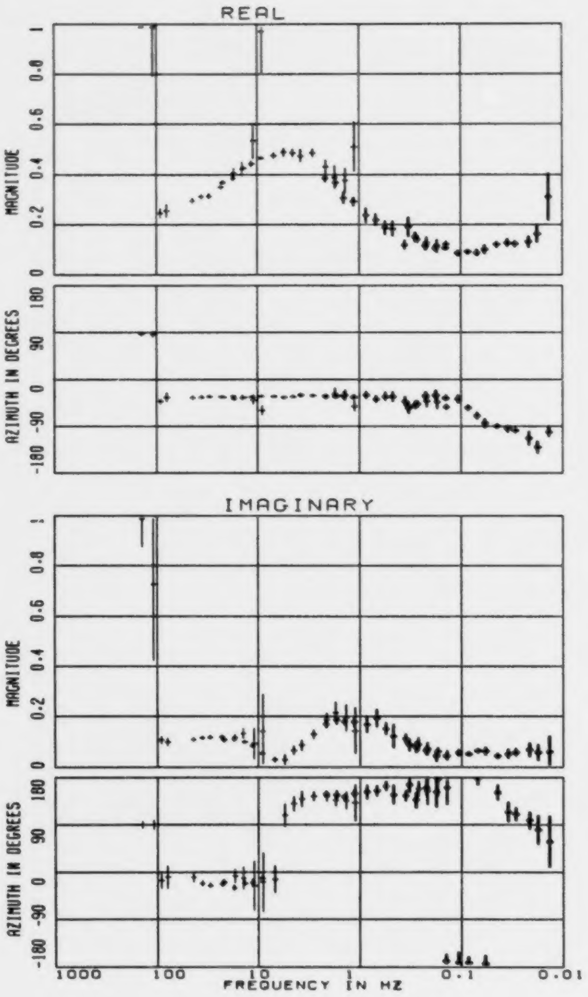

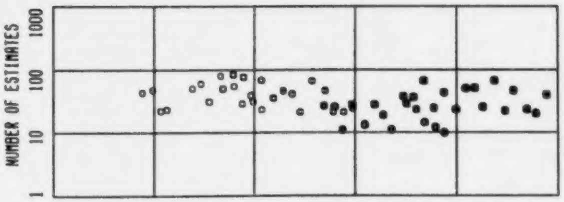

SITE : 206 TELLURIC

CARTRIDGE	:	S2060	S2061	S2062	S2063
BAND	:	0	1	2	3
COMPONENTS	:	5	5	5	5
SAMPLES/WINDOW	:	256	256	256	256
NUMBER WINDOWS	:	48	48	48	48
SAMPLE RATE HZ	:	512	64	8	1
PLOT HPF	:	8.0	1.0	0.1	0.010
PLOT LPF	:	180.0	24.0	3.0	0.380
FREQS/DECADE	:	10	10	10	10
FREQS/BAND	:	19	14	14	15
MIN COHERENCY	:	0.80	0.80	0.80	0.80
REJECTION LOOPS	:	2	2	2	2

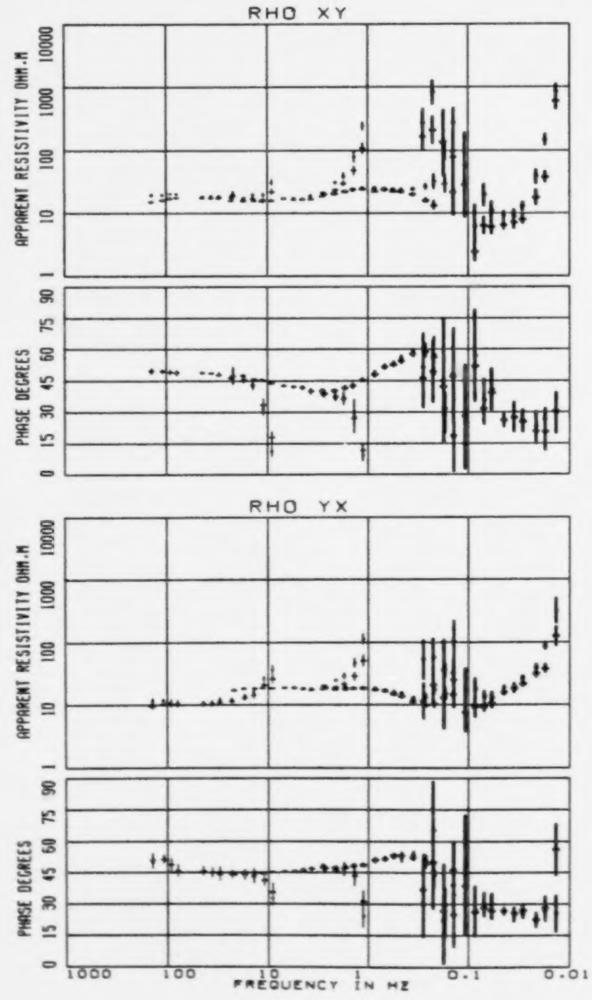

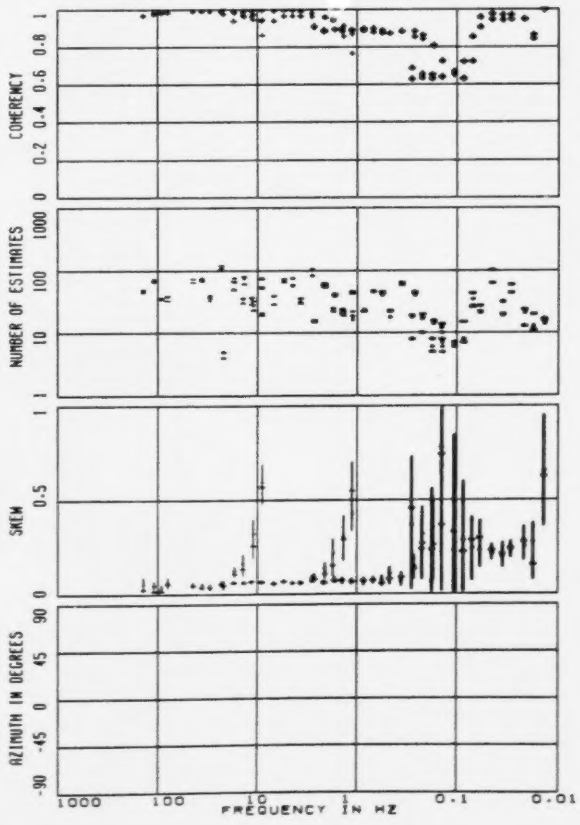

SITE : 206 TELLURIC

CARTRIDGE	S2060	S2061	S2062	S2063
BAND	0	1	2	3
COMPONENTS	5	5	5	5
SAMPLES/WINDOW	256	256	256	256
NUMBER WINDOWS	48	48	48	48
SAMPLE RATE HZ	512	64	8	1
PLOT HPF	8.0	1.0	0.1	0.010
PLOT LPF	180.0	24.0	3.0	0.350
FREQS/DECADE	10	10	10	10
FREQS/BAND	13	14	14	15
MIN COHERENCY	0.80	0.80	0.80	0.80
REJECTION LOOPS	2	2	2	2

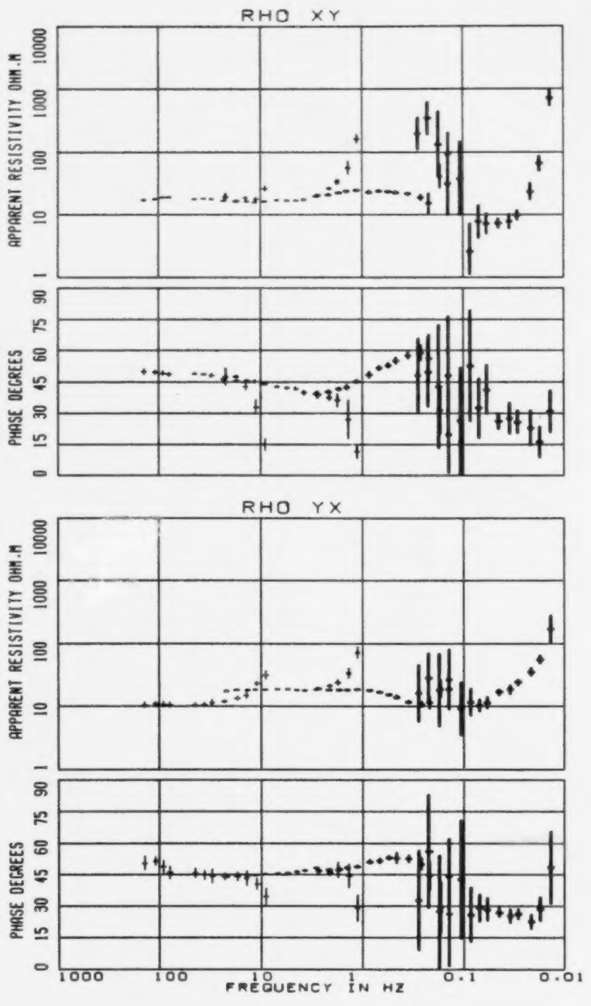

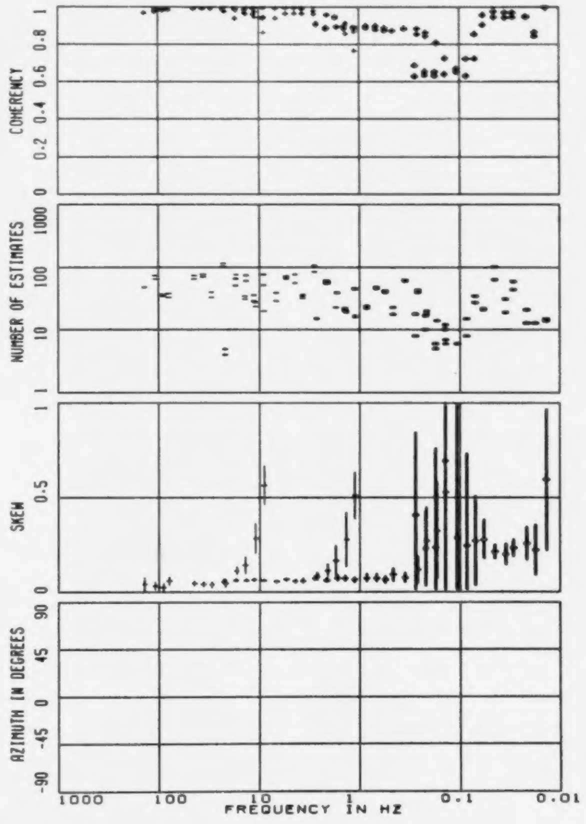

SITE : 206 TELLURIC

```
CARTRIDGE       : S2060  S2061  S2062  S2063
BAND            : 0      1      2      3
COMPONENTS      : 5      5      5      5
SAMPLES/WINDOW  : 256    256    256    256
NUMBER  WINDOWS : 48     48     48     48
SAMPLE RATE HZ  : 512    64     8      1
PLOT     HPF    : 8.0    1.0    0.1    0.010
PLOT     LPF    : 180.0  24.0   8.0    0.080
FREQS/DECADE    : 10     10     10     10
FREQS/BAND      : 13     14     14     15
MIN COHERENCY   : 0.80   0.80   0.80   0.80
REJECTION LOOPS : 2      2      2      2
```

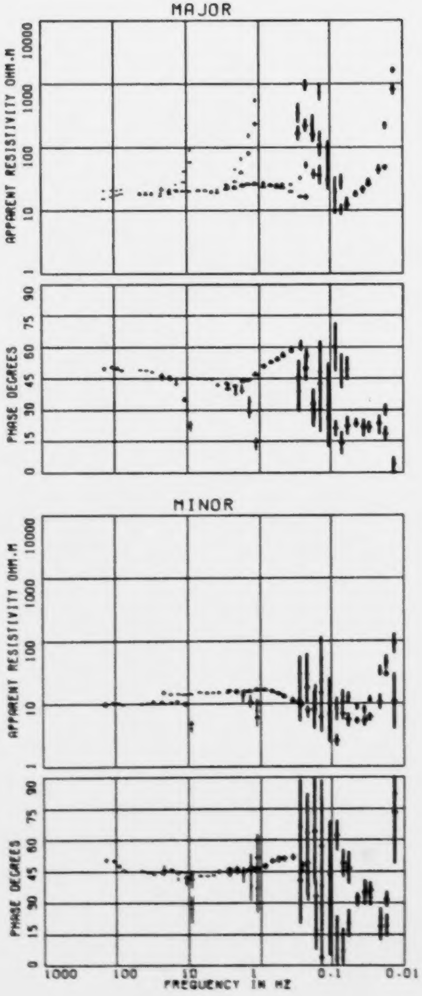

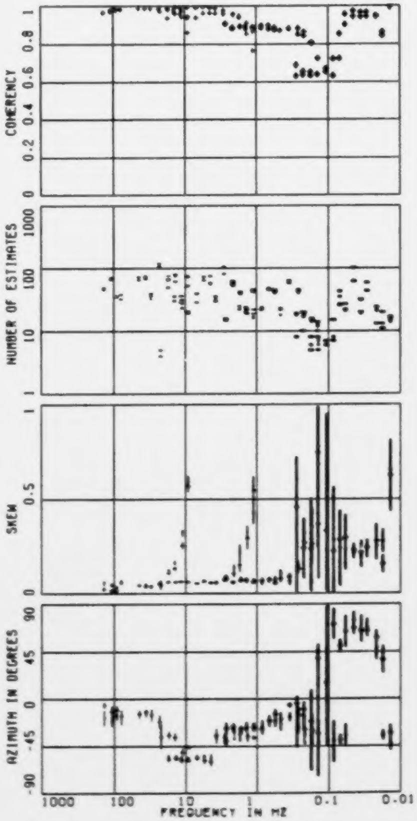

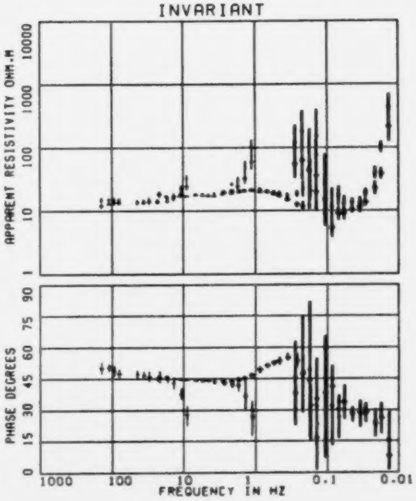

SITE : 206 TELLURIC

CARTRIDGE	: S2060	S2061	S2062	S2063
BAND	: 0	1	2	3
COMPONENTS	: 5	5	5	5
SAMPLES/WINDOW	: 256	256	256	256
NUMBER WINDOWS	: 48	48	48	48
SAMPLE RATE HZ	: 512	64	8	1
PLOT HPF	: 8.0	1.0	0.1	0.010
PLOT LPF	: 180.0	24.0	8.0	0.080
FREQS/DECADE	: 10	10	10	10
FREQS/BAND	: 13	14	14	15
MIN COHERENCY	: 0.80	0.80	0.80	0.80
REJECTION LOOPS	: 2	2	2	2

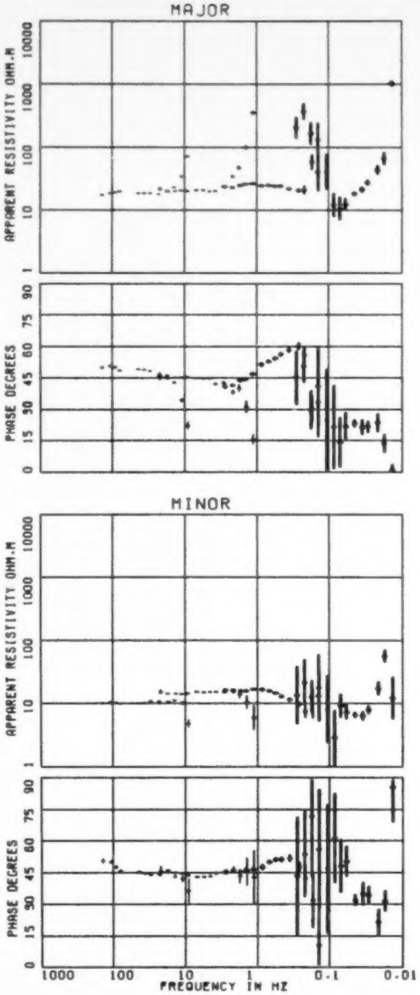

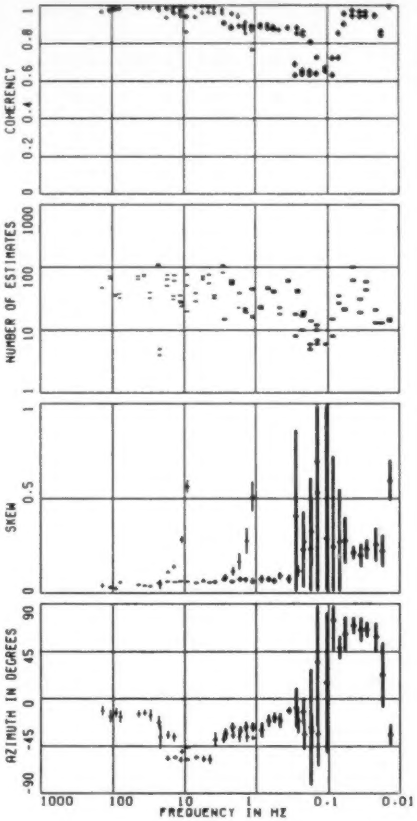

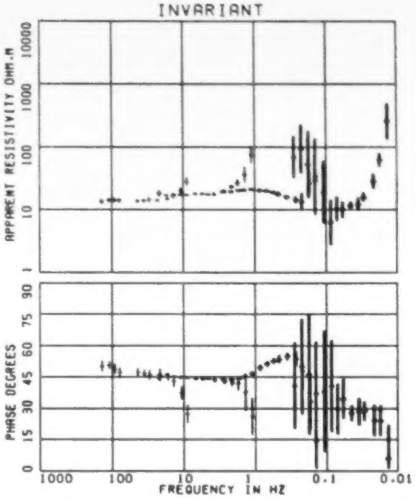

SITE : 206 MAGNETIC

```
CARTRIDGE        : 52060   52061   52062   52063
BAND             : 0       1       2       3
COMPONENTS       : 5       5       5       5
SAMPLES/WINDOW   : 256     256     256     256
NUMBER  WINDOWS  : 48      48      48      48
SAMPLE RATE HZ   : 512     64      8       1
PLOT     HPF     : 8.0     1.0     0.1     0.010
PLOT     LPF     : 180.0   24.0    3.0     0.350
FREQS/DECADE     : 10      10      10      10
FREQS/BAND       : 13      14      14      13
MIN COHERENCY    : 0.70    0.70    0.70    0.70
REJECTION LOOPS  : 2       2       2       2
```

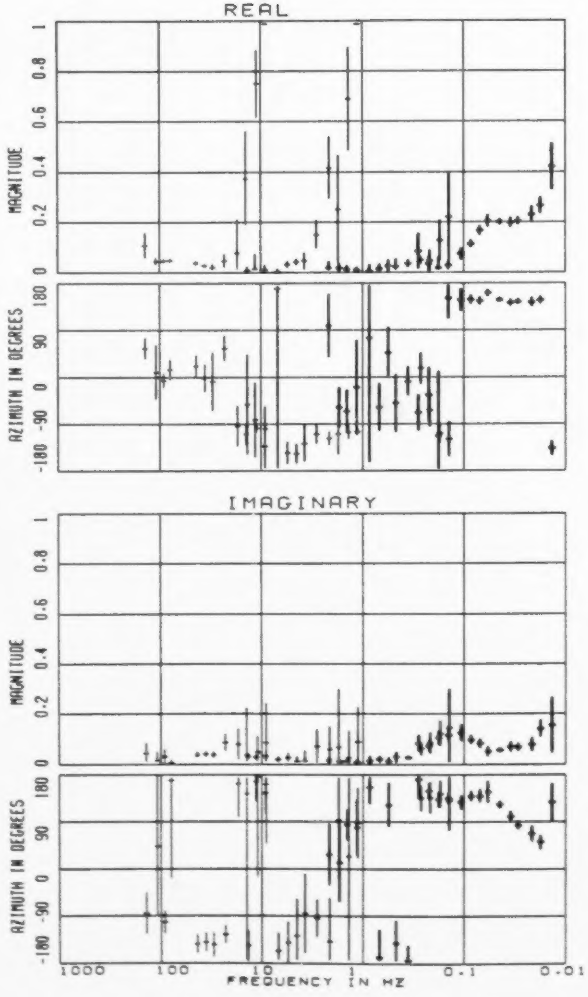

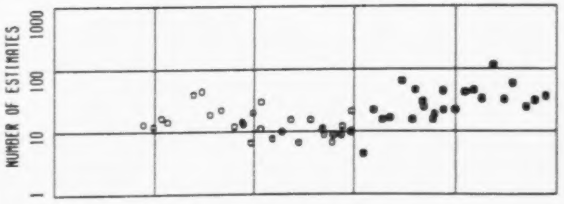

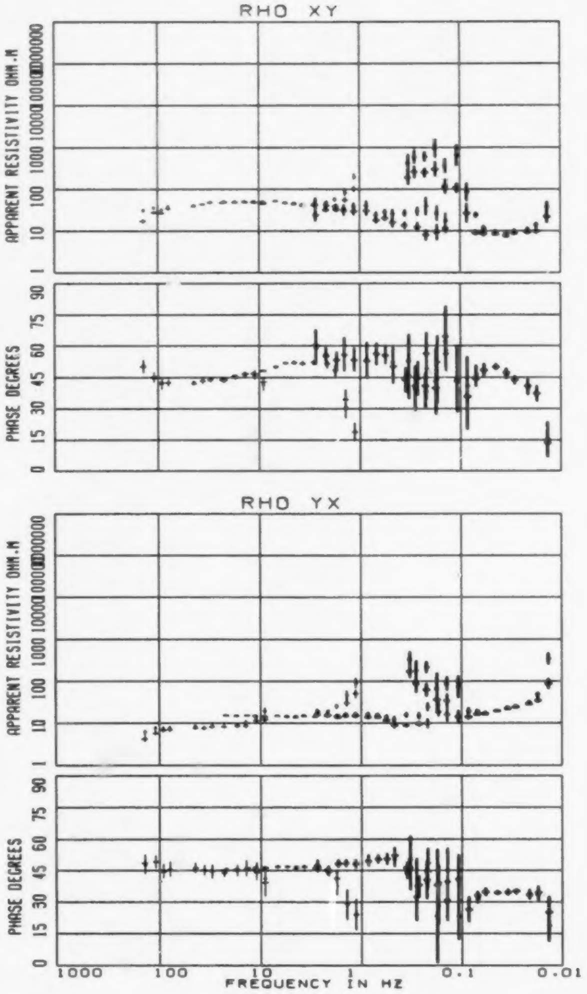

SITE : 207 TELLURIC

CARTRIDGE :	S2070	S2071	S2072	S2073
BAND :	0	1	2	3
COMPONENTS :	5	5	5	5
SAMPLES/WINDOW :	256	256	256	256
NUMBER WINDOWS :	48	48	48	48
SAMPLE RATE HZ :	512	64	8	1
PLOT HPF :	8.0	1.0	0.1	0.010
PLOT LPF :	180.0	24.0	3.0	0.350
FREQS/DECADE :	10	10	10	10
FREQS/BAND :	15	14	14	15
MIN COHERENCY :	0.80	0.80	0.80	0.80
REJECTION LOOPS :	2	2	2	2

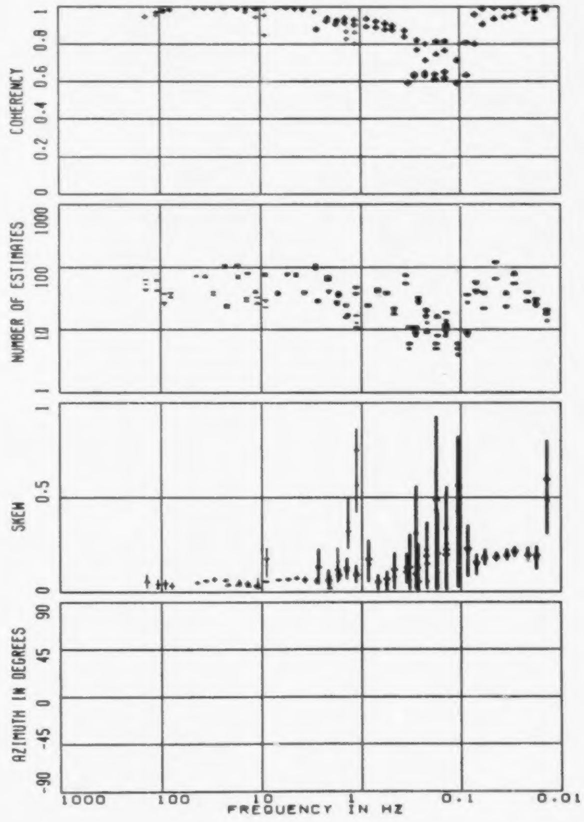

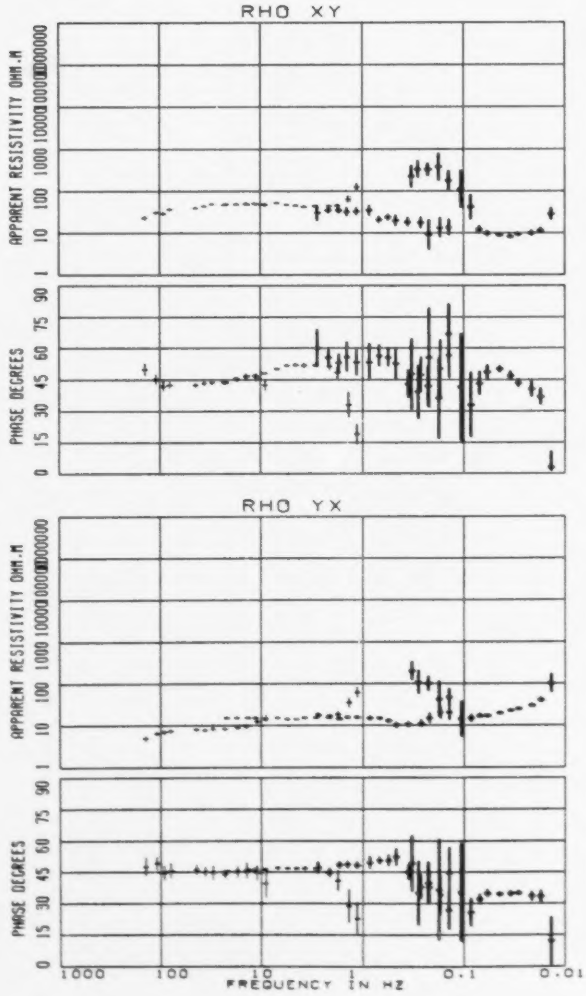

SITE : 207 TELLURIC

CARTRIDGE	: 52070	52071	52072	52073
BAND	: 0	1	2	3
COMPONENTS	: 5	5	5	5
SAMPLES/WINDOW	: 256	256	256	256
NUMBER WINDOWS	: 48	48	48	48
SAMPLE RATE HZ	: 512	64	8	1
PLOT HPF	: 8.0	1.0	0.1	0.010
PLOT LPF	: 180.0	24.0	3.0	0.350
FREQS/DECADE	: 10	10	10	10
FREQS/BAND	: 13	14	14	15
MIN COHERENCY	: 0.80	0.80	0.80	0.80
REJECTION LOOPS	: 2	2	2	2

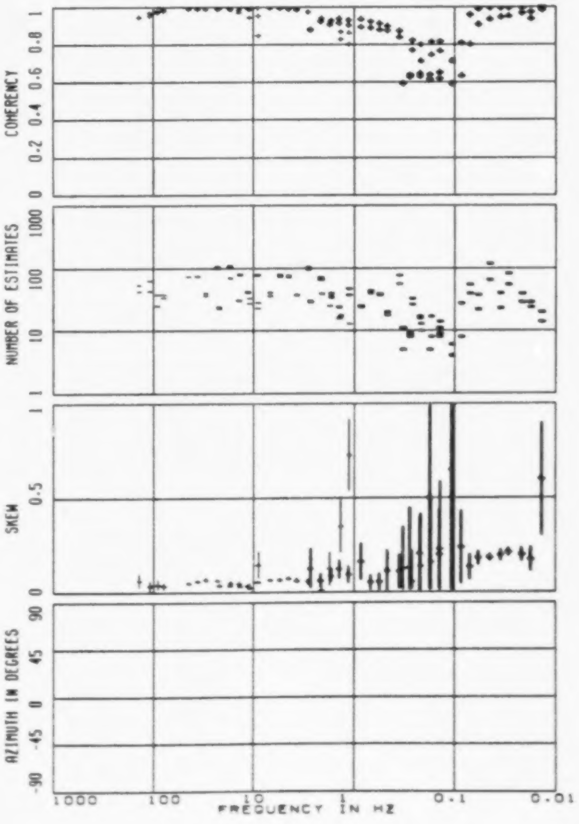

SITE : 207 TELLURIC

CARTRIDGE	: S2070	S2071	S2072	S2073
BAND	: 0	1	2	3
COMPONENTS	: 5	5	5	5
SAMPLES/WINDOW	: 256	256	256	256
NUMBER WINDOWS	: 48	48	48	48
SAMPLE RATE HZ	: 512	64	8	1
PLOT HPF	: 8.0	1.0	0.1	0.010
PLOT LPF	: 180.0	24.0	3.0	0.050
FREQS/DECADE	: 10	10	10	10
FREQS/BAND	: 13	14	14	15
MIN COHERENCY	: 0.80	0.80	0.80	0.80
REJECTION LOOPS	: 2	2	2	2

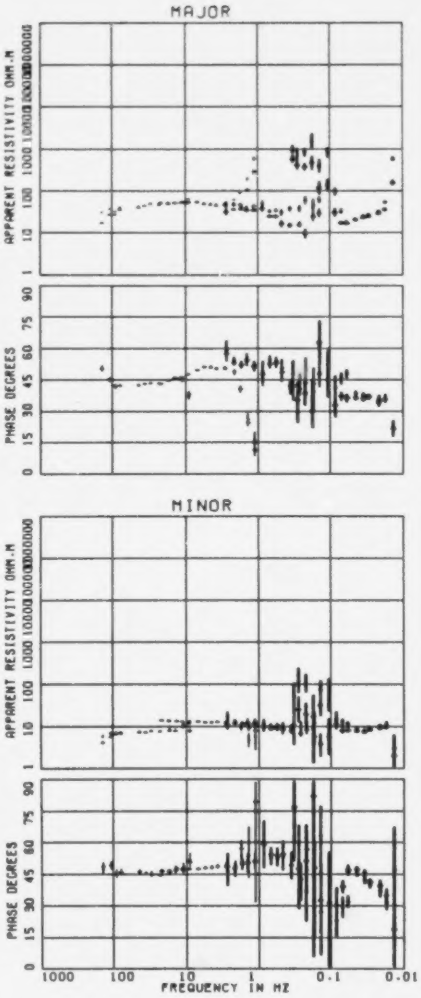

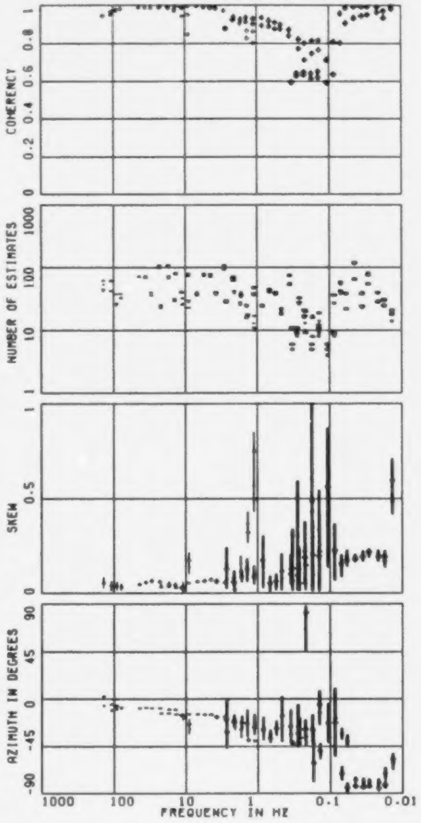

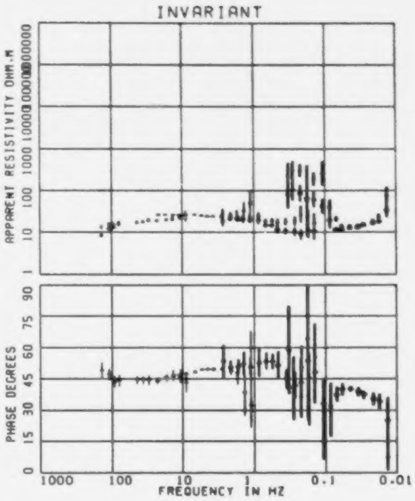

SITE : 207 TELLURIC

CARTRIDGE :	52070	52071	52072	52073
BAND :	0	1	2	3
COMPONENTS :	5	5	5	5
SAMPLES/WINDOW :	256	256	256	256
NUMBER WINDOWS :	48	48	48	48
SAMPLE RATE HZ :	512	64	8	1
PLOT HPF :	8.0	1.0	0.1	0.010
PLOT LPF :	180.0	24.0	3.0	0.350
FREQS/DECADE :	10	10	10	10
FREQS/BAND :	13	14	14	15
MIN COHERENCY :	0.80	0.80	0.80	0.80
REJECTION LOOPS :	2	2	2	2

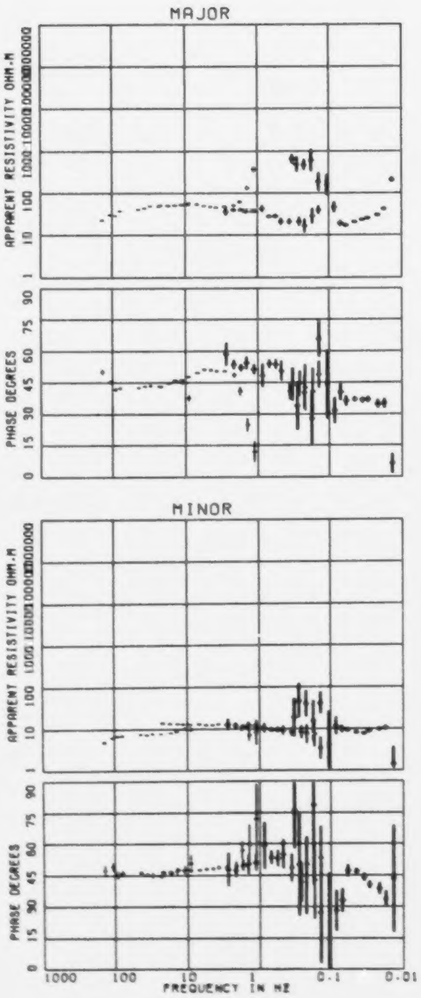

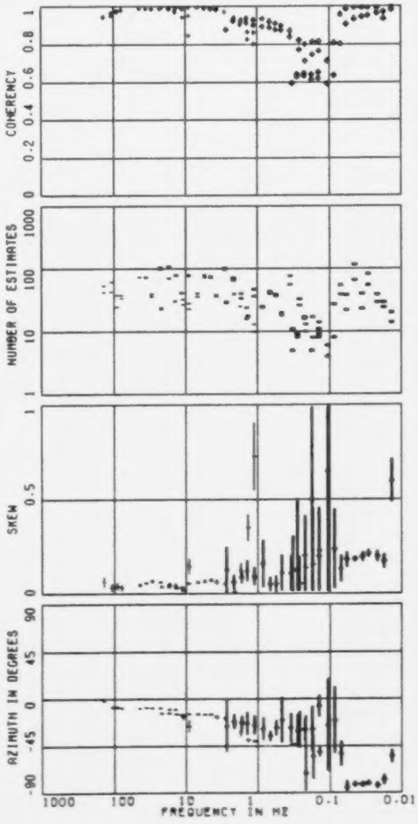

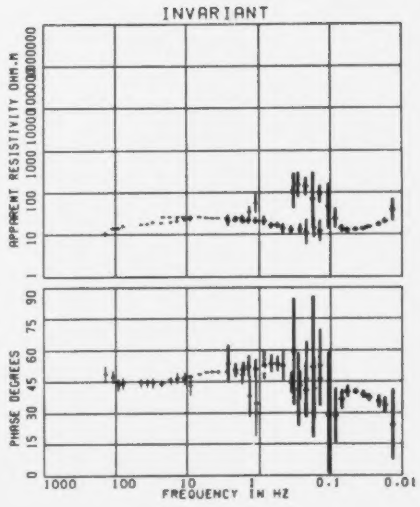

SITE : 207 MAGNETIC

CARTRIDGE :	S2070	S2071	S2072	S2073
BAND :	0	1	2	3
COMPONENTS :	5	5	5	5
SAMPLES/WINDOW :	256	256	256	256
NUMBER WINDOWS :	48	48	48	48
SAMPLE RATE HZ :	512	64	8	1
PLOT HPF :	8.0	1.0	0.1	0.010
PLOT LPF :	180.0	24.0	3.0	0.350
FREQS/DECADE :	10	10	10	10
FREQS/BAND :	13	14	14	15
MIN COHERENCY :	0.70	0.70	0.70	0.70
REJECTION LOOPS :	2	2	2	2

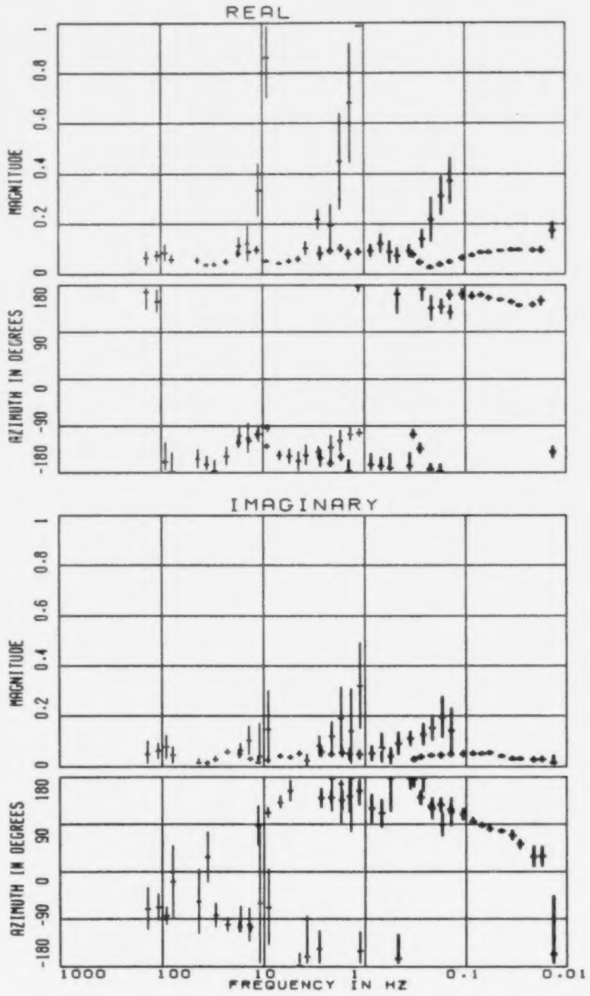

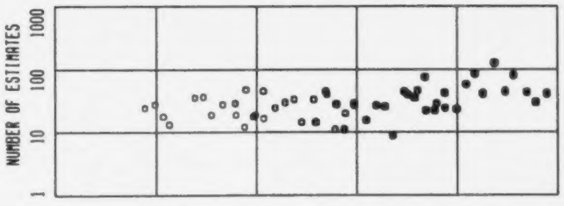

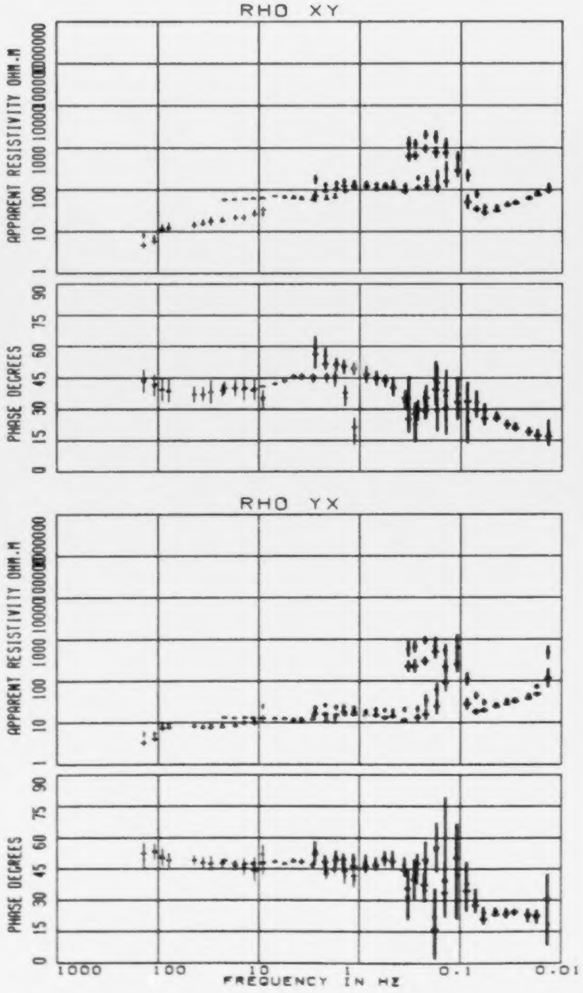

SITE : 208 TELLURIC

CARTRIDGE	:	52080	52081	52082	52083
BAND	:	0	1	2	3
COMPONENTS	:	5	5	5	5
SAMPLES/WINDOW	:	256	256	256	256
NUMBER WINDOWS	:	48	48	48	48
SAMPLE RATE HZ	:	512	64	8	1
PLOT HPF	:	8.0	1.0	0.1	0.010
PLOT LPF	:	180.0	24.0	3.0	0.350
FREQS/DECADE	:	10	10	10	10
FREQS/BAND	:	19	14	14	15
MIN COHERENCY	:	0.80	0.80	0.80	0.80
REJECTION LOOPS	:	2	2	2	2

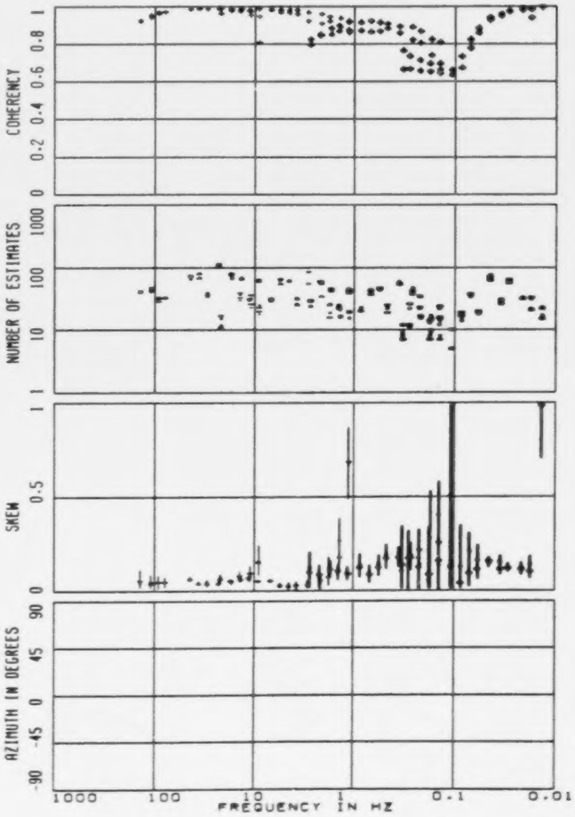

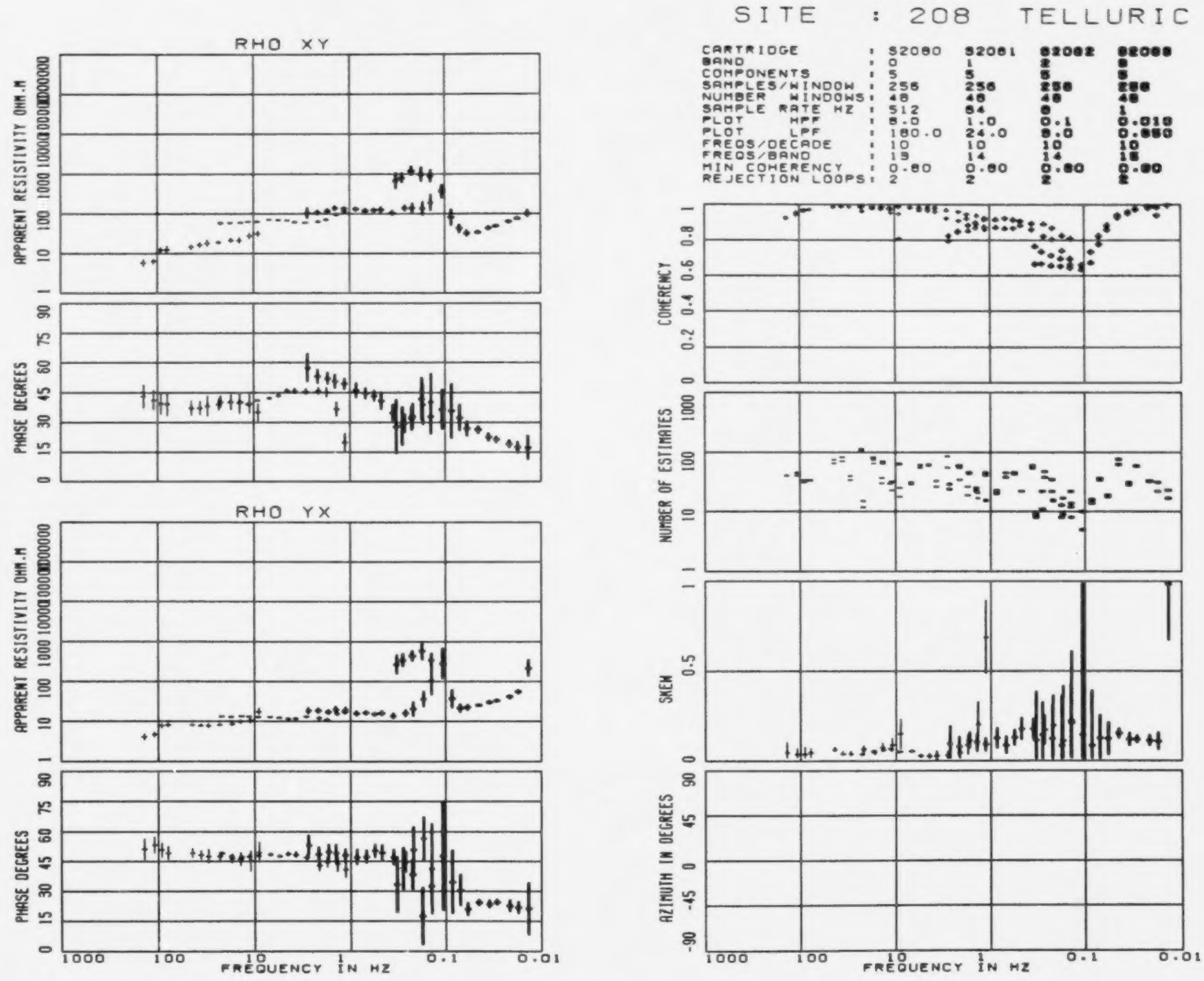

SITE : 208 TELLURIC

```
CARTRIDGE        : S2080   S2081   S2082   S2083
BAND             : 0       1       2       3
COMPONENTS       : 5       5       5       5
SAMPLES/WINDOW   : 256     256     256     256
NUMBER  WINDOWS  : 48      48      48      48
SAMPLE RATE HZ   : 512     64      8       1
PLOT     HPF     : 8.0     1.0     0.1     0.010
PLOT     LPF     : 180.0   24.0    3.0     0.350
FREQS/DECADE     : 10      10      10      10
FREQS/BAND       : 13      14      14      15
MIN COHERENCY    : 0.80    0.80    0.80    0.80
REJECTION LOOPS  : 2       2       2       2
```

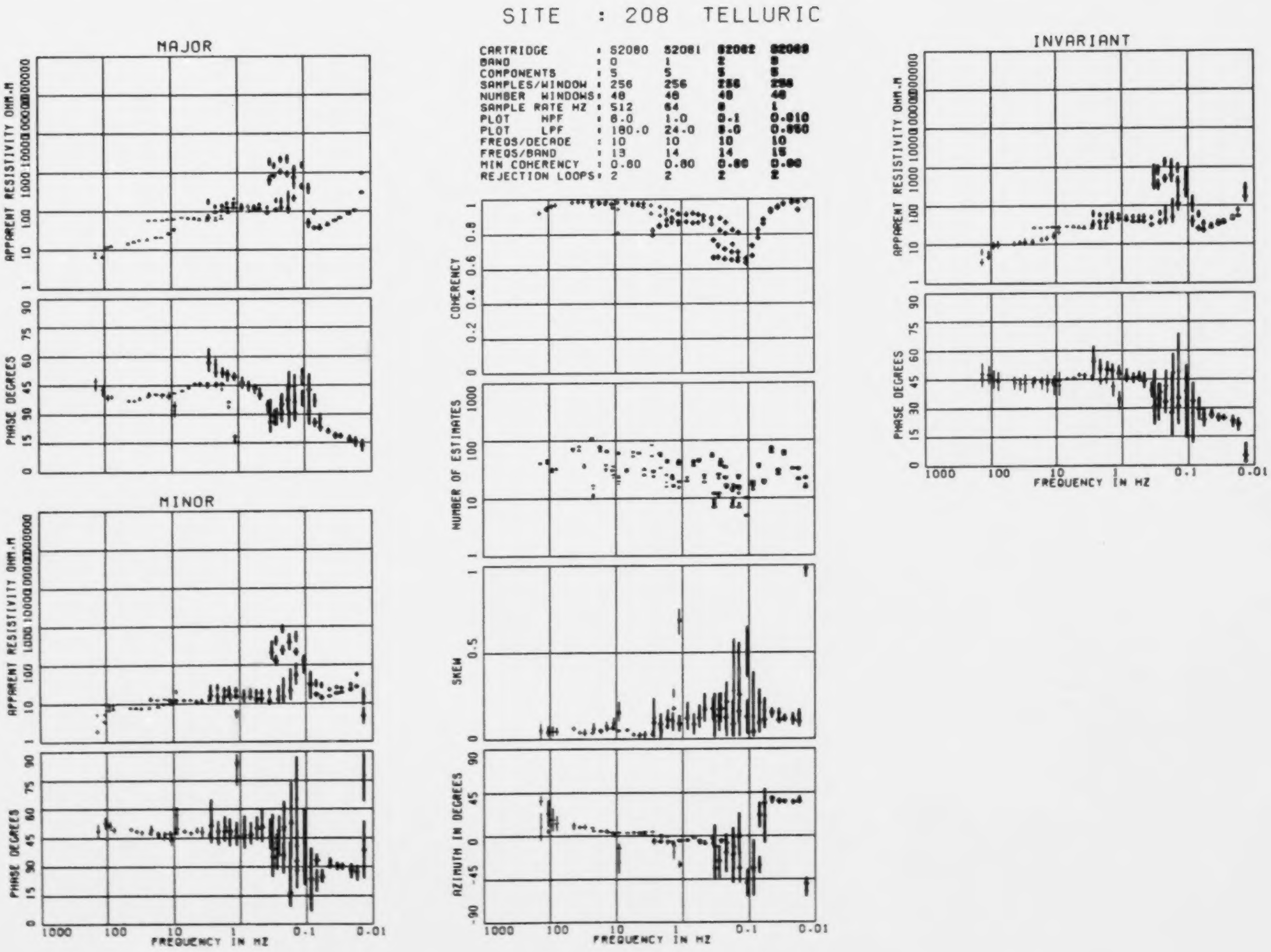

SITE : 208 TELLURIC

CARTRIDGE	: S2080	S2081	S2082	S2083
BAND	: 0	1	2	3
COMPONENTS	: 5	5	5	5
SAMPLES/WINDOW	: 256	256	256	256
NUMBER WINDOWS	: 48	48	48	48
SAMPLE RATE HZ	: 512	64	8	1
PLOT HPF	: 8.0	1.0	0.1	0.010
PLOT LPF	: 180.0	24.0	8.0	0.080
FREQS/DECADE	: 10	10	10	10
FREQS/BAND	: 13	14	14	15
MIN COHERENCY	: 0.80	0.80	0.80	0.80
REJECTION LOOPS	: 2	2	2	2

SITE : 208 TELLURIC

CARTRIDGE	:	S2080	S2081	S2082	S2083
BAND	:	0	1	2	3
COMPONENTS	:	5	5	5	5
SAMPLES/WINDOW	:	256	256	256	256
NUMBER WINDOWS	:	48	48	48	48
SAMPLE RATE HZ	:	512	64	8	1
PLOT HPF	:	8.0	1.0	0.1	0.010
PLOT LPF	:	180.0	24.0	3.0	[illegible]
FREQS/DECADE	:	10	10	10	10
FREQS/BAND	:	13	14	14	15
MIN COHERENCY	:	0.80	0.80	0.80	0.80
REJECTION LOOPS	:	2	2	2	2

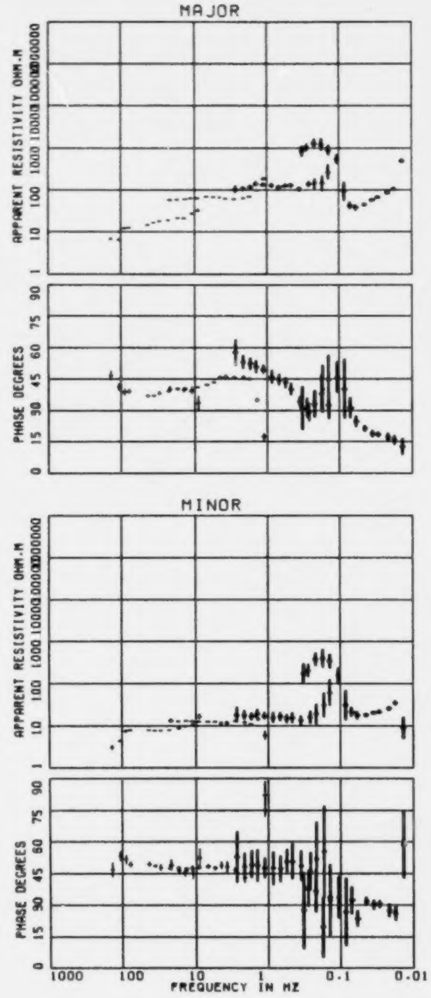

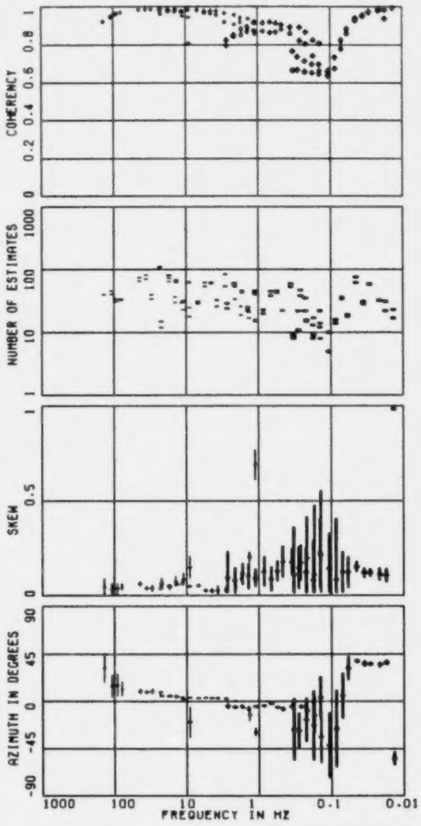

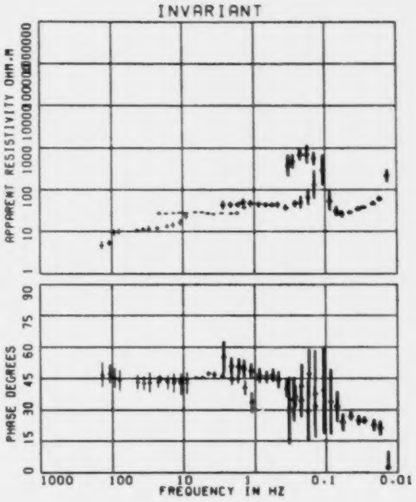

SITE : 208 MAGNETIC

CARTRIDGE :	S2080	S2081	S2082	S2083
BAND :	0	1	2	3
COMPONENTS :	5	5	5	5
SAMPLES/WINDOW :	256	256	256	256
NUMBER WINDOWS :	48	48	48	48
SAMPLE RATE HZ :	512	64	8	1
PLOT HPF :	8.0	1.0	0.1	0.010
PLOT LPF :	180.0	24.0	3.0	0.350
FREQS/DECADE :	10	10	10	10
FREQS/BAND :	13	14	14	15
MIN COHERENCY :	0.70	0.70	0.70	0.70
REJECTION LOOPS :	2	2	2	2

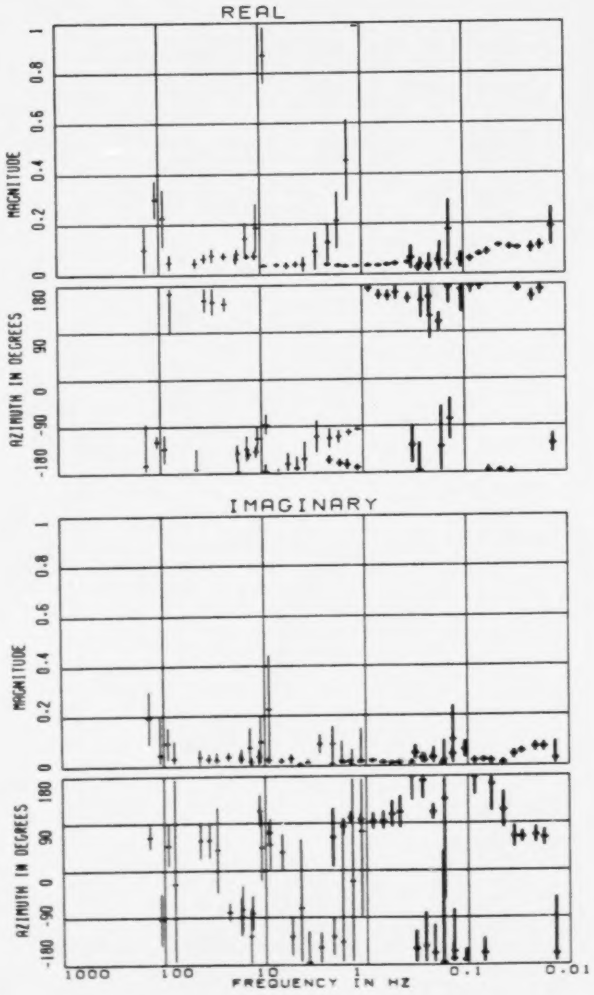

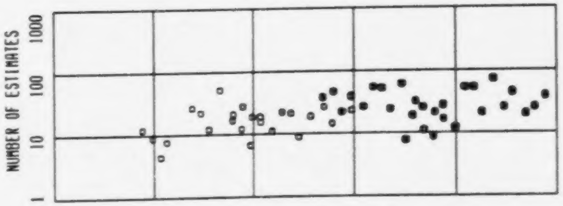

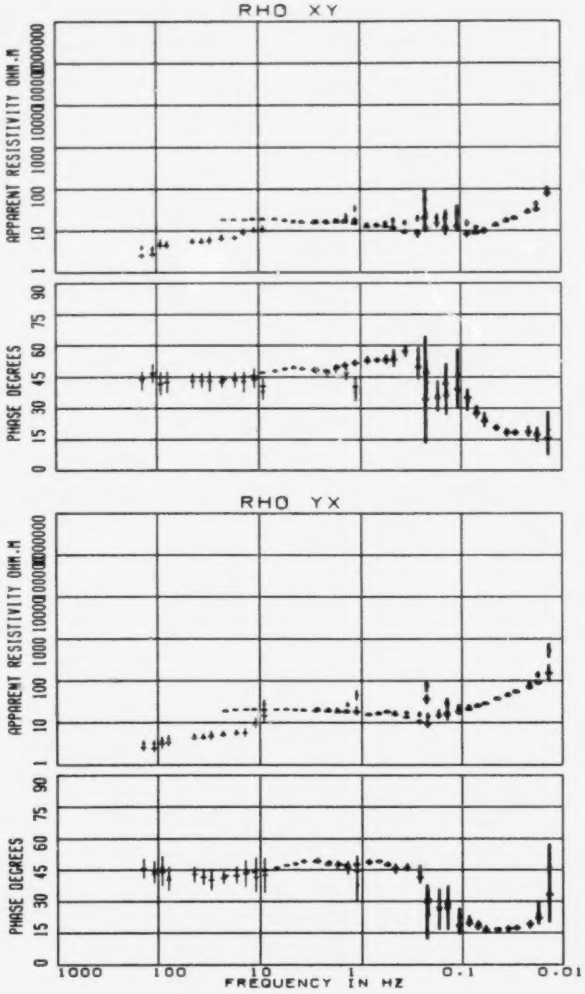

SITE : 209 TELLURIC

CARTRIDGE	:	S2090	S2091	S2092	S2093
BAND	:	0	1	2	3
COMPONENTS	:	5	5	5	5
SAMPLES/WINDOW	:	256	256	256	256
NUMBER WINDOWS	:	48	48	48	48
SAMPLE RATE HZ	:	512	64	8	1
PLOT HPF	:	8.0	1.0	0.1	0.010
PLOT LPF	:	180.0	24.0	3.0	0.350
FREQS/DECADE	:	10	10	10	10
FREQS/BAND	:	19	14	14	15
MIN COHERENCY	:	0.80	0.80	0.80	0.80
REJECTION LOOPS	:	2	2	2	2

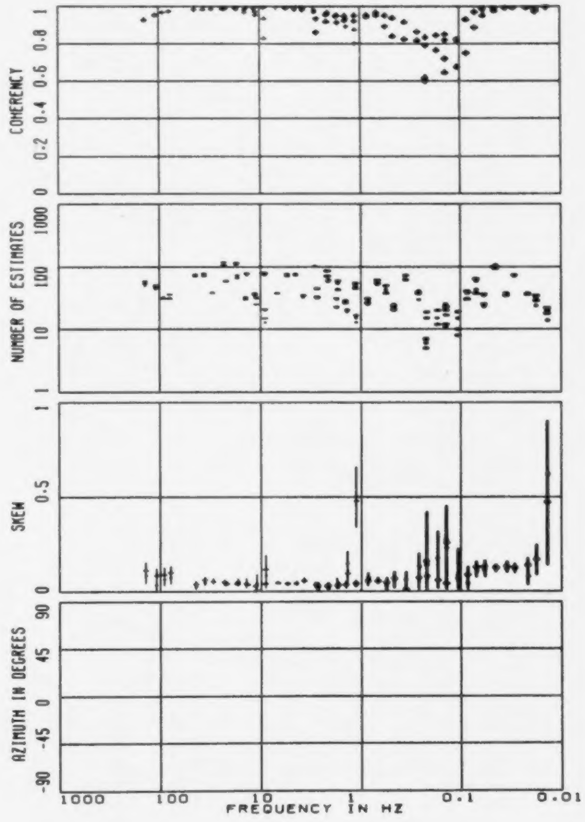

SITE : 209 TELLURIC

CARTRIDGE	S2090	S2091	S2092	S2093
BAND	0	1	2	3
COMPONENTS	5	5	5	5
SAMPLES/WINDOW	256	256	256	256
NUMBER WINDOWS	48	48	48	48
SAMPLE RATE HZ	512	64	8	1
PLOT HPF	8.0	1.0	0.1	0.010
PLOT LPF	180.0	24.0	3.0	0.350
FREQS/DECADE	10	10	10	10
FREQS/BAND	19	14	14	15
MIN COHERENCY	0.80	0.80	0.80	0.80
REJECTION LOOPS	2	2	2	2

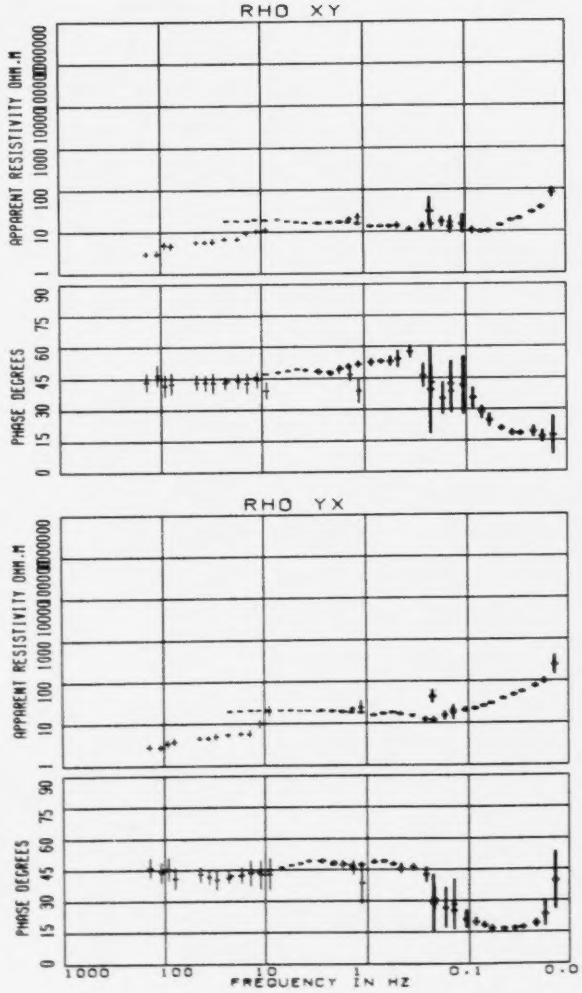

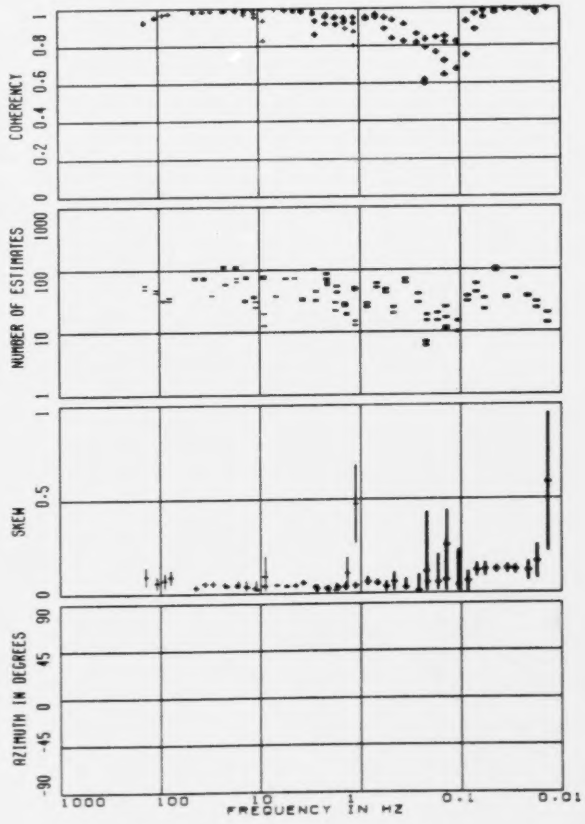

SITE : 209 TELLURIC

CARTRIDGE	:	82090	82091	82092	82093
BAND	:	0	1	2	3
COMPONENTS	:	5	5	5	5
SAMPLES/WINDOW	:	256	256	256	256
NUMBER WINDOWS	:	48	48	48	48
SAMPLE RATE HZ	:	512	64	8	1
PLOT HPF	:	8.0	1.0	0.1	0.010
PLOT LPF	:	180.0	24.0	3.0	0.360
FREQS/DECADE	:	10	10	10	10
FREQS/BAND	:	13	14	14	15
MIN COHERENCY	:	0.80	0.80	0.80	0.80
REJECTION LOOPS	:	2	2	2	2

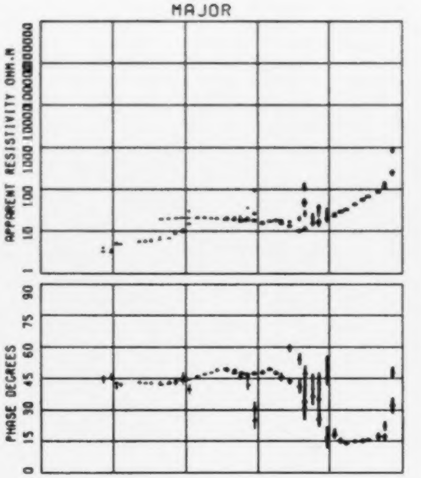
MAJOR

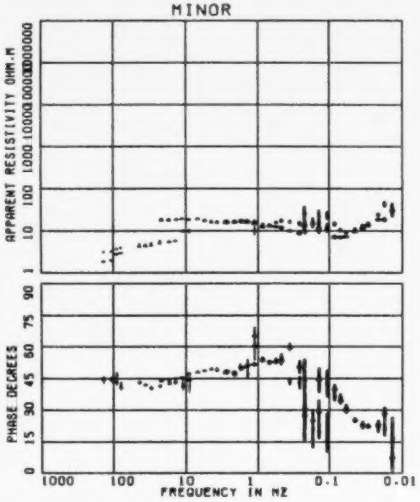
MINOR

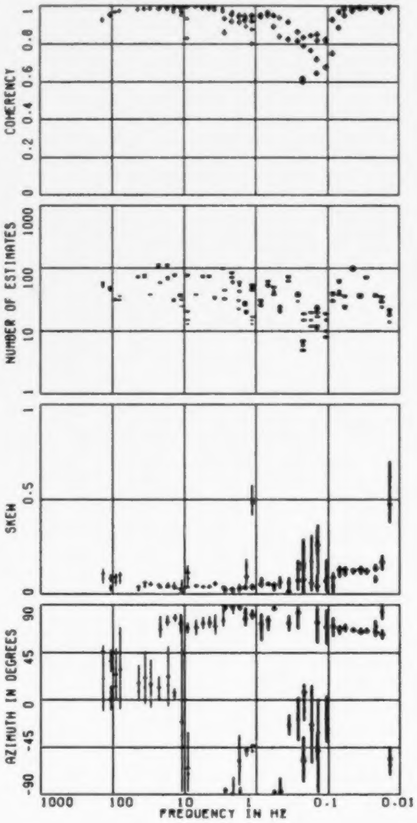

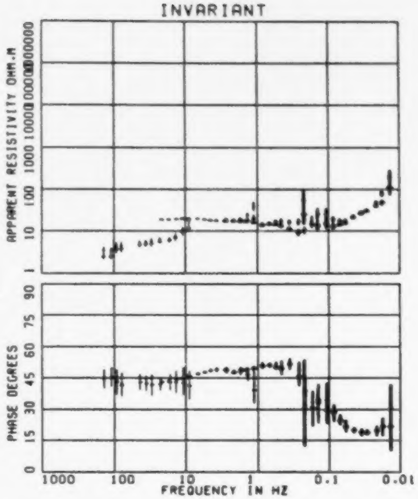
INVARIANT

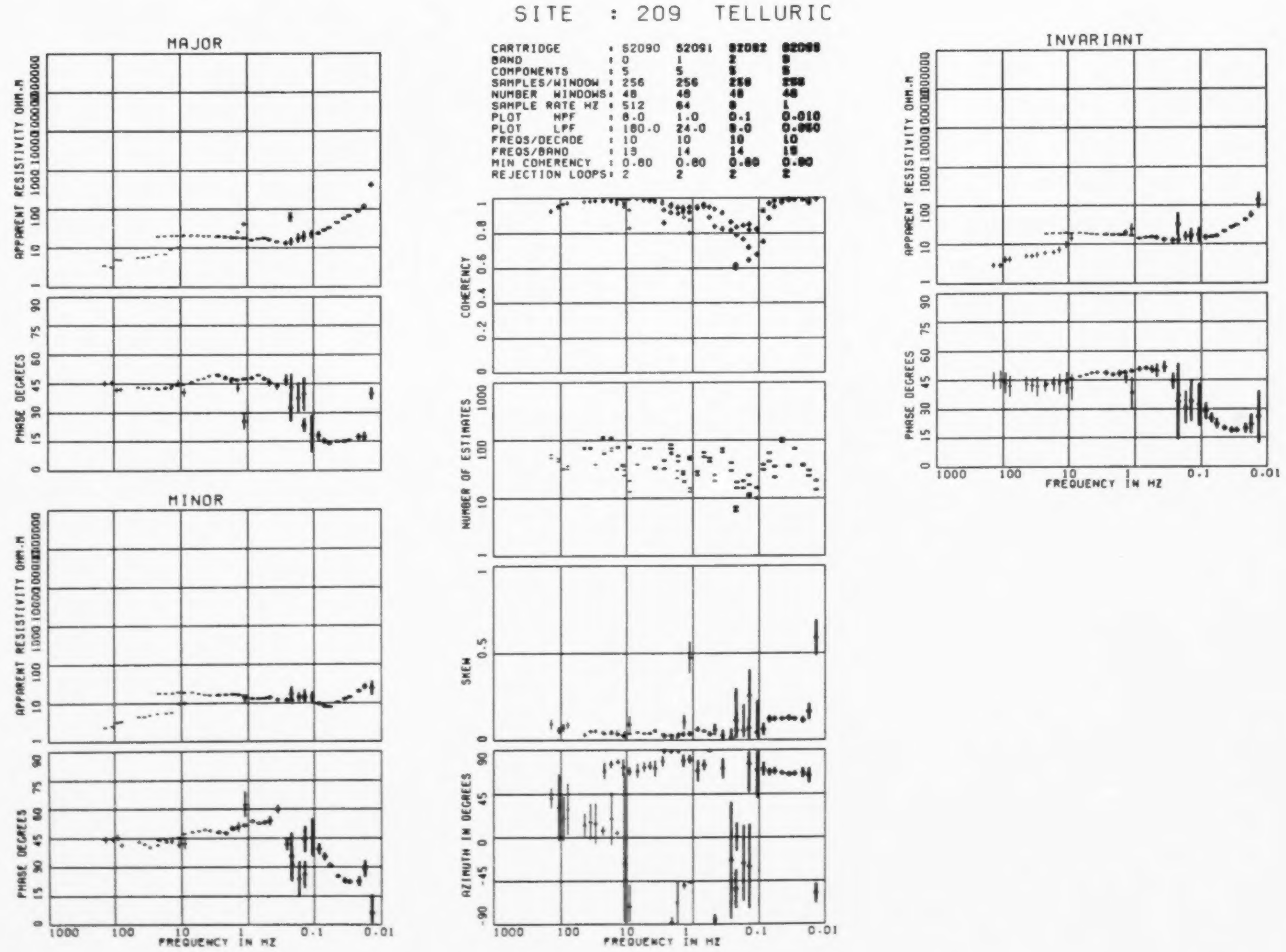

SITE : 209 TELLURIC

CARTRIDGE	: 52090	52091	52092	52093
BAND	: 0	1	2	3
COMPONENTS	: 5	5	5	5
SAMPLES/WINDOW	: 256	256	256	256
NUMBER WINDOWS	: 48	48	48	48
SAMPLE RATE HZ	: 512	64	8	1
PLOT HPF	: 8.0	1.0	0.1	0.010
PLOT LPF	: 180.0	24.0	3.0	0.350
FREQS/DECADE	: 10	10	10	10
FREQS/BAND	: 13	14	14	15
MIN COHERENCY	: 0.80	0.80	0.80	0.80
REJECTION LOOPS	: 2	2	2	2

```
SITE   : 209   MAGNETIC

CARTRIDGE        : S2090   S2091   S2092   S2093
BAND             : 0       1       2       3
COMPONENTS       : 5       5       5       5
SAMPLES/WINDOW   : 256     256     256     256
NUMBER  WINDOWS  : 48      48      48      48
SAMPLE RATE HZ   : 512     64      8       1
PLOT     HPF     : 8.0     1.0     0.1     0.010
PLOT     LPF     : 180.0   24.0    3.0     0.350
FREQS/DECADE     : 10      10      10      10
FREQS/BAND       : 13      14      14      15
MIN COHERENCY    : 0.70    0.70    0.70    0.70
REJECTION LOOPS  : 2       2       2       2
```

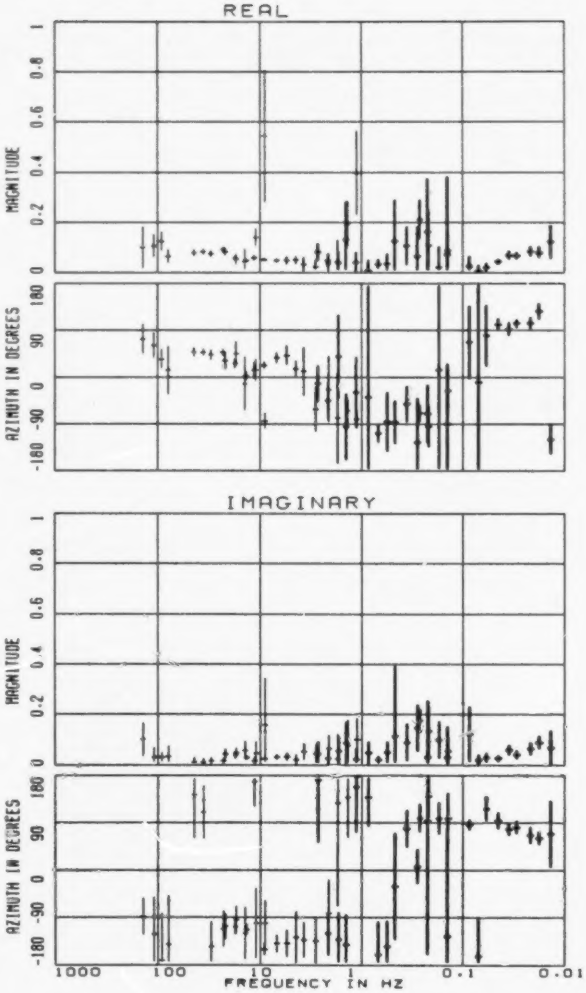

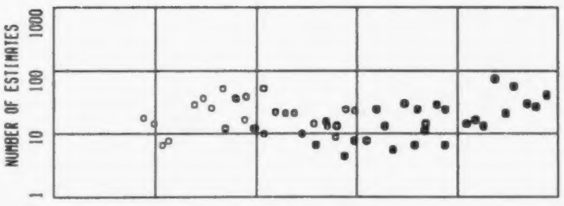

APPENDIX B

All the figures in Appendix B appear in the same order as Figs.4.6a and 4.6b. The site numbers are contained in the first line of the figures as in '1D-INVERSE AT 163 (pol:invariant)', the number 163 indicating the site number.

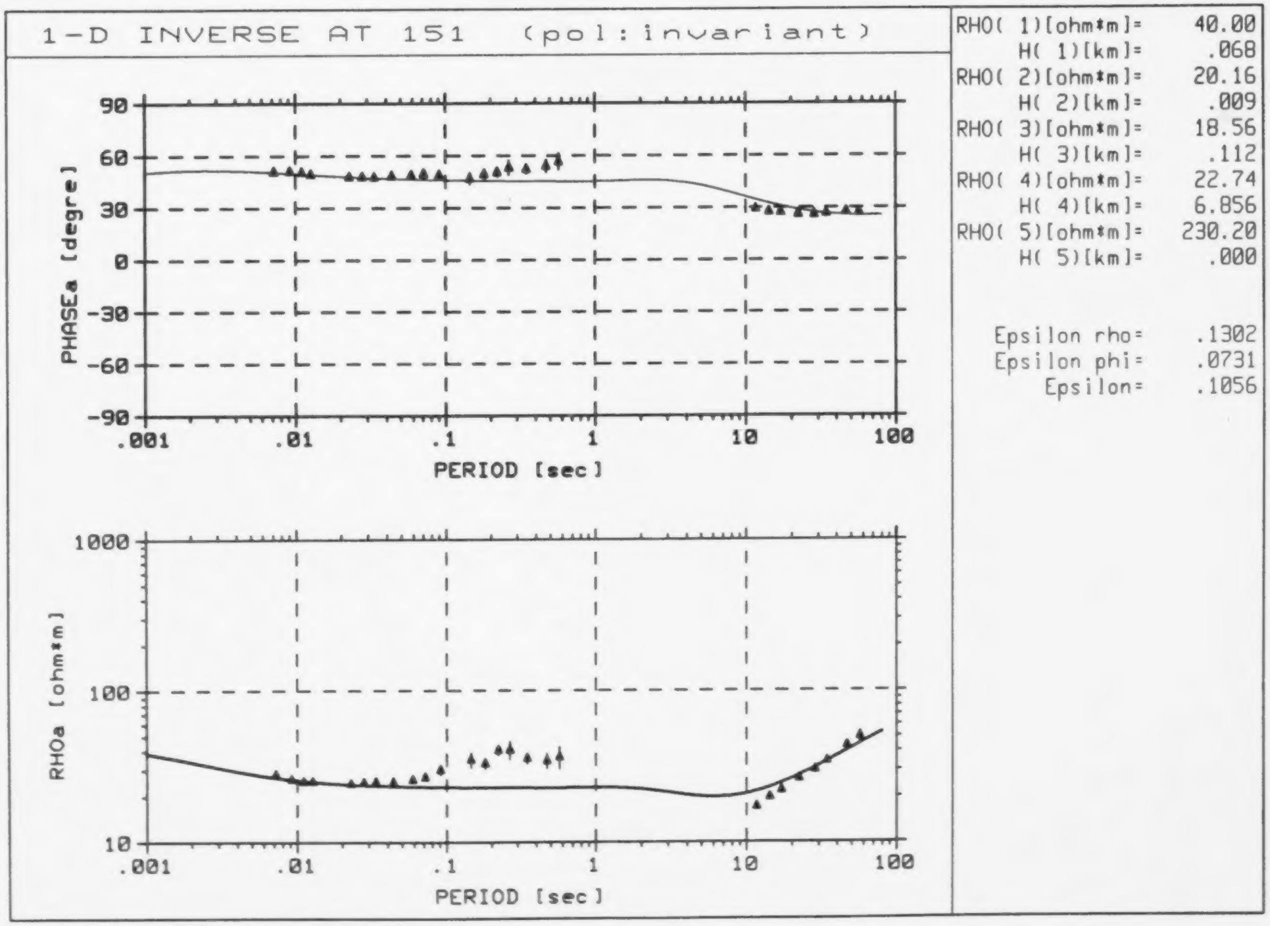

1-D INVERSE AT 151 (pol:invariant)

```
RHO( 1)[ohm*m]=    40.00
   H( 1)[km]=       .068
RHO( 2)[ohm*m]=    20.16
   H( 2)[km]=       .009
RHO( 3)[ohm*m]=    18.56
   H( 3)[km]=       .112
RHO( 4)[ohm*m]=    22.74
   H( 4)[km]=      6.856
RHO( 5)[ohm*m]=   230.20
   H( 5)[km]=       .000


  Epsilon rho=     .1302
  Epsilon phi=     .0731
     Epsilon=      .1056
```

1-D INVERSE AT 151 (pol:invariant)

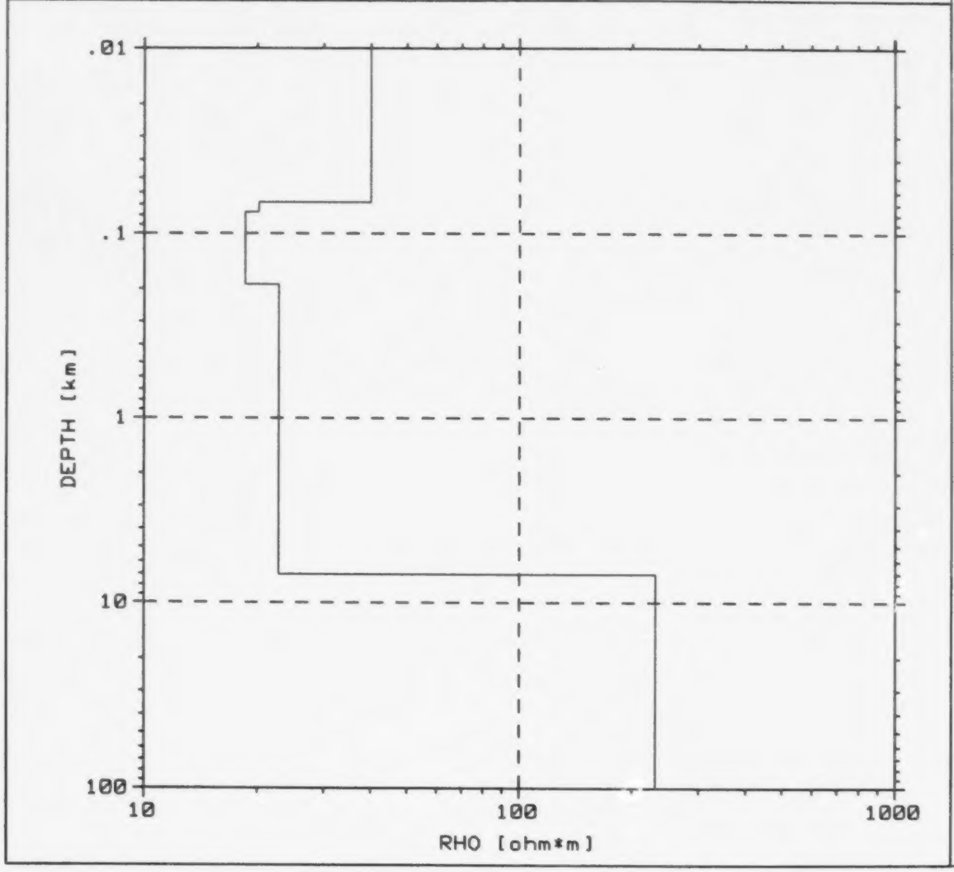

```
RHO( 1)[ohm*m]=   40.00
     H( 1)[km]=    .068
RHO( 2)[ohm*m]=   20.16
     H( 2)[km]=    .009
RHO( 3)[ohm*m]=   18.56
     H( 3)[km]=    .112
RHO( 4)[ohm*m]=   22.74
     H( 4)[km]=   6.856
RHO( 5)[ohm*m]=  230.20
     H( 5)[km]=    .000


  Epsilon rho=    .1302
  Epsilon phi=    .0731
      Epsilon=    .1056
```

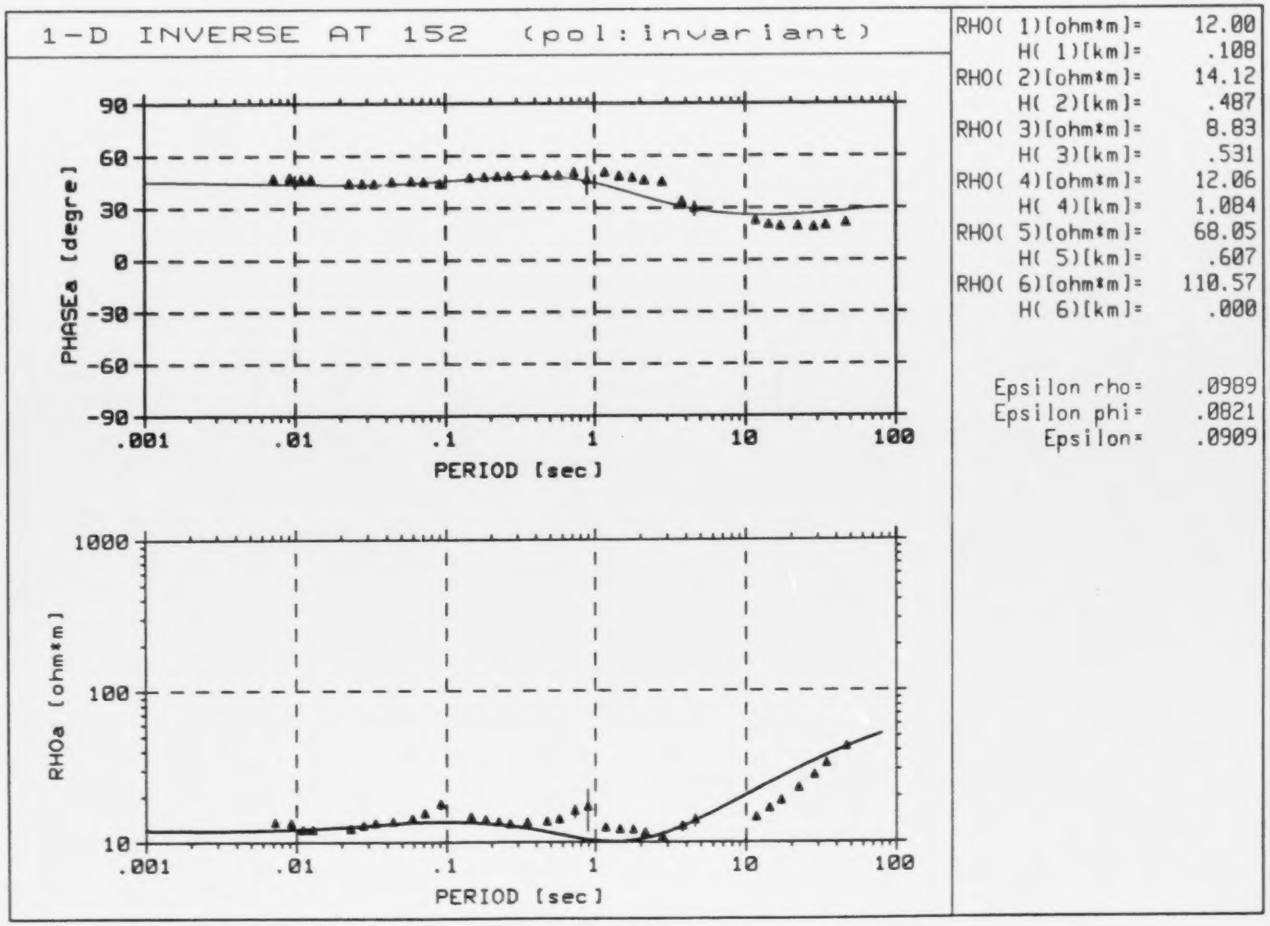

1-D INVERSE AT 152 (pol:invariant)

```
RHO( 1)[ohm*m]=    12.00
     H( 1)[km]=     .108
RHO( 2)[ohm*m]=    14.12
     H( 2)[km]=     .487
RHO( 3)[ohm*m]=     8.83
     H( 3)[km]=     .531
RHO( 4)[ohm*m]=    12.06
     H( 4)[km]=    1.084
RHO( 5)[ohm*m]=    68.05
     H( 5)[km]=     .607
RHO( 6)[ohm*m]=   110.57
     H( 6)[km]=     .000


  Epsilon rho=     .0989
  Epsilon phi=     .0821
     Epsilon=      .0909
```

1-D INVERSE AT 152 (pol:invariant)

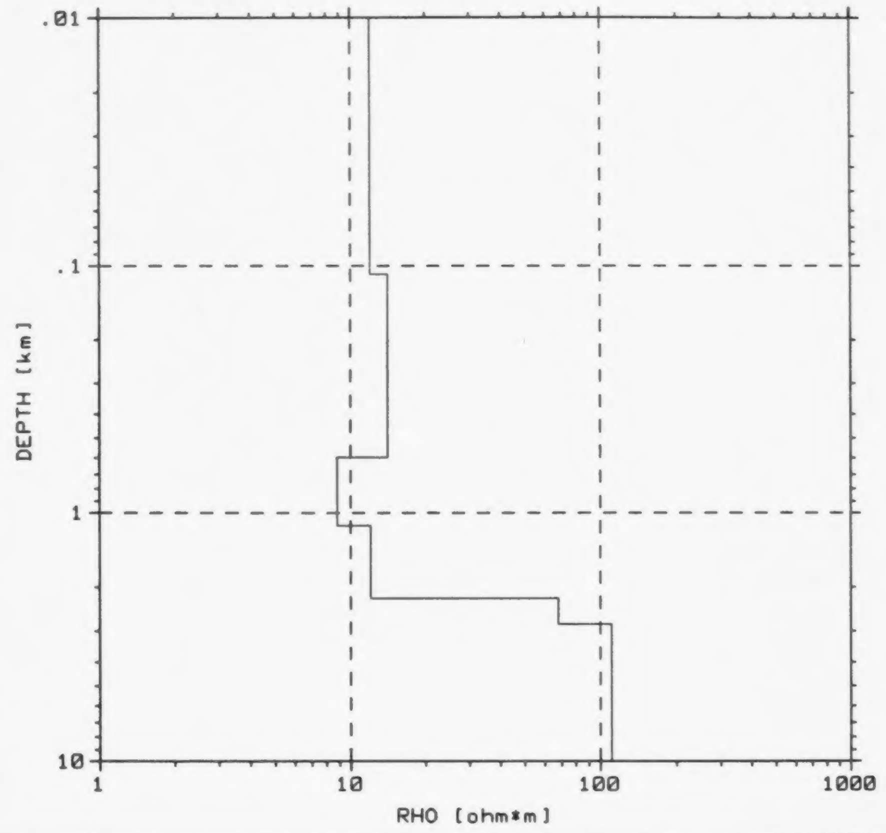

```
RHO( 1)[ohm*m]=    12.00
   H( 1)[km]=       .108
RHO( 2)[ohm*m]=    14.12
   H( 2)[km]=       .487
RHO( 3)[ohm*m]=     8.83
   H( 3)[km]=       .531
RHO( 4)[ohm*m]=    12.06
   H( 4)[km]=      1.084
RHO( 5)[ohm*m]=    68.05
   H( 5)[km]=       .607
RHO( 6)[ohm*m]=   110.57
   H( 6)[km]=       .000


  Epsilon rho=     .0989
  Epsilon phi=     .0821
      Epsilon=     .0909
```

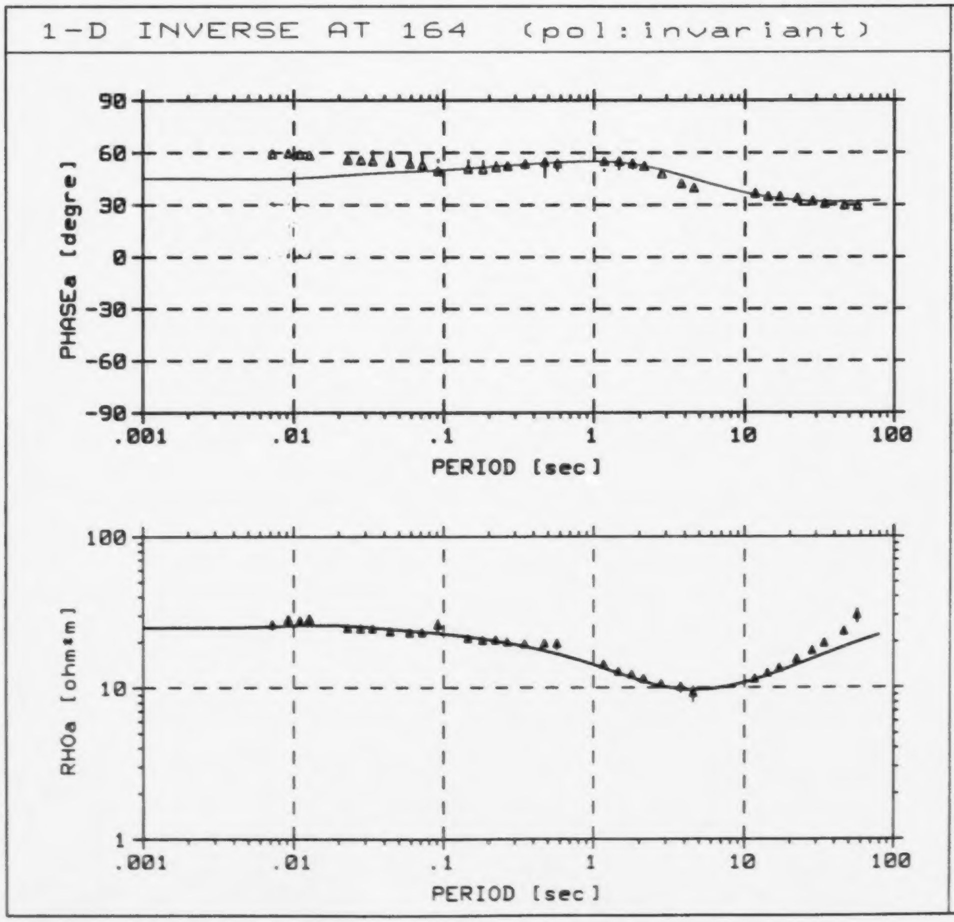

```
RHO( 1)[ohm*m]=     25.00
      H( 1)[km]=      .364
RHO( 2)[ohm*m]=     14.51
      H( 2)[km]=      .626
RHO( 3)[ohm*m]=      7.25
      H( 3)[km]=     2.044
RHO( 4)[ohm*m]=     47.61
      H( 4)[km]=      .000


    Epsilon rho=     .0507
    Epsilon phi=     .0968
        Epsilon=     .0772
```

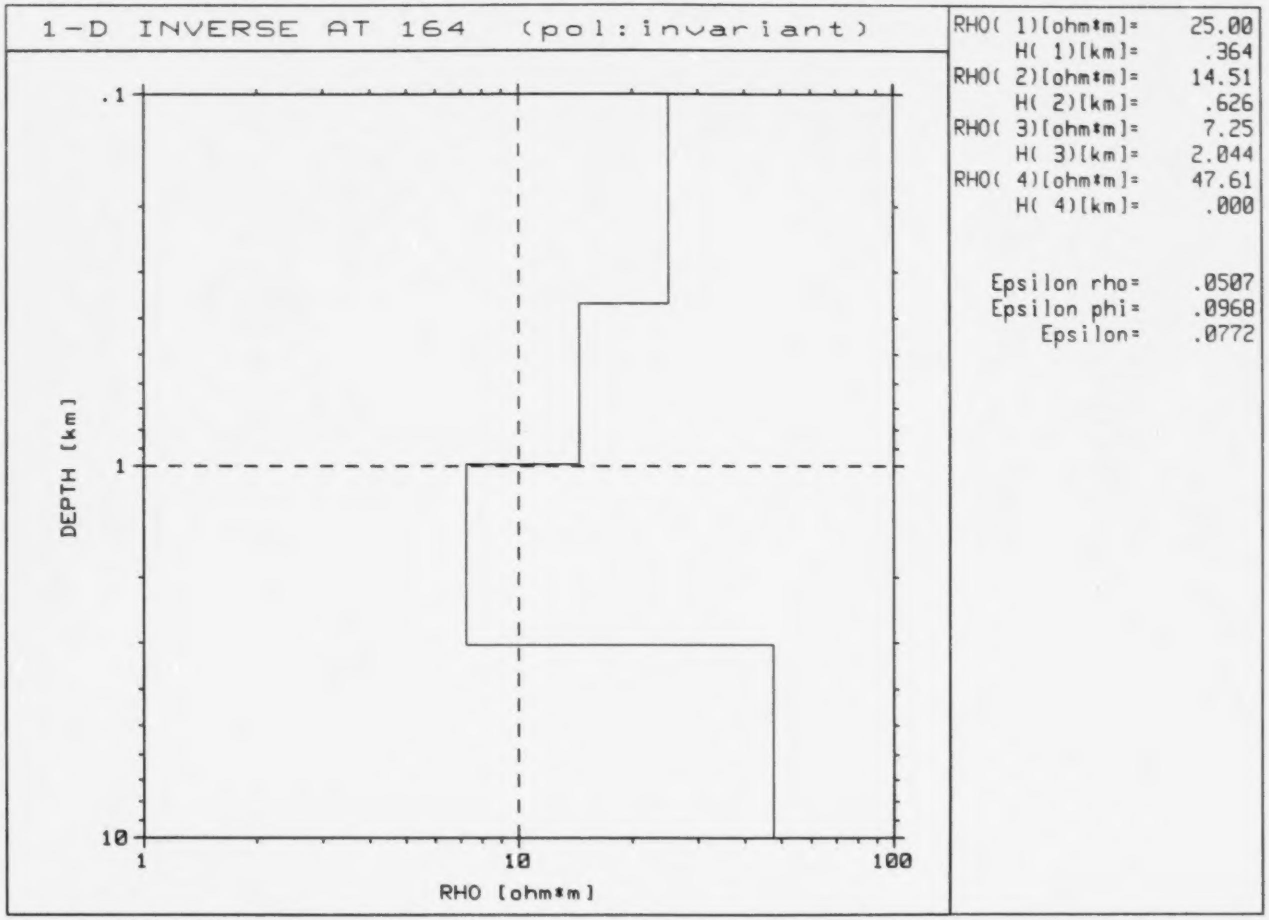

```
RHO( 1)[ohm*m]=   25.00
   H( 1)[km]=      .364
RHO( 2)[ohm*m]=   14.51
   H( 2)[km]=      .626
RHO( 3)[ohm*m]=    7.25
   H( 3)[km]=     2.044
RHO( 4)[ohm*m]=   47.61
   H( 4)[km]=      .000

  Epsilon rho=    .0507
  Epsilon phi=    .0968
      Epsilon=    .0772
```

1-D INVERSE AT 201   (pol:invariant)

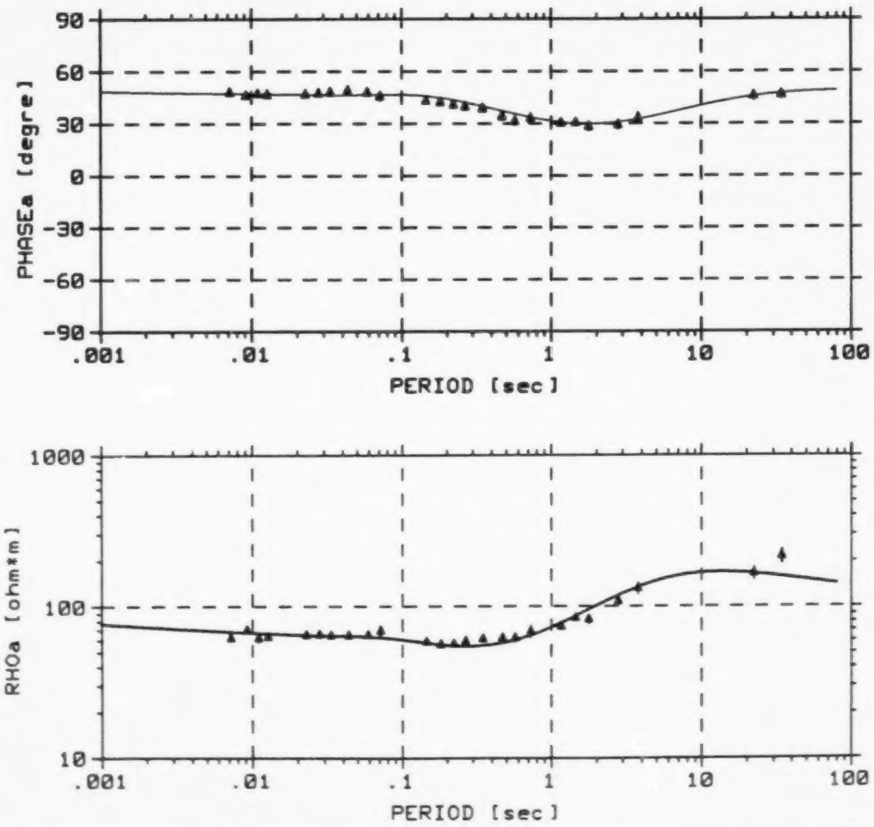

```
RHO( 1)[ohm*m]=   100.00
    H( 1)[km]=      .044
RHO( 2)[ohm*m]=    54.65
    H( 2)[km]=      .038
RHO( 3)[ohm*m]=    67.98
    H( 3)[km]=      .090
RHO( 4)[ohm*m]=    59.63
    H( 4)[km]=     2.185
RHO( 5)[ohm*m]=   360.27
    H( 5)[km]=    13.858
RHO( 6)[ohm*m]=   102.95
    H( 6)[km]=      .000


  Epsilon rho=     .0430
  Epsilon phi=     .0324
     Epsilon=      .0381
```

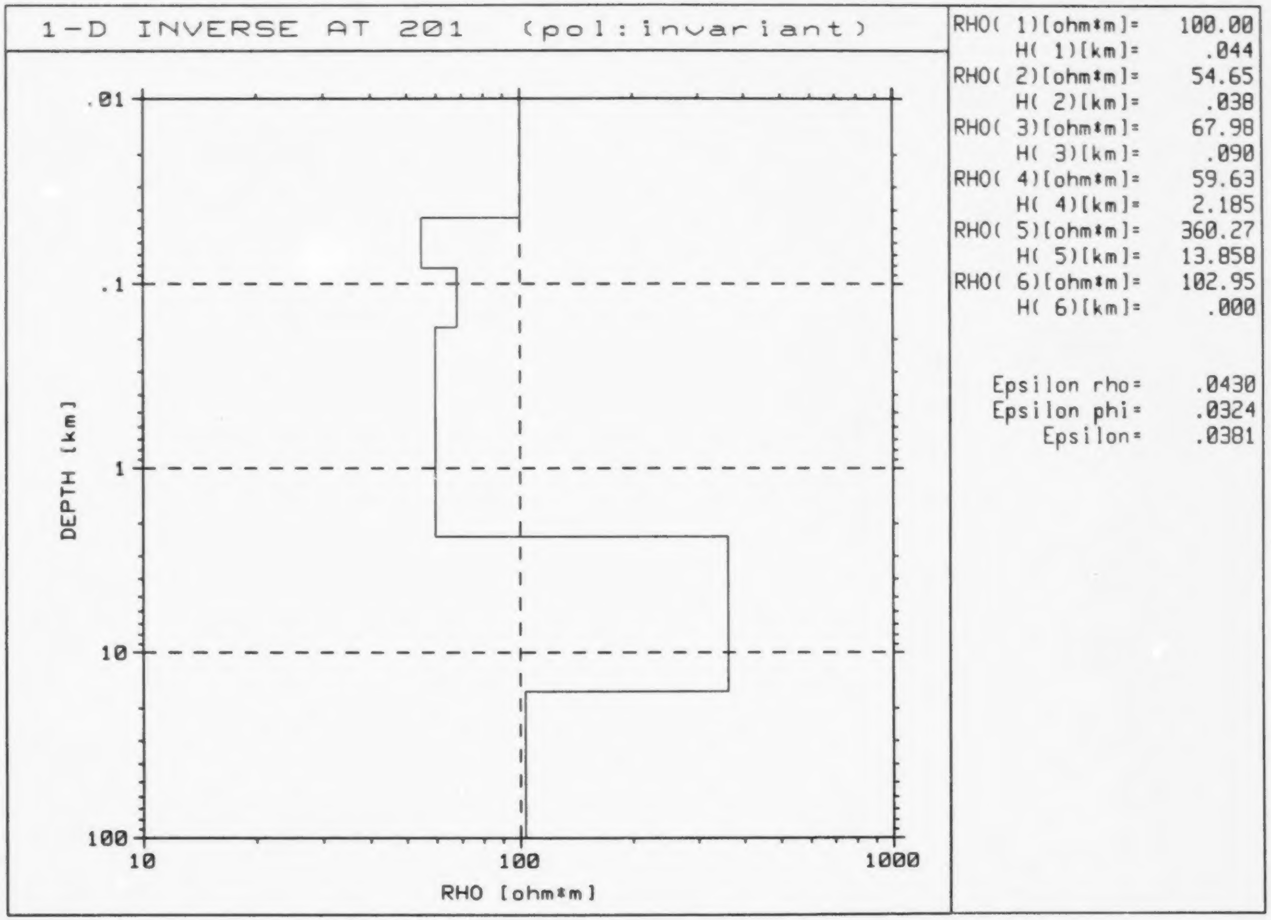

1-D INVERSE AT 201 (pol:invariant)

```
RHO( 1)[ohm*m]=   100.00
     H( 1)[km]=     .044
RHO( 2)[ohm*m]=    54.65
     H( 2)[km]=     .038
RHO( 3)[ohm*m]=    67.98
     H( 3)[km]=     .090
RHO( 4)[ohm*m]=    59.63
     H( 4)[km]=    2.185
RHO( 5)[ohm*m]=   360.27
     H( 5)[km]=   13.858
RHO( 6)[ohm*m]=   102.95
     H( 6)[km]=     .000


  Epsilon rho=     .0430
  Epsilon phi=     .0324
     Epsilon=      .0381
```

1-D INVERSE AT 202 (pol:invariant)

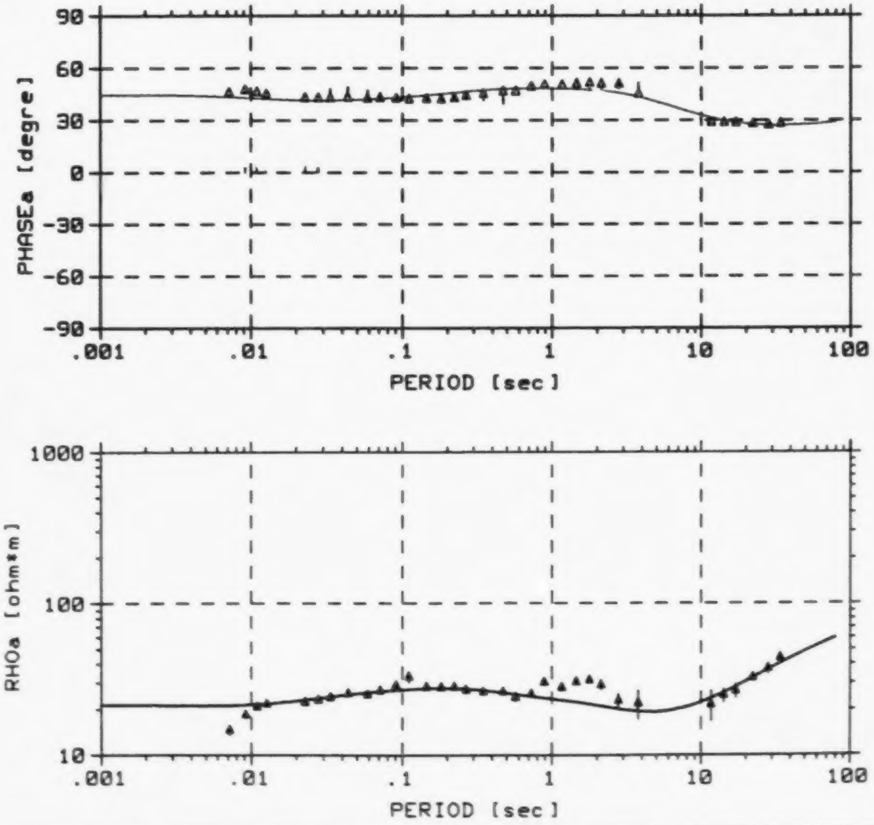

```
RHO( 1)[ohm*m]=    20.00
      H( 1)[km]=     .008
RHO( 2)[ohm*m]=    14.16
      H( 2)[km]=     .000
RHO( 3)[ohm*m]=    21.86
      H( 3)[km]=     .171
RHO( 4)[ohm*m]=    28.05
      H( 4)[km]=     .095
RHO( 5)[ohm*m]=    33.04
      H( 5)[km]=     .425
RHO( 6)[ohm*m]=    30.66
      H( 6)[km]=     .037
RHO( 7)[ohm*m]=    21.90
      H( 7)[km]=     .838
RHO( 8)[ohm*m]=    15.01
      H( 8)[km]=     .916
RHO( 9)[ohm*m]=    27.93
      H( 9)[km]=    4.482
RHO(10)[ohm*m]=   400.05
      H(10)[km]=   14.496
RHO(11)[ohm*m]=   145.01
      H(11)[km]=     .000


   Epsilon rho=    .0725
   Epsilon phi=    .0405
       Epsilon=    .0587
```

1-D INVERSE AT 202 (pol:invariant)

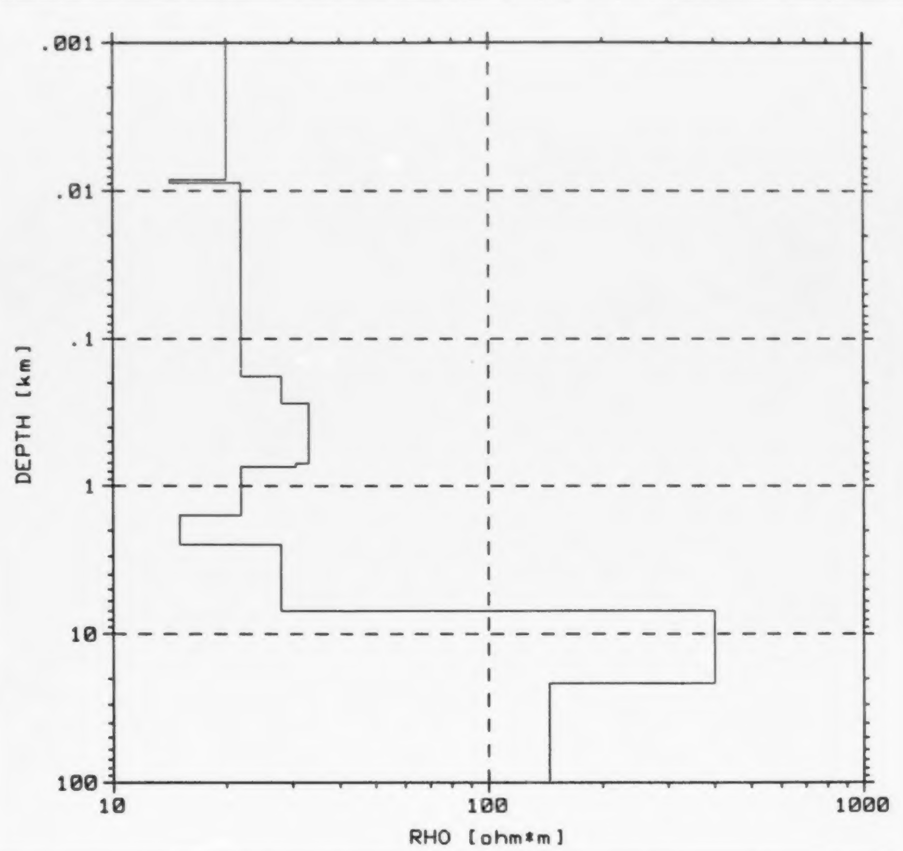

```
RHO( 1)[ohm*m]=   20.00
   H( 1)[km]=      .008
RHO( 2)[ohm*m]=   14.16
   H( 2)[km]=      .000
RHO( 3)[ohm*m]=   21.86
   H( 3)[km]=      .171
RHO( 4)[ohm*m]=   28.05
   H( 4)[km]=      .095
RHO( 5)[ohm*m]=   33.04
   H( 5)[km]=      .425
RHO( 6)[ohm*m]=   30.66
   H( 6)[km]=      .037
RHO( 7)[ohm*m]=   21.90
   H( 7)[km]=      .838
RHO( 8)[ohm*m]=   15.01
   H( 8)[km]=      .916
RHO( 9)[ohm*m]=   27.93
   H( 9)[km]=     4.482
RHO(10)[ohm*m]=  400.05
   H(10)[km]=    14.496
RHO(11)[ohm*m]=  145.01
   H(11)[km]=      .000


  Epsilon rho=    .0725
  Epsilon phi=    .0405
      Epsilon=    .0587
```

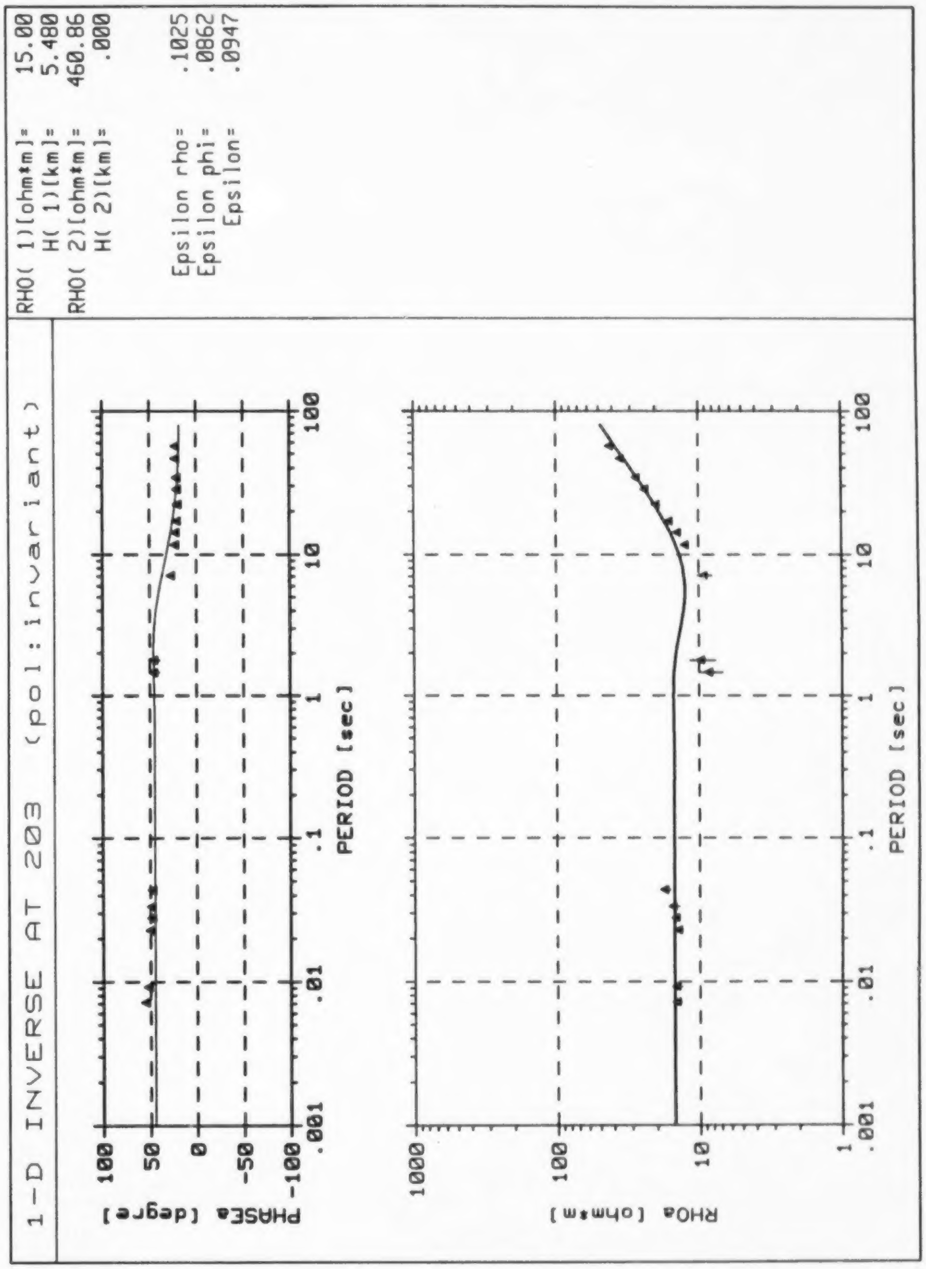

RHO(1)[ohm*m]= 15.00
H(1)[km]= 5.480
RHO(2)[ohm*m]= 460.86
H(2)[km]= .000

Epsilon rho= .1025
Epsilon phi= .0862
Epsilon= .0947

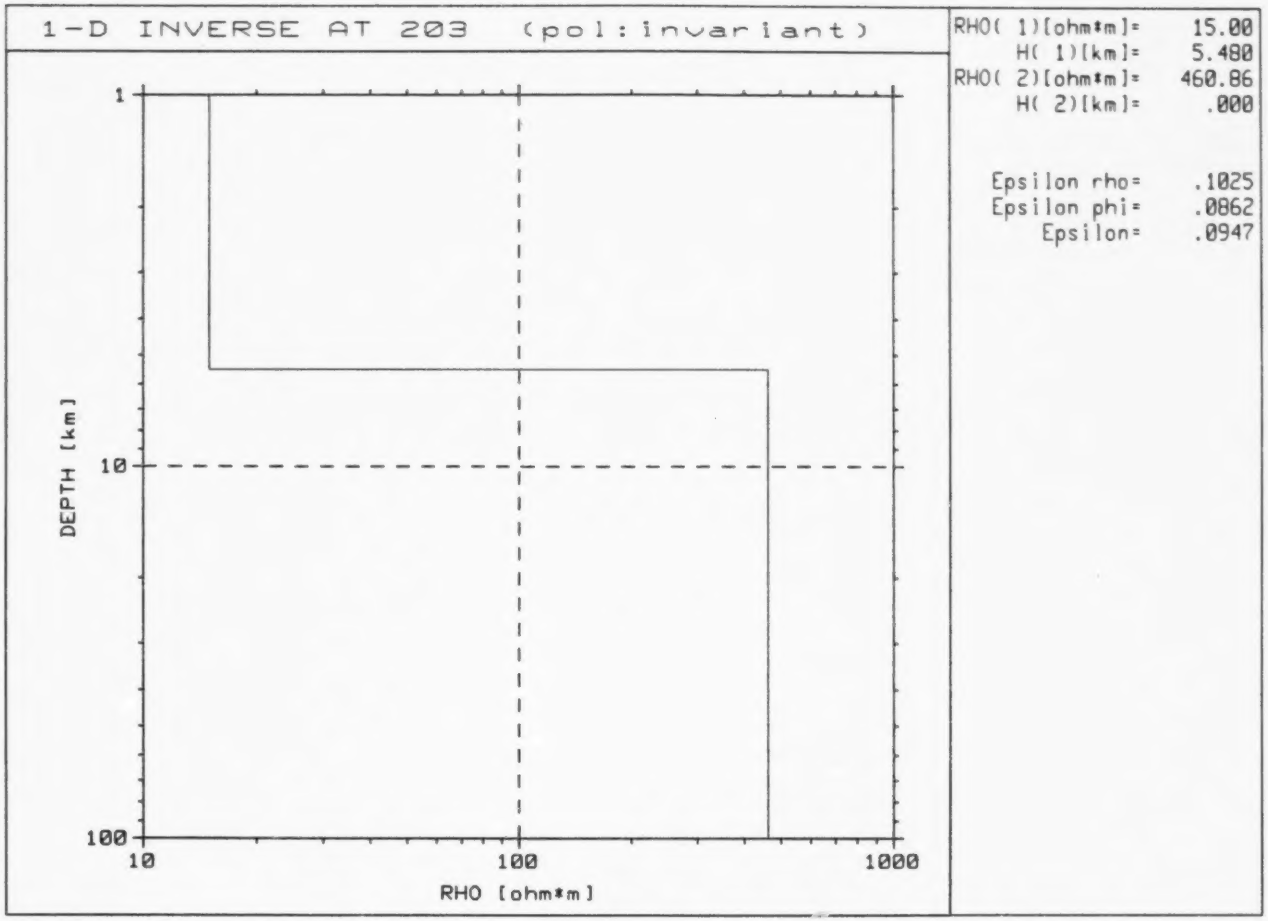

```
RHO( 1)[ohm*m]=     15.00
   H( 1)[km]=       5.480
RHO( 2)[ohm*m]=    460.86
   H( 2)[km]=        .000


  Epsilon rho=      .1025
  Epsilon phi=      .0862
      Epsilon=      .0947
```

1-D INVERSE AT 204 (pol:invariant)

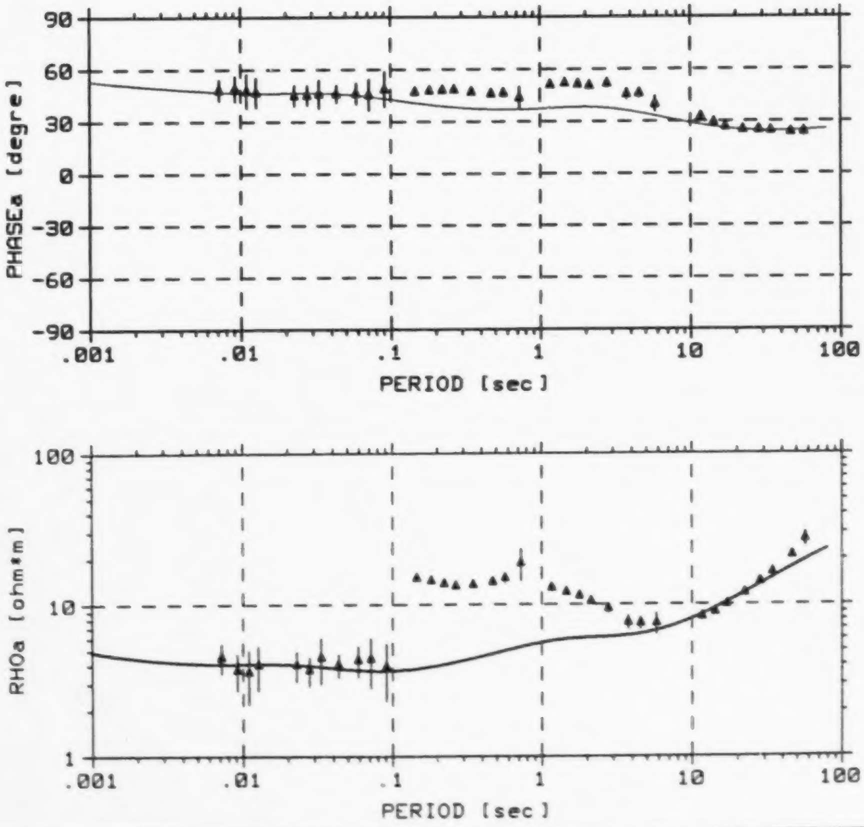

```
RHO( 1)[ohm*m]=   20.00
    H( 1)[km]=     .006
RHO( 2)[ohm*m]=    4.00
    H( 2)[km]=     .006
RHO( 3)[ohm*m]=    3.19
    H( 3)[km]=     .019
RHO( 4)[ohm*m]=    3.89
    H( 4)[km]=     .072
RHO( 5)[ohm*m]=    4.62
    H( 5)[km]=     .031
RHO( 6)[ohm*m]=    3.67
    H( 6)[km]=     .084
RHO( 7)[ohm*m]=    2.49
    H( 7)[km]=     .054
RHO( 8)[ohm*m]=    9.56
    H( 8)[km]=    3.325
RHO( 9)[ohm*m]=   83.94
    H( 9)[km]=     .000


  Epsilon rho=    .3179
  Epsilon phi=    .1258
      Epsilon=    .2417
```

1-D INVERSE AT 204 (pol:invariant)

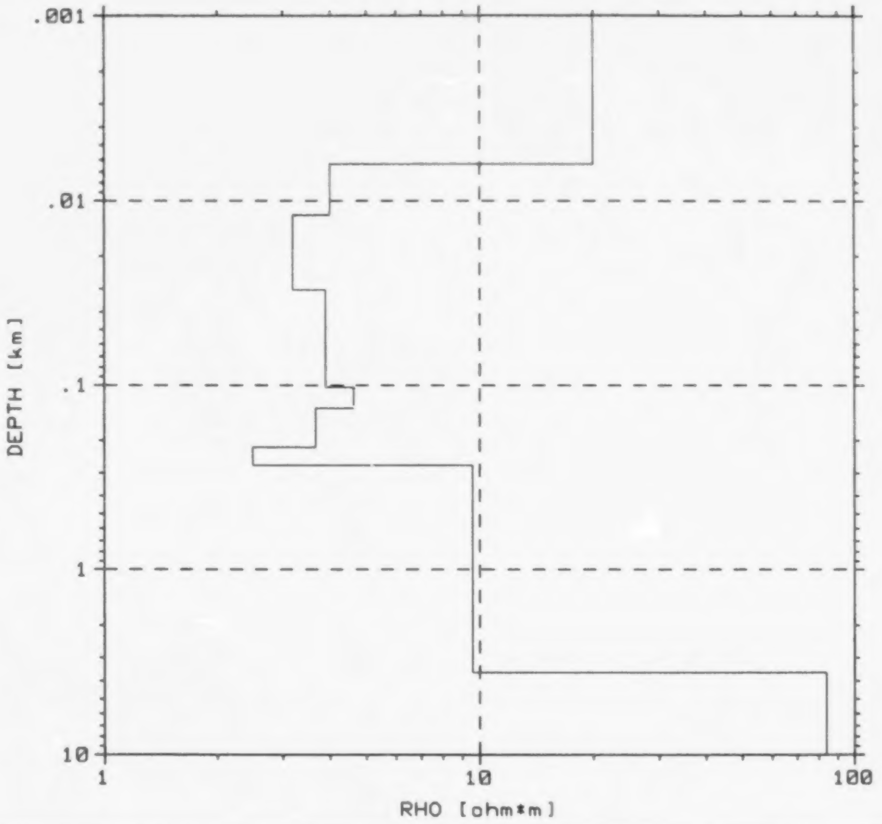

```
RHO( 1)[ohm*m]=   20.00
     H( 1)[km]=    .006
RHO( 2)[ohm*m]=    4.00
     H( 2)[km]=    .006
RHO( 3)[ohm*m]=    3.19
     H( 3)[km]=    .019
RHO( 4)[ohm*m]=    3.89
     H( 4)[km]=    .072
RHO( 5)[ohm*m]=    4.62
     H( 5)[km]=    .031
RHO( 6)[ohm*m]=    3.67
     H( 6)[km]=    .084
RHO( 7)[ohm*m]=    2.49
     H( 7)[km]=    .054
RHO( 8)[ohm*m]=    9.56
        8)[km]=   3.325
RHO( 9)[ohm*m]=   83.94
     H( 9)[km]=    .000


  Epsilon rho=    .3179
  Epsilon phi=    .1258
      Epsilon=    .2417
```

1-D INVERSE AT 205 (pol:invariant)

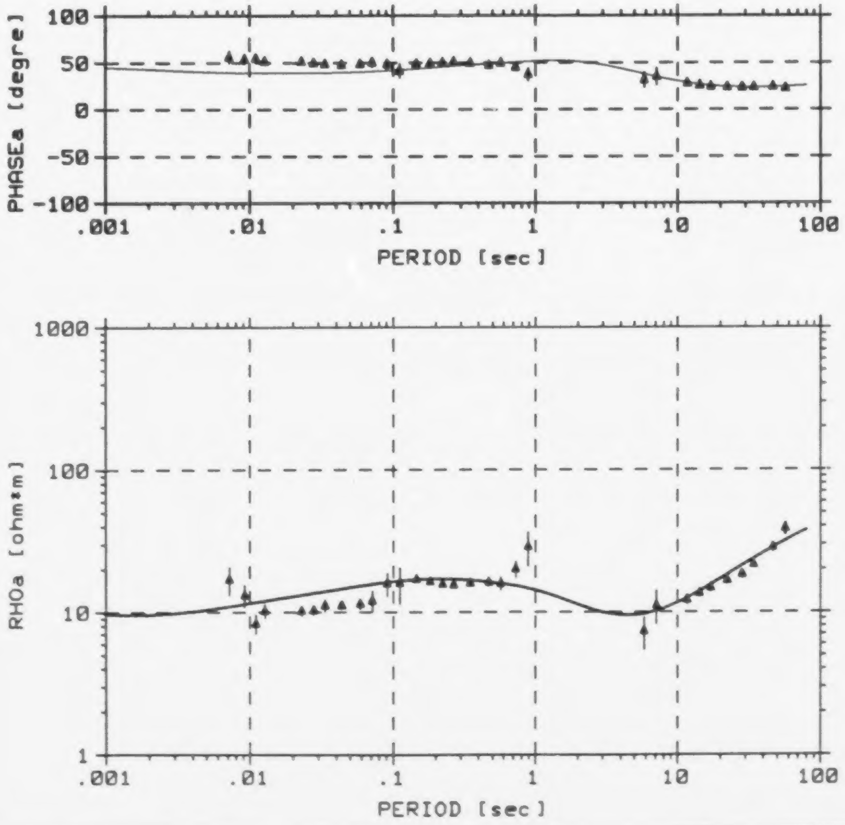

RHO(1)[ohm*m]= 10.00
H(1)[km]= .075
RHO(2)[ohm*m]= 19.05
H(2)[km]= .707
RHO(3)[ohm*m]= 11.62
H(3)[km]= .356
RHO(4)[ohm*m]= 8.15
H(4)[km]= 2.352
RHO(5)[ohm*m]= 287.49
H(5)[km]= 4.593
RHO(6)[ohm*m]= 298.52
H(6)[km]= 10.399
RHO(7)[ohm*m]= 117.14
H(7)[km]= .000

Epsilon rho= .1096
Epsilon phi= .1328
Epsilon= .1218

1-D INVERSE AT 205 (pol:invariant)

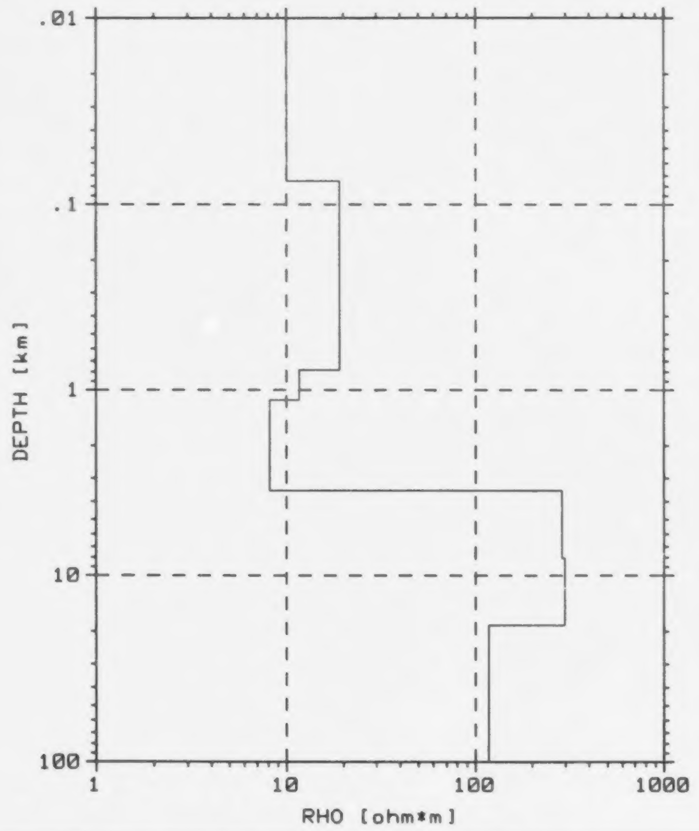

```
RHO( 1)[ohm*m]=   10.00
     H( 1)[km]=    .075
RHO( 2)[ohm*m]=   19.05
     H( 2)[km]=    .707
RHO( 3)[ohm*m]=   11.62
     H( 3)[km]=    .356
RHO( 4)[ohm*m]=    8.15
     H( 4)[km]=   2.352
RHO( 5)[ohm*m]=  287.49
     H( 5)[km]=   4.593
RHO( 6)[ohm*m]=  298.52
     H( 6)[km]=  10.399
RHO( 7)[ohm*m]=  117.14
     H( 7)[km]=    .000


   Epsilon rho=   .1096
   Epsilon phi=   .1328
       Epsilon=   .1218
```

1-D INVERSE AT 206 (pol:invariant)

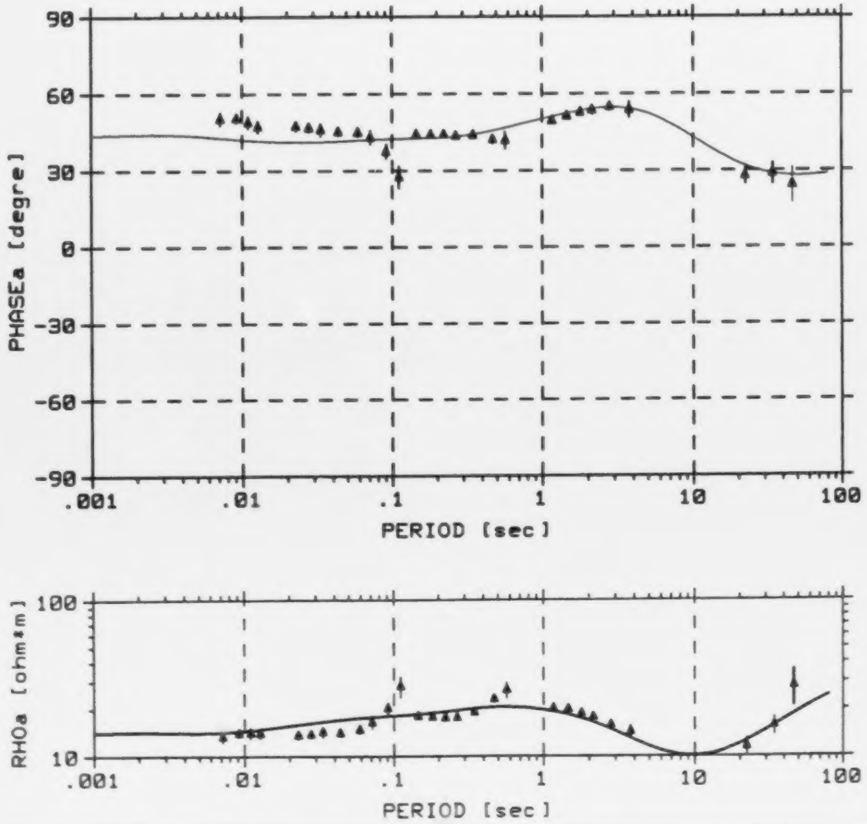

```
RHO( 1)[ohm*m]=     11.00
    H( 1)[km]=       .005
RHO( 2)[ohm*m]=     14.91
    H( 2)[km]=       .138
RHO( 3)[ohm*m]=     18.60
    H( 3)[km]=       .096
RHO( 4)[ohm*m]=     34.41
    H( 4)[km]=       .088
RHO( 5)[ohm*m]=    118.80
    H( 5)[km]=       .005
RHO( 6)[ohm*m]=     17.44
    H( 6)[km]=       .043
RHO( 7)[ohm*m]=     19.55
    H( 7)[km]=      1.555
RHO( 8)[ohm*m]=      5.93
    H( 8)[km]=      1.014
RHO( 9)[ohm*m]=      8.75
    H( 9)[km]=      2.417
RHO(10)[ohm*m]=    943.53
    H(10)[km]=     17.008
RHO(11)[ohm*m]=     51.31
    H(11)[km]=       .000


  Epsilon rho=      .0774
  Epsilon phi=      .0834
      Epsilon=      .0805
```

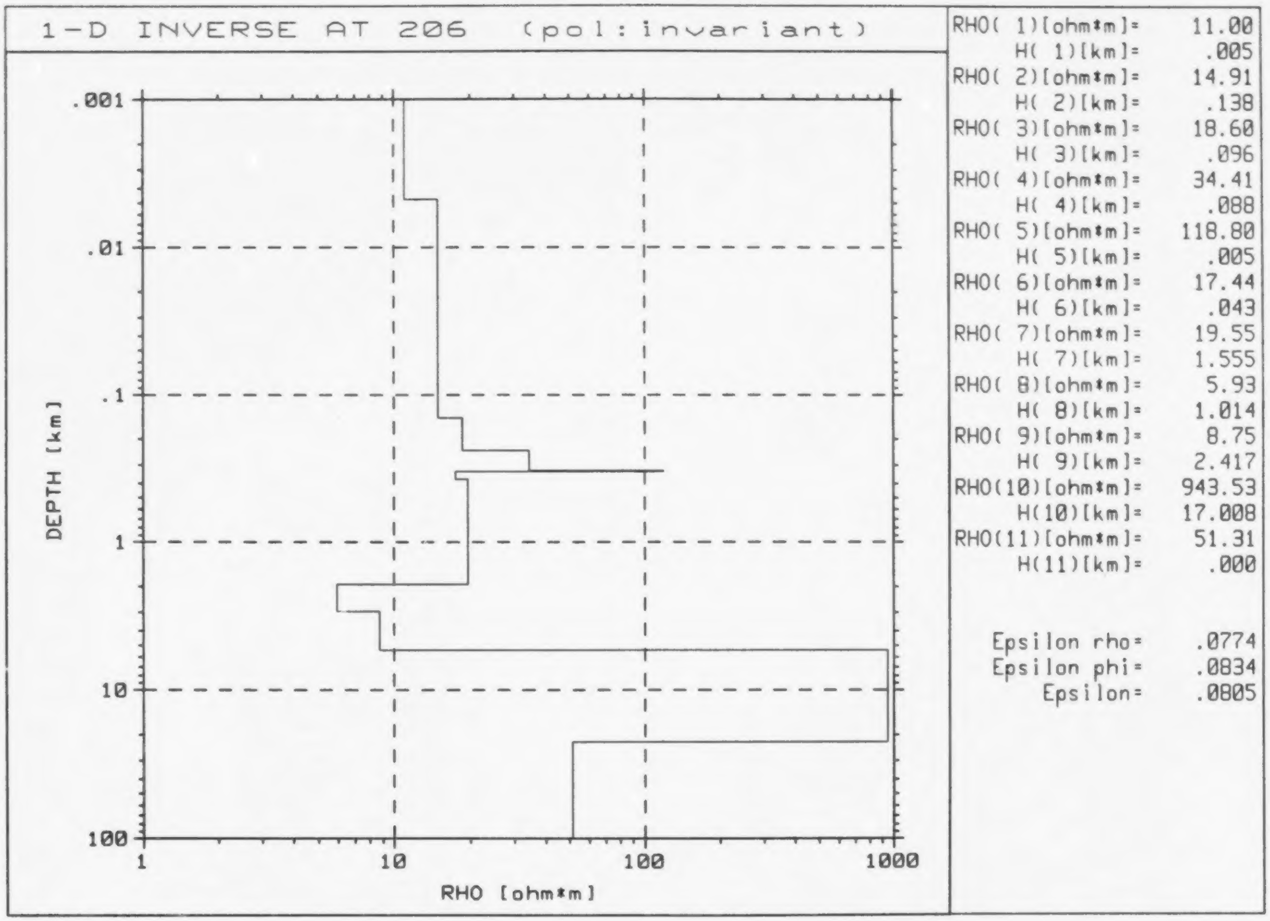

1-D INVERSE AT 206 (pol:invariant)

```
RHO( 1)[ohm*m]=    11.00
     H( 1)[km]=     .005
RHO( 2)[ohm*m]=    14.91
     H( 2)[km]=     .138
RHO( 3)[ohm*m]=    18.60
     H( 3)[km]=     .096
RHO( 4)[ohm*m]=    34.41
     H( 4)[km]=     .088
RHO( 5)[ohm*m]=   118.80
     H( 5)[km]=     .005
RHO( 6)[ohm*m]=    17.44
     H( 6)[km]=     .043
RHO( 7)[ohm*m]=    19.55
     H( 7)[km]=    1.555
RHO( 8)[ohm*m]=     5.93
     H( 8)[km]=    1.014
RHO( 9)[ohm*m]=     8.75
     H( 9)[km]=    2.417
RHO(10)[ohm*m]=   943.53
     H(10)[km]=   17.008
RHO(11)[ohm*m]=    51.31
     H(11)[km]=     .000


  Epsilon rho=     .0774
  Epsilon phi=     .0834
     Epsilon=      .0805
```

1-D INVERSE AT 207 (pol:invariant)

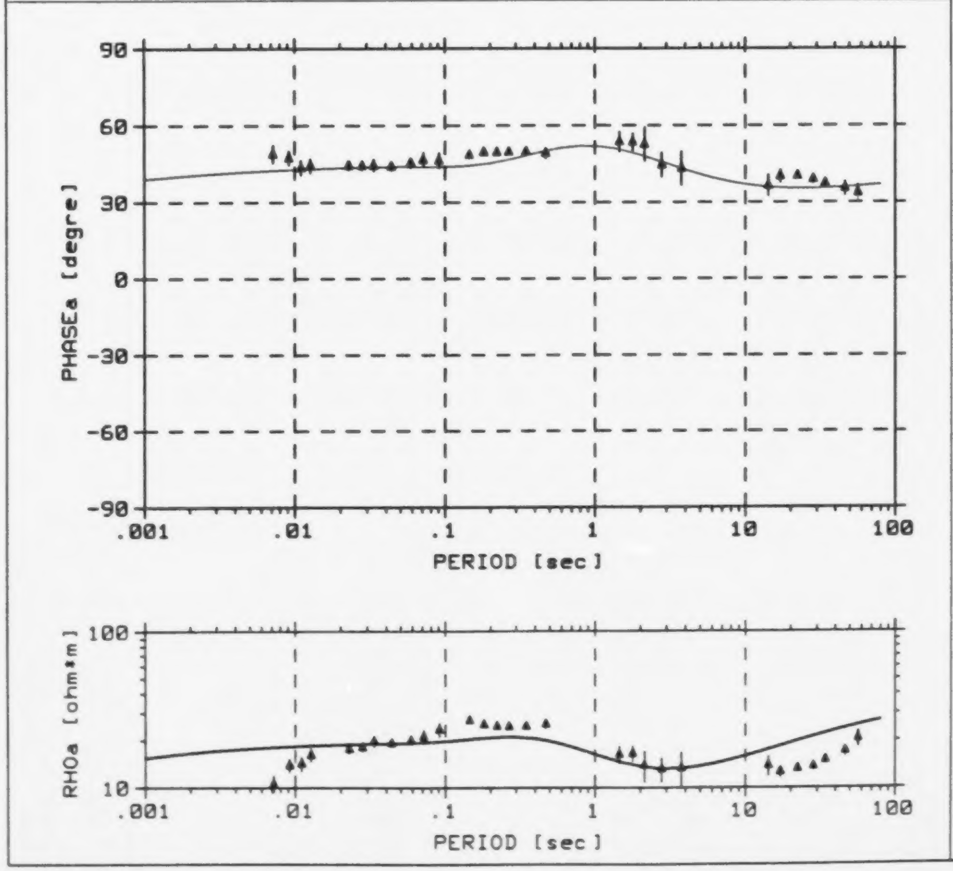

```
RHO( 1)[ohm*m]=    5.00
    H( 1)[km]=     .003
RHO( 2)[ohm*m]=   15.07
    H( 2)[km]=     .001
RHO( 3)[ohm*m]=   19.98
    H( 3)[km]=    1.347
RHO( 4)[ohm*m]=    7.27
    H( 4)[km]=    1.101
RHO( 5)[ohm*m]=   58.11
    H( 5)[km]=     .122
RHO( 6)[ohm*m]=   41.64
    H( 6)[km]=     .000


  Epsilon rho=    .1200
  Epsilon phi=    .0517
      Epsilon=    .0924
```

1-D INVERSE AT 207 (pol:invariant)

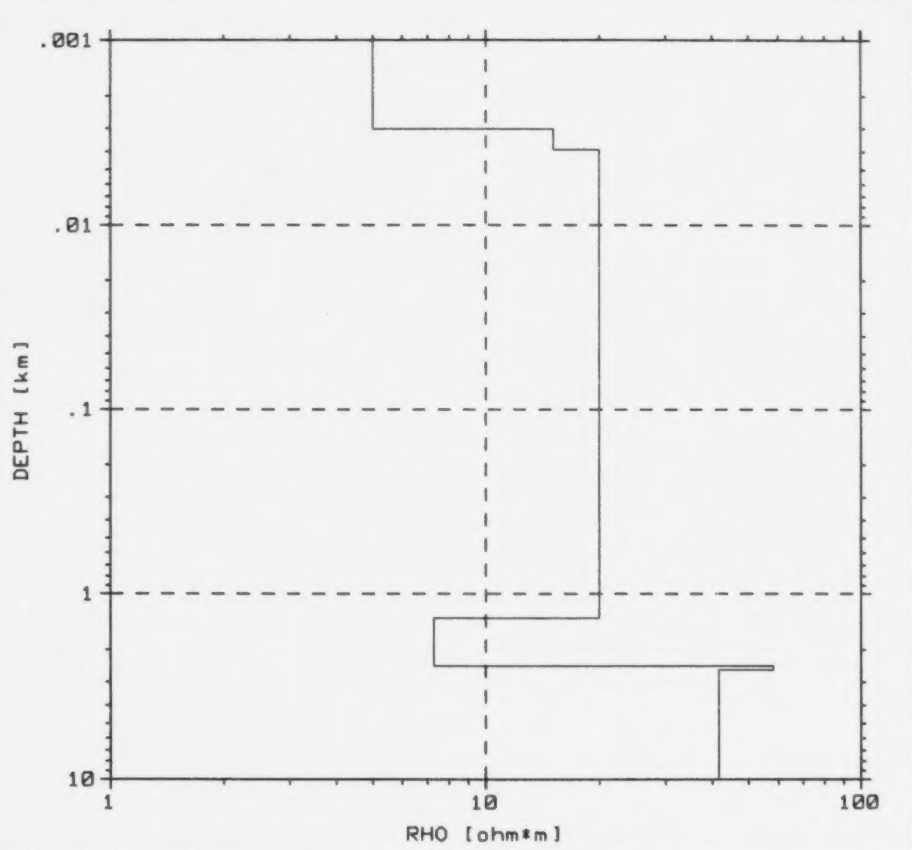

```
RHO( 1)[ohm*m]=     5.00
    H( 1)[km]=      .003
RHO( 2)[ohm*m]=    15.07
    H( 2)[km]=      .001
RHO( 3)[ohm*m]=    19.98
    H( 3)[km]=     1.347
RHO( 4)[ohm*m]=     7.27
    H( 4)[km]=     1.101
RHO( 5)[ohm*m]=    58.11
    H( 5)[km]=      .122
RHO( 6)[ohm*m]=    41.64
    H( 6)[km]=      .000


  Epsilon rho=     .1200
  Epsilon phi=     .0517
      Epsilon=     .0924
```

1-D INVERSE AT 208 (pol:invariant)

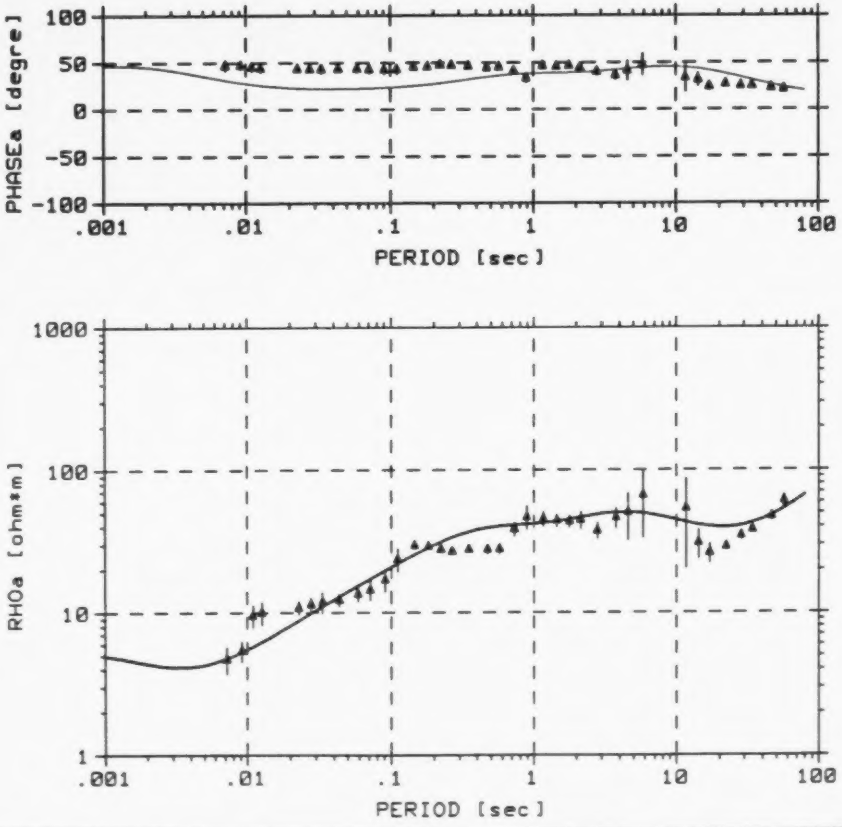

```
RHO( 1)[ohm*m]=      5.00
     H( 1)[km]=      .038
RHO( 2)[ohm*m]=      4.11
     H( 2)[km]=      .032
RHO( 3)[ohm*m]=     78.59
     H( 3)[km]=     2.470
RHO( 4)[ohm*m]=     22.36
     H( 4)[km]=      .084
RHO( 5)[ohm*m]=     23.76
     H( 5)[km]=      .327
RHO( 6)[ohm*m]=     35.36
     H( 6)[km]=     1.317
RHO( 7)[ohm*m]=    133.22
     H( 7)[km]=     3.204
RHO( 8)[ohm*m]=     40.58
     H( 8)[km]=     3.766
RHO( 9)[ohm*m]=       .09
     H( 9)[km]=      .010
RHO(10)[ohm*m]=    399.30
     H(10)[km]=    25.169
RHO(11)[ohm*m]=   1577.35
     H(11)[km]=    14.346
RHO(12)[ohm*m]=   4531.77
     H(12)[km]=      .000


  Epsilon rho=      .1075
  Epsilon phi=      .2474
     Epsilon=      .1907
```

1-D INVERSE AT 208 (pol:invariant)

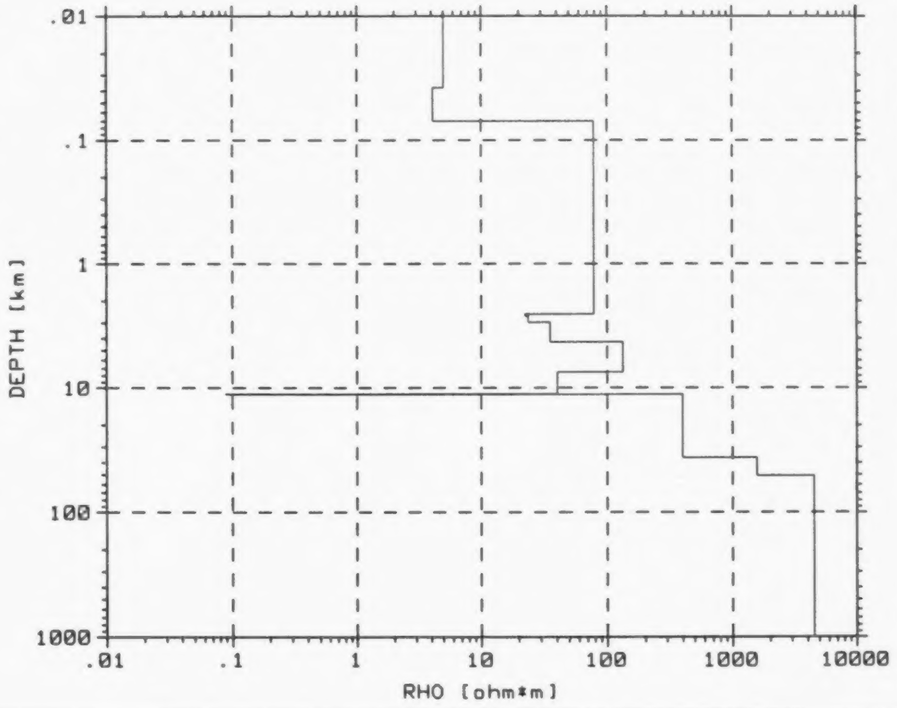

```
RHO( 1)[ohm*m]=      5.00
    H( 1)[km]=       .038
RHO( 2)[ohm*m]=      4.11
    H( 2)[km]=       .032
RHO( 3)[ohm*m]=     78.59
    H( 3)[km]=      2.470
RHO( 4)[ohm*m]=     22.36
    H( 4)[km]=       .084
RHO( 5)[ohm*m]=     23.76
    H( 5)[km]=       .327
RHO( 6)[ohm*m]=     35.36
    H( 6)[km]=      1.317
RHO( 7)[ohm*m]=    133.22
    H( 7)[km]=      3.204
RHO( 8)[ohm*m]=     40.58
    H( 8)[km]=      3.766
RHO( 9)[ohm*m]=       .09
    H( 9)[km]=       .010
RHO(10)[ohm*m]=    399.30
    H(10)[km]=     25.169
RHO(11)[ohm*m]=   1577.35
    H(11)[km]=     14.346
RHO(12)[ohm*m]=   4531.77
    H(12)[km]=       .000


  Epsilon rho=      .1075
  Epsilon phi=      .2474
      Epsilon=      .1907
```

1-D INVERSE AT 209 (pol:invariant)

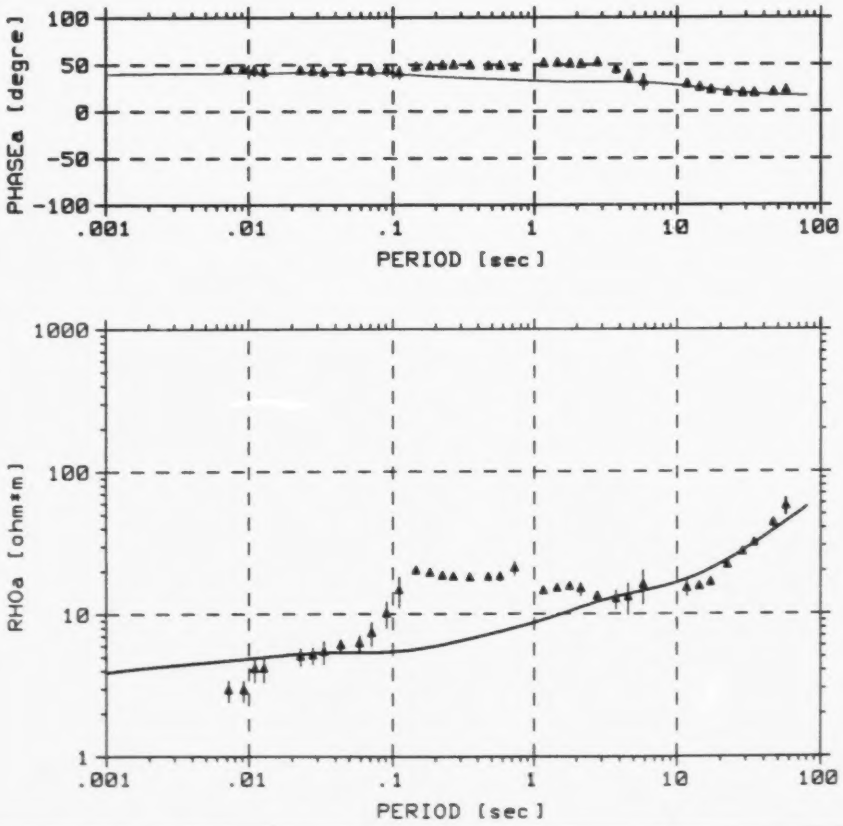

RHO(1)[ohm*m]= 2.90
H(1)[km]= .007
RHO(2)[ohm*m]= 4.36
H(2)[km]= .004
RHO(3)[ohm*m]= 5.39
H(3)[km]= .069
RHO(4)[ohm*m]= 6.55
H(4)[km]= .381
RHO(5)[ohm*m]= 19.19
H(5)[km]= 1.760
RHO(6)[ohm*m]= 43.93
H(6)[km]= 8.813
RHO(7)[ohm*m]= 745.57
H(7)[km]= .000

Epsilon rho= .2860
Epsilon phi= .1670
Epsilon= .2342

1-D INVERSE AT 209 (pol:invariant)

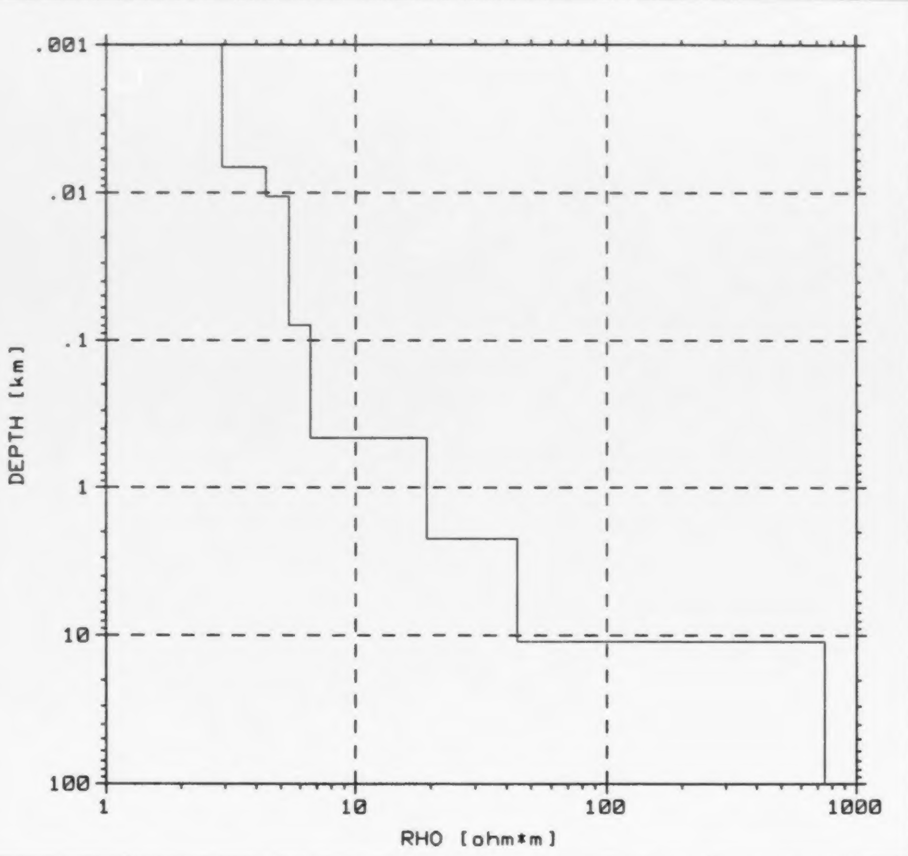

```
RHO( 1)[ohm*m]=      2.90
    H( 1)[km]=       .007
RHO( 2)[ohm*m]=      4.36
    H( 2)[km]=       .004
RHO( 3)[ohm*m]=      5.39
    H( 3)[km]=       .069
RHO( 4)[ohm*m]=      6.55
    H( 4)[km]=       .381
RHO( 5)[ohm*m]=     19.19
    H( 5)[km]=      1.760
RHO( 6)[ohm*m]=     43.93
    H( 6)[km]=      8.813
RHO( 7)[ohm*m]=    745.57
    H( 7)[km]=       .000


   Epsilon rho=     .2860
   Epsilon phi=     .1670
       Epsilon=     .2342
```